Contribution à l'étude de l'épitaxie d'hétérostructuresà base de semi-conducteurs III-V phosphorés

Xavier Wallart

Mémoire

Présenté à

L'Université des Sciences et Technologies de Lille

par

Xavier WALLART

pour obtenir

l'Habilitation à Diriger des Recherches

Contribution à l'étude de l'épitaxie d'hétérostructures à base de semi-conducteurs III-V phosphorés

Soutenu le 22 novembre 2005, devant la commission d'examen :

A. CAPPY	**Président**
J.C. HARMAND	**Rapporteur**
J. MASSIES	**Rapporteur**
E. TOURNIE	**Rapporteur**
F. MOLLOT	**Directeur des Recherches**
N. MAGNEA	**Examinateur**
C. PRIESTER	**Examinateur**

A Nathalie,
Edouard et Arthur

Remerciements

Ces travaux ont été réalisés principalement à l'Institut d'Electronique, de Microélectronique et de Nanotechnologie (IEMN - UMR 8520) dirigé par Monsieur Alain CAPPY, dans le groupe Epiphy. Je n'oublie pourtant pas les débuts, antérieurs à la création de l'IEMN, où le soutien de l'Institut Supérieur d'Electronique et du Numérique (ISEN) a été déterminant pour la suite.

A ce titre, je remercie les directions de L'ISEN et de l'IEMN pour la confiance qu'elles m'ont témoignée au long de ces années.

Monsieur Alain CAPPY fut mon voisin de bureau avant d'être appelé aux fonctions qui sont les siennes aujourd'hui. Ce fut pour moi l'occasion de discussions toujours intéressantes avec un scientifique et un pédagogue passionné et je suis très heureux qu'il ait accepté de présider ce jury.

Je remercie chaleureusement Messieurs Jean-Christophe HARMAND, Eric TOURNIE et Jean MASSIES d'avoir accepté de rapporter sur ce travail. Une reconnaissance particulière envers Monsieur Jean MASSIES, un des pionniers de l'Epitaxie par Jets Moléculaires en France, qui m'a initié à cet univers lors d'un séjour de quelques semaines au Centre de Recherche sur l'Hétéro-Epitaxie et ses Applications en 1990.

J'exprime mes sincères remerciements à Monsieur Noël MAGNEA pour voir accepté d'examiner ce travail.

C'est grâce à Madame Catherine PRIESTER que nombre de résultats expérimentaux ont pu trouver une interprétation satisfaisante. Je tiens à lui dire combien j'ai apprécié sa collaboration chaleureuse et son enthousiasme communicatif.

L'expérience de Monsieur Francis MOLLOT constitua un atout précieux dans mon travail de recherche. Il a su m'en faire profiter, a guidé ma démarche et m'a permis d'acquérir, au fil du temps, mon indépendance. J'ai beaucoup appris à son contact, aiguillonné en permanence par sa rigueur et son exigence scientifiques. Je l'en remercie vivement.

Je ne peux oublier mes compagnons de fortune et d'infortune en épitaxie : Messieurs Christophe COINON et Jean-Louis CODRON. Je leur témoigne toute ma gratitude pour l'ambiance sympathique qu'ils contribuent à entretenir autour des bâtis.

L'épitaxie a besoin de caractérisations : un grand merci à Dominique VIGNAUD et à Dominique DERESMES pour la photoluminescence et la microscopie à force atomique ainsi que pour leurs analyses critiques des résultats qui m'ont été précieuses.

J'associe pleinement à ces remerciements les doctorants avec lesquels j'ai travaillé : les travaux présentés leur doivent beaucoup.

Enfin, je remercie les collègues des groupes Composants et du groupe Physique de l'IEMN avec qui j'ai eu de nombreuses discussions et collaborations.

Curriculum Vitae

Etat Civil

Nom : WALLART
Prénoms : Xavier François Emmanuel
Date et lieu de naissance : 6 mai 1962 à Hazebrouck (59)
Nationalité : Française
Situation familiale : marié, 2 enfants
Adresse personnelle : 41, Rue Marcel Hénaux
59160 LOMME
tél : 03 20 08 21 37

Diplômes

juillet 1984 : Diplôme d'Ingénieur en Electronique, Institut Supérieur d'Electronique du Nord, Lille

juillet 1984 : Diplôme d'Etudes Approfondies, spécialité Sciences des Matériaux, Université des Sciences et Technologies de Lille I

juillet 1988 : Doctorat d'Université, spécialité Sciences des Matériaux, Université des Sciences et Technologies de Lille I

Activité et situation professionnelles

1985-1988 : Thésard et enseignant à l'Institut Supérieur d'Electronique du Nord
1988-1991 : Enseignant chercheur à l'Institut Supérieur d'Electronique du Nord
Depuis 1991 :

- Chargé de recherche de 1ère classe au CNRS à l'Institut d'Electronique, de Microélectronique et de Nanotechnologie au sein de l'équipe « Epitaxie » dirigée par Francis Mollot, directeur de recherche au CNRS
- Enseignant à l'Institut Supérieur d'Electronique et du Numérique

Date d'entrée au CNRS : 1er octobre 1991, CR1

Rattachement administratif : CNRS
Délégation régionale Nord-Pas de Calais et Picardie
2, Avenue des Canonniers,
59046 Lille Cedex

Adresse professionnelle :
Institut d'Electronique, de Microélectronique et de Nanotechnologie
U.M.R.-C.N.R.S. 8520,
Avenue Poincaré, B.P.69,
59652 Villeneuve d'Ascq Cedex
tél : 03 20 19 78 57
fax : 03 20 19 78 92
e-mail : Xavier.Wallart@iemn.univ-lille1.fr

Plan

Introduction

Faire le point de 17 années de recherche n'est pas chose aisée. Mon activité a connu des changements thématiques importants et comporté différents aspects qu'il n'était pas possible de détailler tous. C'est pourquoi j'ai choisi de me focaliser uniquement sur ce qui a constitué le cœur de mon travail, l'épitaxie d'hétérostrutures à base de semi-conducteurs III-V phosphorés.

Néanmoins, il m'a paru intéressant de préciser la trajectoire que j'avais suivie et le contexte dans lequel s'est déroulé ce travail : ceci est l'objet de la première partie.

La seconde partie entre dans le vif du sujet et détaille mes principales contributions à l'élaboration d'hétérostructures de semi-conducteurs III-V.

Dans la troisième partie, j'esquisse mon projet de recherche pour les années à venir, consacré aux hétérostructures de semi-conducteurs III-V antimoniés.

La quatrième partie résume mes autres activités, notamment l'enseignement de Mécanique Quantique et Physique des Solides auquel je suis particulièrement attaché et les différents encadrements d'étudiants de DEA et thésards.

Enfin, les annexes sont regroupées dans la cinquième partie avec la liste de mes publications et communications et une sélection de publications.

1ère partie

Mon parcours dans la recherche

Dans cette partie, je présente rapidement les thèmes de recherche que j'ai abordés à l'exception de l'épitaxie d'hétérostructures de semi-conducteurs III-V qui est détaillée dans la seconde partie. Si, pour certaines de ces activités telle l'étude des couches minces de siliciures, la page est tournée d'autres telle l'analyse de surfaces par spectroscopie de photoélectrons continue de faire partie de mon paysage quotidien.

Les débuts

J'ai commencé durant la thèse d'Université par l'étude des siliciures de titane, puis ai poursuivi comme enseignant chercheur à l'ISEN par l'étude du siliciure de fer semi-conducteur et l'oxydation des alliages SiGe. Cette période m'a permis d'aborder le monde des matériaux semi-conducteurs, les problèmes d'interface liés aux films minces de quelques nanomètres d'épaisseur et d'acquérir une expérience en techniques d'analyse de surfaces.

Quelques mots sur les siliciures

Tout commence avec le silicium !

Dans la fabrication des composants silicium, les siliciures interviennent comme matériaux de faible résistivité pouvant avantageusement remplacer le polysilicium comme matériau de grille. Le siliciure de titane s'avère particulièrement intéressant puisqu'il présente l'une des plus faibles résistivités parmi les siliciures. C'est dans ce contexte que j'ai entrepris mon travail de thèse au sein du Laboratoire d'Etude des Surfaces et Interfaces (LESI, URA 253) dirigé par Michel Lannoo. Le sujet portait sur la caractérisation de la réaction en phase solide lors du recuit d'un film mince de titane (1-5 nm) déposé sur un substrat de silicium dans une enceinte ultra-vide. Sur le plan expérimental, les conditions étaient particulières puisqu'il m'a fallu "démarrer" le système ultra-vide associé à cette étude, avec l'aide de Jean-Philippe Nys, aujourd'hui ingénieur d'études CNRS. Les techniques expérimentales que j'ai mises en œuvre sont essentiellement les spectroscopies Auger et de pertes d'énergie d'électrons et la diffraction d'électrons lents.

Au cours de cette étude, j'ai approfondi 2 aspects de la spectroscopie Auger :

- l'analyse quantitative qui m'a permis de déterminer la composition des siliciures formés à l'interface ainsi que leur mode de croissance

- l'analyse de la forme de la raie Auger SiLVV et son interprétation à l'aide des densités d'états partielles en bande de valence qui m'ont donné accès à l'environnement chimique du silicium à l'interface et dans les films minces. Cette partie de l'étude a fait l'objet d'une collaboration avec l'équipe théorique du laboratoire (Isabelle Devos-Lefèbvre, Michel Lannoo) pour le calcul des densités d'états pour les différents siliciures [1,2].

Durant ce travail, j'ai participé au Groupement Circuits Intégrés Silicium (GCIS) et bénéficié de son soutien financier.

Après ma soutenance de thèse en juillet 1988, les études sur les siliciures métalliques étaient déjà bien avancées au niveau international. Le sujet a connu alors un regain d'intérêt avec les siliciures semi-conducteurs et particulièrement le siliciure de fer β-$FeSi_2$. Après discussion avec Paul Friedel, je me suis lancé dans l'aventure en encadrant mon premier

thésard, Hong Sheng Zeng (directeur de thèse : Didier Stièvenard)[3], et les mêmes outils que précédemment. J'y ai adjoint une technique nouvelle : la spectroscopie de structures fines de pertes d'énergie des électrons. Cette dernière, apparentée à l'EXAFS, permet de déterminer l'ordre atomique local en surface et est bien adaptée à l'étude des régions interfaciales amorphes ou polycristallines rencontrées dans les systèmes silicium-métaux [4,5].

Les siliciures de fer ont été mon premier contact avec l'épitaxie (dans ce cas en phase solide) puisque la phase β-$FeSi_2$ peut s'épitaxier sur les surfaces Si(111) et (100). La qualité cristalline du matériau obtenu par réaction en phase solide s'est avérée mauvaise et, malgré l'utilisation d'un procédé de coévaporation de fer et silicium, je n'ai pu obtenir du matériau de qualité suffisante pour prétendre à une application de type semi-conducteur. Les principales raisons en sont :

- plusieurs orientations d'épitaxie équivalentes sur Si(111)
- la difficulté de contrôle de la stœchiométrie dans le cas de la coévaporation.

Ce sujet a été l'occasion d'une collaboration avec les laboratoires du LEP et du CRMC2 (CRMCN depuis) dans le cadre d'un contrat DRET sur la faisabilité d'un détecteur à base de β-$FeSi_2$ [6,7].

Oxydation des alliages SiGe

Des alliages prometteurs

Les années 80 voient le développement de l'épitaxie des semi-conducteurs III-V mais également des alliages SiGe sur substrat silicium. Ces alliages permettent d'améliorer les performances des composants bipolaires silicium avec le TBH à base SiGe et à effet de champ avec les MOSFET à canal SiGe (ou Si contraint plus récemment). Au début des années 90, l'utilisation des alliages SiGe comme matériau de canal de transistor MOS semble prometteuse puisqu'elle améliore la dynamique des trous qui est l'un des facteurs limitant les performances des paires CMOS. La fabrication de l'oxyde de grille sur un alliage SiGe par oxydation thermique n'est plus envisageable dans ce cas car nécessite des températures trop élevées. C'est ainsi qu'après discussion avec Didier Stièvenard, j'ai abordé l'oxydation assistée par plasma des alliages SiGe. Ce travail a fait l'objet de la thèse de Claude Tételin dont j'ai assuré l'encadrement, Didier Stièvenard étant directeur de thèse [8]. Les échantillons épitaxiés par dépôt en phase vapeur (CVD) ont été fournis par Lili Vescan (Institut für Schicht and Ionentechnik, Forschungszentrum, Jülich). Cette étude a détaillé la cinétique d'oxydation de ces alliages en fonction de leur composition et a montré qu'elle s'accompagne de la formation de SiO_2 en surface et d'un empilement de germanium à l'interface Si-SiO_2. Pour mener à bien ce travail, j'ai associé la spectroscopie d'électrons Auger à un canon ionique permettant une analyse chimique en profondeur. Cette technique d'analyse fournit des résultats délicats à interpréter mais par une optimisation des conditions de profilage, un étalonnage sur des échantillons test et un traitement des données prenant en compte la plupart des effets indésirables (ion mixing,...), j'ai pu remonter à des profils de concentration "réalistes" sur des échelles d'épaisseur de l'ordre du nanomètre [9,10].

Le tournant : la création de l'IEMN

En 1991, dans la perspective de la création de l'IEMN, j'ai intégré le CNRS comme chargé de recherche avec à la clé :

- une mission : définition, choix et mise en oeuvre d'un appareillage de spectroscopie de photoélectrons (ESCA) couplé à des bâtis d'épitaxie par jets moléculaires (EJM).

- un changement thématique puisque mon programme de recherche portait sur l'épitaxie d'hétérostructures à base de semi-conducteurs III-V pour applications micro-ondes.

Une constante de mon activité : l'analyse de surfaces

Surface, quand tu nous tiens…

Parmi les investissements réalisés à la création de l'IEMN, il est décidé de renforcer la caractérisation physique de matériaux et en particulier de coupler un système d'analyse de surfaces (ESCA) aux bâtis d'EJM. Compte tenu de mon activité antérieure dans le domaine, je me suis investi dans ce projet. En collaboration avec mes collègues de l'EJM, j'ai défini le système, opéré le choix du fabricant et surtout me suis assuré de la compatibilité avec les bâtis EJM. C'est ce dernier point qui m'a demandé le plus d'énergie puisqu'aucune solution commerciale n'existait et qu'il a donc fallu l'inventer. Malgré un retard de livraison et quelques péripéties, le système est installé début 1995 et donne encore aujourd'hui toute satisfaction

Depuis lors, j'ai en charge cet équipement d'analyse et j'ai développé son activité autour de 3 pôles essentiels :

- l'étude de surfaces et d'interfaces entre semi-conducteurs III-V élaborées par épitaxie par jets moléculaires (cf. 2ème partie)
- l'étude de couches organiques greffées sur substrats de silicium au laboratoire et en collaboration avec l'extérieur
- la caractérisation d'étapes technologiques lors de la fabrication de composants

Etude de couches moléculaires greffées sur silicium

Depuis quelques années se développe le greffage de couches organiques sur silicium. La sensibilité de surface de l'XPS en fait un outil d'analyse privilégié pour ces structures où l'épaisseur des couches est de l'ordre de 1 à 2 nm. L'ESCA de l'IEMN disposant d'une source X monochromatisée, des spectres XPS haute résolution peuvent être obtenus afin de caractériser l'environnement chimique des différents constituants de la molécule greffée. Ce travail a fait l'objet d'une collaboration avec l'équipe de P. Allongue de l'Université Pierre et Marie Curie à Paris dans le cadre du Programme Matériaux du CNRS (1998-2000) [11-13] et avec le groupe physique de l'IEMN [14].

L'action menée avec P. Allongue visait à étudier le greffage de molécules de type alcènes C_nH_{2n+1} sur substrats Si(111). Le greffage étant réalisé sur des substrats monocristallins, les effets de diffraction des photoélectrons peuvent altérer fortement l'analyse quantitative des résultats. Ils sont dus aux interférences entre l'onde électronique émanant de l'atome émetteur et les ondes diffusées (surtout vers l'avant pour des énergies électroniques supérieures à 500 eV) par les atomes voisins. Pour un cristal homogène, les variations d'intensité mesurées peuvent atteindre plusieurs dizaines de % suivant les angles polaire et azimutal de détection. Ceci a nécessité de développer une méthodologie permettant de s'affranchir le plus possible de ces effets. La solution retenue consiste à opérer une moyenne azimutale pour chaque angle polaire (angle entre la surface et la direction d'émission des photoélectrons) [15]. L'analyse des échantillons est effectuée suivant différents angles polaires (de 25 à 75°) permettant une variation de la profondeur sondée d'un facteur 2 environ. L'atténuation de l'intensité de la raie du silicium Si 2p donne alors accès à l'épaisseur de la couche greffée ou plus précisément au rapport d/λ où d est l'épaisseur de la couche greffée et λ le libre parcours moyen des électrons dans la couche. La méthode a été testée avec succès sur des échantillons de silicium recouverts d'oxyde natif. Pour l'étendre

aux couches moléculaires, des spectres et des intensités de référence pour les éléments Si, C et O, constituants majoritaires des couches greffées, ont été relevés sur des échantillons Si(111)-H, carbone graphite et SiO_2. Les valeurs de λ obtenues sont en bon accord avec des déterminations précédentes portant sur des couches de thiols greffées sur des substrats d'or. Les différences peuvent s'interpréter par un greffage imparfait : nous avons montré que le taux de couverture est compris entre 0.45 et 0.5 pour un taux théorique de 0.5. Ces résultats sont confirmés par une détermination indépendante de la densité en atomes de carbone de la couche obtenue à partir de celle du graphite [13].

Avec le groupe Physique de l'IEMN, j'ai abordé la fonctionnalisation de surfaces Si(111) par des molécules de semi-carbazine servant ultérieurement à l'accrochage de peptides dans le cadre de travaux menés à l'interface physique-biologie. Plus précisément, c'est dans ce cas la sensibilité de l'XPS à l'environnement chimique des atomes de carbone qui a été mise à profit pour démontrer de greffage covalent de cette molécule complexe et pour comparer différentes méthodes de greffage (cf. figure I.1).

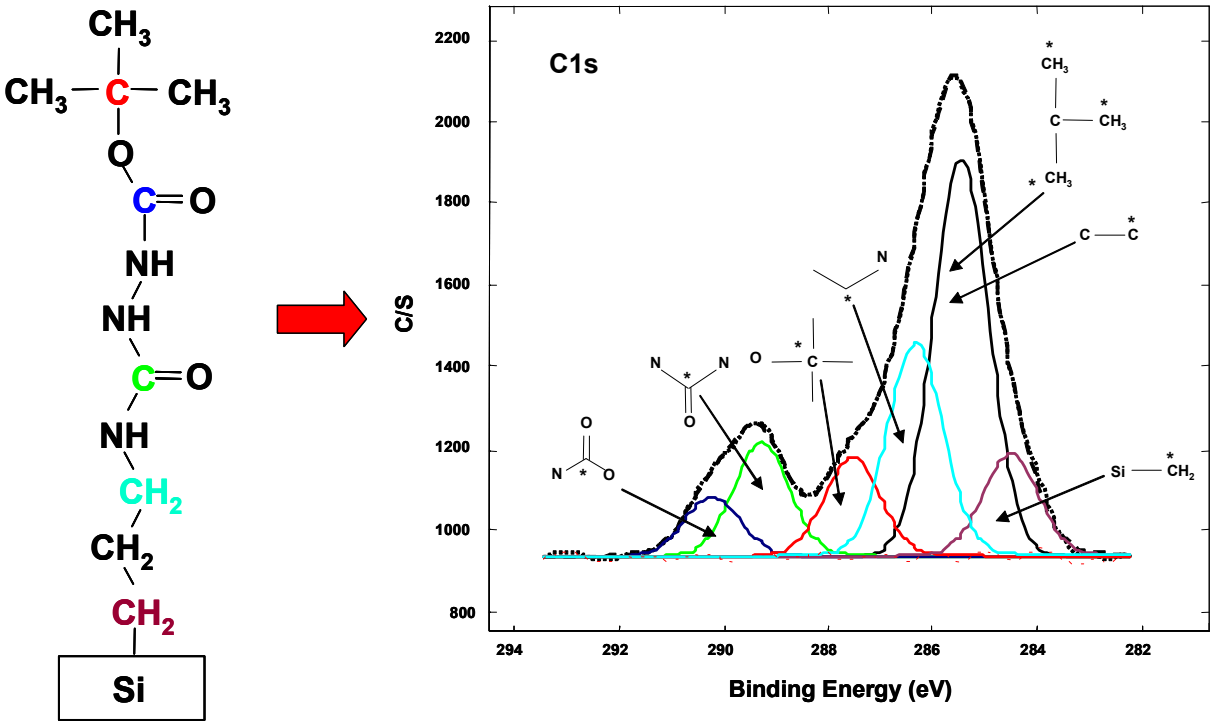

Figure I.1 : Schéma de principe du greffage de la molécule de semi-carbazine sur une surface de silicium (à gauche) et spectre XPS de la raie C1s obtenu après greffage permettant d'identifier les différents environnements chimiques des atomes de carbone.

Caractérisation d'étapes technologiques

L'une des activités importantes du laboratoire est la technologie des semi-conducteurs III-V pour la réalisation de dispositifs opto et micro-électroniques. Dans ce cadre, l'XPS permet de caractériser les différentes opérations technologiques telles que gravure, recuit.... et j'ai été fréquemment amené à collaborer avec les équipes « composants » du laboratoire à ce sujet [16]. A titre d'exemple, je peux citer l'étude menée sur les traitements de désoxydation des alliages InGaAs et InAlAs pour l'optimisation du contact Schottky de grille des transistors HEMT dans la filière InAlAs/InGaAs. Cette étude a déterminé les meilleures

attaques acides pour désoxyder la couche de contact InGaAs avant gravure du fossé de grille puis la couche barrière InAlAs avant le dépôt de la grille. Le même type de caractérisation a été mené sur les matériaux nitrures GaN, AlGaN [17].

Plus récemment, j'ai collaboré avec E. Dubois dans le cadre du programme européen SODAMOS sur la fabrication de transistors MOS silicium ultimes [18]. Il s'agit dans ce cas d'étudier la formation de contacts Schottky à très faible hauteur de barrière sur substrats SOI. Parmi les candidats possibles, nous avons étudié les siliciures de platine et d'iridium formés par recuit thermique sous azote d'un film métallique déposé sur silicium. L'analyse XPS couplée à l'érosion ionique a eu pour but de déterminer les réactions d'interface, la composition et la cinétique de croissance des siliciures formés en fonction de la température de recuit. Ces résultats ont été corrélés avec des mesures électriques [19-21].

Le cœur de mon travail : l'épitaxie de semi-conducteurs

Mon intégration dans l'équipe "Epitaxie " de l'IEMN s'est faite avec pour but de développer la croissance d'hétérostructures InAlAs/InGaAs sur subtrat InP pour la fabrication de composants de type HEMT rapides. Je dois à Yves Druelle, professeur et à Jean-Luc Lorriaux, ingénieur de recherche, mon initiation à l'EJM des semi-conducteurs III-V. Francis Mollot, directeur de recherche au CNRS, m'a ensuite guidé dans toutes les subtilités du métier. J'ai pu mesurer à cette occasion l'écart qui existe entre la mise en oeuvre de l'ultra-vide pour les études matériaux et pour l'élaboration de matériaux semi-conducteurs pour la fabrication de composants.

A mon arrivée en 1991, l'équipe "Epitaxie" a déjà acquis une expérience dans la réalisation de structures de type HEMT à canal GaAs ou InGaAs pseudomorphique sur substrat GaAs mais n'a pas encore développé de croissances sur substrat InP. J'ai développé cette activité en tentant d'allier une recherche portant sur la croissance des matériaux à une démarche spécifiquement tournée vers les composants. Plus récemment, j'ai tenté de diversifier le volet « matériaux » en tentant une approche de l'épitaxie de diamant par jets moléculaires

Epitaxie d'hétérostructures de semi-conducteurs III-V

Ce travail est exposé en détail dans la seconde partie et je n'en donne ci-dessous qu'un résumé.

J'ai orienté l'aspect matériaux vers les problèmes d'interfaces et la croissance des semi-conducteurs phosphorés contraints. J'ai abordé le problème des interfaces à anion commun pour lequel nous avons proposé un modèle cinétique prenant en compte l'effet de la température de croissance sur les mécanismes d'échange et de ségrégation en surface. Pour les interfaces différant par leurs anions, la corrélation des résultats de diverses techniques m'a amené à une description précise de la composition chimique de ces interfaces en fonction des conditions de croissance et de son influence sur les propriétés électroniques de l'hétérostructure. Les séquences de croissance ont ensuite été optimisées pour réaliser les interfaces les plus abruptes possible. Cette optimisation m'a conduit à étudier la réactivité de surface des arséniures sous flux de phosphore pour laquelle, avec C. Priester du groupe Physique de l'IEMN, nous avons déterminé les facteurs essentiels : dimères d'anions en surface et énergie de liaison des binaires impliqués. L'effet de la contrainte sur la morphologie des couches de semi-conducteurs phosphorés présente des similitudes et des différences avec le cas des arséniés. Nous avons proposé une interprétation de ces différences soulignant le rôle des reconstructions de surface spécifiques aux phosphorés.

Concernant les composants, j'ai initié au sein de l'IEMN la croissance d'hétérostructures à modulation de dopage sur substrat InP. Les applications visées sont les composants micro-ondes de puissance ou faible bruit. J'ai ainsi été conduit à optimiser la croissance de structures à double plan de dopage, celle de barrière InAlAs à fort taux d'aluminium et celle de canaux composites pour les applications de puissance. Pour le faible bruit, mon effort a porté sur la croissance de canaux contraints en InGaAs à fort taux d'indium et de structures à dimensions ultimes pour les longueurs de grille les plus courtes.

Une diversification à haut risque : l'homoépitaxie de diamant

Durant les années 97-98, le laboratoire a entrepris une réflexion prospective sur les matériaux sous forme d'une commission que j'ai animée. Suite aux travaux de cette commission que j'ai présentés en Conseil de Laboratoire, il a été décidé d'entreprendre l'homoépitaxie de diamant en vue d'applications électroniques.

Le diamant, de par ses propriétés thermique, optique et électronique exceptionnelles, tient une place à part dans la famille des matériaux. Il se distingue par sa capacité à supporter des environnements extrêmes en pression, température et puissance dissipée. Cependant, les dispositifs électroniques à base de diamant n'en sont qu'à leur premier stade, du fait de problèmes inhérents à l'élaboration de substrats diamant de pureté et de qualité cristalline suffisantes et de dopage. La croissance de diamant dopé n n'a été démontrée que récemment (1997) et a relancé l'intérêt de la communauté scientifique pour ce matériau.

Avec Francis Mollot et Dominique Vignaud, j'ai participé activement au choix de la technique de croissance et à la définition du système d'épitaxie, opérant ainsi une diversification de mon activité de croissance de matériaux. La méthode d'élaboration retenue est l'Epitaxie par Jets Moléculaires à Sources Gazeuses (EJMSG). Elle se démarque nettement des techniques usuelles d'épitaxie du diamant, l'Epitaxie en Phase Vapeur à Filament Chaud (EPVFC) ou Assistée par Plasma (EPVAP). Ces deux techniques utilisent un mélange gazeux, composé d'un hydrocarbure (le plus souvent le méthane) et d'hydrogène, activé soit par des filaments de tungstène placés à quelques millimètres de l'échantillon et portés à plus de 2000°C, soit par un plasma micro-ondes. Ceci conduit à d'importantes concentrations de radicaux méthyles et d'hydrogène atomique en surface de l'échantillon, les deux espèces supposées nécessaires à la croissance de diamant.

Le choix de l'EJMSG est motivé par les inconvénients présentés par ces deux techniques. En EPVFC, la disposition des filaments à proximité de la surface en croissance est propice à l'incorporation d'impuretés métalliques. De plus, la carburation des filaments rend le craquage des gaz injectés progressivement moins efficace. En EPVAP, l'échantillon en croissance est placé dans le plasma et donc exposé aux espèces ionisées plus ou moins énergétiques qui peuvent induire des défauts cristallins, voire contribuer à l'incorporation d'impuretés dans le diamant épitaxié. Enfin, si ces deux techniques permettent d'obtenir des films monocristallins dopés de type p par ajout d'une espèce contenant du bore, elles ne permettent que très difficilement la croissance de films dopés de type n. Le projet de l'IEMN a donc deux objectifs majeurs :

- étudier la faisabilité de l'épitaxie de diamant par EJMSG qui est une technique plus douce et conduite dans un environnement plus propre (ultra-vide) que les précédentes. Ceci est un véritable défi car jusqu'à présent, les quelques tentatives relevées dans la littérature se sont soldées par des croissances de films de qualité médiocre et à des vitesses très faibles
- tenter d'améliorer l'efficacité du dopage de type n par rapport à l'épitaxie en phase vapeur.

Le bâti d'épitaxie, comportant de nombreux éléments prototypes, a été installé en salle blanche à l'automne 2000. Le travail de thèse de Thomas Géhin [22] dont j'ai été co-directeur a porté sur 3 aspects :

- la préparation des surfaces de diamant monocristallin pour l'épitaxie
- la recherche et la mise en œuvre d'une source intense d'hydrogène atomique et d'une source de radicaux méthyles, précurseurs de la croissance de diamant
- la recherche de conditions de croissance favorisant la croissance de la phase diamant et non graphite

A partir des substrats reçus du fournisseur, à l'aide de caractérisations XPS et AFM, nous avons mis au point une procédure de nettoyage chimique permettant d'éliminer toutes traces d'impuretés et de résidus de carbone amorphe à la surface. Cependant, la rugosité des surfaces due au polissage des substrats est telle que, après recuit dans la chambre de croissance, seuls certains échantillons présentent une reconstruction (2x1), observée en RHEED, caractéristique des surfaces atomiquement propres.

La mise au point et la caractérisation des sources radicalaires a nécessité l'utilisation intensive de la spectrométrie de masse à ionisation de seuil afin de confirmer et de quantifier la formation des radicaux souhaités. Le craquage thermique de l'hydrogène moléculaire dans une cellule de type capillaire n'a permis d'obtenir que des flux d'hydrogène atomique de l'ordre de 1 10^{15}/cm^{2}s. Seule l'utilisation d'une cellule à craquage assisté par plasma RF nous a permis d'atteindre des valeurs environ 10 fois supérieures, de l'ordre de 1 à 2 10^{16} H/cm^{2}s à la surface de l'échantillon.

La fabrication d'une source efficace de radicaux méthyles s'avère plus délicate car le craquage d'hydrocarbures assisté par plasma conduit rapidement à un dépôt de carbone à l'intérieur de la cavité radiofréquence, rendant la cellule inutilisable. Seul le craquage thermique est possible mais nécessite l'utilisation d'un craqueur haute température (jusque 1800°C), compte tenu des énergies de liaison en jeu. Nous avons également fait varier le régime d'écoulement du gaz dans le craqueur (laminaire, moléculaire) en modifiant la conductance du diffuseur de sortie. Le craquage thermique du méthane (hydrocarbure utilisé en EPV) ne fournit des quantités significatives de radicaux méthyles (1 10^{15}/cm^{2}s par sccm de CH_4) qu'en écoulement laminaire dans le craqueur, favorisant l'accommodation thermique. Dans le cas de l'éthane, une efficacité légèrement supérieure a été obtenue (5 10^{15}/cm^{2}s par sccm de C_2H_6) mais cette fois en régime moléculaire. Pour accroître le flux de radicaux méthyles, nous nous sommes alors tournés vers des précurseurs originaux : l'isobutène et l'acétone pour lesquels les énergies de liaison sont plus faibles. Avec ces derniers, nous avons ainsi pu obtenir des flux nettement supérieurs (de l'ordre de 1 à 2 10^{16}/cm^{2}s par sccm de gaz précurseur). Cependant, dans le cas de l'isobutène, la production de radicaux méthyles s'accompagne de celle de radicaux allyles (C_3H_5) alors que le craquage de l'acétone conduit à la formation simultanée de CO, molécule très stable [23].

Nous avons ensuite exploré la recherche des conditions de croissance de la phase diamant sur substrats silicium et diamant. Par analogie avec les techniques EPVFC et EPVAP, nous dirigeons sur la surface un flux de radicaux méthyles et un flux d'hydrogène atomique. Nous avons exploré une gamme de température de substrat allant de l'ambiante à 1100°C. Sur substrat silicium, en utilisant le craquage thermique du méthane, de l'éthane ou de l'acétone nous avons observé la formation de SiC polycristallin pour des températures supérieures à 650°C, mais aucune nucléation de la phase diamant. Par contre, aucune croissance n'est détectée sur substrat diamant quels que soient la température et le rapport des flux hydrogène atomique/radicaux méthyles (de 1 à 20).

Le craquage thermique de l'isobutène conduit à des résultats différents. En effet, sur silicium, nous avons pu déposer des films de type DLC (plusieurs centaines de nanomètres d'épaisseur) à température ambiante. Hélas, ces films se subliment au-delà de 500°C et n'ont

pas pu servir de base à la nucléation de la phase diamant. Sur substrat diamant, nous avons obtenu de faibles dépôts de carbone amorphe (quelques nanomètres d'épaisseur) plus ou moins hydrogéné suivant la température de croissance mais là encore, jamais de croissance de la phase diamant. Les dépôts observés avec l'isobutène sont probablement dus aux radicaux allyles (C_3H_5) issus du craquage de l'isobutène, et non aux radicaux méthyles.

Les schémas réactionnels permettant la croissance de diamant en EPV sont donc inopérants en EJM. L'une des raisons en est sans doute le trop faible flux d'hydrogène atomique obtenu en EJM (quelques $10^{16}/cm^2s$) comparé à celui utilisé en EPV (quelques $10^{19}/cm^2s$). L'hydrogène atomique est à l'origine des réactions d'activation de la surface, d'abstraction et de recombinaison sur les radicaux méthyles permettant finalement l'incorporation de ces radicaux en diamant. Le faible flux utilisé en EJM pénalise donc fortement la fréquence de ces réactions durant la durée de vie des radicaux méthyles en surface, limitée par la désorption thermique. L'augmentation de la durée de vie des radicaux par une diminution de la température du substrat ne permet pas d'améliorer la situation car, dans ce cas, les phénomènes de gravure deviennent prépondérants.

Le couple radicaux méthyles-hydrogène atomique ne fonctionne donc pas en EJM. L'augmentation significative du flux d'hydrogène atomique pour se rapprocher des conditions EPV paraît très difficile à réaliser techniquement. L'alternative consiste alors à utiliser des radicaux plus réactifs que les radicaux méthyles et ayant donc une durée de vie supérieure à la surface : c'est cette voie que nous explorons actuellement.

Références

[1] : X. Wallart, J.P. Nys, G. Dalmai, I. Lefebvre, M. Lannoo, Europhys. Lett. **10**, 587 (1989)
[2] : X. Wallart, J.P. Nys, H.S. Zeng, G. Dalmai, I. Lefebvre, M. Lannoo,, Phys.Rev. **B41**, 3781 (1990)
[3] : H.S. Zeng, *Etude de la formation de films minces de siliciures de fer par spectroscopies d'électrons*, thèse de l'Université des Sciences et Technologies de Lille I, spécialité Sciences des Matériaux, octobre 1991.
[4] : H.S. Zeng, X. Wallart, J.P. Nys, G. Dalmai, P. Friedel, Phys.Rev. **B44**, 13811 (1991)
[5] : X. Wallart, J.P. Nys, C. Tételin, Phys.Rev.**B49**, 5714 (1994)
[6] : J.P. André, H. Alaoui, A. Deswarte, Y. Zheng, J.F. Petroff, X. Wallart, J.P. Nys, J.Cryst.Growth **144**, 29 (1994)
[7] : *Photodétecteur intégrable en siliciure de fer - épitaxie sur silicium,* Contrat MRT N° 90 S 0248.
[8] : C. Tételin, *Oxydation basse température assistée par plasma des alliages silicium-germanium*, thèse de l'Université des Sciences et Technologies de Lille I, spécialité Sciences des Matériaux, mars 1996.
[9] : C. Tételin, X. Wallart, D. Stièvenard, J.P. Nys, D.J. Gravesteijn, J. Vac. Sci. Technol. **B16**, 137 (1998)
[10] : C. Tételin, X. Wallart, J.P. Nys, L. Vescan, D.J. Gravesteijn, J. Appl. Phys. **83**, 2842 (1998)
[11] : *Films moléculaires greffés directement sur silicium : fonctionnalisation et nanostructuration,* Programme Matériaux CNRS, appel d'offres 1998
[12] : P. Allongue, C. Henry De Villeneuve, J. Pinson, F. Ozanam, J.N. Chazalviel, X. Wallart, Electrochemical Acta **43**, 2791 (1998)
[13] : X. Wallart, C. Henry de Villeneuve, P. Allongue, accepté à J. Am. Chem. Soc.
[14] : Y. Coffinier, C. Olivier, A. Perzyna, B. Grandidier, X. Wallart, J.-O.Durand, O. Melnyk, D. Stiévenard, Langmuir **21**, 1489 (2005)
[15] : M. Seelmann-Eggebert and H. J. Richter, Phys. Rev. **B43** (1991) 9578
[16] : I. Roch, L. Buchaillot, X. Wallart, D. Collard, J. Vac. Sci. Technol. **B19**, 305 (2001)
[17] : B. Boudart, S. Trassaert, X. Wallart, J.C. Pesant, O. Yaradou, D. Théron, Y. Crosnier, H. Lahreche, F. Omnes, Journal of Electronic Materials **29**, 603 (2000)
[18] : Projet européen SODAMOS IST-2000-26475
[19] : G. Larrieu, *Elaboration et caractérisation de transistors MOS Schottky en regime nanométrique*, thèse de l'Université des Sciences et Techniques de Lille I, spécialité Electronique, avril 2004.
[20] : G. Larrieu, E. Dubois, X. Wallart, X. Baie, J. Katcki, J. Appl. Phys. **94**, 7801 (2003)
[21] : A. Laszcz, J. Katcki, J. Ratajczak, G. Larrieu, E. Dubois, X. Wallart, J. Alloy and Compounds **382,** 24 (2004)
[22] : T. Géhin, *Mise en oeuvre de l'épitaxie par jets moléculaires pour la synthèse de diamant monocristallin*, thèse de l'Université des Sciences et Techniques de Lille I, spécialité Science des Matériaux, décembre 2004
[23] : T. Géhin, X. Wallart, D. Vignaud, Surface and bulk defects in CVD diamond X, Hasselt (2005)

2ème Partie

Hétérostructures à base de semi-conducteurs III-V phosphorés

De la physique des surfaces aux composants

Mon travail en Epitaxie par Jets Moléculaires de semi-conducteurs III-V a comporté de nombreux aspects. Cela m'a permis d'aborder différentes problématiques, allant de la physique des surfaces aux composants hyperfréquences. Je ne mentionnerai ici que mes contributions les plus significatives que j'ai regroupées en quatre thèmes principaux.

Le premier concerne les reconstructions de surface qui jouent un rôle primordial dans la croissance épitaxiale. Je discuterai particulièrement les reconstructions de surface des phosphures qui présentent des différences notables avec celles plus documentées des arséniures. Une autre caractéristique majeure des hétérostructures est la qualité de leurs interfaces que j'aborderai ensuite, suivant qu'elles mettent en jeu des semi-conducteurs à anion commun ou non. La contrainte tient également une place de choix en épitaxie puisqu'elle fixe les limites au-delà desquelles il n'est pas toujours bon d'aller, quoique…Enfin, la croissance d'hétérostructures vise le plus souvent la réalisation de dispositifs opto ou microélectroniques. J'illustrerai dans cette dernière partie les résultats obtenus sur des structures à modulation de dopage, de type HEMT.

Reconstructions de surfaces

Un vieux problème… toujours d'actualité

Les reconstructions de surface sont observées sur la plupart des surfaces de monocristaux, métalliques ou semi-conducteurs. Dans le cas des semi-conducteurs III-V, elles dépendent de la composition de la surface en élément III ou V. A ce titre, leur connaissance est un guide précieux lors de l'épitaxie puisqu'il permet par observation du diagramme RHEED, d'estimer la composition de la surface en croissance. Ces différentes reconstructions correspondent à des énergies spécifiques différentes qui peuvent favoriser la diffusion de surface des espèces incidentes mais aussi la transition d'un mode de croissance bidimensionnel vers un mode tridimensionnel. Historiquement, les reconstructions de surface de GaAs ont servi de prototype à toute discussion sur d'autres semi-conducteurs III-V. Je commence donc par un bref retour sur les reconstructions les plus courantes des surfaces GaAs (001) et InAs (001) avant de présenter le cas des phosphures GaP (001) et InP (001).

Les surfaces GaAs et InAs (001)

A tout seigneur, tout honneur : la surface GaAs(001)

Lors de la croissance de GaAs, l'observation des diagrammes RHEED révèle principalement 3 reconstructions que l'on peut classer suivant leur concentration décroissante en arsenic : c(4x4), (2x4) et (4x2). La c(4x4) est une reconstruction très riche en arsenic avec plus d'une monocouche d'arsenic en surface tandis que la (4x2) est enrichie en gallium. Pour ces raisons, la croissance de GaAs s'effectue le plus souvent en (2x4), pour laquelle la composition en arsenic est de l'ordre de 0.5-0.75 monocouche. Une caractéristique importante de la surface de GaAs (comme des autres arséniures) est la possibilité d'observer la transition d'une surface riche en arsenic à une surface riche en gallium en suivant le passage d'un diagramme RHEED (2x4) à un diagramme (4x2).

La reconstruction (2x4) de GaAs a suscité de nombreuses études expérimentales (photoémission, STM, RDS,…) et théoriques (calculs ab initio d'énergie de différents modèles de reconstruction) [1-8]. Lors de la croissance épitaxiale de GaAs, des changements d'intensité des raies fractionnaires du diagramme (2x4) permettent de distinguer les reconstruction (2x4) α, β et γ. Il existe actuellement un consensus suivant lequel l'arrangement le plus stable correspond au modèle β2 (2x4) (figure II.1), dans lequel le taux de couverture en arsenic est de 0.75.

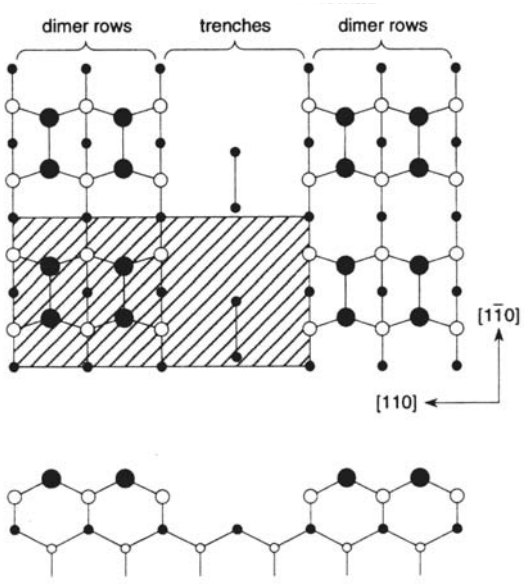

Plus précis : GaAs (2x4)

Figure II. 1 : vues de dessus et de profil de la reconstruction GaAs β2(2x4)(d'après [8]).

La reconstruction riche gallium est plus complexe et ce n'est que récemment que le modèle ξ(4x2), permettant de rendre compte de toutes les observations expérimentales, a été élaboré [9-12].

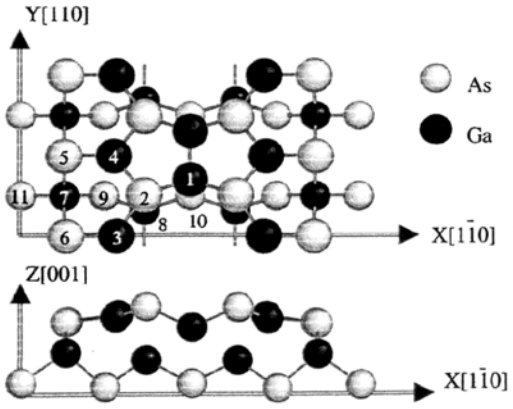

Cela peut devenir complexe….

Figure II.2 : vues de dessus et de profil de la reconstruction GaAs ξ(4x2)(d'après [11]).

Finalement, la reconstruction c(4x4),la plus riche en arsenic, fait encore débat puisque si jusqu'alors, elle était décrite avec plusieurs dimères d'arsenic en surface [13,14] conduisant à un taux de couverture en arsenic de 1.75, des résultats récents tendent à prouver qu'elle est caractérisée par 3 dimères mixtes Ga-As et un taux de couverture de 1.0 en arsenic [15]. Néanmoins, cette dernière valeur semble faible car très proche de celle relevée sur la

reconstruction β2 (2x4) alors que ces 2 reconstructions apparaissent expérimentalement pour des pressions d'arsenic ou des températures de substrat très distinctes.

Dans le cas de la surface InAs (001) (2x4), des mesures en diffraction de rayons X rasants ont conclu au même modèle β2 que pour la surface de GaAs [16]. Néanmoins , des observations récentes en STM démontrent que l'arrangement atomique correspondant aux surfaces (2x4) est plutôt un mélange des reconstructions β2 et α2 [17,18] (figure II.3).

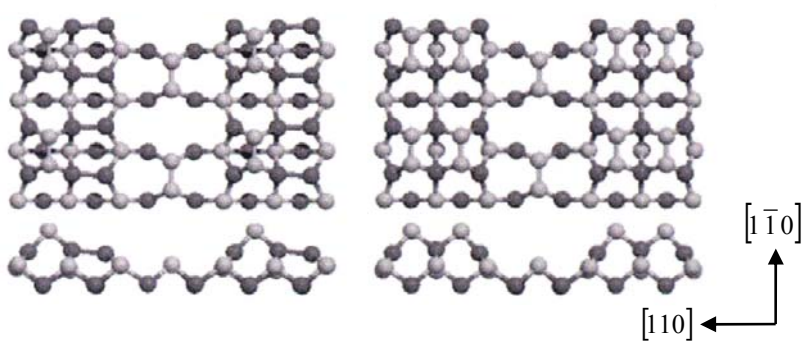

Figure II.3 : vues de dessus et de profil des reconstructions α2 (2x4) (gauche) et β2 (2x4) (droite) rencontrées sur les surfaces InAs (d'après [17]).

Etude des surfaces de phosphures par RHEED et photoémission

Par comparaison, les reconstructions de surface des phosphures ont été beaucoup moins étudiées et ce n'est que récemment qu'ont émergé des modèles convaincants. J'ai pour

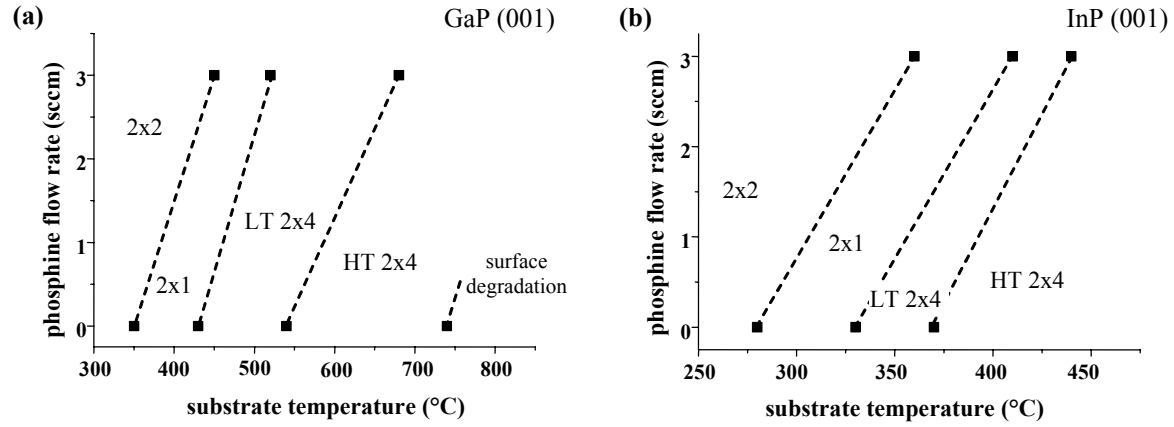

Figure II.4 : reconstruction de surface en fonction de la température de recuit avec ou sans flux de phosphore

ma part étudié les reconstructions de surface de GaP et InP(001) par RHEED et photoémission induite par rayons X (XPS) [19].

Des surfaces riches en phosphore ont été préparées en exposant à un flux de phosphore à basse température des couches épitaxiées de GaP et InP. Nous avons suivi ensuite l'évolution du diagramme RHEED lors du chauffage de ces surfaces sous ultra-vide. La séquence d'apparition des reconstructions lors de la montée en température est similaire dans les 2 cas, à savoir une (2x2) suivie d'une (2x1) puis d'une (2x4) basse température (BT) et

enfin une (2x4) haute température (HT) (figure II.4). Ces résultats sont en bon accord avec ceux de LaBella et al. [20]. Une des différences essentielles avec le cas des arséniures est qu'il n'existe pas de reconstruction (4x2).

Nous nous sommes intéressés plus particulièrement aux reconstructions (2x4). Les mesures XPS résolues angulairement montrent que la (2x4) BT est riche phosphore alors que la (2x4) HT est riche cation. Les spectres XPS haute résolution sur la raie P2p révèlent une composante de surface à plus faible énergie de liaison pour la (2x4) HT, en bon accord avec la littérature (figure II.5). Le modèle structural de cette reconstruction a été reporté récemment, consistant en une surface riche cation terminée par un dimère mixte (figure II.6) [21-24]. Le taux de couverture en phosphore suivant ce modèle est de 1/8 : il s'agit bien d'une surface riche cation. Pour la GaP(2x4) BT, une seconde composante à plus forte énergie de liaison apparaît (figure II.5). Ceci témoigne de 2 sites atomiques différents pour les atomes de phosphore en surface de la (2x4) BT. Dans le cas d'InP par contre, apparaît une 3ème composante de surface à plus haute énergie de liaison correspondant à du phosphore élémentaire adsorbé sur la surface. Pour InP, la (2x4) BT est donc vraisemblablement une reconstruction de transition entre la (2x1) et la (2x4)HT.

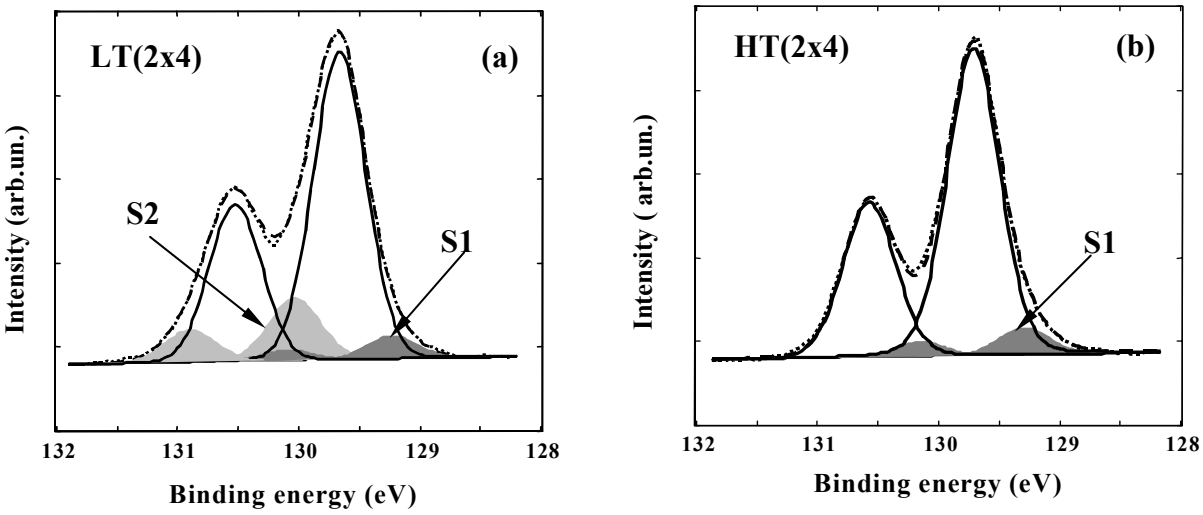

Figure II.5 : spectre P2p du phosphore enregistré sur une surface GaP(001) (2x4) BT (a) et (2x4) HT (b).

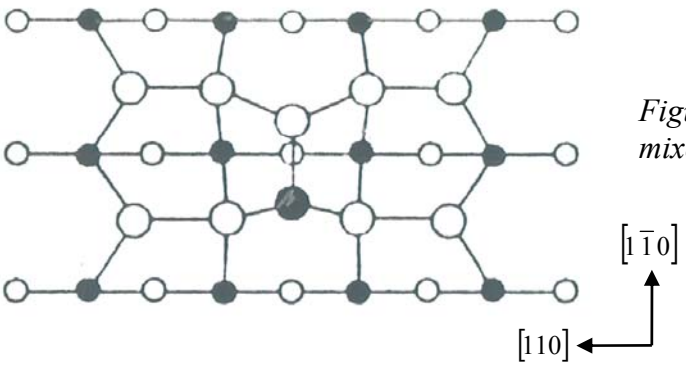

Figure II.6 : modèle de reconstruction (2x4) mixed-dimer (d'après [21]).

Les interfaces

Des zones bien mystérieuses

L'une des caractéristiques des hétérostructures à base de semi-conducteurs III-V est qu'elles mettent en jeu des couches de faible épaisseur, typiquement quelques dizaines de nanomètres ou moins. La fabrication de telles structures impose un contrôle précis des vitesses de croissance mais requiert également la maîtrise de la réalisation des interfaces. L'EJM est techniquement bien armée pour affronter ces exigences puisqu'avec des vitesses de croissance typiques de 1µm/h et des changements de matériaux en des temps inférieurs à la seconde, on peut espérer contrôler les épaisseurs et les interfaces à la monocouche atomique près. Néanmoins, on peut identifier 3 sources essentielles d'élargissement des interfaces :

- l'interdiffusion des espèces
- la rugosité du front de croissance
- la ségrégation
- les effets mémoire du système

Aux températures de croissance de l'EJM, l'interdiffusion des éléments III et V est négligeable [25-27], contrairement au cas de la MOCVD, opérant à plus hautes températures. La rugosité du front de croissance intervient quelle que soit l'interface considérée, dépend des paramètres de croissance et de l'état de contrainte de la couche : je n'en discuterai pas davantage dans cette partie. Les 2 derniers effets interviennent différemment suivant l'interface considérée. Les interfaces à anion commun et ne différant que par leur cation ne sont influencées que par la ségrégation. En effet, aux températures de croissance, il n'existe aucun effet mémoire lié aux cations dont la pression de vapeur est très faible. Par contre, ces effets mémoire doivent être pris en compte pour les interfaces différant par leurs anions.

Ce travail a débuté en 1994 avec la thèse d'Olivier Dehaese [28] que j'ai encadrée et dont le directeur de thèse était Didier Stièvenard. A cette époque, la ségrégation des éléments III était déjà avérée [29] et nous avions pour but dans cette thèse d'étudier la ségrégation des éléments V, notamment As par rapport à P. Cependant, les modèles proposés jusque là pour décrire la ségrégation nous ont semblé insuffisants et cela nous a amené à développer un modèle cinétique de ségrégation, d'abord mis en œuvre et validé sur les éléments III.

En passant aux éléments V, nous nous sommes rapidement aperçus que l'élargissement des interfaces différant par leurs anions était davantage dû à des effets expérimentaux qu'à la ségrégation. Notre travail dans ce domaine s'est donc orienté vers une optimisation de la procédure de commutation des anions. Cette partie doit également beaucoup au travail de thèse d'Olivier Schuler [30].

La mise en œuvre de cette optimisation nécessite d'exposer la surface d'un phosphure à un flux d'arsenic ou vice-versa. C'est pourquoi nous nous sommes ensuite intéressés à l'évolution des surfaces d'arséniures sous flux de phosphore, en collaboration avec C. Priester.

Interfaces à anion commun

La ségrégation

Un phénomène général

La ségrégation est un phénomène général dans la métallurgie des alliages. Elle se manifeste par l'enrichissement de la surface en l'un des constituants de l'alliage lors de traitements thermiques. Lors de l'épitaxie d'hétérostructures de semi-conducteurs III-V à anion commun, la ségrégation se manifeste par l'enrichissement de la surface en l'un des cations. Ainsi, lors de la croissance du binaire BV sur le binaire AV, si A est l'élément

ségrégant, A s'incorpore lors de la croissance de BV. De même, lors de la croissance de l'alliage ABV, la surface est enrichie en A.

La ségrégation est gouvernée par 2 processus de base :

- la minimisation de l'énergie de surface
- la minimisation de l'énergie élastique et donc de la contrainte

La surface en croissance possède toujours un nombre important de liaisons insatisfaites dont le coût énergétique dépend des éléments. Ainsi, il est énergétiquement plus favorable que le composé ayant la plus faible énergie de surface ségrége vers la surface. Lors de la croissance d'alliages contraints, le binaire présentant le plus fort désaccord de maille avec le substrat a intérêt à ségréger pour diminuer l'énergie élastique emmagasinée et relaxer partiellement la contrainte en surface. Ces 2 processus peuvent se cumuler ou entrer en compétition.

Historiquement, la ségrégation du gallium par rapport à l'aluminium [29] et celle de l'indium par rapport au gallium [29, 31, 32] ont été rapidement mises en évidence.

Les modèles et leur limitation

La diffusion des éléments pouvant être négligée, tous les modèles décrivent la ségrégation par un processus d'échange entre la monocouche atomique en croissance et celle immédiatement en dessous appelée monocouche de volume (figure II.7). De plus, aux températures de croissance, la réévaporation des éléments III est nulle, correspondant à un coefficient de collage de 1 [33]. Ceci autorise l'utilisation d'une équation de conservation de la matière qui permet de calculer itérativement la concentration de chaque monocouche. Avant notre travail sur le sujet, on distinguait :

- le modèle à taux d'échange constant
- le modèle à l'équilibre thermodynamique

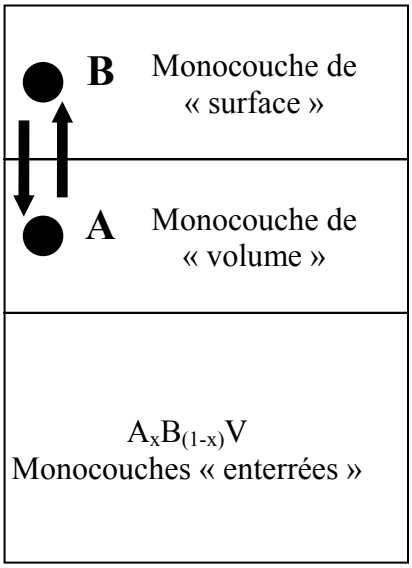

Figure II.7 : représentation schématique de l'échange.

Un modèle empirique

Considérons à nouveau 2 binaires AV et BV pour lesquels il y a ségrégation à la surface de l'élément A par rapport à B. La composition en élément A de la monocouche en croissance est égale à la composition nominale à laquelle on ajoute une partie due à la ségrégation. Dans le modèle à taux d'échange constant, cette dernière est supposée égale à R

fois la composition en élément A de la dernière monocouche de volume [29,31,32]. Un calcul itératif permet de calculer la concentration en A tout au long de la croissance.

Ce modèle permet de décrire correctement la ségrégation par ajustement du paramètre R sur des données expérimentales. Par contre, il n'a pas de caractère prédictif : si les conditions de croissance sont modifiées, une nouvelle valeur de R est nécessaire. Par ailleurs, le fait de garder R fixe pour toute composition n'est pas justifié et, sans autre précaution, conduit dans certains cas à des valeurs de concentration supérieures à 1 [28]. Cette difficulté est levée dans le modèle à l'équilibre thermodynamique.

Mieux : faisons entrer la thermodynamique

Dans le modèle à l'équilibre thermodynamique [34-36], les concentrations en A et B sur la monocouche en croissance et la dernière monocouche de volume sont régies par un équilibre de constante :

$$K = \exp(E_s/kT) \qquad \text{(II.1)}$$

où E_s est l'énergie de ségrégation. E_s est le seul paramètre du modèle et représente le gain énergétique au cours de l'échange. L'interprétation physique simple de ce modèle a contribué à son succès. Néanmoins, il pose la question de savoir si l'on peut considérer que la croissance de semi-conducteurs III-V se fait à l'équilibre thermodynamique ou s'il faut prendre en compte la cinétique. La réponse est fournie par des résultats expérimentaux mettant en évidence une diminution de la ségrégation lorsque la température de croissance décroît [35-39]. Or ce modèle, à E_s fixée, prédit une augmentation de K et donc de la ségrégation si l'on baisse la température. C'est pour lever cette contradiction que nous avons développé un modèle cinétique de ségrégation.

Le modèle cinétique de ségrégation

Tentons de rendre compte de l'expérience

La prise en compte de la cinétique de croissance à travers les deux paramètres importants que sont la température et la vitesse de croissance est l'objectif principal de tout modèle cinétique. Pour y parvenir, il est possible de développer une méthode de simulation microscopique, généralement basée sur la méthode de Monte-Carlo ou de traiter le problème à un niveau macroscopique en s'inspirant de méthodes statistiques utilisées par exemple en cinétique chimique. Pour modéliser la ségrégation des éléments III au cours de la croissance de semi-conducteurs III-V, nous avons choisi cette seconde approche qui permet de rester dans la continuité du modèle d'échange à l'équilibre thermodynamique. Tout comme ceux présentés précédemment, notre modèle cinétique suppose un échange entre un atome de la monocouche de volume et un autre de celle de surface ainsi que l'absence de réévaporation des éléments III afin de pouvoir ajouter une équation de conservation. Le diagramme II.8 schématise l'échange entre l'élément A ségrégant et l'élément B non. La prise en compte de la cinétique intervient par l'introduction des barrières énergétiques E_1 et E_2 qui permettent de définir des taux d'échange et de contre-échange. Ces derniers sont introduits dans des équations différentielles du premier ordre par rapport au temps pour décrire l'évolution temporelle des concentrations [40].

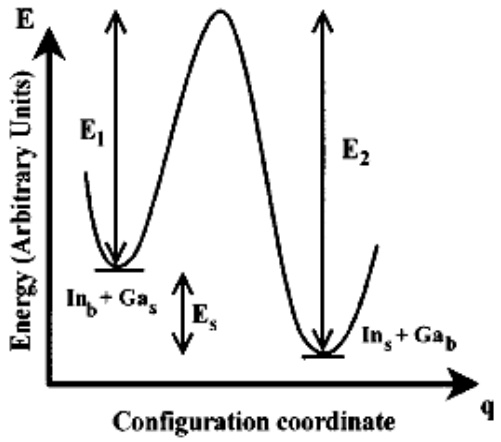

Figure II.8. diagramme de configuration pour un échange In/Ga.

Avant notre étude, la mise en évidence expérimentale de la ségrégation s'était faite principalement par des mesures de photoluminescence sur des puits quantiques judicieusement choisis. La ségrégation ayant pour effet d'introduire des zones graduelles aux interfaces, les énergies des transitions optiques s'en trouvent modifiées. L'écart entre les énergies attendues et celles mesurées caractérise alors la ségrégation. Cependant, ceci ne permet pas de remonter à un profil de concentration aux interfaces car plusieurs modèles peuvent donner des énergies de transition optique très voisines.

L'apport de l'XPS

Pour tenter de préciser les profils de concentration aux interfaces, nous avons utilisé la photoémission induite par rayons X (XPS) résolue angulairement. En effet, la profondeur sondée par cette technique est $3\lambda \sin\theta$ où λ est le libre parcours inélastique moyen des photoélectrons et θ l'angle polaire d'émission des photoélectrons repéré par rapport au plan de surface. Ainsi, en faisant varier θ, on sonde plus ou moins profondément le matériau. Dans le cas d'une interface entre un binaire BV déposé sur un binaire AV, on peut, en choisissant correctement l'épaisseur de BV, sonder soit BV seul, soit BV et les dernières monocouches de AV. L'intensité d'un niveau de cœur de l'élément A mesurée en XPS est proportionnelle à la concentration de A sur l'épaisseur sondée. Cependant, l'évolution des intensités XPS en fonction de l'épaisseur sondée ne permet pas de remonter directement à un profil de concentration. Les intensités relevées pour différents angles d'émission sont donc comparées aux intensités calculées en supposant différents modèles de concentration.

Néanmoins, lors de mesures XPS réalisées sur des monocristaux, apparaissent des phénomènes de photodiffraction suivant les principales directions cristallographiques. Clairement, ces effets se superposent aux variations d'intensité liées aux changements de concentration et, sans précaution particulière, rendent toute détermination de concentration aléatoire. Pour remédier à ce problème, nous avons utilisé une moyenne azimutale du signal XPS en faisant tourner l'échantillon sur lui-même pendant l'acquisition à un angle polaire fixé (cf. 1ère partie « *Etude de couches moléculaires greffées sur silicium* ») . Pour s'affranchir des variations du dispositif expérimental, nous avons de plus utilisé des rapports d'intensité.

Notre modèle cinétique de ségrégation a ainsi pu être testé sur l'interface GaAs sur GaInAs. La figure II.9 illustre l'accord obtenu entre notre modèle et l'expérience dans le cas d'une couche de 10 mc de GaAs épitaxiée sur une couche de 100 Å de GaInAs sur substrat GaAs. Avec les mêmes valeurs des barrières E1 et E2 (1.74 et 1.91 eV respectivement), nous parvenons à modéliser correctement les mesures à 400 et 500°C. En particulier, notre modèle

rend compte de la diminution de la ségrégation lorsque l'on baisse la température de croissance.

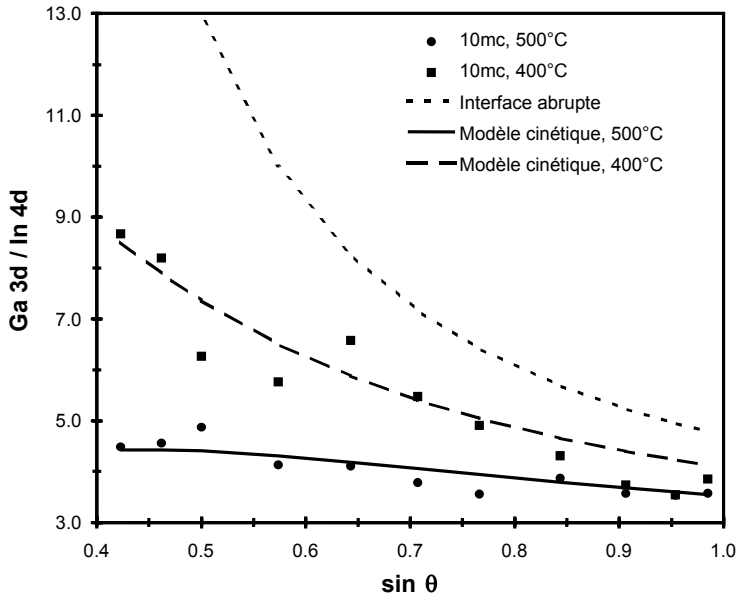

Figure II.9 : Rapport d'intensité Ga3d/In4d mesurés sur un échantillon comportant 10mc de GaAs épitaxiées à 400 et 500°C sur GaInAs.

Les interfaces différant par leurs anions

Quel est le problème ?

Contrairement au cas des interfaces à anion commun (As) avec commutation de cations (Ga, Al, In) dont l'élargissement est bien expliqué par des phénomènes d'échange et de ségrégation, aucun modèle physique ne rend compte de la formation d'interfaces différant par leur anion bien que celles-ci s'avèrent souvent diffuses. L'une des raisons est la difficulté expérimentale à commuter de façon abrupte As et P dans les techniques de croissance usuelles, l'autre étant la nature de l'incorporation des éléments V, intrinsèquement différente de celle des éléments III. Ceci rend très délicate la distinction entre effets expérimentaux extrinsèques et effets intrinsèques liés au système de matériaux étudié.

Le problème posé par les interfaces différant par leurs anions n'est pas symétrique car l'arsenic s'incorpore plus facilement dans une couche de phosphure que le phosphore dans une couche d'arséniure. C'est pourquoi nous avons surtout étudié l'interface GaInP/GaAs. La croissance est réalisée sur le bâti EJM à sources gazeuses pour les éléments V (AsH_3, PH_3), équipé d'une cellule à craquage thermique commune pour les 2 hydrures. Nous avons appliqué la méthode d'analyse angulaire des intensités XPS pour les raies P2p et As3d corrélée avec des mesures de photoluminescence.

Pour tester l'interface GaInP sur GaAs, nous avons utilisé des puits quantiques asymétriques comportant 19 mc de GaAs avec une barrière supérieure en GaInP et une barrière inférieure en AlGaAs. Sans précaution particulière quant à la commutation des gaz, le spectre de photoluminescence relevé à 10K montre que l'énergie de la transition optique est décalée de plus de 25 meV par rapport à la valeur attendue (fig. II.10). Ce décalage ne peut s'interpréter par une incertitude sur l'épaisseur du puits qui devrait être de plusieurs monocouches pour expliquer une telle différence.

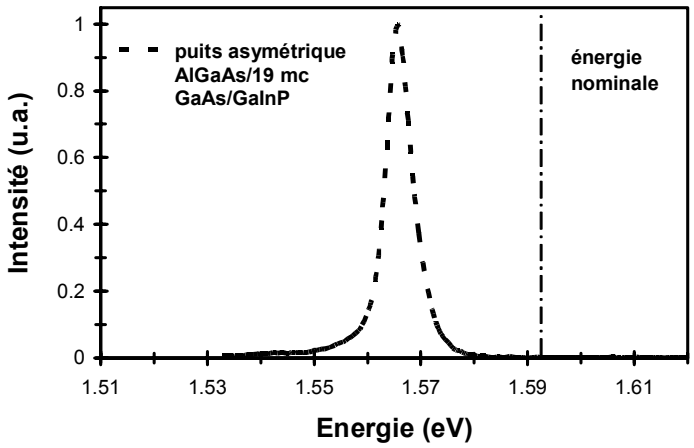

Figure II.10 : spectre de photoluminescence relevé sur un puits asymétrique de 19 mc GaAs.

Pour tenter d'expliquer cela par la ségrégation de l'arsenic dans GaInP , nous avons relevé les intensités XPS sur une interface composée de 5mc de GaInP sur GaAs à différentes températures de croissance (figure II.11). Aux 3 températures, le rapport expérimental As3d/P2p est nettement supérieur à celui calculé pour une interface abrupte, pour tous les angles polaires. Ceci démontre la présence d'arsenic dans la couche supérieure de GaInP. Nous avons alors tenté de modéliser cet excès d'arsenic par de la ségrégation en utilisant le modèle à l'équilibre thermodynamique avec une valeur de Es élevée, 0.4 eV. Dans ces conditions, l'échange est quasi-total. Les valeurs ainsi calculées sont proches de l'expérience

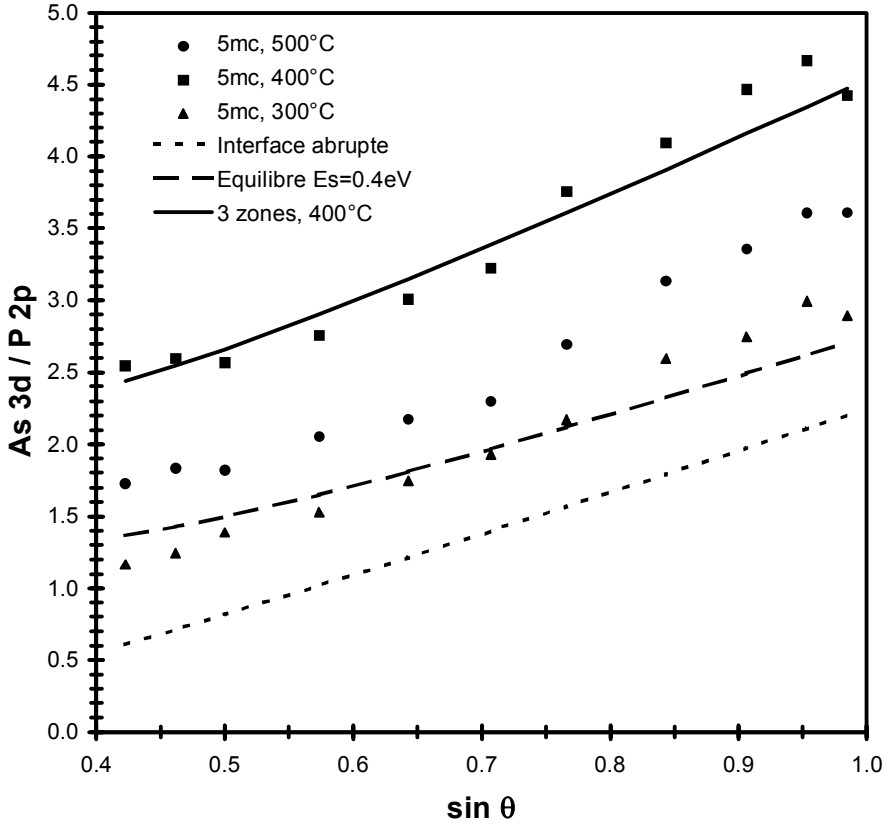

Figure II.11 : Intensités XPS relevées sur une interface composée de 5 mc de GaInP sur GaAs à différentes températures et comparaison avec différents modèles.

à 300°C mais nettement en-dessous de celles à 400 et 500°C. Pour ces températures, il n'est pas possible de rendre compte de l'évolution des intensités XPS par un modèle de ségrégation de l'As par rapport à P, quel qu'il soit. Nous avons alors modélisé l'interface par un modèle comportant différentes zones de composition constante. La figure II.12 illustre un tel profil pour une température de croissance de 400°C. On y voit clairement la formation d'un puits de GaInAsP sur 3 mc au moins. Le même effet a été observé lors de la croissance de InP sur GaInAs durant laquelle se forme un puits parasite d'InAsP à l'interface.

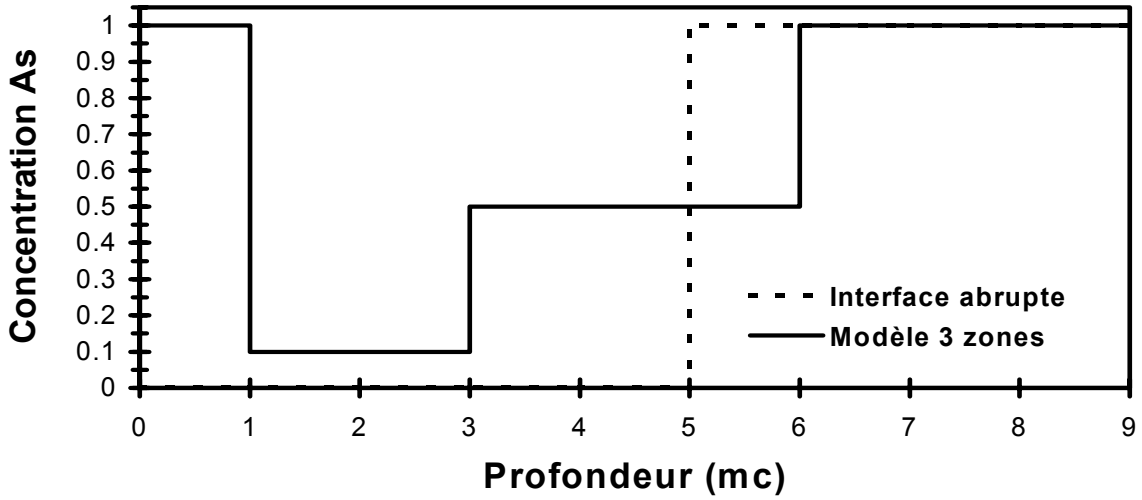

Figure II.12 : Profil de concentration en As d'une interface comportant 5 mc de GaInP sur GaAs épitaxiée à 400°C.

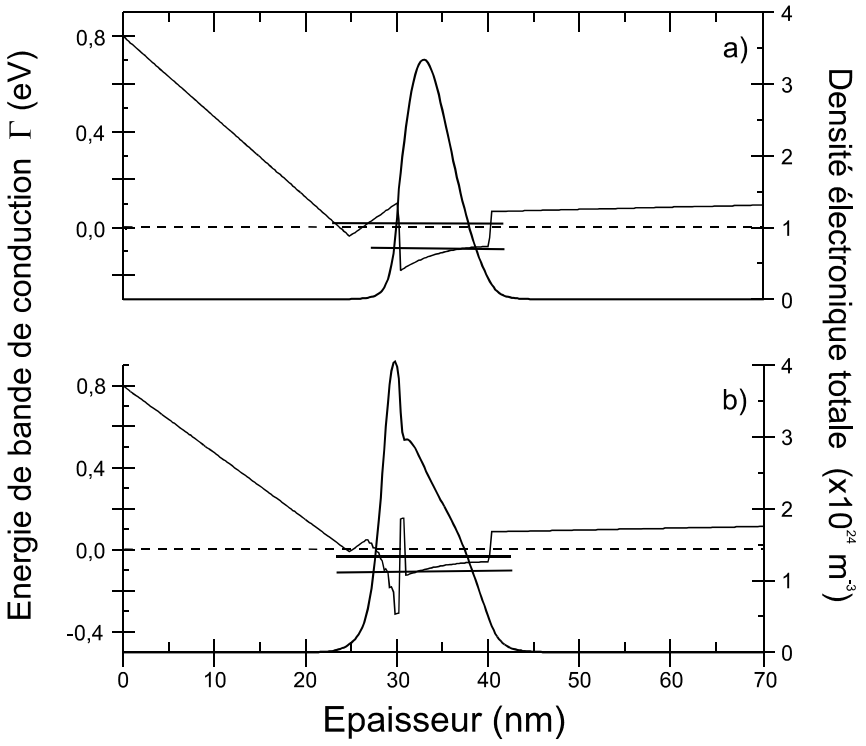

Figure II.13 : bande de conduction, densité électronique et position des 2 premiers niveaux d'énergie d'une structure à modulation de dopage GaInP/InGaAs. (a) : structure nominale, (b) : structure à interface diffuse

Dans les hétérostructures à modulation de dopage GaInP/GaInAs, ce puits parasite piège les électrons du gaz 2D. Ceci est mis en évidence sur la figure II.13 où l'on observe que la densité électronique est maximale à l'endroit du puits parasite dans le cas de l'interface diffuse. Ceci conduit à une diminution sensible de la mobilité électronique qui ne dépasse pas 1 500 $cm^2/V.s$ à 300 et 77K [41].

Les remèdes

L'incorporation d'arsenic dans le phosphure ne peut s'expliquer par un phénomène de ségrégation seul mais fait intervenir ce qu'il est convenu d'appeler « les effets mémoire » du système. Ceux-ci, dans notre cas, peuvent avoir 3 origines :

- une pression résiduelle d'arsenic trop importante dans le bâti lors du début de la croissance du phosphure
- des phénomènes de « cross-talk » au niveau de la ligne d'évent du craqueur d'hydrures
- le craqueur thermique lui-même qui peut piéger l'arsenic dans des volumes morts.

L'identification de la cause principale a été un travail de longue haleine et nous avons utilisé des parades pour mener à bien nos études avant de finaliser l'optimisation de ces interfaces. Ainsi, pour tenter de préciser l'effet de la ségrégation d'arsenic, nous avons utilisé des interfaces réalisées avec une longue interruption de croissance (plusieurs heures) de sorte que les effets mémoire du système soient supprimés. Dans ce cas, les intensités XPS sont très proches de celles attendues pour une interface abrupte et ne témoignent donc que d'une faible ségrégation de l'As. Le dépouillement de ces résultats conduit à une énergie de ségrégation de 0.12 eV. Par ailleurs, on observe sur la figure II.11 que la concentration d'arsenic est plus faible à 500°C qu'à 400°C, ce qui est contraire à notre modèle cinétique de ségrégation. Ceci s'explique par la ré-évaporation de l'arsenic en surface à 500°C avec un coefficient voisin de 0.1. Sur ces interfaces quasi-abruptes, nous avons pu mesurer l'offset de bande de valence entre GaInP et GaAs par photoémission [42]. Nous trouvons une valeur de 0.3 ± 0.05 eV, en bon accord avec les prédictions théoriques [43] et les résultats de la littérature [44].

Lors de la croissance de l'hétérostructure GaInP/InGaAs, un arrêt de croissance de plusieurs heures à l'interface n'est pas concevable. Dans ce cas, nous avons intercalé une couche d'AlInP à l'interface GaInP/InGaAs. Ainsi, l'incorporation d'arsenic dans le phosphure se fait dans AlInP et conduit à la formation du quaternaire AlInAsP, qui est encore un matériau grand gap : la formation d'un puits parasite est évitée. Des mesures par effet Hall en fonction de l'épaisseur d'AlInP intercalé ont montré un accroissement de la mobilité électronique jusqu'à une épaisseur de 6-8 mc. Ceci confirme le caractère diffus de l'interface sur au moins 2 nm.

Après de nombreuses expériences, il s'est avéré que la cause principale d'incorporation de l'As dans le phosphure était un effet mémoire de la cellule à craquage thermique. Ceci se traduit par le fait qu'au moment de la commutation arsine/phosphine, le craqueur continue à envoyer de l'arsenic sur le substrat : tout se passe comme s'il fallait un temps de purge du craqueur au changement de gaz. Nous avons alors optimisé la procédure en introduisant un temps de 5 à 10 secondes pendant lequel la surface de l'arséniure est exposée au flux de phosphore (ou plus exactement au mélange arsenic-phosphore résultant de la purge du craqueur) avant de commencer la croissance du phosphure (GaInP ou InP). La figure II.14 confirme qu'avec un temps de 10 secondes, la position du pic de photoluminescence correspond à celle attendue.

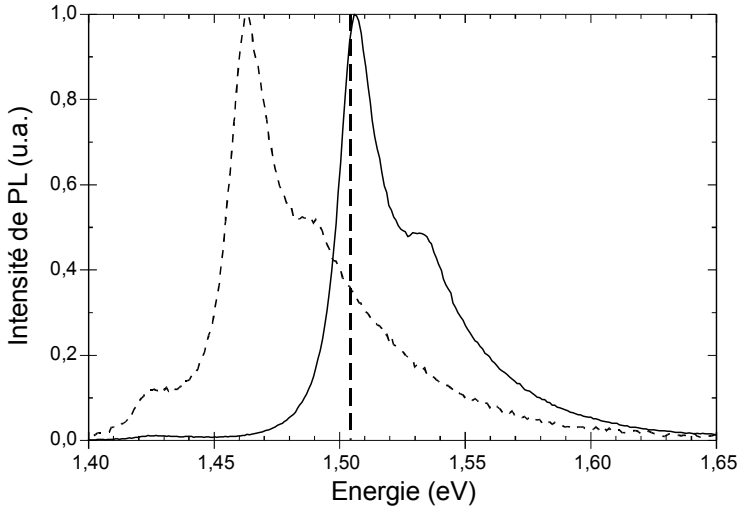

Fig. II.14 : Spectres de photoluminescence à 300K de puits asymétriques de 19 mc GaAs avec (trait plein) et sans (pointillés) anticipation de 10 secondes.

Surfaces d'arséniures exposées à un flux de phosphore

Où une procédure de commutation nous ramène à un problème de surface

Cette procédure nous a conduit à mener une étude détaillée de la réactivité des surfaces d'arséniures exposées à un flux de phosphore combinant RHEED, XPS et AFM. Nous avons considéré les deux binaires GaAs et InAs ainsi que les alliages $Ga_{0.47}In_{0.53}As$ adapté en maille sur InP et $Ga_{0.8}In_{0.2}As$ contraint en compression sur GaAs. Les surfaces ont été préparées pour présenter des reconstructions typiques riches As (2x4 ou 2x3) avant l'exposition au phosphore. Les observations RHEED et AFM ont montré que les surfaces de GaAs et des 2 alliages se rugosifient sous l'effet de l'exposition au phosphore alors que la surface d'InAs conserve son caractère bidimensionnel même pour de longues expositions (figure II.15).

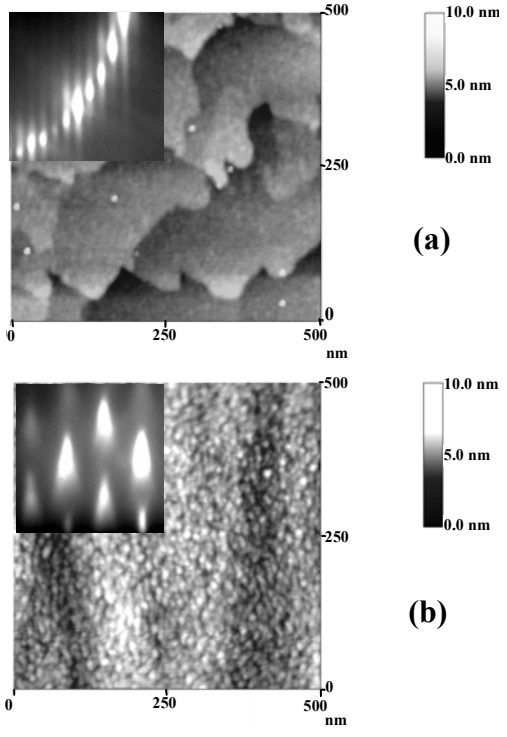

Figure II.15 : Images AFM d'une surface InAs (2x4) exposée 10 min. (a) et d'une surface GaAs (2x4) exposée 5 min (b) à un flux de phosphore à 500°C. Les insertions montrent les diagrammes RHEED correspondants suivant l'azimut [110].

Les mesures XPS indiquent que la quantité de phosphore incorporé pour un même temps d'exposition est équivalente dans les différents échantillons. Avec Catherine Priester, nous avons montré que cette différence de comportement entre les 2 binaires GaAs et InAs est reliée à la différence d'énergie élastique liée à l'incorporation du phosphore dans les 2 matériaux [45].

Nous avons également mis en évidence le rôle des dimères d'anions de surface qui créent des sites favorables (sous les dimères) et défavorables (entre les dimères) pour l'incorporation de phosphore [46] (figure II.16). L'ordre induit par ces mêmes dimères dans les premiers plans de cations de l'alliage $Ga_{0.47}In_{0.53}As$ adapté en maille sur InP permet de rendre compte des observations expérimentales pour cet alliage. Par contre, dans le cas de l'alliage $Ga_{0.8}In_{0.2}As$ contraint sur GaAs, la rugosification de la surface après exposition au phosphore tient en partie son origine de la faible rugosité initiale induite par la croissance contrainte [47].

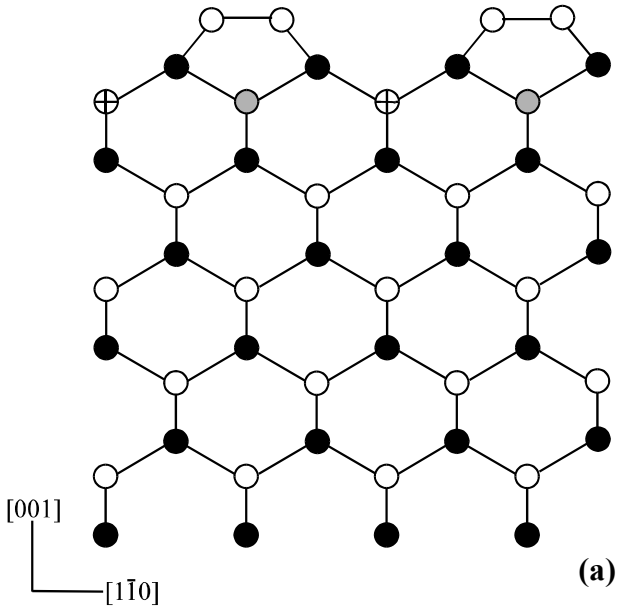

Figure II.16 : Schéma montrant l'existence de sites favorables et défavorables pour l'incorporation de phosphore dans le second plan d'anion pour une reconstruction (2x1) riche anion. Les circles pleins représentent les cations, les circles évidés les anions. Les cercles gris pointent les sites favorables et les croix les sites défavorables.

Croissance contrainte

Dans le cadre de l'optimisation des structures pour composants HEMT, j'ai abordé la croissance contrainte de l'alliage InGaAs sur InP et de l'alliage InGaP sur GaAs.

Croissance contrainte d'InGaAs sur InP

Dans le but d'obtenir des composants à fréquence de coupure élevée, l'utilisation d'une zone active en InGaAs contraint s'avère intéressante. En effet, cet alliage possède une dynamique de transport électronique d'autant plus favorable que le taux d'indium est élevé. C'est par ce biais que j'ai abordé la croissance des alliages InGaAs contraints sur InP.

Ce sujet a suscité l'intérêt de plusieurs équipes et notamment en France, celle du LEOM. Ces travaux ont mis en évidence les deux modes de relaxation de contrainte (plastique ou élastique) en fonction de la composition. A une température de croissance d'environ 500°C et dans des conditions riches en arsenic, la relaxation intervient par formation de dislocations (plastique) pour des concentrations inférieures à 0.75-0.8. Pour des valeurs supérieures, la relaxation s'opère via une transition entre un mode de croissance bidimensionnel et un mode tridimensionnel (élastique) [48-53]. Les effets cinétiques ont également été soulignés. Une réduction de la température de croissance de 525°C à 450°C permet d'augmenter l'épaisseur critique tandis qu'une reconstruction riche cation peut changer le mode de relaxation à une température de croissance donnée [54]. De ces études, il ressort que le taux maximum d'indium compatible avec la croissance bidimensionnelle d'une zone active de 10 à 15 nm d'épaisseur est de 75%.

Peut-on tirer parti de la cinétique ?

Mon travail a consisté à examiner l'effet d'une réduction plus importante de la température de croissance et donc de la cinétique de surface sur la relaxation afin de dépasser si possible ce taux maximum de 75%. Pour ce faire, nous avons étudié la croissance d'alliages de composition supérieure à 75% à des températures comprises entre 350°C et 500°C. Nous avons utilisé des observations RHEED in situ, AFM ex-situ et avons caractérisé des hétérostructures InGaAs/InAlAs par effet Hall à 77 et 300K.

En RHEED, nous avons noté soit une rugosification du front de croissance, soit une nette transition 2D-3D. La figure II.17 résume les épaisseurs critiques pour l'apparition de ces phénomènes.

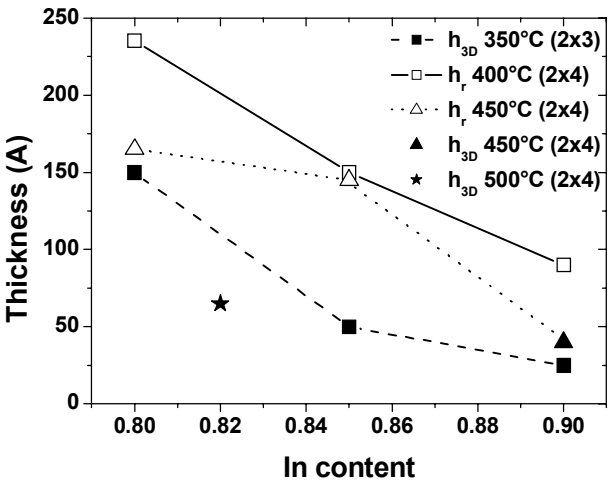

Figure II.17: épaisseur critique pour l'apparition de la transition 2D-3D (h_{3D}) ou la rugosification de surface (h_r) en fonction du taux d'indium de l'alliage contraint InGaAs à différentes températures de croissance et pour 2 reconstructions de surface. La valeur h_{3D} à 500°C, pour comparaison, est tirée de la référence [54].

Le résultat important et surprenant de la figure II.17 est que l'épaisseur critique à 350°C est plus faible qu'à 400 ou 450°C (figure II.18) et se traduit par une relaxation élastique quel que soit le taux d'indium. Ces observations RHEED ont été confirmées par des images AFM et s'avèrent en contradiction totale avec ce qui est attendu de la réduction de la cinétique de surface avec la température de croissance.

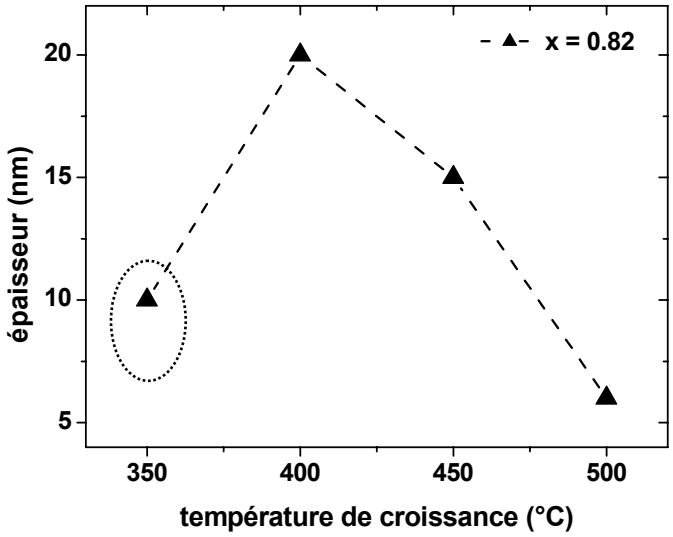

Figure II.18 : épaisseur critique en fonction de la température de croissance pour une composition particulière.

L'importance de la reconstruction de surface

La clé de ce paradoxe réside dans la reconstruction de surface qui, dans nos conditions de croissance, est de type (2x3) à 350°C alors qu'elle est de type (2x4) aux températures supérieures. Pour valider cette hypothèse, nous avons examiné l'effet de la reconstruction de surface à 350°C en modulant le flux d'arsenic de telle sorte que la surface lors de la croissance bidimensionnelle du film présente soit une reconstruction (2x3) très riche As, soit une (2x4) riche As, soit enfin une (4x2) riche cation.

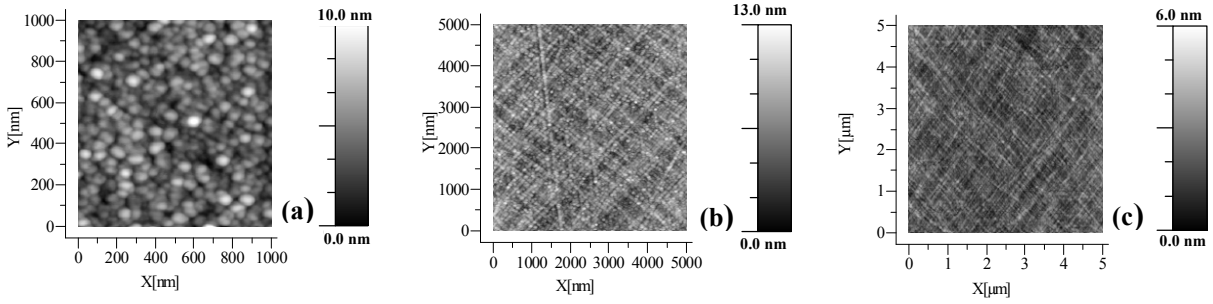

(2x3)
h_{3D} = 5 nm

(2x4)
h_r = 9 nm

(4x2)
h_r = 13 nm

Figure II.19 : Images AFM d'un film d'$In_{0.85}Ga_{0.15}As$ après relaxation à 350°C pour 3 reconstructions de surface initiales et épaisseurs critiques associées.

La figure II.19 résume les observations AFM et RHEED et démontre clairement que la reconstruction (2x3) très riche As favorise la transition 2D-3D. Par contre, les reconstructions moins riches As, voire riches cation permettent de conserver une croissance bidimensionnelle,

la relaxation étant alors plastique. Ceci est relié à l'énergie de surface. En effet, les surfaces riches As présentent davantage de liaisons pendantes sur les atomes As qui ont un coût énergétique inférieur aux liaisons pendantes de cations. Néanmoins, même dans le cas des reconstructions (2x4) et (4x2), l'épaisseur critique demeure plus faible à 350°C qu'à 400 ou 450°C. Ceci est dû au développement d'une rugosité à petite échelle à basse température qui favorise la nucléation de dislocations. Dans ce cas, la limitation de la cinétique en surface est trop importante et a l'effet inverse de celui recherché.

Pour valider ces observations RHEED et AFM, nous avons épitaxié des hétérostructures InAlAs en accord de maille sur InP/InGaAs contraint et les avons caractérisé par effet Hall. Il s'est avéré que l'épaisseur critique pour la relaxation plastique était inférieure à celle déterminée par RHEED pour la rugosification de surface à 400 et 450°C. Ainsi, l'observation AFM de couches de 12 nm d'épaisseur d'alliages à 85% d'indium épitaxiés à 400°C et à 82% d'indium épitaxié à 450°C révèle l'apparition des premières dislocations. Ceci nous a contraint à restreindre le taux maximum d'indium à 80%. Par ailleurs, à cette composition (x= 0.8), des mesures Hall réalisées sur une structure épitaxiée à 450°C et une autre à 500°C montrent que la mobilité électronique est supérieure à 500°C. Ceci est lié à l'inévitable incorporation d'impuretés durant l'arrêt de croissance nécessaire à la diminution de la température du substrat avant le canal, la couche tampon étant réalisée à 500°C. A cette température, des mesures de photoluminescence ont permis d'établir que le taux d'indium maximum avant le début de la relaxation plastique pour une épaisseur de 12 nm est de 75%, conformément aux études antérieures. Nous avons donc finalement obtenu nos meilleurs résultats pour une température de croissance de 500°C et un taux d'indium de 75%, avec des mobilités de 16 000 et 140 000 cm^2/Vs à 300 et 77 K respectivement [55]. Ces valeurs sont parmi les meilleures publiées à ce jour pour ce système de matériaux.

Croissance des alliages InGaP contraints

L'hétérojonction AlGaAs/(In)GaAs est la première à avoir été réalisée et étudiée et continue à susciter l'intérêt. C'est elle qui a donné lieu aux premiers composants à dopage modulé, de type HEMT. De ce point de vue, l'utilisation de l'alliage AlGaAs pose quelques problèmes technologiques, tel l'apparition de centres profonds (DX) pour des concentrations d'aluminium supérieures à 0.4 et son oxydation rapide à l'atmosphère ambiante. Une alternative possible est son remplacement par l'alliage InGaP qui permet de s'affranchir des problèmes de centres DX. De plus, lors des étapes technologiques, la sélectivité de gravure entre la couche de contact arséniée et la couche barrière en InGaP peut être mise à profit.

Cependant, l'offset de bande de conduction entre InGaP et GaAs est assez faible (de l'ordre de 150 meV) et donc peu favorable au transfert électronique. L'utilisation d'alliages InGaP contraints en tension permettrait d'accroître le décalage de bande de conduction et donc le transfert électronique. Pourtant, la croissance des alliages InGaP contraints est beaucoup moins documentée que celle des alliages InGaAs. Il n'est cependant pas certain que les connaissances acquises sur les alliages InGaAs puissent être transposées directement aux alliages InGaP compte tenu des différences d'enthalpie de mélange et de reconstruction de surface entre les 2 familles. C'est pourquoi j'ai entrepris une étude de la croissance des alliages InGaP contraints, d'abord sur substrat GaAs.

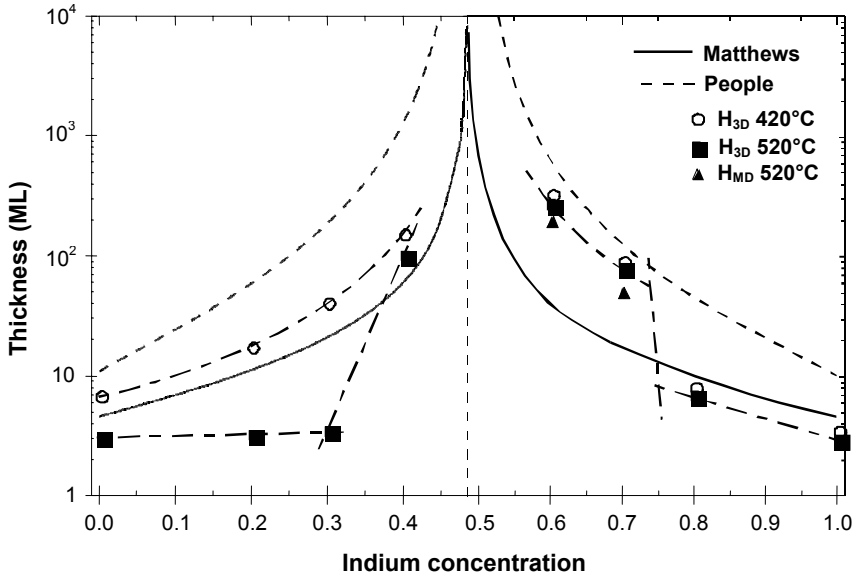

Figure II.20 : Evolution de l'épaisseur critique d'un film de $In_xGa_{1-x}P$ épitaxié sur GaAs, en compression ou en tension.

Le comportement observé pour une contrainte en compression (taux d'indium supérieur à 50%) et une température de croissance de 520°C est voisin de celui relevé pour le système InGaAs/InP. En effet, la relaxation de la contrainte s'opère par nucléation de dislocations (plastique) pour les plus faibles taux d'indium ($x<0.75$) puis par croissance tridimensionnelle pour $x>0.75$. Par contre, dans le cas de la contrainte en tension, la transition 2D-3D est observée pour environ 3 monocouches déposées pour une composition en indium variant de 0 à 0.35 (figure II.20). Sur substrat InP, pour la même contrainte en tension (mais pas la même composition), ce comportement anormal n'est pas observé : il s'agit donc bien plutôt d'un effet de composition que d'un effet de contrainte [56]. Ces observations pourraient être expliquées par la décomposition spinodale de l'alliage InGaP reportée dans la littérature pour des compositions en indium inférieures à 50% vers 500°C [57]. Pour tester cette

hypothèse, nous avons abordé l'étude de la croissance de l'alliage contraint en compression sur GaP : cette fois, la composition est identique au cas de l'alliage contraint en tension sur GaAs mais la contrainte est inversée. La décomposition spinodale ne dépendant pas du signe de la contrainte, elle devrait également se manifester dans ce cas. Or, il n'en est rien et l'évolution de l'épaisseur critique en fonction du taux d'indium dans le système InGaP/GaP est très similaire à celle relevée pour le système InGaAs/GaAs (figure II.21). En nous appuyant sur des modélisations réalisées par C. Priester, nous avons montré que cette décomposition de l'alliage est favorisée à la fois par la contrainte en tension, la composition en indium (20-30%) et la ségrégation verticale et latérale de l'indium [58].

L'étude de la croissance sur substrat GaP s'est poursuivie avec pour but une comparaison avec le système InGaAs/GaAs [59]. Deux différences marquantes sont apparues. La première concerne la morphologie des couches pour des taux d'indium compris entre 25 et 50% où il y a formation de structures filaires orientées suivant la direction [110] (figure II.22). La seconde est relative à la taille des îlots (~1 μm) observés lors de la croissance d'InP sur GaP (figure II.23). Nous avons expliqué ces observations grâce aux travaux récents publiés sur les reconstructions de surface des phosphures [60] (cf. paragraphe « reconstructions de surfaces »). En effet, il s'avère que GaP et InP présentent une reconstruction de surface (2x4) riche cation, faisant intervenir des dimères de cations orientés suivant [110], favorisant une

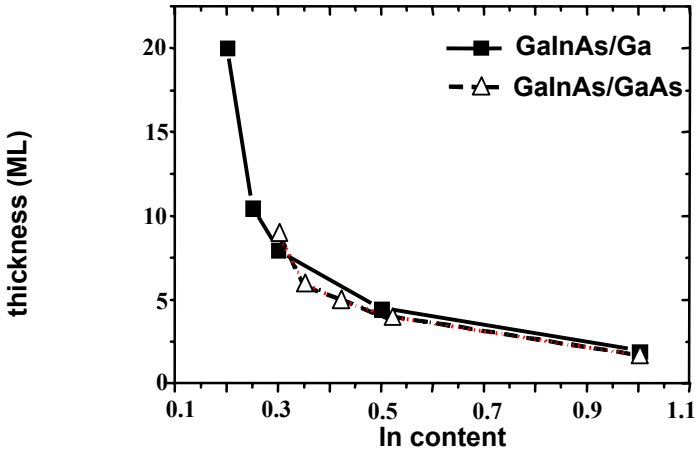

Figure II.21 : Comparaison de l'évolution de l'épaisseur critique en fonction du taux d'indium de l'alliage pour les systèmes InGaAs/GaAs et InGaP/GaP.

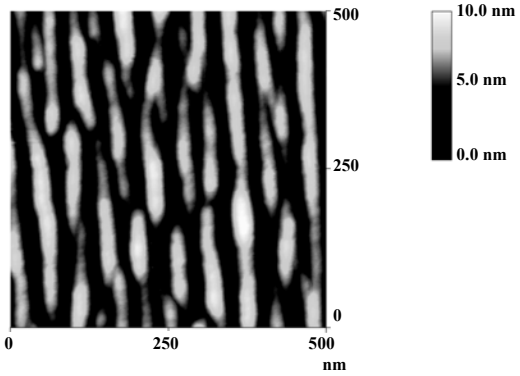

Figure II.22 : Image AFM d'un film de 75Å de $In_{0.25}Ga_{0.75}$ P épitaxié à 520°C sur substrat GaP.

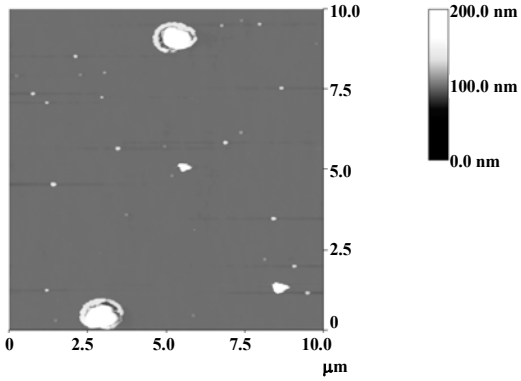

Figure II.23 : Image AFM après croissance de 3.3 monocouches d'InP épitaxiées sur GaP à 520°C

anisotropie de diffusion des espèces à la surface et donc le développement de structures 3D suivant cette direction. Par ailleurs, cette surface riche cation est caractérisée par une très forte mobilité des espèces, à l'origine des îlots de très grande taille.

Application aux hétérostructures pour composants micro-ondes

Ce travail a été le fil rouge de mon activité, visant à optimiser des structures de type HEMT sur InP pour les composants micro-ondes de puissance ou faible bruit. Il m'a permis de mettre à profit les connaissances acquises lors des études présentées plus haut concernant notamment les phénomènes de ségrégation, les interfaces et les couches contraintes.

Le double plan de dopage et la structure inversée

A nouveau la ségrégation

La réalisation de transistors HEMT de puissance sur InP est pénalisée par une mauvaise tenue en tension. Pour y pallier, nous avons fait le pari d'obtenir des courants importants à l'aide de structures à double plan de dopage. Ceci nous a conduit à aborder les problèmes liés à la ségrégation du dopant silicium lors de la croissance de la structure inversée (figure II.24). Cette ségrégation du silicium est particulièrement pénalisante puisqu'à

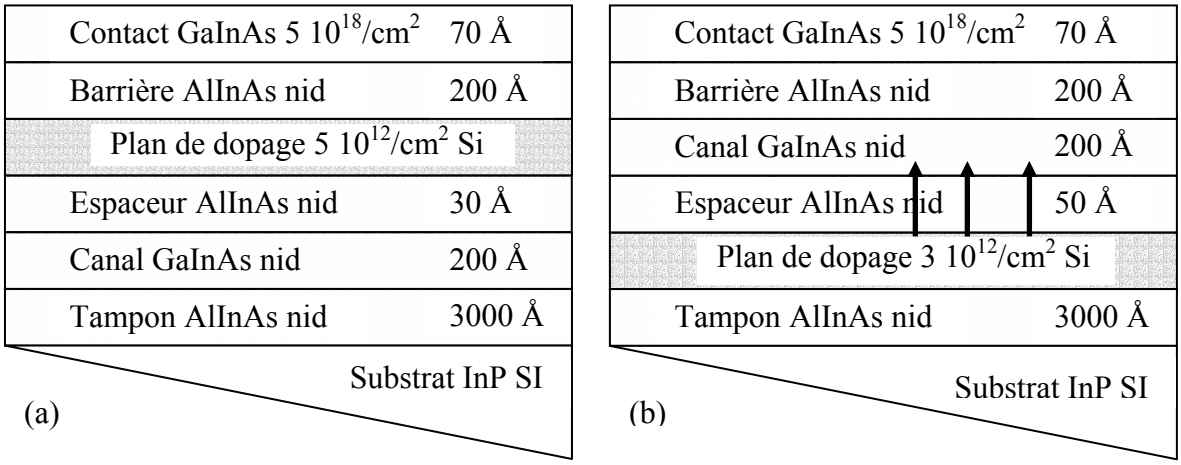

Figure II.24 : Exemple de structures de type HEMT directe (a) et inverse (b). Les flèches de la figure (b) symbolisent la ségrégation du silicium dans le canal.

	Sans optimisation de température		Avec optimisation de température	
	300 K	77 K	300 K	77 K
nH en cm-^{2}	1.52 10^{12}	1.95 10^{12}	2.32 10^{12}	2.86 10^{12}
µH en cm^2/V.s	3850	6670	8970	25900

Tableau II.I : Densité de porteurs et mobilité de Hall mesurée sur l'hétérostructure inverse (b) avec et sans optimisation de la température de croissance.

la température de croissance standard pour ces structures (500-520°C), le silicium ségrége à la surface et s'incorpore dans le canal, réduisant de façon dramatique la mobilité des électrons. Nous avons mis au point une procédure de croissance qui diminue fortement la cinétique de la ségrégation. Elle consiste essentiellement à baisser la température du substrat vers 450°C durant les quelques premières monocouches de la couche espaceur, de sorte à « enterrer » les

atomes de silicium du plan de dopage et ainsi à en limiter la ségrégation. La température de croissance est ensuite rétablie aux environs de 500-520°C pour l'épitaxie de la zone active. Les valeurs de la mobilité électronique pour les structures directe et inverse sont alors comparables (cf. tableau II.I). La maîtrise acquise a permis la participation à un contrat DRET sur la filière InP [61]. A titre d'exemple, dans le cadre de la thèse de Frédéric Diette (équipe « Composants de puissance » de l'IEMN), nous avons épitaxié une structure à compensation de contrainte composée d'un canal InGaAs à 65% d'indium, d'une barrière InAlAs à 35% d'indium et de 2 plans de dopage qui a fourni des transistors dont les caractéristiques étaient à l'état de l'art [62,63]. En effet, à 60 GHz, nous avons obtenu une densité de puissance de 370 mW/mm, un rendement en puissance ajoutée supérieur à 28% et un gain en puissance au-delà de 5dB pour un transistor à grille de 0.25 µm.

Dans le cas des composants faible bruit à faible longueur de grille, le report sur des substrats plus isolants permet de réduire considérablement les effets de canal court. Ce thème a fait l'objet d'une collaboration avec le LETI en vue de réaliser des composants hyperfréquences sur substrat InP reportés sur substrats Si ou GaAs par collage moléculaire afin de pallier les problèmes relatifs à l'utilisation des substrats InP (coût, fragilité,...). Lors de la croissance, compte tenu de l'étape de report, la structure doit être épitaxiée inversée. Là encore, la difficulté majeure est de minimiser la ségrégation du silicium dans le canal et nous avons appliqué la même procédure que précédemment. Après collage et élimination du substrat, un transistor HEMT de longueur de grille 0.12 µm a été réalisé, présentant des fréquences de coupure f_t de 185 GHz et f_{max} de 280 GHz, comparables à un composant non reporté [64].

Les canaux mixtes et phosphorés

Où l'on retrouve les interfaces

Afin de réduire l'ionisation par impact liée aux porteurs énergétiques, nous avons introduit des structures à canal mixte InP/InGaAs ou à canal phosphoré (InAsP ou InP). Dans le cas du canal mixte (thèse de Pascal Chevalier, 1998), les porteurs se déplacent d'abord dans l'alliage InGaAs puis, lorsqu'ils ont suffisamment d'énergie, transfèrent dans InP et perdent ainsi de l'énergie cinétique, ce qui réduit le phénomène d'ionisation par impact. Les mesures obtenues sur des structures adaptées en maille à canal mixte InP/InGaAs montrent une réduction d'un facteur 2 de la transconductance de sortie, ce qui confirme la diminution de l'ionisation par impact. Sur ces structures, à 60 GHz et pour un transistor de 0.15µm de longueur de grille, nous avons mesuré une densité de puissance supérieure à 350 mW/mm, un gain en puissance entre 5 et 6dB et un rendement en puissance ajoutée de l'ordre de 13% [65,66]. Ces performances sont assez comparables à la structure à double plan de dopage en termes de densité de puissance et de gain en puissance mais avec un simple plan de dopage. Le canal phosphoré (thèse de Fahrid Medjdoub, 2004) présente une tenue en tension nettement supérieure à celle du canal InGaAs mais est pénalisé par une dynamique des porteurs moins favorable, surtout pour InP. L'utilisation d'une grille courte (100 nm ou moins) est alors indispensable pour autoriser la montée en fréquence. Le respect des règles d'échelle impose alors de réduire l'épaisseur de barrière à 10 nm ou moins. Dans ce cas, le potentiel de surface dans les zones découvertes du fossé de grille déserte en partie le canal et déforme les caractéristiques $I_{DS}=f(V_{DS})$. Pour contrer cet effet, nous avons utilisé une barrière composite InAlAs/InP permettant de réaliser un double fossé de grille et d'éloigner la surface du canal tout en conservant un rapport d'aspect correct. C'est ainsi que récemment ont été réalisés des

transistors à grille de 100 nm présentant l'état de l'art en puissance à 94 GHz, avec une densité de puissance de 260 mW/mm, un gain en puissance de 5.9 dB et un rendement en puissance ajoutée supérieur à 10%.

Vers des canaux à haute mobilité

L'augmentation du taux d'indium de l'alliage InGaAs dans le canal permet un gain en dynamique des porteurs. Du point de vue de l'épitaxie, deux voies ont été explorées, utilisant des structures $In_xGa_{1-x}As/In_yAl_{1-y}As$ pseudomorphiques ou métamorphiques sur substrat InP. Dans le premier cas, durant le stage de DEA de Bastien Pinsard, nous avons montré que pour une zone active de 12-15 nm d'épaisseur, les meilleurs résultats sont obtenus pour un taux d'indium de 75% (cf. paragraphe « croissance contrainte d'InGaAs sur InP »). Nous avons déterminé l'influence des paramètres de la structure sur la mobilité dans le canal. Nous avons ainsi montré que la mobilité à 77K croît avec la densité de porteurs jusqu'à des valeurs de 9 $10^{11}/cm^2$, mettant ainsi en évidence l'effet collectif d'écrantage du gaz 2D. De même, la mobilité augmente avec l'épaisseur de l'espaceur jusqu'à une épaisseur de 20 nm, permettant une réduction de l'interaction coulombienne entre les porteurs et les donneurs ionisés. Grâce à cette optimisation, nous avons pu obtenir des mobilités de 16 000 et 140 000 cm^2/Vs à 300 et 77 K respectivement, avec une densité de porteurs correspondante de 9 $10^{11}/cm^2$ [55]. Ces valeurs sont parmi les meilleures publiées sur des structures pseudomorphiques dans ce système de matériaux.

La littérature fournit quelques valeurs supérieures pour des structures métamorphiques que nous avons étudiées dans le cadre du DEA de Julien Lastennet. Le but visé avec de telles structures était la croissance d'une zone active en InAs de 10-15 nm grâce à une couche tampon métamorphique en $In_yAl_{1-y}As$ servant d'adaptation de paramètre de maille avec le substrat InP. Pour la croissance de la couche d'adaptation, nous nous sommes appuyés sur l'expérience acquise par l'équipe ces dernières années. Cependant, les matériaux utilisés imposent une contrainte en compression du canal InAs, d'autant plus importante que le taux d'indium final de la couche d'adaptation en InAlAs est faible. Ce taux ne peut pourtant pas être trop élevé sous peine de réduire fortement l'offset de bande de conduction et nuire au transfert : nous avons ainsi fixé le taux maximum d'indium de la couche métamorphique à 80%. Dans ce cas, il s'est avéré impossible d'épitaxier un canal InAs de 10 à 15 nm d'épaisseur sans relaxation plastique, quelles que soient les conditions de croissance. Ceci est probablement dû à la rugosité inévitable de la couche métamorphique relaxée. Par contre, nous avons pu obtenir d'excellents résultats avec un canal mixte composé de 7 nm d'InAs avec de part et d'autre 4 nm de $In_{0.8}Ga_{0.2}As$. La mobilité électronique est alors de 21 500 $cm^2/V.s.$ à 300K t 179 000 $cm^2/V.s.$ à 77K pour une densité de porteurs de 9 $10^{11}/cm^2$. Là encore, ces valeurs se situent très honorablement par rapport à la concurrence internationale.

Références

[1] : C. Deparis and J. Massies, J. Crystal Growth **108** (1991) 157.
[2] : H.H. Farrell and C.J. Palmstrom, J. Vac. Sci. Technol. **B8** (1990) 903.
[3] : J.E. Northrup and S. Froyen, Phys. Rev. **B50** (1994) 2015.
[4] : T. Hashizume, Q.K. Xue, J. Zhou, A. Ichimiya and T. Sakurai, Phys. Rev. Lett. **73** (1994) 2208.
[5] : G.P. Srivastava and S.J. Jenkins, Phys. Rev. **B53** (1996) 12 589.
[6] : V.P. LaBella, H. Yang, D.W. Bullock, P.M. Thibado, P. Kratzer and M. Scheffler, Phys. Rev. Lett. **83** (1999) 2989.
[7] : V.P. LaBella, D.W. Bullock, C. Emery, Z. Ding and P.M. Thibado, Appl. Phys. Lett. **79** (2001) 3065.
[8] : M. Itoh, G.R. Bell, A.R. Avery, T.S. Jones, B.A. Joyce, D.D. Vvedensky, Phys. Rev. Lett. **81**, 633 (1998)
[9] : S.-H. Lee, W. Moritz, M. Scheffler, Phys. Rev. Lett. **85** (2000) 3890
[10] : C. Kumpf, L.D. Marks, D. Ellis, D. Smilgies, E. Landemark, M. Nielsen, R. Feidenhans, J. Zegenhagen, O. Bunk, J.H. Zeysing, Y. Su and R.L. Johnson, Phys. Rev. Lett. **86** (2001) 3586.
[11] : D. Paget, Y. Garreau, M. Sauvage, P. Chiaradia, R. Pinchaux and W.G. Schmidt, Phys. Rev. **B64** (2001) 161 305.
[12] : A. Ohtake, S. Tsukamoto, M. Pritovsek, N. Koguchi, M. Ozeki, Phys. Rev. **B65** (2002) 233 311.
[13] : M. Sauvage-Simkin, R. Pinchaux, J. Massies, P. Claverie, N. Jedrecy, J. Bonnet and I.K. Robinson, Phys. Rev. Lett. **62** (1989) 563.
[14] : C. Xu, J.S. Burnham, R.M. Braun, S.H. Goss and N. Winograd, Phys. Rev. **B52** (1995) 5172.
[15] : A. Ohtake, J. Nakamura, S. Tsukamoto, N. Koguchi, A. Natori, Phys. Rev. Lett. **89** (2002) 206 102.
[16] : M. Göthelid, Y. Garreau, M. Sauvage-Simkin, R. Pinchaux, A. Cricenti, G. Le Lay, Phys. Rev. B59 (1999) 15 285.
[17] : W. Barvosa-Carter, R.S. Ross, C . Ratsch, F. Grosse, J.H.G. Owen, J.J. Zinck, Surf. Sci. 499 (2002) L129.
[18] : F Grosse, W. Barvosa-Carter, J.J. Zinck, M.F. Gyure, Phys. Rev. B66 (2002) 075 321.
[19] : X.Wallart, Surf. Sci. **506** (2002) 203
[20] : V.P. LaBella, Z. Ding, D.W. Bullock, C. Emery and P.M. Thibado, J. Vac. Sci. Technol. **A18** (2000) 1492.
[21] : W.G. Schmidt, F. Bechstedt, N. Esser, M. Pritovsek, C. Schultz and W. Richter, Phys. Rev. **B57** (1998) 14 596.
[22] : N. Esser, W.G. Schmidt, J. Bernholc, A.M. Frisch, P. Vogt, M. Zorn, M. Pritovsek, W. Richter, F. Bechstedt, T. Hannapel, S. Visbeck, J. Vac. Sci. Technol. **B17** (1999) 1691.
[23] : A.M. Frisch, W.G. Schmidt, J. Bernholc, M. Pritovsek, N. Esser and W. Richter, Phys. Rev. **B60** (1999) 2488.
[24] :K. Lüdge, P. Vogt, O. Pulci, N. Esser, F. Bechstedt and W. Richter, Phys. Rev. **B62** (2000) 11 046.

[25]: S.V. Ivanov, P.S. Kop'ev, N.N. Ledentsov, J. Cryst. Growth **104** (1990) 345.
[26] : B. Jusserand, E. Alexandre, D. Paquet, G. Leroux, Appl. Phys. Lett. **47** (1985) 301.
[27] : N. Imata, Y. Matsumoto, T. Baba, Jpn. J. Appl. Phys. **24** (1985) L17.

[28] : O. Dehaese, thèse d'université, Université des Sciences et Technologies de Lille1, juillet 1997
[29] : J.M. Moison, C. Guille, F. Houzay, F. Barthe, M. Van Rompay, Phys. Rev. **B 40** (1989) 6149.
[30] : O. Schuler, thèse d'université, Université des Sciences et Technologies de Lille1, novembre 1998.
[31] : K. Muraki, S. Fukatsu, Y. Shiraki, R. Ito, Appl. Phys. Lett. **61** (1992) 557.
[32] : H. Toyoshima, T. Niwa, J. Yamazaki, A. Okamoto, Appl. Phys. Lett. **63** (1993) 821.
[33] : J.R. Arthur, J. Appl. Phys. **39** (1968) 4032.
[34] : J.M. Gerard, J.Y. Marzin, Phys. Rev. **B 45** (1992) 6313.
[35] : J. Nagle, J.P. Landesman, M. Larive, C. Mottet, P. Bois, J. Cryst. Growth **127** (1993) 550.
[36] : M. Larive, J. Nagle, J.P. Landesman, X. Marcadet, C. Mottet, P. Bois, J. Vac. Sci. Tech. **B11** (1993) 1413.
[37] : B. Jusserand, F. Mollot, J.M. Moison, G. Le Roux, Appl. Phys. Lett. **57** (1990) 560.
[38] : J. Massies, F. Turco, A. Saletes, J.P. Contour, J. Cryst. Growth **80** (1987) 307.
[39] : G. Grenet, E. Bergignat, M. Gendry, M. Lapeyrade, G. Hollinger, Surf. Sci. **352-354** (1996) 734.
[40] : O. Dehaese, X. Wallart, F. Mollot, Appl.Phys.Lett.**66** (1995) 52
[41] : O. Schuler, O. Dehaese, X. Wallart, F. Mollot, J. Appl. Phys. **84** (1998) 766
[42] : O. Dehaese, X. Wallart, O. Schuler, F. Mollot, J. Appl. Phys**. 84** (1998) 2127
[43] : Y. Foulon, C. Priester, G. Allan, J.C. Garcia, J.P. Landesman, M. Leroux, Phys. Rev.**B46** (1992) 1886
[44] : M. Leroux, M.L. Fille, B. Gil, J.P. Landesman, J.C. Garcia, Phys. Rev**. B47** (1993) 6465
[45] : X. Wallart, C. Priester, D. Deresmes, T. Gehin, F. Mollot, Appl. Phys. Lett.**81** (2002) 1086
[46] : S.B. Zhang, A. Zunger, Appl. Phys. Lett **71** (1997) 677
[47] : X. Wallart, C. Priester, Phys. Rev. **B68** (2003) 235314

[48] : J. Massies, J. Rochette, P. Delescluse, P. Etienne, J. Chevrier and N.T. Linh, Electronics Lett. **18**, 758 (1982)
[49] : J. Massies and M. Sauvage-Simkin, Appl. Phys. **A 32**, 27 (1983)
[50] : M. Gendry, V. Drouot, C. Santinelli, G. Hollinger, C. Miossi and M. Pitaval, J. Vac. Sci. Technol. **B10**, 1829 (1992)
[51] : S.Z. Chang, S.C. Lee, C.R. Chen and L.J. Chen, J. Appl. Phys. **75**, 1511 (1994)
[52] : S. Jourba, M. Gendry, P. Regreny and G. Hollinger, J. Crystal Growth **201/202**, 1101 (1999)
[53] : D. Lacombe, A. Ponchet, S. Fréchengues, V. Drouot, N. Bertru, B. Lambert and A. Le Corre, J. Crystal Growth **201/202**, 252 (1999)
[54] : M. Gendry, V. Drouot, G. Hollinger and S. Mahajan, Appl. Phys. Lett **66**, 40 (1995)
[55] : X. Wallart, B. Pinsard, F. Mollot, J. Appl. Phys.**97**, (2005) 053706
[56] : X. Wallart, O. Schuler, D. Deresmes and F.Mollot., Appl. Phys. Lett. **76** (2000) 2080
[57] : S.H. Wei, L.G. Ferreira and A. Zunger, Phys.Rev.**B41** (1990) 8240
[58] : X. Wallart, C. Priester, D. Deresmes and F. Mollot, Appl. Phys. Lett.**77** (2000) 253
[59] : X. Wallart, D. Deresmes and F. Mollot, J. Crystal Growth.**227-228** (2001) 255
[60] : X. Wallart, D. Deresmes and F. Mollot, Appl. Phys. Lett. **78** (2001) 2961

[61] : Contrat DRET91/113, *Etude prospective des potentialités de transistors à effet de champ à base de GaInAs sur InP*
[62] : S. Piotrowicz, C. Gaquière, B. Bonte, E. Bourcier, D. Théron, X. Wallart, Y. Crosnier, IEEE Microwave and Guided Wave Lett. **8**, 10 (1998)
[63] : F. Diette, D. Théron, X. Wallart, M. Muller, M. François, E. Delos, C. Gaquière, Y. Crosnier, IEEE Proceedings of IPRM96, 20 (1996)
[64] : S. Bollaert, X. Wallart, S. Lepilliet, A. Cappy, E. Jalaguier, S. Pocas, B. Aspar, El. Device Lett.**23**, 73 (2002)
[65] : P. Chevalier, X. Wallart, B. Bonte, R. Fauquembergue, Electronics Letters **34**, 409 (1998)
[66] : M. Boudrissa, E. Delos, X. Wallart, D. Théron, J.C. De Jaeger, El. Device Lett. **22**, 257 (2001)

3ème partie : projet de recherche

Epitaxie d'hétérostructures à base d'antimoniures

L'évolution future de mon activité de recherche est déjà amorcée et découle de mon expérience: le développement de la croissance d'hétérostructures à base de semi-conducteurs III-V antimoniés.

Ce projet s'insère dans la thématique "composants rapides" du laboratoire et constitue une prolongation de mes activités de croissance d'hétérostructures sur InP pour composants micro-ondes. En effet, dans la course à la haute fréquence, l'intégration de matériaux antimoniés dans les hétérojonctions à modulation de dopage ou dans les transistors bipolaires à hétérojonction permet de franchir un pas supplémentaire.

Contexte national et international

C'est sans nul doute les chercheurs de Santa Barbara emmenés par le prix Nobel H. Kroemer qui furent les pionniers dans l'épitaxie des antimoniures dès la fin des années 1980. Ils démontrèrent les potentialités de l'hétérostructure AlSb/InAs avec des mobilités électroniques record de l'ordre de 30 000 $cm^2/V.s$ à 300K et 900 000 $cm^2/V.s$ à 4K [1-4]. L'équipe initiale a essaimé et actuellement, le groupe de C. Bolognesi de l'Université Simon Fraser au Canada est également très actif dans le domaine. Le « Naval Research Laboratory » (NRL) américain est également engagé fortement dans le domaine et on lui doit nombre d'études sur les surfaces d'antimoniures et leurs interfaces avec les arséniures [5-8].

Les chercheurs de Santa Barbara comme ceux du NRL ont réalisé des transistors de type HEMT basés sur l'hétérojonction AlSb/InAs. Pour une longueur de grille de 0.1 µm, le NRL atteint des fréquences de coupure f_T et f_{Max} aux environs de 200GHz [9, 10] tandis que pour une grille de 0.2 µm, l'équipe de Santa Barbara obtient 160 et 140 GHz respectivement [11]. Ces résultats sont assez décevants compte tenu des propriétés remarquables de l'hétérostructure AlSb/InAs : grande discontinuité de bande de conduction (1.35 eV) et mobilité électronique très élevée dans InAs. Ceci s'explique essentiellement par les phénomènes d'ionisation par impact dans le canal InAs à petit gap mais aussi par les difficultés technologiques (contacts,…) rencontrées avec les antimoniures : la technologie est beaucoup moins mature que celle sur substrat GaAs ou InP. Par ailleurs, les composants étudiés sont épitaxiés sur substrat GaAs avec une couche tampon métamorphique pour adapter le paramètre de maille : l'influence d'une forte densité de dislocations émergentes dans la zone active doit également être considérée.

L'utilisation de l'antimoine dans la base de transistors à hétérojonction a permis une avancée significative. En effet, en utilisant comme matériau de base un alliage GaAsSb en accord de maille sur InP, C.Bolognesi et al. ont montré que l'on peut atteindre des fréquences de coupure voisines de 300 GHz sans technologie complexe, valorisant ainsi l'apport des antimoniures dans la structure TBH sur InP [12]. Ces performances n'avaient été atteintes précédemment par M. Rodwell et al. qu'au prix d'une technologie complexe impliquant notamment une étape de report [13]. Par rapport à une base en InGaAs, la base en GaAsSb améliore le blocage des trous à la jonction émetteur-base et surtout favorise l'injection des électrons à la jonction base-collecteur (figure III.1).

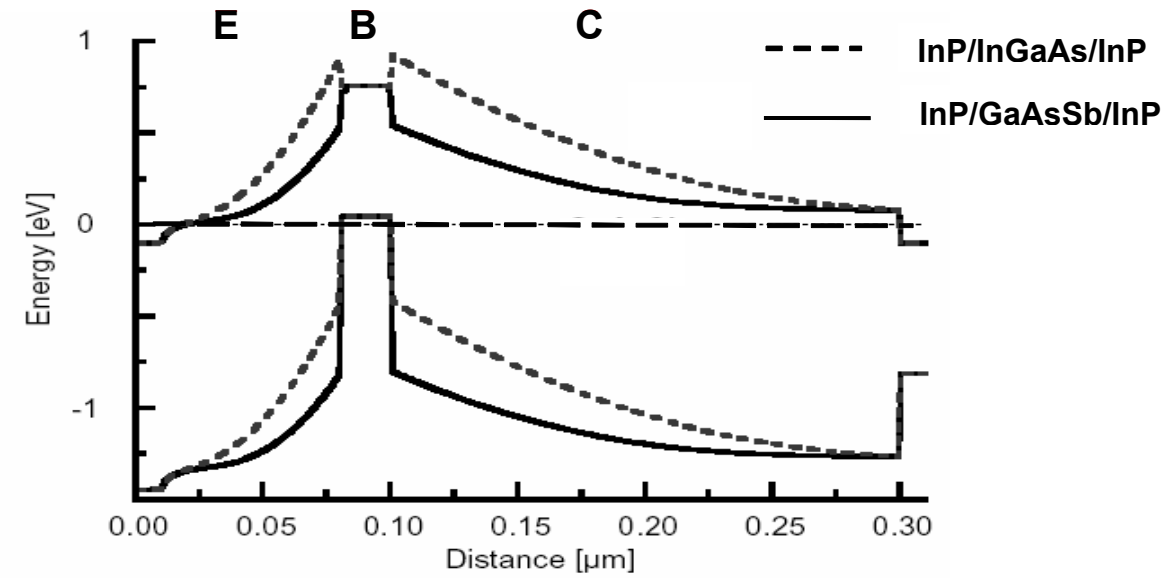

Figure III.1 : schéma des bandes de valence et de conduction le long d'un HBT à base InGaAs ou GaAsSb sans polarisation (d'après C. Bolognesi et al.)

Enfin, il faut souligner la réalisation au début des années 1990 d'une diode à effet Tunnel résonnant à double barrière AlSb par les chercheurs du MIT présentant une fréquence maximum d'oscillation de 712GHz constituant encore aujourd'hui le record en la matière [14].

En France, les principaux laboratoires impliqués dans la croissance d'antimoniures par EJM sont le CEM2 à Montpellier, le LPN à Marcoussis et le laboratoire de recherche de Thalès à Corbeville. Les applications visées sont essentiellement optoélectroniques, dans l'infra-rouge. Par ailleurs, des industriels tel OMMIC à Limeil-Brévannes s'intéressent fortement aux structures HBT à base antimoniée.

Le projet : hétérostructures antimoniées pour électronique très rapide

Les éléments présentés ci-dessus tendent à prouver que le futur de la montée en fréquence passe par l'utilisation des matériaux antimoniés. Plus récemment, des sociétés telle Intel ont également montré l'intérêt des antimoniures pour réduire la puissance dissipée dans les futurs dispositifs [15,16]. Au niveau national, aucun laboratoire universitaire n'est fortement impliqué dans la recherche sur les composants rapides à base d'antimoine. Compte tenu de l'expérience de l'IEMN dans ce domaine, il apparaît donc naturel qu'il entreprenne un programme d'élaboration d'hétérostructures pour des composants haute fréquence utilisant l'antimoine.

Ce programme abordera les structures à modulation de dopage, les TBH et s'appuiera sur des études plus fondamentales liées à la croissance.

Hétérostructures à dopage modulé

Ces hétérostructures visent d'abord la fabrication de transistors de type HEMT à canal InAs. Comme il a été mentionné plus haut, la structure métamorphique $In_xGa_{1-x}As/In_yAl_{1-y}As$

demeure délicate à mettre en œuvre et présente d'importantes limitations en terme notamment d'offset de bande de conduction. Aussi, pour s'affranchir de ces limitations, de la contrainte et permettre l'utilisation d'InAs dans la zone active, l'emploi d'antimoniures comme matériau de barrière est incontournable.

L'hétérojonction AlSb/InAs présente la plus importante discontinuité de bande de conduction (1.35 eV) parmi les semi-conducteurs III-V, très favorable au transfert électronique. Le canal InAs permet quant à lui d'atteindre des mobilités électroniques élevées grâce à la faible masse effective des électrons dans InAs (0.025 m_0). Cependant, la faible bande interdite d'InAs associée à l'hétérojonction AlSb/InAs de type II conduit à une importante concentration de trous, non confinés dans le canal, générés par ionisation par impact. Ces trous participent alors à un courant de grille et à une charge positive du substrat, 2 phénomènes parasites du fonctionnement du transistor HEMT.

Nous nous proposons donc de développer des solutions permettant de réduire l'ionisation par impact et d'améliorer le confinement des trous créés dans le canal. Les premières sont basées sur des canaux mixtes alliant InAs à un alliage de plus grande bande interdite. Cette approche a déjà été expérimentée par le groupe de Santa Barbara avec des canaux mixtes InAs/InAlAs [17] et InAs/InAsP [18]. Des composants ont été réalisés et ont démontré une amélioration par rapport à ceux à canal InAs, notamment du point de vue de l'ionisation par impact. Les longueurs de grille utilisées étaient relativement longues (0.5 et 0.7 µm) et ne permettent pas de juger des performances ultimes de ce type de composants. Nous nous proposons de continuer dans cette voie avec des longueurs de grille de 0.1 µm ou moins pour explorer les potentialités de cette approche. L'amelioration du confinement des trous passe par l'utilisation d'alliages $Al(Ga)As_xSb_{1-x}$ comme matériau de couche tampon et de barrière afin que l'hétérojonction $Al(Ga)As_xSb_{1-x}$/InAs soit de type I. Des premiers pas en ce sens ont été entrepris par les chercheurs de Santa Barbara avec l'insertion d'une couche d $AlAs_xSb_{1-x}$ dans la barrière [19] mais en gardant AlSb comme couche tampon, la collection du courant de trous vers le substrat se faisant par une grille arrière [20]. Le retour à une hétérostructure de type I nous paraît préférable et les excellents résultats obtenus par les chercheurs d'Intel sur l'hétérojonction AlInSb/InSb (de type I) [15,16], malgré la très faible bande inerdite d'InSb (~0.2 eV), nous encouragent en ce sens.

Enfin, les structures à dopage modulé peuvent également déboucher sur des aspects plus originaux comme les composants balistiques. L'émergence des structures balistiques vient du rapprochement des longueurs maintenant technologiquement accessibles, de l'ordre de 100 nm, et du libre parcours moyen des électrons entre deux collisions à température ambiante dans certains matériaux. C'est le cas des alliages InGaAs, d'autant plus que le taux d'In est élevé, le meilleur candidat étant InAs. Dans le cadre du projet européen Nanotera [21], le laboratoire a déjà entrepris une action sur ces structures à base d'alliages InGaAs sur substrat InP.

Le transistor bipolaire à hétérojonction

Les résultats récents sur les transistors TBH à base GaAsSb en font un candidat de choix pour la montée en fréquence. Notre travail portera dans un premier temps sur l'optimisation de la structure à double hétérojonction InP/GaAsSb/InP. Nous nous appuierons sur l'expérience acquise au laboratoire dans la réalisation de TBH InP/InGaAs/InP ces dernières années [22,23]. Puis, à plus long terme, le degré de liberté supplémentaire apporté par l'antimoine dans l'ingénierie des structures de bandes permet d'envisager la réalisation de TBH dans une filière 6.1Å, c'est-à-dire adaptée en maille à GaSb.

Les études liées à la croissance

Comme tout au long de mon activité passée, les objectifs finalisés décrits ci-dessus reposeront sur des études plus fondamentales. D'ores et déjà, j'identifie 3 pistes principales.

Les couches tampon métamorphiques

La première est l'élaboration de couches tampons métamorphiques isolantes, nécessaires à la croissance de structures pour composants. En effet, il n'existe ni substrats GaSb, ni a fortiori de substrats InAs semi isolants. Il est donc nécessaire d'utiliser des substrats GaAs ou InP semi isolants sur lesquels il faut épitaxier une couche tampon, typiquement en $Al(Ga)As_xSb_{1-x}$, isolante électriquement et qui permette l'adaptation du paramètre de maille entre le substrat et la zone active [4, 24, 25]. Pour ce faire, je m'appuierai sur l'expérience de l'équipe « Epitaxie » acquise lors de la croissance métamorphique sur substrats GaAs et InP [26, 27]. Néanmoins, la croissance métamorphique des alliages InGa(Al)As sur GaAs ou InP repose exclusivement sur des gradients de composition en éléments III (Ga-In ou Al-In) alors que dans le cas des antimoniés, ces gradients concernent les éléments V As et Sb. La tache sera plus ardue car l'incorporation respective de As et Sb dépend des conditions de croissance, ce qui n'est pas le cas pour les éléments III pour lesquels le coefficient de collage est toujours 1. Une étude préalable de l'incorporation de As et Sb en fonction des conditions de croissance (température de croissance, rapport des flux V/III) sera donc nécessaire et pourra bénéficier utilement des résultats déjà obtenus par l'équipe de Thalès [28]. D'un point de vue expérimental, cela nécessite un contrôle précis des flux d'éléments V qui exige l'utilisation de cellules à vanne.

Le dopage n utilisant le tellure

Le second aspect à maîtriser est le dopage de type n des antimoniures qui n'est pas possible directement avec le silicium. Deux solutions existent. La première consiste à épitaxier des barrières sous forme de super-réseaux AlSb/InAs à courte période dans lesquels le dopage se fait grâce au silicium dans la couche InAs [29]. La seconde nécessite l'emploi du tellure. Pour ce faire, des sources binaires tel GaTe sont préférées car ces matériaux présentent une pression de vapeur beaucoup plus faible que le tellure élémentaire et sont donc plus compatibles avec l'environnement EJM [30]. Le tellure a été également utilisé comme surfactant lors de la croissance contrainte d'alliages InGaAs par exemple [31], dans laquelle est mise à profit sa tendance à ségréger en surface. Dans le cas du dopage, il me faudra au contraire travailler pour limiter au maximum cette ségrégation.

Où l'on retrouve les interfaces et les surfaces

Le troisième sujet d'étude à aborder est le contrôle des interfaces arséniures/antimoniures et phosphures/antimoniures. Les chercheurs du laboratoire de recherche de Thalès ainsi que ceux de l'université de Montpellier ont déjà travaillé sur ce sujet dans le cadre d'applications optiques [32,33]. Il me faudra reprendre ce sujet en visant une optimisation pour des composants électroniques. Ce point est particulièrement délicat puisque dans les applications envisagées, il y a à la fois commutation d'anions et de cations aux interfaces, InP/GaAsSb pour les transistors bipolaires à hétérojonction et AlSb/InAs pour les hétérostructures à dopage modulé. L'effet de la séquence de commutation aux interfaces sur les propriétés électroniques a été très tôt mis en évidence par le groupe de Santa Barbara [34] et demeure un sujet d'actualité [35,36]. Je bénéficierai de notre expérience passée de

l'étude des interfaces arséniures/phosphures et de l'ensemble expérimental de l'IEMN disposant d'un système d'analyse de surfaces couplé aux bâtis EJM.

Enfin, poursuivant mon investigation de l'influence des reconstructions de surface sur la croissance des matériaux, je m'attacherai à mener une étude des reconstructions de surface spécifiques aux antimoniures car elles sont de loin moins bien documentées que celles des arséniures ou phosphures. Les travaux antérieurs indiquent que les reconstructions rencontrées sur AlSb sont assez voisines de celles observées sur AlAs, à savoir une c(4x4) pour les surfaces riches Sb puis une (1x3). Par contre, les reconstructions observées sur GaSb sont très différentes de celles de GaAs puisque lorsque le taux de couverture en Sb de la surface diminue, apparaissent successivement une (2x5), une (1x5) puis une c(2x6) et enfin une (1x3) [37-40]. Ces reconstructions ont fait l'objet d'études RHEED et STM mais ont donné lieu à assez peu d'analyses par photoémission [41,42]. C'est ce type de travaux que je pourrai développer en tirant partie de l'ensemble expérimental de l'IEMN.

Références

[1] : G. Tuttle, H. Kroemer, J.H. English, J. Appl. Phys. **67** (1990) 3032
[2] : C.R. Bolognesi, H. Kroemer and J.H. English, Appl. Phys. Lett. **61** (1992) 213
[3] : C. Nguyen, B. Brar, C.R. Bolognesi, J.J. Pekarik, H. Kroemer and J.H. English, J. Electronic Materials **22** (1993) 255
[4] : M. Thomas, H.R. Blank, K.C. Wong and H. Kroemer, J. Crystal Growth **175/176** (1997) 894
[5] : P.M. Thibado, B.R. Bennett, B.V. Shanabrook, L.J. Whitman, J. Crystal Growth **175/176** (1997) 317
[6] : B.Z. Nosho, W.H. Weinberg, W. Barvosa-Carter, A.S. Bracker, R. Magno, B.R. Bennett, J.C. Culbertson, B.V. Shanabrook, L.J. Whitman, J. Vac. Sci. Technol. **B17** (1999) 1786
[7] : W. Barvosa-Carter, A.S. Bracker, J.C. Culbertson, B.Z. Nosho, B.V. Shanabrook, L.J. Whitman, Phys. Rev. Lett. **84** (2000) 4649
[8] : A.S. Bracker, M.J. Yang, B.R. Bennett, J.C. Culbertson, W.J. Moore, J. Crystal Growth **220** (2000) 384
[9] : J.B. Boos, M.J. Yang, B.R. Bennett, D. Park, W. Kruppa, C.H. Yang, and R. Bass, Electronics Letters **34**, (1998) 1525-1526.
[10] : R. Tsai, M. Barsky, J. B. Boos, B. R. Bennett, J. Lee, N. A. Papanicolaou, R. Magno, C. Namba, P. H. Liu, D. Park, R. Grundbacher, and A. Gutierrez, Proceedings of the 2003 IEEE GaAs IC Symposium (2003).
[11] : C. Kadow, M. Dahlström, J.U. Bae, H.K. Lin, A.C. Gossard, M.J.W. Rodwell, B. Brar, G.J. Sullivan, G. Naguy, J.I. Bergman, IEEE Trans El. Devices **52** (2005) 151
[12] : M.W. Dvorak, C.R. Bolognesi, O.J. Pitts, S.P. Watkins, IEEE El. Device Lett. **22** (2001) 361.
[13] : M.J.W. Rodwell, M. Urteaga, T. Mathew, D. Scott, D. Mensa, Q. Lee, J. Guthrie, Y. Betser, S.C. Martin, R.P. Smith, S. Jaganathan, S. Krishnan, S.I. Long, R. Pullela, B. Argaval, U. Bhattacharya, L. Samoska, M. Dahlstrom, IEEE Trans. El. Devices **48** (2001) 2606.
[14] : E.R. Brown, J.R. Söderström, C.D. Parker, L.J. Mahoney, K.M. Molvar, T.C. McGill, Appl. Phys. Lett. **58** (1991) 2291.
[15] : S. Datta, R. Chau, T. Ashley, A. R. Barnes, L. Buckle, A. B. Dean, M. T. Emeny, M. Fearn, D. G. Hayes,K. P. Hilton, R. Jefferies, T. Martin, K. J. Nash, T. J. Phillips, W. H. A. Tang and P. J. Wilding, The 7th International Conference on Solid-State and Integrated-Circuit Technology, ICSICT 2004, Beijing, Chine, octobre 2004.
[16] : R. Chau, 2005 IEEE VLSI-TSA International Symposium on VLSI Technology, Hsinchu, Taiwan, avril 2005.
[17] : H.K. Lin, C. Kadow, J.U. Bae, M.J.W. Rodwell, A.C. Gossard, B. Brar, G. Sullivan, G. Nagy, J. Bergman, J. Appl. Phys. **97** (2005) 024505.
[18] : H.K. Lin, C. Kadow, M. Dahlström, J.U. Bae, M.J.W. Rodwell, A.C. Gossard, B. Brar, G. Sullivan, G. Nagy, J. Bergman, Appl. Phys. Lett. **84** (2004) 437.
[19] : C.R. Bolognesi, J.D. Werking, E.J. Caine, H. Kroemer, E.L. Hu, El. Device Lett. **14** (1993) 13.
[20] : B. Brar, H. Kroemer, El. Device Lett.**16** (1995) 548.
[21] : Contrat européen Nano-Tera IST-2001-32517, *Ballistic Nanodevices for Terahertz Data Processing.*
[22] : E. Lefebvre, M.Zaknoune, F.Mollot, R.Teissier, D.Sicault and J.L.Pelouard, IEEE Proceedings of the 14th Indium Phosphide and Related Materials, Stockholm (2002) 615.
[23] : E. Lefebvre, M.Zaknoune, Y.Cordier and F.Mollot, IEEE Proceedings of the 15th Indium Phosphide and Related Materials, Santa Barbara (2003) 409.

[24] : S. Miya, S. Muramatsu, N Kuze, K. Nagase, T. Iwabuchi, A. Ichii, M. Ozaki, I Shibasaki, J. Electronic Materials **25** (1996) 415.
[25] : P.M. Thibado, B.R. Bennett, M.E. Twigg, B.V. Shanabrook, L.J.Whitman, J. Vac. Sci. Technol. **A14** (1996) 885
[26] : Y.Cordier, D.Ferré, J.-M.Chauveau and J.DiPersio, Appl. Surf. Sci. **166** (2000) 442
[27] : E. Lefebvre, M.Zaknoune, Y.Cordier and F.Mollot, IEEE Proceedings of the 15th Indium Phosphide and Related Materials, Santa Barbara (2003) 409.
[28] : C. Renard, X. Marcadet, J. Massies, R. Bisaro, O. Durand, M. Garcia, C. Sirtori, Proceedings of the 13th European Molecular Beam Epitaxy Workshop, Grindelwald (2005).
[29] : C.R. Bolognesi, J.E. Bryce, D.H. Chow, Appl. Phys. Lett. **69** (1996) 3531
[30] : A. Furukawa, M. Mizuta, Electron. Lett. **24** (1988) 1378.
[31] : N. Grandjean, J. Massies, Phys. Rev. **B53** (1996) R1323.
[32] : I. Prevot, X. Marcadet, O. Durand, R. Bisaro, A. Bouchier, F.H. Julien, J. Crystal Growth **227/228** (2001) 566.
[33] : I. Prevot, B. Vinter, X. Marcadet, J. Massies, Appl. Phys. Lett. **81** (2002) 3362.
[34] : G. Tuttle, H. Kroemer, J.H. English, J. Appl. Phys. **67** (1990) 3032
[35] : B.Z. Nosho, W.H. Weinberg, J.J. Zinck, B.V. Shanabrook, B.R. Bennett, L.J. Whitman, J. Vac. Sci. Technol. **B16** (1998) 2381
[36] : M. Zhong, J. Steinshnider, M. Weimer, R. Kaspi, J. Vac. Sci. Technol. **B22** (2004) 1593
[37] : P.M. Thibado, B.R. Bennett, B.V. Shanabrook, L.J. Whitman, J. Crystal Growth **175/176** (1997) 317
[38] : W. Barvosa-Carter, A.S. Bracker, J.C. Culbertson, B.Z. Nosho, B.V. Shanabrook, L.J. Whitman, H. Kim, N.A. Modine, E. Kaxiras, Phys. Rev. Lett. **84** (2000) 4649
[39] : A.S. Bracker, M.J. Yang, B.R. Bennett, J.C. Culbertson, W.J. Moore, J. Crystal Growth **220** (2000) 384.
[40] : M.C. Righi, R. Magri, C.M. Bertoni, Phys. Rev. **B71** (2005) 075323.
[41] : G.E. Franklin, D.H. Rich, A. Samsavar, E.S. Hirscorn, F.M. Leibsle, T. Miller, T.C. Chiang, Phys. Rev. **B41** (1990) 12619.
[42] : M.T. Sieger, T. Miller, T.C. Chiang, Phys. Rev. B52 (1995) 8256.

Conclusion

Durant ces 17 années, j'ai abordé différents thèmes de recherche et bénéficié du contexte favorable de l'IEMN. Après des débuts consacrés à l'étude des siliciures, mon activité s'est rapidement centrée sur l'épitaxie par jets moléculaires d'hétérostructures de semi-conducteurs III-V.

Ma contribution principale a porté sur les surfaces des semi-conducteurs phosphorés GaP et InP, les phénomènes d'échange et de ségrégation, les interfaces arséniés/phosphorés et la croissance contrainte d'alliages InGaP. Tout au long de ce travail, j'ai cherché à corréler les résultats de différentes techniques de caractérisation avec une attention particulière portée à la spectroscopie de photoélectrons, tirant ainsi partie du dispositif expérimental de l'IEMN. Le développement de la spectroscopie de photoélectrons a par ailleurs donné lieu à de nombreuses collaborations tant à l'intérieur de l'IEMN, au sein du groupe « Physique » et des groupes impliqués en technologie, qu'à l'extérieur. Grâce aux multiples compétences réunies à l'IEMN, j'ai pu allier cette recherche dite « amont » sur les matériaux à une recherche plus « appliquée » destinée aux composants. Cette interaction avec les équipes « composants », l'aller-retour incessant amont-aval et les collaborations qu'ils impliquent m'ont permis de contribuer à l'obtention de résultats significatifs dans le domaine des composants.

C'est cette approche que je souhaite continuer à développer dans mon projet de croissance d'hétérostructures antimoniées pour applications microélectroniques. Même s'il existe déjà des études sur ce sujet, les propriétés des antimoniures et de leurs interfaces demeurent bien moins connues que celles des arséniures et phosphures. Le champ d'investigation est vaste : propriétés des surfaces, des interfaces, croissance pseudo et métamorphique….La réussite de ce projet passera donc par une collaboration avec les groupes « Physique » et « Compsants » de l'IEMN ainsi qu'avec les équipes nationales déjà engagées dans des travaux sur les antimoniures.

4ème partie

Autres activités

Enseignement

J'ai dispensé mon enseignement à l'Institut Supérieur d'Electronique et du Numérique (ISEN) à Lille, en 1ère et 2ème années de cycle Ingénieur (niveau 2ème cycle universitaire).

1985-1988 : Travaux dirigés de Mécanique Quantique
1988-1991 : Travaux dirigés de Mécanique Quantique
Travaux dirigés de Physique du solide
1991-2000 : Cours de Mécanique Quantique
Travaux dirigés de Mécanique Quantique
Travaux dirigés de Physique du solide
2001-2004 : Cours de Mécanique Quantique
Travaux dirigés de Mécanique Quantique et de Physique du Solide
Cours et Travaux Pratiques d'analyse de surfaces
Cours sur l'élaboration d'hétérostructures de semi-conducteurs par Epitaxie par Jets Moléculaires

Encadrement

Diplôme d'Etudes Approfondies

- Claude TETELIN

Etude de la formation d'interfaces ytterbium-silicium (111) et siliciures d'ytterbium-silicium par spectroscopie et diffraction d'électrons, DEA de Sciences des Matériaux, LilleI, juillet 1991

- Olivier DEHAESE

Caractérisation de siliciures de fer obtenus par coévaporation, DEA de Sciences des Matériaux, Université des Sciences et Technologies de Lille I, juillet 1992

- Bouchta LAYATI

Croissance du GaInAs et de l'AlInAs sur InP par épitaxie par jets moléculaires, DEA d'Electronique, Université des Sciences et Technologies de Lille I, juillet 1992

- Emmanuelle DERON

Analyse de profils Auger lors de l'oxydation plasma d'alliages SiGe, DEA de Sciences des Matériaux, Université des Sciences et Technologies de Lille I, juillet 1994.

- Serge ROSCISZEWSKI

Etude de l'oxyde formé par oxydation assistée par plasma d'alliages SiGe, DEA de Sciences des Matériaux, Université des Sciences et Technologies de Lille I, juillet 1996.

- Thomas GEHIN

Etude et optimisation de l'interface entre semiconducteurs III-V phosphorés et arséniés épitaxiés par jets moléculaires, DEA de Sciences des Matériaux, Université des Sciences et Technologies de Lille I, juillet 2000.

- Sébastien DHELLEMMES

Etude des surfaces de semi-conducteurs phosphorés par spectroscopie de photoélectrons, DEA de Sciences des Matériaux, Université des Sciences et Technologies de Lille I, juillet 2002.

- Bastien PINSARD

Croissance d'hétérostructures de semi-conducteurs III-V pour composants balistiques, Université des Sciences et Technologies de Lille I, juin 2003.

- Julien LASTENNET

Croissance d'hétérostructures de semi-conducteurs III-V à canal InAs pour composants balistiques, Université des Sciences et Technologies de Lille I, en cours

Participation à l'encadrement de thèses

- Hong Sheng ZENG

Etude de la formation de films minces de siliciures de fer par spectroscopies d'électrons, spécialité Sciences des Matériaux, Université des Sciences et Technologies de Lille I, octobre 1991.

- Claude TETELIN

Oxydation basse température assistée par plasma des alliages silicium-germanium, spécialité Sciences des Matériaux, Université des Sciences et Technologies de Lille I, mars 1996.

- Bouchta LAYATI

Contribution à l'étude d'hétérostructures AlInAs/GaInAs épitaxiées par jets moléculaires sur substrats InP, spécialité Electronique, Université des Sciences et Technologies de Lille I, décembre 1996.

- Olivier DEHAESE

Contribution à l'étude d'interfaces de semiconducteurs III-V par spectroscopies de photoélectrons : cas de l'interface GaAs-GaInP, spécialité Sciences des Matériaux, Université des Sciences et Technologies de Lille I, juillet 1997.

- Thomas GEHIN (co-directeur)

Mise en œuvre de l'épitaxie par jets moléculaires pour la croissance de diamant monocristallin, spécialité Sciences des Matériaux, Université des Sciences et Technologies de Lille I, décembre 2004.

- Sébastien DHELLEMMES (co-directeur)

Epitaxie par jets moléculaires à grande échelle de semi-conducteurs phosphorés, en cours.

Participation à des jurys de thèse

- Hong Sheng ZENG

Etude de la formation de films minces de siliciures de fer par spectroscopies d'électrons, spécialité Siences des Matériaux, Université des Sciences et Technologies de Lille I, octobre 1991

- Jean-Marc ROGEZ

Caractérisation électrique d'hétérostructures III-V, étude de l'influence de défauts d'irradiation et d'interface, spécialité Siences des Matériaux, Université des Sciences et Technologies de Lille I, octobre 1993

- Claude TETELIN

Oxydation basse température assistée par plasma des alliages silicium-germanium, spécialité Siences des Matériaux, Université des Sciences et Technologies de Lille I, mars 1996

- Bouchta LAYATI

Contribution à l'étude d'hétérostructures AlInAs/GaInAs épitaxiées par jets moléculaires sur substrats InP, spécialité Electronique, Université des Sciences et Technologies de Lille I, décembre 1996

- Olivier DEHAESE

Contribution à l'étude d'interfaces de semiconducteurs III-V par spectroscopies de photoélectrons : cas de l'interface GaAs-GaInP, spécialité Siences des Matériaux, Université des Sciences et Technologies de Lille I, juillet 1997

- Frédéric DIETTE

Etude des transistors à effet de champ de type HEMT sur substrat GaAs et InP pour l'amplification de puissance en gamme millimétrique, spécialité Electronique, Université des Sciences et Technologies de Lille I, janvier 1998

- Pascal CHEVALIER

Conception et réalisation de transistors à effet de champ de la filière AlInAs/GaInAs sur substrat InP. Application à l'amplification faible bruit en ondes millimétriques, spécialité Electronique, Université des Sciences et Technologies de Lille I, novembre 1998

- Fahrid MEDJDOUB

spécialité Electronique, Université des Sciences et Technologies de Lille I, décembre 2004

- Thomas GEHIN

Mise en œuvre de l'épitaxie par jets moléculaires pour la croissance de diamant monocristallin, spécialité Sciences des Matériaux, Université des Sciences et Technologies de Lille I, décembre 2004.

Organisation de conférences

- Participation à l'organisation de la 15ème European Conference on Surface Science, Lille, septembre 1995 – responsable de l'exposition de matériel scientifique.
- Participation à l'organisation des Journées Surfaces et Interfaces 2003, Villeneuve d'Ascq, janvier 2003.
- Participation à l'organisation du Congrès général de la Société Française de Physique, Lille, septembre 2005 – responsable de l'exposition de matériel scientifique.

Valorisation

- Contrat MRT N° 90 S 0248

Photodétecteur intégrable en siliciure de fer - épitaxie sur silicium,
Caractérisation par spectroscopie Auger de couches de siliciures obtenues de fer obtenues par épitaxie en phase solide et par dépôt en phase vapeur aux organométalliques

Epitaxie d'hétérostructures à base de semi-conducteurs III-V

L'expérience acquise dans ce domaine m'a permis de participer à divers contrats ayant pour objet la réalisation de transistors ou de circuits micro-ondes.

- Contrat DRET91/113

Etude prospective des potentialités de transistors à effet de champ à base de GaInAs sur InP,

- Contrats DGA 94-160 et 97-057

Transistors des filières InP, Métamorphiques et phosphure

- Contrat européen Nano-Tera IST-2001-32517

Ballistic Nanodevices for Terahertz Data Processing

Caractérisation XPS

- Programme Matériaux CNRS, appel d'offres 1998

Films moléculaires greffés directement sur silicium : fonctionnalisation et nanostructuration

- Projet européen SODAMOS IST-2000-26475

5ème partie

Annexes

Liste des publications et communications

Revues à comité de lecture

1. Wallart X., Nys J.P., Dalmai G., Lefebvre I., Lannoo M.
Combined experimental and theoretical study of the Si $L_{23}VV$ Auger line shape during Ti-Si interface formation, Europhys. Lett. **10**, 587 (1989)

2. Wallart X., Nys J.P., Zeng H.S., Dalmai G., Lefebvre I., Lannoo M.
Auger and electron-energy-loss spectroscopy study of interface formation in the Ti-Si system, Phys.Rev. **B41**, 3781 (1990)

3. Wallart X., Zeng H.S., Nys J.P., Dalmai G., Friedel P.
An Auger and electron energy loss study of the Ti-SiO2 interface reactivity, J.Appl.Phys.**69**, 8168 (1991)

4. Stievenard D., Wallart X., Mathiot D.
Deep level transient spectroscopic characterization of silicon-silicon interfaces, J.Appl.Phys. **69**, 7640 (1991)

5. Zeng H.S., Wallart X., Nys J.P., Dalmai G., Friedel P.
Probing the local atomic environment at the interfaces in the Fe-Si system by the surface-extended energy-loss fine-structure technique, Phys.Rev. **B44**, 13811 (1991)

6. Wallart X., Nys J.P., Tételin C.
Growth of ultra-thin iron silicide films : observation of the γ-$FeSi_2$ phase by electron spectroscopies, Phys.Rev.**B49**, 5714 (1994)

7. Vignaud D., Wallart X., Mollot F.
InAlAs/InP heterostructures : influence of a thin InAs layer at the interface, J.Appl.Phys.**76**, 2324 (1994)

8. André J.P., Alaoui H., Deswarte A., Zheng Y., Petroff J.F., Wallart X., Nys J.P.
Iron silicides growth on Si(111) substrate using metal-organic vapour phase epitaxy, J.Cryst.Growth **144**, 29 (1994)

9. Dehaese O., Wallart X., Mollot F.
Kinetic model of element III segregation during molecular beam epitaxy of III-III'-V semiconductor compounds, Appl.Phys.Lett.**66**, 52 (1995)

10. Dehaese O., Wallart X., Schuler O., Mollot F.
As surface segregation during the growth of GaInP on GaAs, J. Journ. Appl. Phys. **36**, 6620 (1997)

11. Tételin C., Wallart X., Stièvenard D., Nys J.P., Gravesteijn D.J.
Evidence of Ge island formation during thermal annealing of SiGe alloys : combined atomic force microscopy and Auger electron spectroscopy study, J. Vac. Sci. Technol. **B16**, 137 (1998)

12. Tételin C., Wallart X., Nys J.P., Vescan L., Gravesteijn D.J.
Kinetics and mechanism of low-temperature atomic oxygen-assisted oxidation of SiGe layers, J. Appl. Phys. **83**, 2842 (1998)

13. Vignaud D., Wallart X., Mollot F.
Direct and inverse equivalent InAlAs-InP interfaces grown by gas-source molecular beam epitaxy, Appl. Phys. Lett. **72**, 1075 (1998)

14. Vignaud D., Wallart X., Mollot F., Sermage B.
Photoluminescence study of the interface in type II InAlAs_InP heterostructures, J. Appl. Phys. **84**, 2138 (1998)

15. Grandidier B., Stièvenard D., Nys J.P. , Wallart X.
Microscopic behaviour of silicon in silicon delta-doped layer in GaAs, Appl. Phys. Lett. **72**, (1998)

16. Allongue P., Henry De Villeneuve C., Pinson J., Ozanam F., Chazalviel J.N., Wallart X.
Organic monolayers on Si(111) by electrochemical method, Electrochemical Acta **43**, 2791 (1998)

17. Schuler O., Dehaese O., Wallart X., Mollot F.
Interface quality and electron transfert at the GaInP on GaAs interface, J. Appl. Phys. **84**, 766 (1998)

18. Dehaese O., Wallart X., Schuler O., Mollot F.
X-ray photoemission characterization of interface abruptness and band offset of $Ga_{0.5}In_{0.5}P$ grown on GaAs, J. Appl. Phys**. 84**, 2127 (1998)

19. Chevalier P., Wallart X., Bonte B., Fauquembergue R.
V-band high-power/low voltage InGaAs/InP composite channel HEMTs, Electronics Letters **34**, 409 (1998)

20. Piotrowicz S., Gaquière C., Bonte B., Bourcier E., Théron D., Wallart X., Crosnier Y.
Best combination between power density, efficiency, and gain at V-band with an InP-based PHEMT structure, IEEE Microwave and Guided Wave Lett. **8**, 10 (1998)

21. Duez V., Vanbésien O., Lippens D., Vignaud D., Wallart X., Mollot F.
Type II and mixed type I-II radiative recombinations in AlInAs-InP heterostructures, J. Appl. Phys.**85**, 2202 (1999)

22. Hoel V., Boret S., Grimbert B., Apercé G., Bollaert S., Happy H., Wallart X., Cappy A.
94 GHz low noise amplifier on InP in coplanar technology, Microwave Engineering Europe, Novembre, 51 (1999)

23. Wallart X., Schuler O., Deresmes D., Mollot F.
Composition effect on the growth mode, strain relaxation and critical thickness of tensile $Ga_{1-x}In_xP$ layers, Appl. Phys. Lett. **76**, 2080 (2000)

24. Boudart B., Trassaert S., Wallart X., Pesant J.C., Yaradou O., Théron D., Crosnier Y., Lahreche H., Omnes F.
Comparison between TiAl and TiAlNiAu ohmic contacts to n-type GaN, Journal of Electronic Materials **29**, 603 (2000)

25. Wallart X., Priester C., Deresmes D., Mollot F.,
Interplay between segregation, roughness and local strains in the growth of $Ga_{0.75}In_{0.25}P$ alloy, Appl. Phys. Lett.**77**, 253 (2000)

26. Lefebvre-Devos I., Lasalle M., Wallart X., Olivier-Fourcade J., Monconduit L., Jumas J.C.,
Bonding in skutterudites : combined experimental and theoretical characterization of $CoSb_3$, Phys. Rev.**B.63**, 125110 (2001)

27. Roch I ;, Buchaillot L., Wallart X., Collard D.,
Silicon nitride as an effective protection against oxidation of a TiNi thin film in high temperature oxidizing air environment at atmospheric pressure, J. Vac. Sci. Technol. **B19**, 305 (2001)

28. Wallart X., Deresmes D., Mollot F.,
Relationship between surface reconstruction and morphology of strained $Ga_{1-x}In_xP$ layers grown on GaP (001) by Gas Source Molecular Beam Epitaxy, Appl. Phys. Lett. **78**,2961 (2001)

29. Boudrissa M., Delos E., Wallart X., Théron D., De Jaeger J.C.,
A 0.15 mm 60GHz High power composite channel GaInAs/InP HEMT with low gate current, El. Device Lett. **22**, 257 (2001)

30. Wallart X.,
A combined RHEED and photoemission comparison of the GaP and InP (001) (2x4) surface reconstructions, Surf. Sci. **506**, 203 (2002)

31. Bollaert S., Wallart X., Lepilliet S., Cappy A., Jalaguier E., Pocas S., Aspar B.,
0.12 μm Transferred-Substrate $In_{0.52}Al_{0.48}As/In_{0.53}Ga_{0.47}As$ HEMTs on silicon wafer, El. Device Lett.**23**, 73 (2002)

32. Wallart X., Priester C., Deresmes D., Gehin T. and Mollot F.,
Why do (2x4) GaAs and InAs (001) surfaces exposed to phosphorus have so different behavior? Elastic strain arguments, Appl. Phys. Lett.**81,** 1086 (2002)

33. Hackens B., Delfosse F., Faniel S., Gustin C., Boutry H., Wallart X., Bollaert S., Cappy A., Bayot V.,
Long dephasing time and high-temperature conductance fluctuations in an open InGaAs quantum dot, Phys. Rev. **B66**, 241305(R) (2002)

34. Wallart X., Priester C.,
Experimental and theoretical investigation of the $Ga_{1-x}In_xAs$ surface reactivity to phosphorus, Phys. Rev. **B68**, 235314 (2003).

35. Larrieu G., Dubois E., Wallart X., Baie X., Katcki J.,
Formation of Pt-based silicide contacts : kinetics, stoechiometry and current drive capabilities, J. Appl. Phys. **94**, 7801 (2003)

36. Wichmann N., Duszynski I., Wallart X., Bollaert S., Cappy A.,
InAlAs-InGaAs double-gate HEMTs on transferred substrate, El. Device Lett. **25**, 354 (2004)

37. Laszcz A., Katcki J., Ratajczak J., Larrieu G., Dubois E., Wallart X.,
Transmission electron microscopy of irridium silicide contacts for advanced MOSFET structures with Schottky source and drain, J. Alloy and Compounds **382,** 24 (2004)

38. Haeckens B., Gence L., Gustin C., Wallart X., Bollaert S., Cappy A., Bayot V.,
Sign reversal and tunable rectification in a ballistic nanojunction, Appl. Phys. Lett. **85**, 4508 (2004)

39. Coffinier Y., Olivier C., Perzyna A., Grandidier B., Wallart X., Durand J.-O., Melnyk O., Stiévenard D.,
Semicarbazide-functionalized Si(111) surfaces for the site-specific immobilisation of peptides, Langmuir **21**, 1489 (2005)

40. Wallart X., Pinsard B., Mollot F.,
High mobility InGaAs/InAlAs pseudomorphic heterostructures on InP(001), J. Appl. Phys.**97**, 053706 (2005)

41. Soubiron T., Vaurette V., Nys J.P., Grandidier B., Wallart X., Stiévenard D.,
Molecular interactions of PTCDA on Si(100), Surf. Sci. **581**, 178 (2005)

42. Haeckens B., Faniel S., Gustin C., Wallart X., Bollaert S., Cappy A., Bayot V.,
Dwell time limited coherence in open quantum dots, Phys. Rev Lett. **94**, 146802 (2005)

43. Wallart X., Henry de Villeneuve C., Alongue P.,
Truly quantitative XPS characterization of organic monolayers on silicon : Study of alkyl and alkoxy monolayers on H-Si(111), J. Am. Chem. Soc. **127**, 7871 (2005)

44. Wichmann N., Duszynski I., Wallart X., Bollaert S., Cappy A.,
Fabrication and Characterization of 100-nm $In_{0.53}Ga_{0.47}As$-$In_{0.52}Al_{0.48}As$ Double-Gate HEMTs With Two Separate Gate Controls, El. Device Lett. **26**, 601 (2005)

45. Medjdoub F., Zaknoune M., Wallart X., Gaquière C., Theron D.,
94 GHz high power performances of $InAs_{0.4}P_{0.6}$ channel HEMTs on InP, El. Letters **41**, 769 (2005)

46. Boukherroub R., Wallart X., Szunerits S., Marcus B., Bouvier P., Mermoux M.,
Photochemical oxidation of hydrogenated boron-doped diamond surfaces, Electrochemistry Communications **7**, 937 (2005)

47. Wallart X., Lastennet J., Vignaud D., Mollot F.,
Performances and limitations of InAs/InAlAs metamorphic heterostructures on InP for high mobility devices, Appl. Phys. Lett. **87**, 043504 (2005)

48. Ardès-Guisot N., Durand J.O., Granier M., Perzyna A., Coffinier Y., Grandidier B., Wallart X., Stievenard D., *Trichlorosilane Isocyanate as Coupling Agent for Mild Conditions Functionalization of Silica-Coated Surfaces,*Langmuir **21**, 9406 (2005)

49. Medjdoub F., Zaknoune M., Wallart X., Gaquière C., Dessenne F., Thobel J.L., Theron D., *InP HEMT Downscaling for PowerApplications at W Band*, Trans. El. Devices **52**, 2136 (2005)

50. Medjdoub F., Zaknoune M., Wallart X., Gaquière C., Theron D., *High Performances of InP channel Power HEMT at 94-GHz*, accepté à El. Letters (2005)

Actes de colloques à comité de lecture

51. Dalmai G., Nys J.P., Wallart X., *Study of Ti silicides growth on Si heated at different temperatures*, Le Vide, Les Couches Minces **42**, 133 (1987)

52. Wallart X., Nys J.P., Dalmai G., *Early stages characterization of the formation of $TiSi_2$ on Si(100)*, Appl. Surf. Sci. **38**, 49 (1989)

53. Rocher A., Wallart X., Charasse M.N., *Moiré pattern studies on thin layers deposited on (001)Si substrates : cases of $TiSi_2$ and GaAs*, Mat. Res. Soc. Symp. Proc. **148**, 95 (1989)

54. Wallart X., Nys J.P., Zeng H.S., Dalmai G., *Correlation between electrical and microscopic properties of Ti-Si interfaces*, Vacuum **41**,1043 (1990)

55. Wallart X., Zeng H.S., Nys J.P., Dalmai G., *Electron spectroscopy study of the Fe/Si(111) and $FeSi_2$/Si(111) interface formation*, Mat.Sci.Eng. **B9**, 253 (1991)

56. Wallart X., Zeng H.S., Nys J.P., Dalmai G., *Electron spectroscopy study of the Fe/Si(111) interface formation and reactivity upon annealing*, Appl.Surf.Sci. **56-58,** 427 (1992)

57. Wallart X., Nys J.P., Dehaese O., Vincent G., *Study of the epitaxy of β-$FeSi_2$ by codeposition of Fe and Si on Si(111)*, Appl.Surf.Sci. **70-71**, 598 (1993)

58. Westphalen R., Boudart B., Théron D., Wallart X., Druelle Y., Crosnier Y., *Temperature measurements of LT GaAs diodes*, Mat. Sci. and Eng. **B22**, 78 (1993)

59. Mounaix P., Wallart X., Libberecht J.M., Lippens D., *Charge distribution and capacitance of double barrier resonnant tunneling diodes*, Proceedings of the 5th Intenational Conference on Simulation of Semiconductor Devices and Processes, 329, Springer-Verlag (1993)

60. Tételin C., Wallart X., Nys J.P., Vescan L., *Germanium behaviour during the low temperature plasma assisted oxidation of SiGe alloys*, Surf.Int.An. **23**, 363 (1995)

61. Tételin C., Wallart X., Vescan L., Nys J.P., *Plasma assisted oxidation of SiGe layers at 500°C : interface characterization*, Appl.Surf.Sci. **104/105**, 385 (1996)

62. Schuler O., Dehaese O., Wallart X., Mollot F., *A study of GaInP-GaAs interfaces : metallurgical coupling of successive quantum wells*, Superlattices and Microstructures **23**, 265 (1998)

63. Lampin J.F., Wallart X., Gouy J.P., Mollot F.,
Light-hole resonant tunneling through tensile-strained GaInAs quantum wells, Superlattices and Microstructures **24**, 273 (1998)

64. Dehaese O., Wallart X., Schuler O., Mollot F.,
XPS study of GaInP on GaAs interface, Appl. Surf. Sci **123/124**, 527 (1998)

65. Schuler O., Wallart X., Mollot F.,
A gas-source MBE growth study of strained $Ga_{1-x}In_xP$ layers on GaAs, J. Cryst. Growth **201/202**, 280 (1999)

66. Wallart X., Mollot F.,
Strained layer growth of $Ga_{1-x}In_xP$ on GaAs (100) and GaP (100) substrates, Appl. Surf. Sci.**166**, 446 (2000)

67. Wallart X., Deresmes D., Mollot F.,
Growth of strained $Ga_{1-x}In_xP$ layers on GaP (001) by Gas Source Molecular Beam Epitaxy: similarities and differences with the growth of strained arsenides, J. Crystal Growth.**227-228**, 255 (2001)

68. Wallart X., Bollaert S., Lepilliet S., Cappy A., Jalaguier E., Mateos J.,
0.12µm gate length $In_{0.52}Al_{0.48}As/In_{0.53}Ga_{0.47}As$ HEMTs on transferred substrate, Institute of Physics Conference Series **170**, 101 (2002)

69. Hackens B., Faniel S., Delfosse F., Gustin C., Boutry H., Huynen I., Wallart X., Bollaert S., Cappy A., Bayot V.,
Long dephasing time and high temperature ballistic transport in an InGaAs open quantum dot, Proceedings of the International Conference on Superlattices, Nano-structures and Nano-devices (ICSNN 2002), Physica **E 17**, 143 (2003)

70. Wallart X., Pinsard B., Mollot F.,
High In content pseudomorphic InGaAs layers for high mobility heterostructures on InP(001), J. Crystal Growth. **278** (2005) 516.

71. Dhellemmes S., Godey S., Wilk A., Wallart X., Mollot F.,
As–P interface-sensitive GaInP/GaAs structures grown in a production MBE system, J. Crystal Growth **278** (2005) 564.

72. Gehin T., Wallart X., Vignaud D.,
Methyl radical beam sources for ultra high vacuum applications, phys. stat. sol. (a) **202**, 2085 (2005)

Publications dans des revues sans comité

73. Diette F., Théron D., Wallart X., Muller M., François M., Delos E., Gaquière C., Crosnier Y.,
Optimisation of the recess configuration in AlInAs/GaInAs HEMT's, IEEE Proceedings of IPRM96, 20 (1996)

74. Chevalier P., Wallart X., Mollot F., Bonte B., Fauquembergue R.,
Composite channel HEMTs for millimeter-wave power applications, IEEE proceedings of IPRM-X, Tsukuba, 207 (1998)

75. Schuler O., Wallart X., Mollot F.,
An experimental study of the relaxation behaviour of strained GaInP grown on GaAs, IEEE Proceedings of IPRM-X, Tsukuba, 615 (1998)

76. Wallart X., Deresmes D., Mollot F.,
Growth of strained $Ga_{1-x}In_xP$ layers on GaP(001) by Gas source molecular beam epitaxy : comparison with the GaInAs/GaAs system, IEEE Proceedings of IPRM 2000, 231 (2000)

77. Zaknoune M., Schuler O., Wallart X., Piotrowicz S., Mollot F., Théron D., Crosnier Y.,
AlGaInP barrier layer grown by Gas Source Molecular Beam Epitaxy for V-band AlGaInP/InGaAs/GaAs power pseudomorphic HEMT, *IEEE Proceedings of IPRM 2000, 353 (2000)*

78. Boudrissa M., Delos E., Wallart X., Théron D., De Jaeger J.C.,
A 60 GHz High power composite channel GaInAs/InP HEMT on InP substrate with L_G=0.15 µm, IEEE Proceedings of IPRM 2001, 196 (2001)

79. Parenty T., Bollaert S., Mateos J., Wallart X., Cappy A.,
Design and realization of sub 100 nm gate fength HEMTs, IEEE Proceedings of IPRM 2001, 626 (2001)

80. Mateos J., Gonzales T., Pardo D., Bollaert S., Wallart X., Cappy A.,
Improvement of the high frequency performance of HEMTs by bufferless technology, IEEE Proceedings of IPRM 2002, 173 (2002)

81. Bollaert S., Parenty T., Wallart X., Happy H., Dambrine G., Cappy A.,
HEMT design for applications beyond 100 GHz, GaAs 2002, Milan, Italie septembre 2002, 45 (2002)

82. Wichmann N., Duszynski I., Parenty T., Bollaert S., Mateos J., Wallart X., Cappy A.,
Double-gate HEMTs on transferred substrate, IEEE Proceedings of IPRM 2003, 118 (2003)

83. Mateos J., Vasallo B.G., Pardo D., Gonzales T., Boutry H., Hackens B., Bayot V., Bednarz L., Simon P., Huynen I., Galloo J.S., Pichonat E., Roelens Y., Wallart X., Bollaert S., Cappy A.,
Room temperature nonlinear transport in InGaAs/AlInAs based ballistic nanodevices, IEEE Proceedings of IPRM 2003, 484 (2003)

84. Wichmann N., Duszynski I., Bollaert S., Wallart X., Cappy A.,
InAlAs/InGaAs double-gate HEMTs with high extrinsic transconductance, IEEE Proceedings of IPRM 2004, Kagoshima, juin 2004, p.295.

85. Dhellemmes S., Godey S., Wilk A., Wallart X., Mollot F.,
Characterization of As-P interface-sensitive GaAs/GaInP structures grown on a production MBE system, IEEE Proceedings of IPRM 2004, Kagoshima, juin 2004, p.159.

86. Galloo J.S., Pichonat E., Roelens Y., Bollaert S., Wallart X., Cappy A., Mateos J., Gonzales T.,
Transition from ballistic to ohmic transport in T-branch Junctions at room temperature in GaInAs/AlInAs heterostructures, IEEE Proceedings of IPRM 2004, Kagoshima, juin 2004, p.378.

87. Wallart X., Lastennet J., Mollot F.,
High mobility InAs/AlInAs metamorphic heterostructures on InP (001), IEEE Proceedings of the 17th IPRM, Glasgow (2005)

88. Medjdoub F., Zaknoune M., Wallart X., Théron D.,
Power potentiality at 94 GHz of InP HEMTS with large bandgap channels, IEEE Proceedings of the 17th IPRM, Glasgow (2005)

Communications à des congrès, symposium

1. Dalmai G., Nys J.P., Wallart X.,
AES study of the growth of $TiSi_2$ on Si(111), 8th European Conference On Surface Science, Jülich (1986) (poster)

2. Dalmai G., Nys J.P., Wallart X.,
Quantitative model of reactive titanium-silicon interface growth, 4th Conference on Quantitative Surface Analysis, Teddington (1986) (poster)

3. Dalmai G., Nys J.P., Wallart X.,
Study of reactive silicon-titanium interface growth, Conférence de la Société Belge de Physique, Namur (1987) (poster)

4. Dalmai G., Nys J.P., Wallart X.,
Study of Ti silicides growth on silicon heated at different temperatures, European Workshop on refractory metal silicides, Aussois (1987) (poster)

5. Wallart X., Nys J.P., Dalmai G.,
Use of Auger line shape analysis for the study of interface formation in the Ti-Si system, Symposium on the Auger effect, Paris (1989) (poster)

6. Wallart X., Nys J.P., Dalmai G.,
Early stages characterization of the formation of $TiSi_2$ on Si(100), European Workshop on Refractory Metal Silicides, IMEC, Louvain (1989) (orale)

7. Wallart X., Nys J.P., Zeng H.S., Dalmai G.,
Correlation between electrical and microscopic properties of Ti-Si interfaces, 7th International Conference on Solid Surfaces, Cologne (1990) (orale)

8. Wallart X., Nys J.P., Zeng H.S., Dalmai G.,
Electron spectroscopy study of the Fe/Si(111) and $FeSi_2$/Si(111) interface formation, European MRS Fall Meeting, Strasbourg (1990) (poster)

9. Wallart X., Nys J.P., Zeng H.S., Dalmai G.,
An electron spectroscopy study of the Fe-Si system reactivity, Réunion de la Société Belge de Physique, Gand (1991) (poster)

10. Wallart X., Nys J.P., Zeng H.S., Dalmai G.,

Electron spectroscopy study of the Fe/Si(111) interface formation and reactivity upon annealing, 3rd International Conference on the Formation of Semiconductor Interfaces, Rome (1991) (orale)

11. Wallart X., Dehaese O., Nys J.P., Vincent G.,

Study of the epitaxy of β-$FeSi_2$ by codeposition of Fe and Si on Si(111), 8th International Conference on Solid Surfaces, La Haye (1992) (poster)

12. Westphalen R., Théron D., Wallart X., Druelle Y., Crosnier Y.,
Temperature measurements of low temperature grown GaAs Schottky diodes, E-MRS Spring Meeting, Srasbourg (1993) (présentée par Westphalen R.)

13. Mounaix P., Wallart X., Libberecht J.M., Lippens D.,
Charge distribution and capacitance of double barrier resonant Tunneling diodes, 5th International Conference on Simulation of Semiconductor Devices and Processes, Vienne (1993) (présentée par Mounaix P.)

14. Théron D., Boudart B., Westphalen R., Wallart X., Druelle Y.,
Growth of LT GaAs on GaAs under different conditions, 3rd Heterostructure Technology Workshop, Villeneuve d'Ascq (1993) (présentée par Théron D.)

15. Tételin C., Wallart X., Nys J.P., Vescan L.,
Germanium behaviour during the low temperature plasma assisted oxidation of SiGe alloys, 8th International Conference on Quantitative Surface Analysis, Surrey (1994) (poster)

16. Mollot F., Wallart X., Gouy J.P., Vignaud D.,
What is the composition of lattice matched AlInAs on InP?, 8th European Workshop on Molecular Beam Epitaxy, Sierra Nevada, Espagne (1995) (poster)

17. Tételin C., Wallart X., Stièvenard D., Nys J.P., Gravesteijn D.J.,
Ge surface segregation during thermal annealing of SiGe alloys: a study using AES, LEED and AFM, 15th ECOSS, Lille, France (1995) (poster)

18. Tételin C., Wallart X., Vescan L., NYS J.P.,
Plasma assisted oxidation of SiGe layers at 500°C : interface characterization, 5th ICFSI, Princeton (1995) (présentée par Tételin C.)

19. Diette F., Théron D., Wallart X., Muller M., François M., Delos E., Gaquière C., Crosnier Y.,
Optimisation of the recess configuration in AlInAs/GaInAs HEMT's, InP and related Material Conference, Schwäbisch Gmünd, Allemagne (1996) (présentée par Diette F.)

20. Schuler O., Dehaese O., Wallart X., Mollot F.,
A study of GaInP-GaAs interfaces : metallurgical coupling of successive quantum wells, 9th ICSMM, Liège (1996) (présentée par Schuler O.)

21. Lampin J.F., Wallart X., Gouy J.P., Mollot F.,
Light-hole resonant tunneling through tensile-strained GaInAs quantum wells, 9th ICSMM, Liège (1996) (présentée par Lampin J.F.)
22. Dehaese O., Wallart X., Schuler O., Mollot F.,
XPS study of GaInP/GaAs and AlInP/GaAs interfaces composition profile, 5th ICSOS, Aix-en -Provence, (1996) (poster)

23. Tételin C., Nys J.P., Gravesteijn D.J., Vescan L., Wallart X.,
Interface structure of plasma oxidized SiGe layers, 5th ICSOS, Aix-en -Provence (1996) (poster)

24. Tételin C., Wallart X., Nys J.P., Vescan L., Gravesteijn D.J.,
Kinetics and mechanism of low temperature atomic oxygen assisted oxidation of SiGe layers, 16th ECOSS, Gênes, Italie (1996) (présentée par Tételin C.)

25. Dehaese O., Wallart X., Schuler O., Mollot F.,
Interaction of a (2x4) GaAs surface with phosphorus in gas source molecular beam epitaxy, IX Eurpean Workshop on MBE, Oxford (1997) (poster)

26. Schuler O., Dehaese O., Wallart X., Mollot F.,
Interface quality and electron transfer at the GaInP on GaAs heterojunction, IX Eurpean Workshop on MBE, Oxford (1997) (présentée par Schuler O.)

27. Théron D., Piotrowicz S., Wallart X., Diette F., Bonte B., Crosnier Y.,
InP based HEMT structures with a large bandgap barrier layer for power application in V band, WOCSDICE, Scheveningen, Pays-Bas (1997) (présentée par Théron D.)

28. Dehaese O., Wallart X., Schuler O., Mollot F.,
XPS study of GaInP on GaAs interface, 6th Int. Conf. on the Formation of Semiconductor Interfaces, Cardiff (1997) (poster)

29. Chevalier P., Wallart X., Mollot F., Bonte B., Fauquembergue R.,
Composite channel HEMTs for millimeter-wave power applications, Xth Conference on Indium Phosphide and Related Materials, Tsukuba, (1998) (présentée par Chevalier P.)

30. Schuler O., Wallart X., Mollot F.,
An experimental study of the relaxation behaviour of strained GaInP grown on GaAs, Xth Conference on Indium Phosphide and Related Materials, Tsukuba, (1998) (présentée par Schuler O.)

31. Schuler O., Wallart X., Mollot F.,
A gas-source MBE growth study of strained $Ga_{1-x}In_xP$ layers on GaAs, International Conference on MBE, Cannes (1998) (poster)

32. Hoel V., Bollaert S., Wallart X., Grimbert B., Lepillet S., Cappy A.,
A new gate process for the realization of lattice-matched HEMT on InP for high yield MMICs, International Conference on GaAs (1998) (présentée par Hoel V.)

33. Hoel V., Boret S., Grimbert B., Apercé G., Bollaert S., Happy H., Wallart X., Cappy A.,
94 GHz low noise amplifier on InP in coplanar technology, International Conference on GaAs (1998) (présentée par Hoel V.)

34. Wallart X. , Mollot F.,
*Strained layer growth of $Ga_{1-x}In_xP$ on GaAs (100) and GaP (100) substrates***,** International Conference on the Formation of Semiconductor interfaces, Göteborg (1999) (poster)

35. Hoel V., Boret S., Grimbert B., Apercé G., Decaesteke T., Bollaert S., Wallart X., Lepillet S., Cappy A.,
A 94 GHz CPW low noise amplifier on InP, WOCSDICE 99 (présentée par Hoel V.)

36. Roch I., Buchaillot L., Wallart X.,
Fabrication process of shape memory alloy thin films for microactuation, 3rd Conference on Shape Memory and Superelestic Technolgies, Pacific Grove, California (2000) (présentée par Roch I.)

37. Wallart X., Deresmes D., Mollot F.,
Growth of strained $Ga_{1-x}In_xP$ layers on GaP(001) by Gas source molecular beam epitaxy : comparison with the GaInAs/GaAs system, IPRM 2000, Williamsburg (2000) (orale)

38. Zaknoune M., Schuler O., Wallart X., Piotrowicz S., Mollot F., Théron D., Crosnier Y.,
AlGaInP barrier layer grown by Gas Source Molecular Beam Epitaxy for V-band AlGaInP/InGaAs/GaAs power pseudomorphic HEMT, *IPRM 2000, Williamsburg, (2000) (orale)*

39. Wallart X., Deresmes D., Mollot F.,
Growth of strained $Ga_{1-x}In_xP$ layers on GaP(001) by Gas source molecular beam epitaxy : similarities and differences with the growth of strained arsenides, International Conference on MBE, Pékin (2000) (présentée par Mollot F.)

40. Wallart X., Mollot F.,
RHEED and photoemission study of the GaP(001) and InP(001) surface reconstructions, 11ème European Workshop on Molecular Beam Epitaxy, Hinterzarten (2001) (orale)

41. Parenty T., Bollaert S., Mateos J., Wallart X., Cappy A.,
Design and realization of sub 100 nm gate fength HEMTs, IPRM 2001, Nara (présentée par Parenty T.)

42. Wallart X., Bollaert S., Lepilliet S., Cappy A., Jalaguier E., Mateos J.
0.12µm gate length $In_{0.52}Al_{0.48}As/In_{0.53}Ga_{0.47}As$ HEMTs on transferred substrate, ISCS 2001, Tokyo (poster)

43. Bollaert S., Wallart X., Lepilliet S., Cappy A., Jalaguier E., Pocas S., Aspar B.,
0.12 µm Transferred-Substrate $In_{0.52}Al_{0.48}As/In_{0.53}Ga_{0.47}As$ HEMTs on transferred substrate, GaAs 2001, Londres (présentée par Cappy A.)

44. Faniel S., Hackens B., Delfosse F., Gustin C., Boutry H., Huynen I., Bayot V., Wallart X., Bollaert S., Cappy A.,
High temperature conductance fluctuations in an InGaAs/InAlAs open quantum dot, Annual APS March Meeting 2002, Indianapolis (présentée par Faniel S.)

45. Mateos J., Gonzales T., Pardo D., Bollaert S., Wallart X., Cappy A.,
Improvement of the high frequency performance of HEMTs by bufferless technology, IPRM 2002, Stockholm (poster)

46. Wallart X., Priester C., Deresmes D., Mollot F.,
Some key features of the $Ga_{1-x}In_xAs$ surface reactivity to phosphorus, ICMBE XII, San Francisco (2002) (orale)

47. Priester C., Wallart X.,
On the role of strains, surface reconstruction and morphology on interface intermixing during III-V heterostructure growth, MRS Fall Meeting, Boston (2002) (présentée par Priester C.)

48. Wichmann N., Duszynski I., Parenty T., Bollaert S., Mateos J., Wallart X., Cappy A.,
Double-gate HEMTs on Transferred Substrate, IPRM 2003, Santa Barbara (poster)

49. Mateos J., Vasallo B.G., Pardo D., Gonzales T., Boutry H., Hackens B., Bayot V., Bednarz L., Simon P., Huynen I., Ganoo J.S., Roelens Y., Wallart X., Bollaert S., Cappy A.,
Room temperature Nonlinear Transport in InGaAs/AlInAs Based Ballistic Nanodevices, IPRM 2003, Santa Barbara (poster)

50. Larrieu G., Dubois E., Wallart X.,
Performance of platinum silicide for low barrier Schottky contacts p-MOSFET, Spring Meeting du MRS, Boston, avril 2003 (présenté par G. Larrieu)

51. Soubiron T., Vaurette F., Grandidier B., Wallart X., Nys J.P., Stiévenard D.,
Adsorption of PTCDA on Si(001) and Si(001)-H, Nanotech 2004, Boston, mars 2004.

52. Wichmann N., Duszynski I., Bollaert S., Wallart X., Cappy A.,
InAlAs/InGaAs double-gate HEMTs with high extrinsic transconductance, IPRM 2004, Kagoshima, juin 2004 (présenté par Wichmann N.)

53. Dhellemmes S., Godey S., Wilk A., Wallart X., Mollot F.,
Characterization of As-P interface-sensitive GaAs/GaInP structures grown on a production MBE system, IPRM 2004, Kagoshima, juin 2004 (poster)

54. Galloo J.S., Pichonat E., Roelens Y., Bollaert S., Wallart X., Cappy A., Mateos J., Gonzales T.,
Transition from ballistic to ohmic transport in T-branch Junctions at room temperature in GaInAs/AlInAs heterostructures, IPRM 2004, Kagoshima, juin 2004 (poster)

55. X. Wallart, B. Pinsard and F. Mollot
High In content pseudomorphic InGaAs layers for high mobility heterostructures on InP (001), ICMBE XIII, Edimbourg, août 2004 (orale)

56. S. Dhellemmes, S. Godey, A. Wilk, X. Wallart and F. Mollot,
As-P interface-sensitive GaInP/GaAs structures grown in a production MBE system, ICMBE XIII, Edimbourg, août 2004 (présenté par S. Dhellemmes)

57. Wallart X., Lastennet J., Mollot F.,
Metamorphic growth of InAs/InAlAs heterostructures on InP(001) substrates, 13ème European Workshop on Molecular Beam Epitaxy, Grindelwald (2005) (poster)

58. Géhin T., Wallart X., Vignaud D.,
Methyl radical beam sources for ultra high vaccum applications, 10ème Worksop on Surface and Bulk Defects in Diamond, Hasselt (2005) (présenté par T. Géhin)

59. Wallart X., Lastennet J., Mollot F.,
High mobility InAs/AlInAs metamorphic heterostructures on InP (001), IPRM 2005, Glasgow, mai 2005 (présentée par F. Mollot)

60. Medjdoub F., Zaknoune M., Wallart X., Théron D.,
Power potentiality at 94 GHz of InP HEMTS with large bandgap channels, IPRM 2005, Glasgow, mai 2005 (présentée par F. Medjdoub)

Séminaires, workshops

1. Dalmai G., Nys J.P., Wallart X.,
Etude de l'interface silicium-siliciure de titane, Réunion du GCIS, Toulouse (1986) (orale)

2. Dalmai G., Nys J.P., Wallart X.,
Etude de l'oxydation du siliciure de titane, Réunion sur les diélectriques et l'oxydation, Paris (1986) (poster)

3. Dalmai G., Ducroux M.C., Nys J.P., Wallart X.,
Etude par analyse de la forme des raies Auger des interfaces silicium-carbone et silicium-siliciure, Congrès des Matériaux, Paris (1986) (poster)

4. Dalmai G., Nys J.P., Wallart X.,
Etude de la formation de $TiSi_2$ sur silicium chauffé, Réunion du GCIS, Toulouse (1987) (orale)

5. Wallart X., Nys J.P., Dalmai G.,
Etude des modifications des propriétés de l'interface silicium-siliciure de titane après oxydation du siliciure, Réunion du GCIS, Toulouse (1988) (orale)

6. Wallart X., Nys J.P., Dalmai G.,
Analyse de la structure fine des raies Auger des siliciures de titane, Journées de la Matière Condensée, Toulouse (1988) (poster)

7. Wallart X., Nys J.P., Dalmai G.,
Corrélation entre propriétés microscopiques et électriques d'interfaces silicium-siliciures de titane, Journées de la Matière Condensée, Toulouse (1988) (poster)

8. Wallart X., Nys J.P., Dalmai G.,
Caractérisation et corrélation entre propriétés microscopiques et électriques des interfaces silicium-siliciures de titane, Réunion du GCIS, Toulouse (1989) (orale)

9. Druelle Y., Win P., Cappy A., Wallart X., Bouillet A.,
Croissance de matériau GaInAs relaxé sur substrat GaAs, 9ème Séminaire National EJM, St Aygulf (1992) (présentée par Druelle Y.)

10. Wallart X., Nys J.P., Dehaese O.,
Formation and epitaxy of β-$FeSi_2$ films by Fe and Si coevaporation on Si(111), 3èmes Journées de la Matière Condensée, Lille (1992) (poster)

11. Gouy J.P., Wallart X., Mezzour S., Jaffran A., Harari J., Vilcot J.P., Decoster D.,
Photodétecteur métal-semiconducteur-métal sur substrat InP pour applications micro-ondes, 12ème Colloque Optique Hertzienne et Diélectriques, Paris (1993) (présentée par Gouy J.P.)

12. Dehaese O., Wallart X., Mollot F.,
Modèle cinétique d'échange en croissance épitaxiale, 10éme Séminaire national d'épitaxie par jets moléculaires, St Aygulf (1994) (orale)

13. Théron D., Boudart B., Robert C., Wallart X., Druelle Y.,
GaAs basse température : de la croissance à la réalisation de composants MISFET, 5èmes Journées de microélectronique et optoélectronique III-V, Ecully (1994) (présentée par Théron D.)

14. Wallart X., Layati B., Druelle Y.,
Hétérostructure AlInAs/GaInAs à douple plan de dopage sur substrat InP : élaboration et caractérisation, 5èmes Journées de microélectronique et optoélectronique III-V, Ecully (1994) (poster)

15. Tételin C., Wallart X., Nys J.P.,
Redistribution du germanium durant l'oxydation d'alliages SiGe assistée par plasma, 4èmes Journées de la matière Condensée, Rennes (1994) (poster)

16. Wallart X., Nys J.P.,
Croissance du siliciure de fer : rôle d'une couche tampon, 4èmes Journées de la matière Condensée, Rennes (1994) (poster)

17. Lampin J.F., Wallart X., Gouy J.P., Mollot F.,
Effet Tunnel résonnant de trous légers dans des puits quantiques contraints en extension, 5èmes Journées de la Matière Condensée, Orléans (1996) (présentée par Lampin J.F.)

18. Vignaud D., Trentani A., Wallart X., Mollot F.,
Recombinaisons radiatives spatiallement indirectes (type II) dans des hétérostructures InAlAs/InP : une sonde de l'interface, 5èmes Journées de la Matière Condensée, Orléans (1996) (présentée par Trentani A.)

19. Lampin J.F., Wallart X., Mollot F.,
Détermination du décalage de bande entre GaP et GaAs via l'étude de l'hétérostructure contrainte $GaAs_{1-y}P_y/Ga_{1-x}Al_xAs$, 6èmes Journées Nationales de Microélectronique et Optoélectronique III-V, Chantilly (1997) (poster)

20. Schuler O., Dehaese O., Wallart X., Mollot F.,
Etude des interfaces GaInP/GaAs par photoluminescence et ESCA, 6èmes Journées Nationales de Microélectronique et Optoélectronique III-V, Chantilly (1997) (poster)

21. Bonte B., Diette F., Piotrowicz S., Gaquière C., Wallart X., Théron D., Crosnier Y.,
Utilisation d'AlInAs riche en aluminium pour augmenter la tenue en tension des composants HFET's sur InP, 6èmes Journées Nationales de Microélectronique et Optoélectronique III-V, Chantilly (1997) (poster)

22. Chevalier P., Badirou M., Mollot F., Wallart X., Fauquembergue R.,
HEMT sur substrat InP de longueur de grille Lg=0.15 µm : comparaison entre un canal GaInAs et un canal composite GaInAs/InP, Journées Nationales Microondes, St Malo (1997) (présentée par Chevalier P.)

23. Chevalier P., Badirou M., Mollot F., Wallart X., Fauquembergue R.,
HEMT sur substrat InP de longueur de grille Lg=0.15 µm : comparaison entre un canal GaInAs et un canal composite GaInAs/InP, J.N.M., St-Malo (1997) (présentée par Chevalier P.)

24. Schuler O., Wallart X., Mollot F.,
Etude de la croissance par épitaxie par jets moléculaires à sources gazeuses des alliages GaInP contraints sur GaAs et InP, Journées Nationales Micro et Optoélectronique, Font-Romeu (1999) (présentée par Mollot F.)

25. Wallart X., Priester C., Deresmes D., Mollot F.,
Croissance d'alliages GaInP contraints par Epitaxie à Jets Moléculaires à Sources Gazeuses, Séminaire National sur l'épitaxie par jets moléculaires, EJM 2000, St Aygulf (2000) (orale)

26. Wallart X.,.Deresmes D., Mollot F.,
Croissance d'alliages $Ga_{1-x}In_xP$ sur GaP(100) par Epitaxie à Jets Moléculaires à Sources Gazeuses : influence de la reconstruction de surface, 8èmes Journées Nationales Microélectronique et Optoélectronique 2001, Aussois (2001) (poster)

27. Bonte B., Schoendorff B., Zaknoune M., Mollot F., Wallart X., Théron D.,
Evaluation de composants de la filière phosphure pour applications à 60GHz, 8èmes Journées Nationales Microélectronique et Optoélectronique, Aussois (2001) (poster)

28. Théron D., Boudrissa M., Delos E., Wallart X., De Jaeger J.C.,
Influence du dopage dans les transistors HEMT à canal composite pour amplification de puissance en ondes millimétriques, 12èmes Journées Nationales Microondes, Futuroscope Poitiers (2001) (poster)

29. Priester C., Wallart X.,
Etude expérimentale et théorique de la réactivité des surfaces InAs et GaAs (100) à un flux de phosphore, réunion du GDR Relax, Paris, mars 2002 (orale)

30. Wallart X., Priester C., Deresmes D., Mollot F.
Etude de la réactivité des surfaces d'alliages GaInAs (100) à un flux de phosphore, 9èmes Journées Nationales Microélectronique et Optoélectronique, Saint Aygulf (2002) (poster)

31. Wichmann N., Duszynski I., Parenty T., Bollaert S., Wallart X., Cappy A.,
HEMT double-grille sur substrat reporté, Journées Nationales Microondes, Lille, mai 2003 (poster)

32. Duszynski I., Parenty T., Bollaert S., Mateos J., Wallart X., Cappy A.,
Amélioration du Fmax des HEMTs InAlAs/InGaAs sur substrat d'InP de longueur de grille 70nm par optimisation de la structure de couche, Journées Nationales Microondes, Lille, mai 2003 (présentée par Duszynski I.)

33. Wallart X., Henry de Villeneuve C., Allongue P.,
Caractérisation de films d'alcènes greffés sur des surfaces Si(111) par analyse XPS résolue angulairement, ELSPEC 2004, Saclay, mars 2004 (poster)

34. Medjdoub F., Zaknoune M., Wallart X., Théron D.,
HEMT technology for power applications at 94 GHz and above, 13th European Heterostructure Technology Workshop, Koutouloufari, octobre 2004 (présenté par F. Medjdoub).

Sélection de publications

Kinetic model of element III segregation during molecular beam epitaxy of III-III′-V semiconductor compounds

O. Dehaese, X. Wallart, and F. Mollot
Institut d'Electronique et de Microelectronique du Nord, CNRS-U.M.R. 9929, Avenue Poincaré, BP 59, 59652 Villeneuve d'Ascq Cedex, France

(Received 25 July 1994; accepted for publication 25 October 1994)

Segregation of column III atoms during molecular beam epitaxy of III-III′-V semiconductor compounds causes nonabrupt interfaces and a surface composition different from the bulk one. To derive concentration profiles, a thermodynamical equilibrium model has been used for a long time. This model applies well to describe segregation processes at high growth temperatures, but fails in predicting concentration profile variations with substrate temperature. We have thus developed a kinetic model which correctly takes into account the evolution with the growth temperature. We apply this model to the case of indium segregation in the $Ga_xIn_{1-x}As/GaAs$ system. The calculated indium concentration profiles are compared to those obtained with the thermodynamical equilibrium model. A kinetic limitation of segregation is shown to appear at low substrate temperatures and sufficiently high growth rates. This limitation is predicted to arise below 400 °C for a growth rate of 1 monolayer/s for In segregation in the $Ga_xIn_{1-x}As/GaAs$ system. © *1995 American Institute of Physics.*

Advances in growth techniques, such as molecular beam epitaxy (MBE) have allowed high quality materials with complex structures, like quantum wells or superlattices to be built. These structures require formation of abrupt interfaces between different semiconductor compounds. But the perfection of such heterostructures is limited by physical effects and particularly by surface segregation driven by binding and elastic energy differences.[1] Systems such as GaInAs, AlInAs, GaInP, or AlInP on InP or SiGe on Si are likely to present, respectively, In or Ge segregation. In the most studied $Al_xGa_{1-x}As/GaAs$ system, Ga surface segregation is related to a surface roughness increase.[2–4]

In the case of $Ga_xIn_{1-x}As$ grown on GaAs by MBE, In segregates to the growing surface, resulting in a gradual composition of the interface and an In surface enrichment. The indium surface concentration is not zero even after the deposition of several GaAs monolayers (ML) on InAs. These experimental results have been obtained first by surface sensitive techniques: Auger electron spectroscopy, x-ray or ultraviolet photoemission spectroscopy (XPS, UPS).[1,5,6] Other analysis techniques such as reflection high energy electron diffraction (RHEED)[7] or photoluminescence (PL)[8,9] of quantum wells have led to similar results. More recently, the In concentration profile of a MBE grown nominally GaAs/80 Å $Ga_{0.8}In_{0.2}As/GaAs$ quantum well was derived by Zheng *et al.*[10] using cross-sectional scanning tunneling microscopy. It evidences the broadening of interfaces due to In surface segregation.

Except for this last technique, all others need a theoretical model of segregation to build concentration profiles. In this aim a thermodynamical equilibrium model of surface segregation has been proposed referring to metallurgical science.[11,12] This thermodynamical model well describes concentration profiles at high growth temperatures, but fails in predicting profile variations with substrate temperatures. Thus we have developed a kinetic model which allows us to take into account the evolution of concentration profiles with growth parameters. In an M-N alloy where N is segregating to the surface, the bulk composition is different from the surface one. According to McLean,[11] the thermodynamical equilibrium stems from the balance of surface and bulk chemical potentials and can be represented by a chemical equilibrium equation

$$N_b + M_s \leftrightarrow N_s + M_b\,. \tag{1}$$

Surface and bulk composition are linked by

$$\frac{X_s(1-X_b)}{X_b(1-X_s)} = \exp\left(\frac{E_s}{kT}\right), \tag{2}$$

where T is the absolute temperature, k is the Boltzmann constant, X_s and X_b are the concentrations of N in the surface and bulk phases, and E_s is the difference between bulk and surface free energy.

In metallurgical science, atomic motions in alloys are due to diffusion during high temperature anneals. But growth temperatures for MBE of III-V semiconductors are generally lower and bulk diffusion is not operative.[1,13] Thus atomic rearrangements leading to segregation during epitaxy are surface or near-surface processes. They can be seen as an exchange reaction between substrate or epilayer atoms and impinging ones. The surface phase is defined as the last ML grown and the bulk phase as the previous one. In the case of $Ga_xIn_{1-x}As/GaAs$ which we have chosen to illustrate the models presented in this letter, exchange occurs between Ga and In atoms in these two ML. If we denote $X_s(n)$ and $X_b(n)$ the concentration of In, respectively, in the surface and bulk phases after completion of the nth ML, the In mass conservation gives

$$X_s(n) + X_b(n) = X_s(n-1) + X_\phi\,, \tag{3}$$

where X_ϕ is the nominal In mole fraction in the incident flux. A combination of Eqs. (2) and (3) allows us to build layer by layer the In concentration profile assuming that X_b is frozen as soon as the completion of the surface ML is achieved. The "segregation energy," E_s is the single parameter of the model.

 0003-6951/95/66(1)/52/3/$6.00

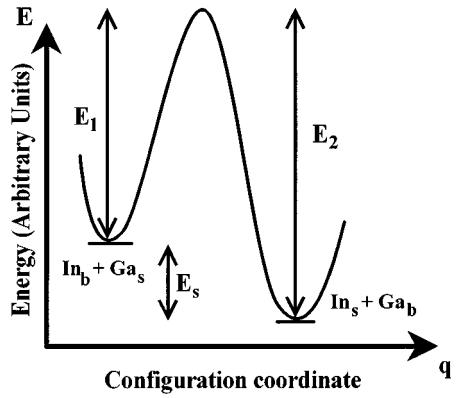

FIG. 1. Configuration diagram for In/Ga exchange process.

With a substrate temperature of ≈500 °C where In reevaporation is negligible, a growth rate of ≈1 ML/s and $E_s=0.2$ eV, calculated In concentration profiles of $Ga_xIn_{1-x}As$ on GaAs are in accordance with experimental measurements of In surface enrichment by XPS,[1] UPS,[6] or RHEED.[7] The failure of this thermodynamical model appears when changing the substrate temperature. When In segregates at the surface, $X_s>X_b$ and considering Eq. (2), it implies that $E_s>0$. The thermodynamical model predicts an increase of segregation because of the term $\exp[E_s/(kT)]$ when decreasing the temperature. On the contrary, experimental results show a decrease of In segregation with temperature. For example, Larive *et al.* have measured the intensity ratio of In $4d$/Ga $3d$ core-level spectra obtained by UPS for 18 ML of $Ga_{0.8}In_{0.2}As$ grown at various temperatures on GaAs substrate.[6] This ratio which is a picture of surface composition, ranges from 1.73 at 490 °C to 2.22 at 560 °C which could be compared to its theoretical value of 0.68 without In surface segregation. This experiment shows unambiguously the increase of segregation with temperature. The same trend is observed for Ga segregation in GaAlAs.[3]

In the case of $Ga_xIn_{1-x}As$ it seems that the assumption of thermodynamical equilibrium is no longer valid below 500 °C for a usual growth rate (≈1 ML/s). Thus, we have developed a kinetic model of exchange processes. Such an approach was first used by Harris *et al.*[14] in the case of Sn segregation in GaAs and by Ni *et al.*[15] for Sb-ion implantation in Si. The difference with In segregation is that Sn or Sb are dopants. Their concentrations in GaAs or Si are orders of magnitude smaller than that of In in $Ga_xIn_{1-x}As$. Thus in the exchange process, dopants always find a free site in the surface phase which is not automatically the case for In atoms. This difference causes a noticeable change in the evolution equation of the In surface concentration which, opposite to Ref. 14, is no longer a first-order differential equation.

The kinetic model is well illustrated by a configuration diagram (Fig. 1) with E being the free energy of the system and q a configuration coordinate. The distance between the energy minima is roughly the ML thickness. Note that E_s is the ''segregation energy'' of the equilibrium model. The exchange process is achieved by overcoming an energy barrier E_1 with a rate

$$P_1=\nu_1 \exp\left(\frac{-E_1}{kT}\right),$$

where ν_1 is a vibration frequency. The reverse exchange is also possible but needs to pass over an $E_2=E_1+E_s$ energy barrier and has a rate

$$P_2=\nu_2 \exp\left(\frac{-E_2}{kT}\right).$$

If we make the assumption that segregation is only due to the exchange process, the evolution of the number of In surface atoms is given by the balance of incoming and leaving In atoms

$$\frac{dX_{\mathrm{In}\,s}(t)}{dt}=\phi_{\mathrm{In}}+P_1X_{\mathrm{In}\,b}(t)X_{\mathrm{Ga}\,s}(t)-P_2X_{\mathrm{In}\,s}(t)X_{\mathrm{Ga}\,b}(t), \tag{4}$$

where ϕ_{In} is the impinging In flux in ML/s and the $X_i(t)$ are time-dependent quantities expressed in fractions of ML. During a time interval dt, the number of In atoms coming in the surface layer is the sum of the impinging In flux and the P_1 rate weighted by the number of exchange possibilities which is simply taken as the product $X_{\mathrm{In}\,b}(t)\ X_{\mathrm{Ga}\,s}(t)$. In the same way, the reverse exchange results in a number of In atoms leaving the surface phase given by $P_2X_{\mathrm{In}\,s}(t)\ X_{\mathrm{Ga}\,b}(t)$. In addition the conservation of In and total surface atom numbers at time t, respectively, leads to

$$X_{\mathrm{In}\,s}(t)+X_{\mathrm{In}\,b}(t)=X_{\mathrm{In}\,s}(0)+X_{\mathrm{In}\,b}(0)+\phi_{\mathrm{In}}t, \tag{5}$$

$$X_{\mathrm{In}\,s}(t)+X_{\mathrm{Ga}\,s}(t)=X_{\mathrm{In}\,s}(0)+X_{\mathrm{Ga}\,s}(0)+(\phi_{\mathrm{In}}+\phi_{\mathrm{Ga}})t. \tag{6}$$

Combination of Eqs. (4)–(6) allows us to obtain a differential equation for $X_{\mathrm{In}\,s}(t)$. The In concentration profile is then built by numerically solving this equation.

The vibration frequencies ν_1 and ν_2 are a combination of surface and bulk lattice vibration frequencies. We have taken $\nu_1=\nu_2=10^{13}\ \mathrm{s}^{-1}$ which seems to be a reasonable value.[15] At high substrate temperature, the rates P_1 and P_2 become sufficiently high to yield the flux term negligible with respect to exchange terms in Eq. (4). Then the stationary state of the system, i.e., $dX_{\mathrm{In}\,s}(t)/dt = 0$ is described by

$$P_1X_{\mathrm{In}\,b}(t)\ X_{\mathrm{Ga}\,s}(t)=P_2X_{\mathrm{In}\,s}(t)\ X_{\mathrm{Ga}\,b}(t)$$

which is the same as Eq. (2). It evidences that at high temperature the kinetic model is equivalent to the thermodynamical one. Thus for the system $Ga_xIn_{1-x}As/GaAs$ we expect the value of $E_s=0.2$ eV (Refs. 1, 6, and 7) deduced from experiments in this condition ($T\geqslant 500$ °C) to be correct. Since the exchange process corresponds to an atomic motion of In and Ga atoms, the energy barrier E_1 must be of the order of element III binding energies in arsenide compounds, i.e., between 1.4 and 2 eV.[1]

Surface segregation limits the formation of abrupt interfaces. Figure 2(a) presents calculated In concentration profiles which show segregation induced broadening of the $Ga_{0.8}In_{0.2}As$ on GaAs interface grown at two different temperatures. Because of segregation effects InAs in GaAs quantum wells are different from nominal ones [Fig. 2(b)].

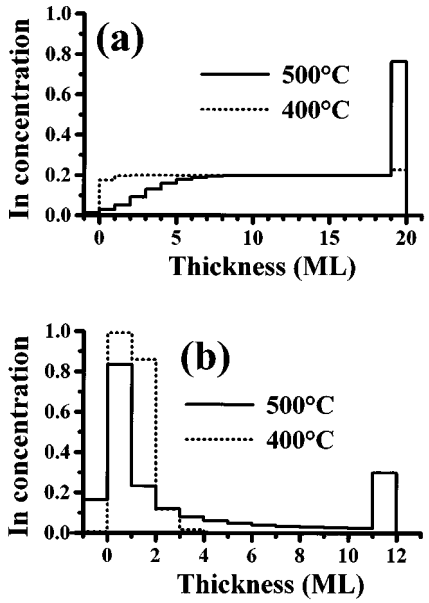

FIG. 2. Indium concentration profile evolution with temperature, growth rate 1 ML/s (a) 20 ML $Ga_{0.8}In_{0.2}As$ on GaAs, (b) 10 ML GaAs/2 ML InAs/GaAs.

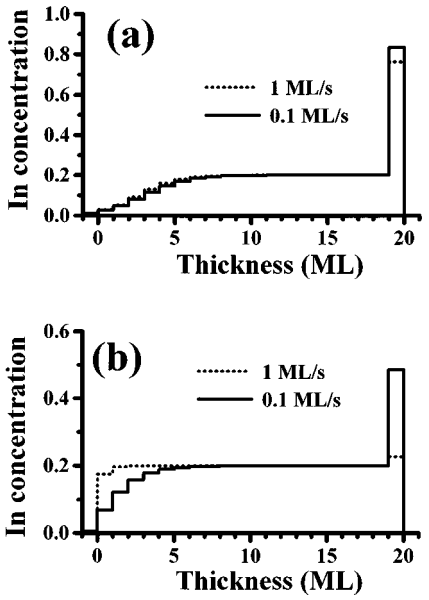

FIG. 3. Indium concentration profiles evolution with growth rate for 20 ML $Ga_{0.8}In_{0.2}As$ on GaAs (a) T=500 °C, (b) T=400 °C.

True profiles had to be taken into account in determining transition energies for PL.[8,9] Indium concentration profiles of Fig. 2 have been obtained with the kinetic model for a 1 ML/s growth rate, E_s=0.2 eV and E_1=1.8 eV. At high temperatures (above 500 °C), these profiles are quite identical to that obtained in similar experimental conditions with the thermodynamical equilibrium model. The assumption of thermodynamical equilibrium seems to be correct for the $Ga_xIn_{1-x}As$/GaAs system at 500 °C as pointed out previously. But when decreasing the substrate temperature without any variation of growth rate, the flux term is no longer negligible with respect to exchange ones in Eq. (4). There is a kinetic limitation of segregation at 400 °C. The evolution with temperature of In concentration profiles as derived by the kinetic model (Fig. 2) is then consistent with experimental results.[6,9]

Moreover the kinetic model is able to predict variations of In segregation with growth rates. Such an effect is quite nonexistent at 500 °C [Fig. 3(a)] because with usual MBE growth rates (0.1–1 ML/s) exchange terms are always much greater than flux ones. The system is near thermodynamical equilibrium and In concentration profiles are weakly sensitive to growth rate variations. At 400 °C and with a growth rate of 1 ML/s, fluxes and exchange terms are in the same order of magnitude resulting in a kinetic limitation of In segregation. To recover near-equilibrium conditions the growth rate needs to be lowered to less than 0.1 ML/s [Fig. 3(b)].

In conclusion, we have developed a kinetic model of element III segregation during growth of ternary semiconductor compounds. Making the assumption of an exchange process limited to the two uppermost ML of the growing sample, this model accounts for the increase of segregation with substrate temperature in accordance with experiments. This was not the case for the thermodynamical equilibrium model. Due to its kinetic form, this model predicts variations of concentration profiles with the growth rate. In summary, our model allows us to define two modes of element III segregation: a near thermodynamical one and a kinetically limited one. In the case of In segregation in the $Ga_xIn_{1-x}As$/GaAs system, near thermodynamical equilibrium is reached at 500 °C for usual MBE growth rate and at 400 °C for low growth rate (<0.1 ML/s). However at 400 °C, our model predicts a kinetic limitation of In segregation for a growth rate of 1 ML/s.

We thank C. Priester for fruitful discussions and J. Massies for invaluable encouragement.

[1] J. M. Moison, C. Guille, F. Houzay, F. Barthe, and M. Van Rompay, Phys. Rev. B **40**, 6149 (1989).
[2] J. Massies, J. F. Rochette, and P. Delescluse, J. Vac. Sci. Technol. B **3**, 613 (1985).
[3] J. Massies, F. Turco, A. Saletes, and J. P. Contour, J. Cryst. Growth **80**, 307 (1987).
[4] B. Jusserand, F. Mollot, J. M. Moison, and G. Le Roux, Appl. Phys. Lett. **57**, 560 (1990).
[5] H. S. Hansen, A. Bensaoula, S. Tougaard, J. Zborowski, and A. Ignatiev, J. Cryst. Growth **116**, 271 (1992).
[6] M. Larive, J. Nagle, J. P. Landesman, X. Marcadet, C. Mottet, and P. Bois, J. Vac. Sci. Technol. B **11**, 1413 (1993).
[7] J. M. Gérard, Appl. Phys. Lett. **61**, 2096 (1992).
[8] J. M. Gérard and J. Y. Marzin, Phys. Rev. B **45**, 6313 (1991).
[9] K. Muraki, S. Fukatsu, and Y. Shiraki, Appl. Phys. Lett. **61**, 557 (1992).
[10] J. F. Zheng, J. D. Walker, M. B. Salmeron, and E. R. Weber, Phys. Rev. Lett. **72**, 2414 (1994).
[11] D. Mc Lean, *Grain Boundaries in Metals* (Oxford University Press, Oxford, 1957).
[12] *Adsorption on Metal Surfaces*, edited by J. Bénard (Elsevier, New York, 1983).
[13] S. V. Ivanov, P. S. Kop'ev, and N. N. Ledentsov, J. Cryst. Growth **104**, 345 (1990).
[14] J. J. Harris, D. E. Ashenford, C. T. Foxon, P. J. Dobson, and B. A. Joyce, App. Phys. **33**, 87 (1984).
[15] W. X. Ni, J. Knall, M. A. Hasan, G. V. Hansson, J. E. Sundgren, S. A. Barnett, L. C. Markert, and J. E. Greene, Phys. Rev. B **40**, 10449 (1989).

Interface quality and electron transfer at the GaInP on GaAs heterojunction

O. Schuler, O. Dehaese, X. Wallart, and F. Mollot
Institut d'Electronique et de Microélectronique du Nord, U.M.R. C.N.R.S. 9929, Avenue Poincaré-B.P. 69-59652 Villeneuve d'Ascq Cedex, France

(Received 4 February 1998; accepted for publication 10 April 1998)

Hall measurements performed on $Ga_{0.50}In_{0.50}P/In_{0.20}Ga_{0.80}As$ structures show abnormally low mobility both at room temperature and at 77 K, and too high electron densities which cannot be attributed to a normal two-dimensional electron gas in the channel. On the other hand, low temperature photoluminescence on asymmetrical AlGaAs/GaAs/GaInP quantum wells and x-ray photoemission spectroscopy measurements reveal the presence of arsenic atoms in the GaInP barrier. Using a one-dimensional Schrödinger–Poisson simulation with a nonabrupt interface model, we show that the presence of arsenic in GaInP leads to the formation of a parasitic GaInAsP well between the δ-doped layer and the channel, trapping the main part of transferred electrons. We experimentally show that the electron transfer can be drastically improved by inserting a thin AlInP layer at the interface. Insertion of at least six monolayers of AlInP is needed to recover a normal electron transfer as high as 2.1×10^{12} cm^{-2}. © *1998 American Institute of Physics.* [S0021-8979(98)02114-8]

I. INTRODUCTION

The GaInP ternary alloy lattice matched to GaAs has drawn much attention as an attractive candidate in view to replace AlGaAs in modulation-doped field-effect transistors. Its large valence band discontinuity with GaAs, its weaker oxidization, and its good chemical etching selectivity with arsenides are the superior characteristics of GaInP over AlGaAs for electronic devices. But in spite of many studies made on growth conditions and element switching sequences,[1–3] it appears that a good control of GaInP/GaAs interfaces is much more difficult than for AlGaAs/GaAs ones. This fact is related to the controversial reported values of the band offset ratio (ΔE_c:ΔE_v) between GaInP and GaAs, which vary over a wide range from 7:93 to 48:52.[4–7] Basically there are at least two issues needed to be considered in achieving good quality arsenide/phosphide interfaces. The first one is related to the experimental setup and concerns the residual incorporation of previous element V during the growth of the succeeding layer. It is often called memory effect. The second one is an intrinsic effect, due to the reactivity of the interface because of the chemical bond energy difference between GaP and GaAs,[8] which could be the driving force for an As/P interdiffusion process. With indium-containing materials, phenomena of surface segregation and desorption of In atoms are added.[9] Recently, Missous *et al.*[10] reported the study of $Ga_{0.52}In_{0.48}P/In_{0.15}Ga_{0.85}As$ high electron mobility transistor structures grown by solid source molecular beam epitaxy (MBE). They show a large reduction of the two-dimensional electron gas (2DEG) mobility when the GaInP spacer layer is placed closer to the InGaAs channel and they need to use an AlGaAs spacer layer to recover good 2DEG characteristics. Diffuse interfaces have been already reported in the growth of GaInP and AlInP on GaAs.[11,12] However, the effect of the GaInP/GaAs interface broadening on 2DEG characteristics have not yet been analyzed. In this work, we report the study of GaInP on (In)GaAs interfaces by means of charge transfer measurements on modulation-doped heterojunctions. These results, but also low temperature photoluminescence and x-ray photoemission spectroscopy (XPS) measurements, lead us to propose an interface profile and an original solution in order to improve electron transfer in these structures, by inserting few AlInP monolayers at the interface.

II. EXPERIMENT

Growth has been carried out in a gas source MBE chamber (Riber 32P) in which arsine and phosphine are cracked in the same cracker cell at 750 °C in order to produce the element V fluxes, whereas standard effusion cells are used to produce element III fluxes. The modulation-doped single heterojunctions are grown on semi-insulating (001) GaAs substrates. Prior to the growth, the GaAs substrate is heated up to 660 °C under an arsenic flux to remove the oxide. Then a 200 nm GaAs buffer layer is grown at 580 °C. The growth is then stopped and the temperature is lowered to and stabilized at 520 °C for the growth of the modulation-doped structure. It consists of a 10 nm $In_{0.20}Ga_{0.80}As$ channel, followed by a 5 nm $Ga_{0.50}In_{0.50}P$ spacer layer and a 5×10^{12} cm^{-2} silicon δ-doped layer. Finally a 25 nm GaInP barrier and a 15 nm Si-doped GaAs cap layer are grown. The commutation sequence at the GaInP on InGaAs interface consists of a 2 s growth interruption without element V, followed by a 1 s of phosphorus (3 sccm PH_3) preceding the opening of Ga and In shutters. During the growth of phosphide layers, the reflection high-energy electron diffraction (RHEED) pattern exhibits a (2×1) reconstruction with no further evolution. It never becomes spotty evidencing a layer-by-layer growth mode. The two-dimensional electron gas structures are characterized by Hall measurements in the standard Van der Pauw configuration at both room temperature and 77 K.

TABLE I. Hall measurements on GaInP/InGaAs and AlInP/InGaAs modulation-doped structure.

	GaInP/InGaAs		AlInP/InGaAs	
	300 K	77 K	300 K	77 K
$n_H(\times 10^{12}\ \mathrm{cm}^{-2})$	3.7	3.7	2.2	2.0
$\mu_H(\mathrm{cm}^2\ \mathrm{V}^{-1}\ \mathrm{s}^{-1})$	1290	1360	5600	17 000

We performed low temperature photo-luminescence (PL) measurements on asymmetrical $Al_{0.30}Ga_{0.70}As/GaAs/Ga_{0.50}In_{0.50}P$ quantum wells using a 488 nm Ar ion laser as the excitation source (30 mW/cm^2) and an InGaAs photocathode photomultiplier as the detector. The use of asymmetrical structures allows to separate the two kinds of GaInP–GaAs interfaces by changing the growth sequence. The growth of these samples had been carried out under the same conditions as the modulation-doped structures. The control of the well thickness was performed by adjusting the GaAs growth rate during the buffer layer by means of RHEED intensity oscillations. It was fixed to 19 monolayers (19 ML, 5.4 nm) with a growth rate of 0.5 ML s^{-1}.

To investigate the As and P profiles through the structure, we used angle dependent XPS measurements on a 5 nm-thick (17 ML) GaInP layer on GaAs with an Al $K\alpha$ x-ray source (1486.6 eV). The direction of photoelectrons is given by the polar angle Θ referred to the surface of the sample and the azimuth which is chosen to be the [110] direction of the (001) GaAs substrate. We calculated the intensity ratio of arsenic and phosphorus core levels (As $3d$/P $2p$) as a function of the polar angle Θ. These two core levels have been chosen because their kinetic energies and then their photoelectron escape depths λ are very close. The total probed thickness is then approximately equal to $3\lambda \sin\Theta$. For low polar angles, the XPS signal is mainly due to the surface of the sample (probed thickness at 25°=3 nm) whereas for high polar angles, both the surface and the interface contributes to the XPS signal (probed thickness at 90°=7.5 nm).

III. RESULTS AND DISCUSSION

A. Hall measurements

Table I summarizes the Hall electron density n_H and Hall mobility μ_H measured for a $Ga_{0.50}In_{0.50}P/In_{0.20}Ga_{0.80}As$ modulation-doped heterojunction. These results do not follow a standard 2DEG behavior for two reasons. The first one is the too high measured electron density which is nearly equal to the electron concentration of the δ-doped layer as if there was no charge transfer. The second one is the abnormally too low Hall mobility, with no increase between room temperature and 77 K. This low mobility cannot be attributed to a 2DEG in the InGaAs channel. However, the same structure with an $Al_{0.50}In_{0.50}P$ barrier instead of the GaInP one exhibits superior characteristics with typical values for a good 2DEG structure (Table I). Nevertheless, AlInP is not a good candidate in view to replace AlGaAs in electronic devices if the purpose is to suppress aluminium. The conduction band offset difference between GaInP and AlInP (110 meV[13]) cannot only explain the wide difference between these experimental results. This wide difference must then be related to the GaInP/(In)GaAs interface.

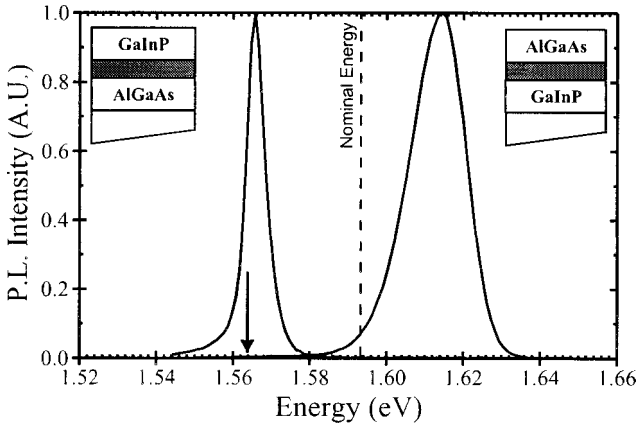

FIG. 1. PL spectra of the two asymmetric AlGaAs/GaAs/GaInP quantum wells. The arrow indicates the PL energy deduced from the XPS As concentration profile for the GaInP-on-GaAs interface.

B. Photoluminescence measurements

We first used PL of asymmetrical AlGaAs/GaAs/GaInP quantum wells to investigate the GaInP–GaAs interface. The experimental PL energies (Fig. 1) were compared to calculations based on the transfer matrix envelope function approximation, well suited for asymmetric structures. A constant binding energy of the quasi-two-dimensional exciton $E_{EX}=10$ meV was assumed. Our calculations were made using a conduction band offset for the GaInP/GaAs system of 145 meV, in agreement with the experimental value determined by Leroux *et al.*[5] The GaAs-on-GaInP sample emits at a slightly higher energy than the calculated one. This blue shift cannot be explained by indium segregation in the GaAs well, otherwise the energy would be red shifted. It is then related to the presence of residual P atoms in the GaAs well. On the contrary, the inverse structure with the GaInP-on-GaAs interface emits at a significant lower energy by about 30 meV. The calculated GaAs well width for this energy is 25 ML, 6 ML more than the nominal thickness. Such a value is out of our precision range for the GaAs thickness. The only way to explain this red shift is the presence of arsenic atoms at the beginning of the GaInP barrier which induces the formation of a small gap GaInAsP alloy after the GaAs well.

C. XPS measurements

This last point had been checked by XPS measurements. In Fig. 2(a), we plotted the intensity ratio of arsenic and phosphorus core levels (As $3d$/P $2p$) as a function of the polar angle Θ. We first tried to fit the experimental data (square dots) by two simple models. Arsenic profiles are shown in Fig. 2(b). The abrupt interface model (dot line) is found to be far away from the experimental data, clearly demonstrating that the GaInP-on-GaAs interface is not abrupt. XPS measurements reveal the presence of As atoms

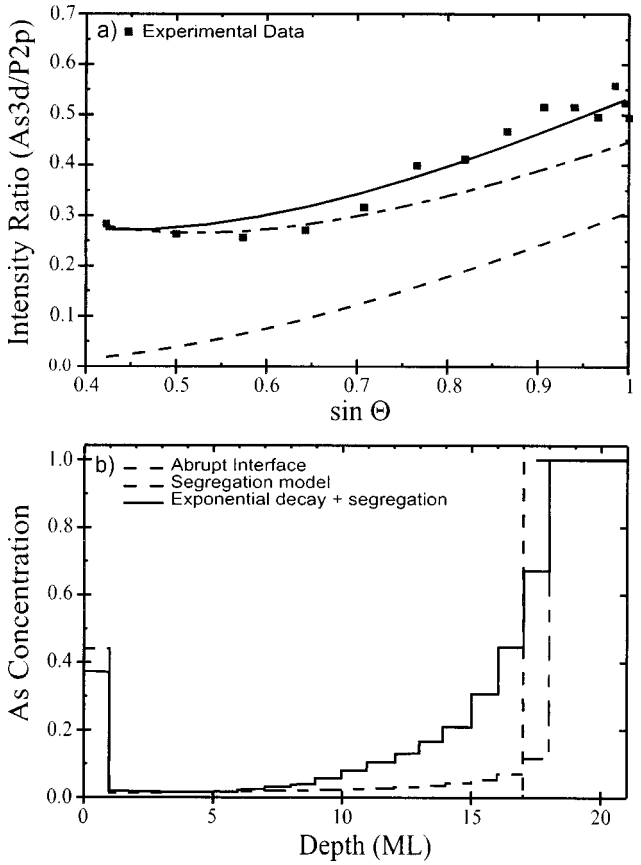

FIG. 2. Angle dependent XPS measurements (a) on a 17 ML thick GaInP layer on GaAs (square dots) and three interface models (b); the nominal abrupt interface model (dash line), the As segregation model (dash-dot line), and an exponential As decay together the segregation model (solid line).

near the surface ($\sin\Theta=0.4$). This fact has been observed even for 500 nm thick GaInP layer and suggests that As segregation occurs during the growth of GaInP.[14] Indeed the segregation model (dash-dot line) using a segregation energy $E_s=0.27$ eV can explain the As concentration near the surface. However the calculated As/P ratio at the interface is systematically below the experimental data. Then the As concentration near the interface cannot be accounted for by an As–P surface exchange mechanism only. It suggests the presence of a noticeable amount of As atoms incorporated during the growth of the GaInP overlayer. In order to test this hypothesis, we modeled the As concentration profile in GaInP (solid line in Fig. 2) by an exponentially decreasing function (decay time of 2.3 s as the adjusted parameter) together with the equilibrium segregation model responsible for the As concentration at the GaInP surface. The overall agreement is better than with the segregation model. More, the same As concentration profile successfully fits the PL energy of the 19 ML GaInP on GaAs-on-AlGaAs asymmetric quantum well and explains the observed red shift (arrow in Fig. 1). This strongly supports the idea of a diffuse GaInP-on-GaAs interface extending on 6–7 MLs. The same model, using an exponentially decreasing function of phosphorus in GaAs, is successfully used in the case of the GaAs-on-GaInP interface to explain the blue shift of the PL line for this interface.

D. Discussion

This GaInP-on-GaAs interface profile has two distinct components. The first one is the small amount of P in GaAs and of As at the surface of GaInP due to the segregation of As atoms through GaInP during the growth. The second one is the large amount of As in GaInP following an exponentially decreasing profile. The origin of this interface broadening could be driven by the chemical bond strength difference between Ga–P and Ga–As as suggested by Anan *et al.*[8] However, the intermixing of P and As at 520 °C for the GaInP-on-GaAs interface is limited to 1–2 ML [Fig. 2(b)] and is not sufficient to explain the large amount of As in GaInP. The main part of As atoms in GaInP is then probably due to a gas mixture during the gas commutation procedure. It is not a simple memory effect because a 1 min purge of the gas cracker cell does not significantly reduce the red shift of the PL line of asymmetrical quantum well. This has been discussed elsewhere.[14]

This interface profile can now be used to explain the Hall measurements of modulation-doped structures. We performed charge transfer calculations using a self-consistent one-dimensional Schrödinger–Poisson solver. The interdiffusion of P atoms in $In_{0.20}Ga_{0.80}As$ induces the formation of a 1–2 ML high gap strained $In_{0.20}Ga_{0.80}As_xP_{1-x}$ layer at the top of the channel acting as a barrier for electrons. On the contrary, exponentially decreasing profile of As atoms in $Ga_{0.50}In_{0.50}P$ leads to the formation of a small gap $Ga_{0.50}In_{0.50}P_xAs_{1-x}$ region which acts as a parasitic well at the bottom of the barrier. Results are summarized in Fig. 3 for a nominal GaInP/InGaAs structure (a) and a diffuse one (b). We plotted the conduction band energy, the total electron density, and the position of the two first electronics levels in the structures. The Fermi level is fixed at 0 eV as the energy reference and the surface potential of GaInP is chosen to be 0.8 eV. The comparison between the simulations of the two profiles clearly shows that in the case of the diffuse interface, about 40% of electrons are localized into the parasitic $Ga_{0.50}In_{0.50}P_xAs_{1-x}$ well instead of the nominal InGaAs channel. This localization is enhanced by the presence of the 1–2 ML $In_{0.20}Ga_{0.80}As_xP_{1-x}$ barrier at the top of the channel. This explains the too high electron density measured on modulation-doped structures because Hall measurements give a weighted average electron density in the case of multiconducting layers. In the case of a diffuse interface, the two first electronics levels are lowered below the Fermi level. The wave function of the first level is mainly localized in the parasitic well with a large extension into the barrier. The second level closed to the first one is related to the InGaAs channel. Whereas the nominal structure has only one level in the InGaAs channel. This has been checked by room temperature photoluminescence measurements on modulation-doped structures. As previously reported, PL spectrum on modulation-doped heterojunctions mainly reveals the transition between the electronics levels below the Fermi level and the first heavy hole level.[15] Curve (a) in Fig. 4 shows the PL spectrum of such structure. The diffuse interface GaInP/InGaAs sample exhibits two transitions corresponding to the two wells in good agreement with the values predicted by

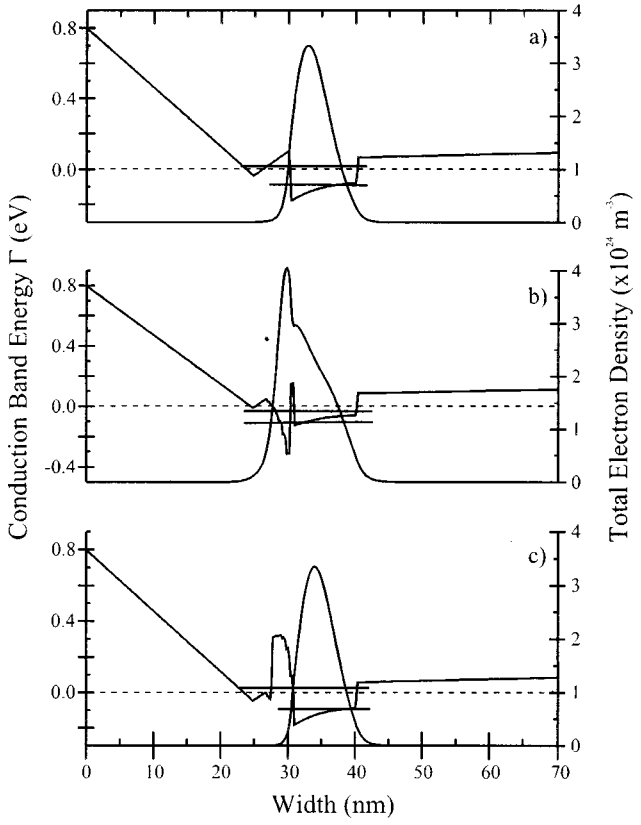

FIG. 3. Self-consistent Schrödinger–Poisson simulation of GaInP/InGaAs modulation-doped structure in the case of a nominal interface (a), a diffuse interface (b), and a diffuse interface with 6 ML of AlInP (c). We plotted the conduction band energy, the total electron density, and the position of the two first electronics levels in the structures. The Fermi level is fixed at 0 eV (dotted line).

our model (arrows in Fig. 4 at, respectively, 1.201 and 1.265 eV). The lower energy peak at about 1.20 eV is attributed to the electronic level in the parasitic well. The presence of a large concentration of electrons in the barrier close to the δ-doped layer and of the 1–2 ML barrier near the center of the 2DEG explain the low values of the Hall mobility.

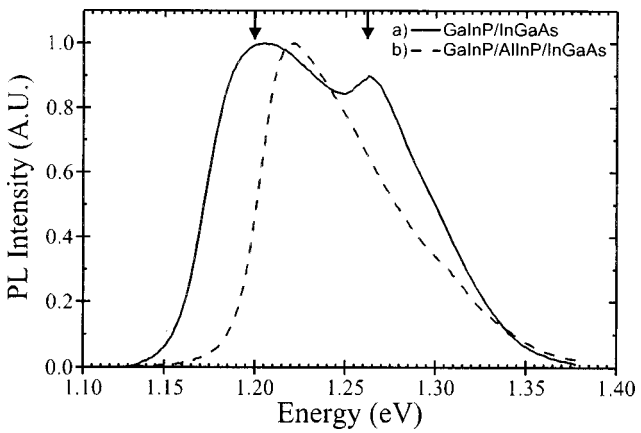

FIG. 4. Room temperature PL measurements of modulation-doped heterojunctions: a GaInP/InGaAs sample (a) and one dressed with 6 ML of AlInP at the interface (b). Arrows indicate the two calculated transitions for a diffuse interface taking into account the XPS As profile.

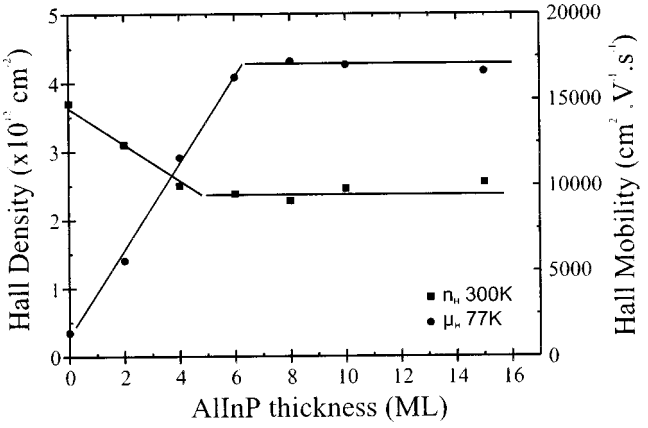

FIG. 5. Hall density and mobility at 77 K as a function of the AlInP additional dressing layer thickness in GaInP/InGaAs modulation-doped structure. (Lines are guides for the eyes.)

Now if the GaInP barrier is replaced by an $Al_{0.50}In_{0.50}P$ one and considering that the As–P incorporation mechanism is the same, the As profile must lead to the formation of a larger gap $Al_{0.50}In_{0.50}P_xAs_{1-x}$ region instead of a $Ga_{0.50}In_{0.50}P_xAs_{1-x}$ one, no longer acting as a well. More, this region can improve the electron confinement in the channel because of its higher conduction band offset [Fig. 3(c)]. We experimentally verified these ideas by dressing the InGaAs–GaInP interface with a few monolayers of AlInP. The total thickness of the spacer layer (i.e., AlInP+GaInP) was kept constant to 5 nm in order to compare the results. We plotted in Fig. 5, the Hall density and mobility at 77 K as a function of the thickness of the AlInP layer. While only 2 MLs improve the 2DEG mobility by a factor of 2, at least 6 MLs of AlInP are needed to recover a normal electron transfer in the channel ($n_H = 2.1\times10^{12}$ cm^{-2}) and a good 2DEG mobility at both room temperature and 77 K [$\mu_H(300\text{ K}) = 5500$ cm^2 V^{-1} s^{-1} and $\mu_H(77\text{ K}) = 17\,000$ cm^2 V^{-1} s^{-1}]. Beyond 6 ML, Hall density and mobility are nearly constant and the effect of the parasitic well is then totally suppressed as expected by simulations [Fig. 3(c)]. We deduce from these experiments that the GaInP-on-InGaAs interface is disrupted on at least 6 ML in the barrier by the presence of arsenic atoms, in good agreement with the XPS As/P profile in which the As concentration after 6 ML is below 10%. Curve (b) in Fig. 4 shows the PL spectrum of a sample, where the beginning of the spacer layer has been replaced by 6 ML of AlInP. Contrary to the sample of curve (a) in Fig. 4, it exhibits only one peak at 1.22 proving that the parasitic well has been suppressed. Of course, this solution does not solve the problem at the arsenide-phosphide interfaces but it suppresses its consequences and can be used as an original solution to ensure good 2DEG characteristics for device applications. No drawbacks due to the presence of this thin AlInP layer have been found (persistent photoconductivity for instance). Based on these results, the GaInP/InGaAs system in spite of its lower conduction band offset, allows as high electron density as the AlGaAs/InGaAs one.[16]

IV. CONCLUSION

The GaInP-on-(In)GaAs interface has been investigated by means of electron transfer measurements in modulation-doped heterostructures. This interface is disrupted on at least 6 ML by the presence of arsenic atoms in the GaInP barrier, probably due to a gas mixture in the cracker cell during the gas commutation procedure. The presence of As atoms in the barrier had been clearly demonstrated by the red shift of the PL lines of asymmetrical AlGaAs/GaAs/GaInP quantum wells and also by angle dependent XPS measurements. The presence of a large amount of As in the bottom of the GaInP barrier leads to the creation of a parasitic GaInAsP quantum well which traps a part of the transferred electrons and lowers their mobility. Further work is required to improve the gas commutation sequence at the interface, however we found an original solution which consists of the insertion of few monolayers of AlInP at the InGaAs/GaInP interface, allowing 2DEG density as high as 2.1×10^{12} cm^{-2}.

ACKNOWLEDGMENT

This work has been supported by DRET/DGA under Contract No. 94160. We gratefully acknowledge C. Coinon for his technical assistance and J. L. Thobel for the one-dimensional Schrödinger–Poisson algorithm and fruitful discussions.

[1] J. M. Kuo, H. C. Kuo, J. Y. Cheng, Y. C. Wang, Y. Lu, and W. E. Mayo, J. Cryst. Growth **158**, 1047 (1996).
[2] M. Usami, Y. Matsushima, and Y. Takahashi, J. Cryst. Growth **150**, 1344 (1995).
[3] M. J. Hafich, J. H. Quigley, R. E. Owens, and G. Y. Robinson, Appl. Phys. Lett. **54**, 2686 (1989).
[4] T. Kobayashi, K. Taira, F. Nakamura, and H. Kawai, J. Appl. Phys. **65**, 4898 (1989).
[5] J. Chen, J. R. Sites, I. L. Spain, M. J. Hafich, and G. Y. Robinson, Appl. Phys. Lett. **25**, 744 (1991).
[6] T. W. Lee, P. A. Houston, R. Kumar, X. F. Yang, G. Hill, M. Hopkinson, and P. A. Claxton, Appl. Phys. Lett. **60**, 474 (1992).
[7] M. Leroux, M. L. Fille, B. Gil, J. P. Landesman, and J. C. Garcia, Phys. Rev. B **47**, 6465 (1993).
[8] T. Anan, S. Sugou, K. Nishi, and T. Ichihashi, Appl. Phys. Lett. **63**, 1047 (1993).
[9] M. Mesrine, J. Massies, C. Deparis, N. Grandjean, and E. Vanelle, Appl. Phys. Lett. **68**, 3579 (1996).
[10] M. Missous, A. A. Aziz, and A. Sandhu, Jpn. J. Appl. Phys., Part 2 **36**, L647 (1997).
[11] H. Y. Lee, M. D. Crook, M. J. Hafich, J. H. Quigley, and G. Y. Robinson, Appl. Phys. Lett. **55**, 2322 (1989).
[12] J. C. Garcia, P. Maurel, P. Bove, and J. P. Hirtz, Jpn. J. Appl. Phys., Part 1 **30**, 1186 (1991).
[13] M. O. Watanabe and Y. Ohba, Appl. Phys. Lett. **50**, 906 (1987).
[14] O. Dehaese, X. Wallart, O. Schuler, and F. Mollot, Jpn. J. Appl. Phys., Part 1 **36**, 6620 (1997).
[15] A. Dodabalapur, V. P. Kesan, D. R. Hinson, D. P. Neikirk, and B. G. Streetman, Appl. Phys. Lett. **54**, 1675 (1989).
[16] L. D. Nguyen, D. C. Radulescu, M. C. Foisy, P. J. Tasker, and L. F. Eastman, IEEE Trans. Electron Devices **36**, 833 (1989).

X-ray photoemission characterization of interface abruptness and band offset of $Ga_{0.5}In_{0.5}P$ grown on GaAs

O. Dehaese,[a] X. Wallart, O. Schuler, and F. Mollot
Institut d'Electronique et de Microélectronique du Nord, UMR CNRS 9929, BP 69, 59652 Villeneuve d'Ascq Cédex, France

(Received 16 December 1997; accepted for publication 9 May 1998)

We have studied by angle resolved x-ray photoemission spectroscopy (XPS) the interface between $Ga_{0.5}In_{0.5}P$ and GaAs grown by gas source molecular beam epitaxy. For cations, we show that the interface is abrupt for a growth temperature of 400 °C and that indium segregation is effective at 500 °C but less than that in GaInAs at the same temperature. For anions, growth of the two layers in rapid succession results in the incorporation of an excess of arsenic in the GaInP epilayers and a diffuse interface. As soon as these predominant experimental effects are suppressed, the abruptness of the interface is limited by a weak arsenic surface segregation. For this quasi-abrupt interface, we report a valence band offset of ≈0.3 eV as determined by XPS. © *1998 American Institute of Physics.* [S0021-8979(98)04716-1]

I. INTRODUCTION

Band offsets at the interface between two III-V semiconductors have received attention for a long time because of their importance for device electronic properties as well as from a fundamental point of view.[1] Nevertheless, in spite of numerous studies devoted to this field, an overall agreement between theoretical predictions and band offset measurements, and sometimes between measurements using different techniques, is only reached for a limited number of interfaces. Among many possible causes of disagreement, one of the most important is probably the lack of precise control of the interface chemistry at the atomic scale. Indeed, it has been shown that for interfaces between III-V semiconductors sharing neither the anions nor the cations (for example InP/GaInAs or GaAs/GaInP), the band offset depends on the exact growth sequence.[2–4] This in turn calls for a detailed picture of the interface formation which, up to now, has only been obtained for interfaces between different arsenides, especially AlAs/GaAs and InAs/GaAs.[5–14] Indeed, in this case, it is now well established that the interface abruptness is limited by segregation during growth rather than by interdiffusion processes. This has been described successfully by several models based either on an exchange mechanism[7,15] or on diffusion length differences[16,17] at the growth surface. Although few results are available, segregation has been reported in phosphides as well but seems to be less active than in arsenides.[18]

On the other hand, for interfaces between arsenides and phosphides, the situation is still unclear. Diffuse interfaces have been reported for both arsenides on InP[19–21] and phosphides on GaAs.[22–26] However, the origin of interface broadening is not well understood. This is due mainly to the difficulty in distinguishing between intrinsic effects related to the material system under study and extrinsic experimental effects. The latter are more or less unavoidable because of the high element V vapor pressure and the element V overpressure used for standard growth conditions in usual techniques such as molecular beam epitaxy (MBE) or metalorganic chemical vapor deposition (MOCVD).

As for the GaAs/GaInP interface, uncertainty concerning the interface chemistry and abruptness has lead to a large dispersion in the measured values of the band offset. For instance, reported results for the valence band offset using several techniques vary from 70 to 430 meV.[27–32] Moreover, most studies relating to the GaAs/GaInP interface make use of characterization techniques such as photoluminescence (PL) or x-ray diffraction (XRD) which are not chemically sensitive and which can not give a detailed picture of the interface chemistry.

In this work, we investigate the GaInP on GaAs interface grown by gas source molecular beam epitaxy (GSMBE) using angle resolved x-ray photoelectron spectroscopy (ARXPS). The chemical sensitivity of XPS combined with angular measurements allow us to determine cation and anion concentration profiles at the interface. These profiles are then used to interpret the origin of the interface broadening. After suppression of the experimental effects, we obtain quasi-abrupt interfaces. This allows us to determine the valence band offset between GaInP and GaAs by XPS.

II. EXPERIMENT

Samples are grown on GaAs ''epiready'' (001) substrates in a gas source Riber 32P epitaxy chamber. Conventional Ga and In MBE effusion cells and cracked AsH_3 and PH_3 are used as element III and V sources, respectively. The same cracker cell working at 750 °C is used for both AsH_3 and PH_3. Prior to growth, the GaAs substrate is heated to 660 °C under an arsenic flux in order to remove the oxide. After the growth of a 2000 Å GaAs buffer layer at 580 °C with an AsH_3 flow of 2 sccm, the temperature is lowered and stabilized at the growth temperature (400 or 500 °C) used for

[a]Also with: Institut de Micro et Optoélectronique, Ecole Polytechnique Fédérale de Lausanne, CH 1015 Ecublens, Switzerland.

the $Ga_{0.5}In_{0.5}P$ epilayers. The duration of this growth interruption is 3 min, and the AsH_3 line is vented when the substrate temperature reaches 550 °C in order to keep a typical As rich (2×4) reflection high energy electron diffraction (RHEED) pattern. $Ga_{0.5}In_{0.5}P$ growth is then initiated by simultaneously opening the Ga and In shutters and activating the phosphine (PH_3 flow: 3 sccm). Immediately the RHEED pattern changes from the (2×4) to a (2×1) reconstruction with no further evolution as long as the growth proceeds and changes back to a (2×4) one once GaInP growth is stopped. The RHEED patterns never become spotty during the growth of $Ga_{0.5}In_{0.5}P$ evidencing a layer by layer growth mode. Phosphide growth rate ($\approx$1 monolayer/s) and composition are regularly determined by RHEED oscillations on GaAs and InP.

Immediately after growth and cooling, samples are transferred under ultrahigh vacuum (1×10^{-10} Torr) to the XPS analysis system. This system is a Physical Electronics model 5600, modified by N.V. SINVACO S.A. in order to analyze 3 in. MBE samples. The angle resolved XPS results presented here have been obtained with a standard Al $K\alpha$ anode (1486.6 eV). The acceptance angle of the analyzer has been set to 14° and the angle between the incident x rays and the analyzer is 54°. The direction of photoelectrons is given by the polar angle θ, as referenced to the sample surface and the azimuth. To obtain angle dependent XPS results, the polar angle is varied from 25° to 90°. The intensity of the various XPS core levels are measured as the peak area after standard background subtraction according to the Shirley procedure.[33] Photodiffraction effects are often prominent on single crystals[34] and, as they superimpose to the XPS signal variations relative to the concentration gradient, they can make concentration profile determination rather difficult. To minimize these effects, we first perform an average of the different XPS core level intensities with respect to the azimuth.[35] Then, we calculate intensity ratios between XPS lines either of two anions (As and P) or two cations (Ga and In) with close binding energies.[36] Since the Ga 3*d* and In 4*d* signals overlap, we apply the deconvolution procedure proposed by Joyce *et al.*[37] to determine the Ga 3*d* and In 4*d* intensities. In this procedure, the Ga 3*d* and In 4*d* lines are described each by a doublet for the 3/2 and 5/2 components. The branching ratios are theoretical ones and the splitting energies are fixed at 0.45 eV between Ga $3d_{3/2}$ and Ga $3d_{5/2}$ and 0.86 eV between In $4d_{3/2}$ and In $4d_{5/2}$, which are typical values for these core levels.[38] These experimental intensity ratios are fitted with simulated ones for various concentration profiles at the interface using photoionization cross section values deduced from measurements on GaAs, InAs, and InP reference samples. The best fit is obtained through a least-square minimization procedure.

For the determination of the valence band offset, we use a monochromatic Al $K\alpha$ x-ray source for which the ultimate overall resolution as measured from the full width half maximum (FWHM) of the Ag $3d_{5/2}$ line is 0.45 eV. We apply a commonly used procedure[39–50] in which the differences between a core level energy (E_1 or E_2) and the valence band maximum (E_{v1} or E_{v2}) are first measured independently on the two semiconductors. Then the separation between the two core level energies ($\Delta E=E_1-E_2$) is obtained on a heterojunction, and the valence band offset is deduced from the equation:

$$\Delta E_v=(E_1-E_{v1})+\Delta E-(E_2-E_{v2}). \tag{1}$$

For the determination of the valence band maxima, the experimental data are fitted with a Gaussian broadened free electron density of states.[32]

III. RESULTS AND DISCUSSION

Since the band offset is sensitive to the interface chemistry, we first focus on the concentration profiles across the interface using ARXPS. Taking advantage of the chemical sensitivity of this technique, we study the anion and cation profiles separately. Figure 1 shows an example set of spectra for the anions (P 2*p*, As 3*d*) and for the cations (Ga 3*d*, In 4*d*) recorded on a 5 monolayer (ML) thick $Ga_{0.5}In_{0.5}P$ on GaAs epilayer grown at 400 °C. In this figure, we display the subtracted background for all spectra and the curve fitting used for the Ga 3*d*–In 4*d* region.

We start with the determination of the cation concentration profiles for 5 ML thick $Ga_{0.5}In_{0.5}P$ on GaAs samples grown at 400 and 500 °C. XPS angular measurements for the Ga 3*d*/In 4*d* intensity ratio are reported in Fig. 2 together with simulations. For a 400 °C growth temperature the agreement is quite good between experimental data and a simulation assuming an abrupt interface for the cations. For a higher growth temperature (500 °C) a slight decrease of the Ga 3*d*/In 4*d* intensity ratio is observed for all the polar angles indicating that the interface is no longer abrupt due to the indium surface segregation. To take into account this segregation we use a thermodynamic equilibrium model[7,11,12] with a segregation energy (E_s) of 0.1 or 0.2 eV. We can see in Fig. 2 that experimental data are well fitted by a simulation with $E_s=0.1$ eV.

These results show that indium segregation occurs in GaInP as in GaInAs. This is in agreement with the results of Mesrine *et al.*[18] relating to GaInP grown at 550 °C by chemical beam epitaxy (CBE). However, since the value of E_s we report for GaInP grown at 500 °C is less than the 0.2 eV, usually determined for GaInAs at the same temperature, the indium segregation seems to be less effective in phosphides than in arsenides. This could be due to a kinetic limitation of the exchange mechanism leading to segregation because of the higher binding energies of Ga and In in GaInP than in GaInAs.[19,51] If true, the indium segregation should be enhanced at higher growth temperature in GaInP as it seems to be for GaInP grown at 550 °C by CBE.[18] This tends to demonstrate the activation of indium segregation with the growth temperature and hence the importance of kinetic factors on the Ga/In exchange mechanism in phosphides. This behavior is quite similar to that observed in GaInAs although equilibrium seems to be reached near 500 °C for GaInAs. For GaInP, it appears to be obtained at higher temperatures.

For the same samples, we also determine the anion concentration profiles. XPS angular measurements for the As 3*d*/P 2*p* intensity ratio are reported in Fig. 3 together with simulations. Assuming an abrupt GaInP on GaAs inter-

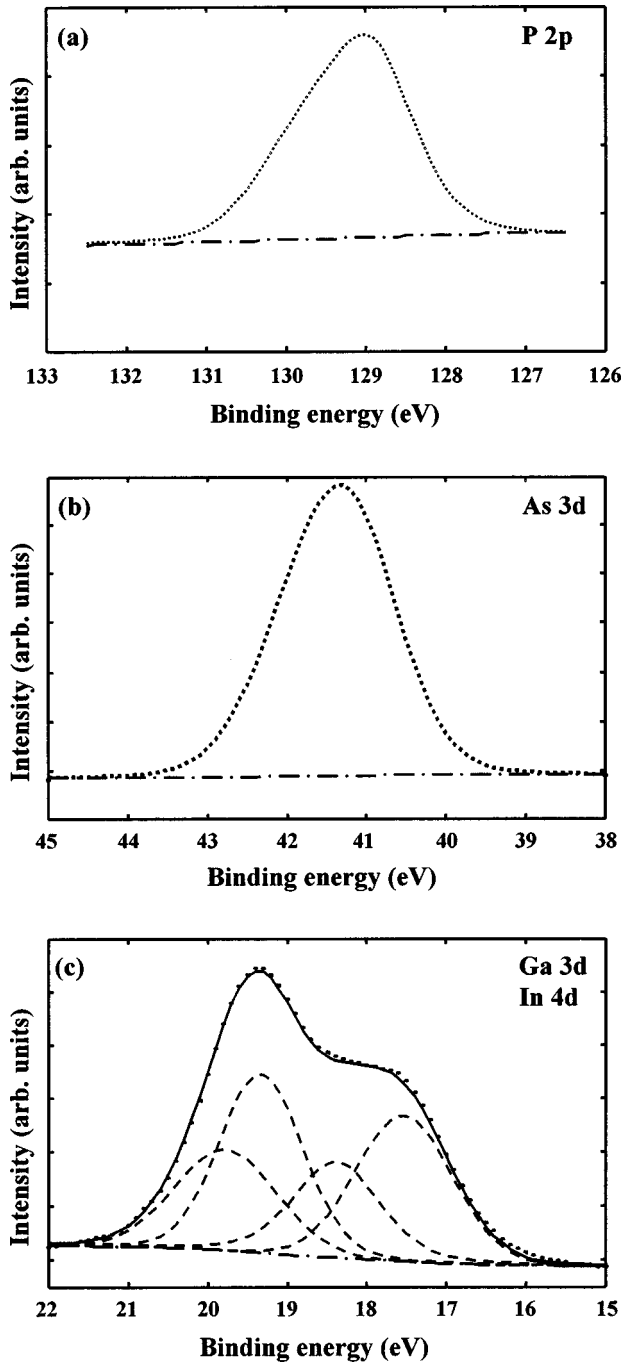

FIG. 1. Example set of spectra recorded on a 5 ML thick GaInP on GaAs epilayer grown at 400 °C. (a) P 2*p* core level (dotted line) and its subtracted background (dashed-dotted line). (b) As 3*d* core level (dotted line) and its subtracted background (dashed-dotted line). (c) Ga 3*d* and In 4*d* core levels (dotted line), associated subtracted background (dashed-dotted line), two doublets (Ga $3d_{3/2}$–Ga $3d_{5/2}$, In $3d_{3/2}$–In $3d_{5/2}$) components (dashed lines), result of the curve fitting (full line).

face, the calculated As 3*d*/P 2*p* intensity ratios are much less than the experimental ones for all the polar angles. This shows that the GaInP on GaAs interface is not abrupt for the anions for a growth temperature of 400 °C or 500 °C and a 3 min growth interruption. Moreover, since the experimental intensity ratios are greater than the calculated ones, we can conclude that some arsenic is incorporated into the GaInP epilayer. The first assumption is that there is a surface segregation of arsenic with respect to phosphorous. This segregation process should be similar to that of indium for cations. Thus we apply the thermodynamic equilibrium model to fit experimental data with calculated As 3*d*/P 2*p* ratios. The single parameter of this fit is the segregation energy E_s. In Fig. 3 we present As 3*d*/P 2*p* intensity ratios calculated for anion concentration profiles deduced by using the thermodynamic equilibrium model with $E_s = 0.4$ eV. For this value of the segregation energy, the exchange process between As and P atoms is quite total and thus the arsenic concentration of the surface monolayer is almost 1. Hence the calculated

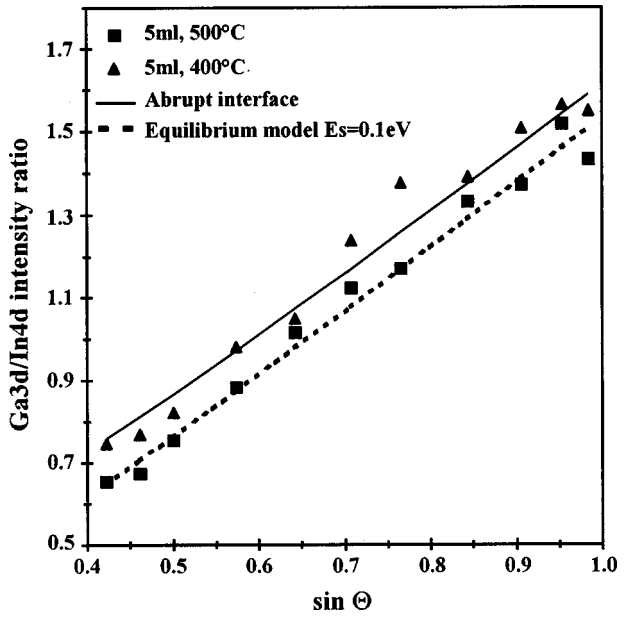

FIG. 2. Experimental and calculated polar angle dependence of the Ga 3*d*/In 4*d* intensity ratio after azimutal average for a nominally 5 ML thick GaInP epilayer grown on GaAs at 400 and 500 °C.

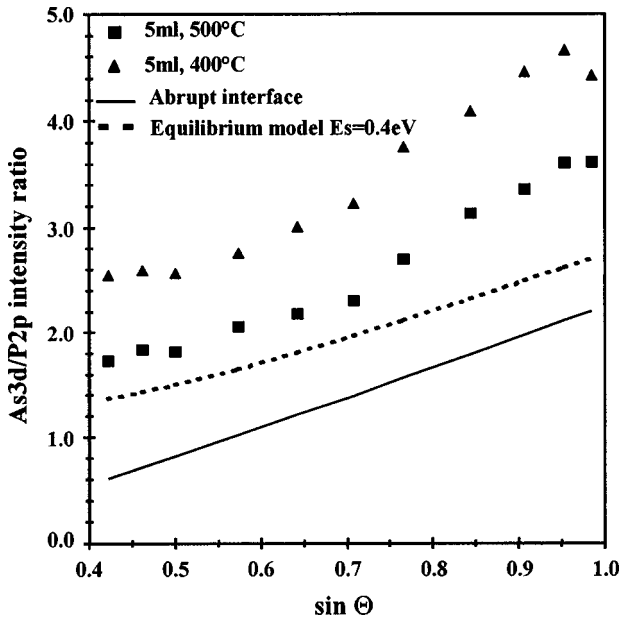

FIG. 3. Experimental and calculated polar angle dependence of the As 3*d*/P 2*p* intensity ratio after azimutal average for a nominally 5 ML thick GaInP epilayer grown on GaAs at 400 and 500 °C.

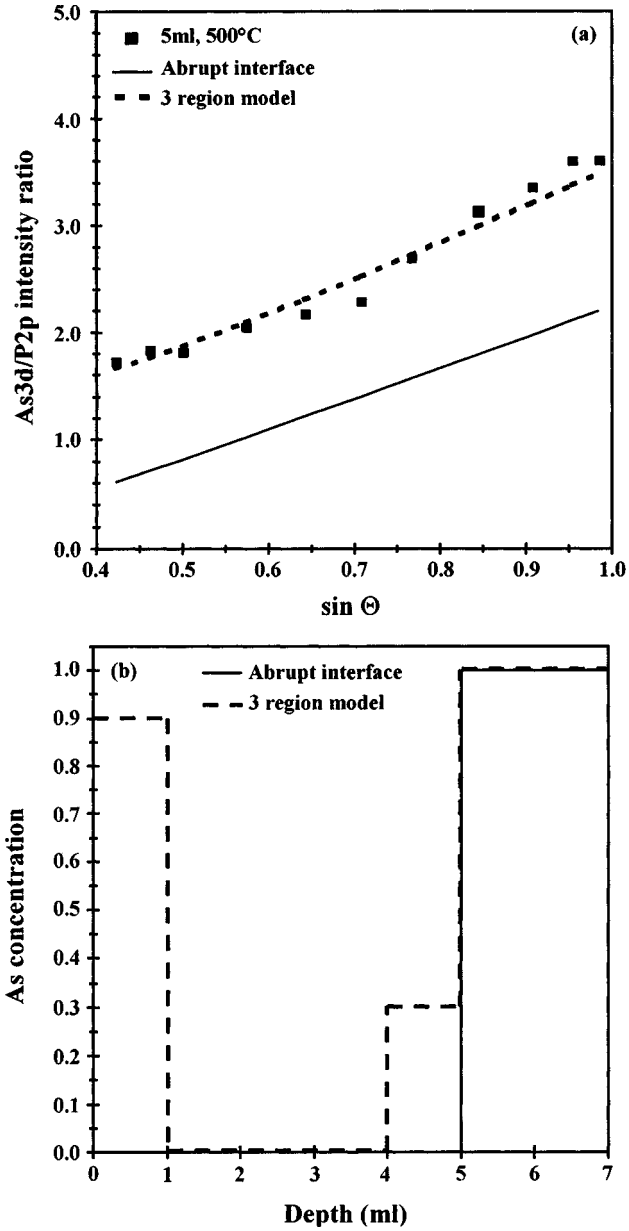

FIG. 4. (a) Experimental and calculated polar angle dependence of the As $3d$/P $2p$ intensity ratio for a nominally 5 ML thick GaInP epilayer grown at 500 °C on GaAs. (b) As concentration profile deduced from the fit to XPS data for a nominally 5 ML thick epilayer grown at 500 °C on GaAs.

As $3d$/P $2p$ ratios represent the maxima we can obtain without assuming the incorporation of an excess of arsenic in the GaInP epilayer. We see in Fig. 3 that these maxima are still less than the experimental data.

To improve the agreement between experiment and simulation we then use a composition profile made up of three regions and the GaAs substrate. Each of these regions is of constant composition in As and so in P. The fit parameters are the three concentrations and the three thicknesses of the regions. The best fit between experiment and simulation for a 500 °C growth temperature [Fig. 4(a)] is obtained with the As concentration profile shown in Fig. 4(b). This profile reveals important features. First, the epilayer surface is enriched in As suggesting the existence of an As segregation process. Since the arsenic surface content is quite important as seen in the concentration profile of Fig. 4(b), the As/P exchange process leading to segregation must be very efficient. However, As segregation alone cannot account for the concentration profile in Fig. 4(b), since the total amount of excess arsenic in the GaInP epilayer is greater than 1 ML. On the other hand, since the experimental As $3d$/P $2p$ intensity ratios are greater at 400 °C than at 500 °C (Fig. 3), we can infer that the incorporated excess of As is greater at 400 °C than at 500 °C. This cannot be explained by an exchange/segregation phenomenon alone. Finally, the concentration profile of Fig. 4(b) shows the absence of phosphorus in the last monolayers of GaAs, which rules out the possibility of a strong As/P interdiffusion process as the origin of the incorporated As in the GaInP epilayer. The above experimental observations lead us to conclude that the apparent interdiffusion at the GaInP on GaAs interface results mainly from experimental effects rather than from intrinsic ones. These effects could be a residual As pressure in the MBE reactor during the GaInP growth or a gas mixture between AsH_3 and PH_3 in the vent line or in the cracker cell. These points are discussed in more detail elsewhere.[52]

Whatever the origin may be, it is necessary to suppress the incorporation of the excess As in GaInP in order to obtain an abrupt interface between GaInP and GaAs. We use a modified growth procedure in which we stop the growth after the GaAs buffer layer and leave the samples under ultrahigh vacuum for one night. This allows us to purge the vent line, the cracker cell, and the MBE reactor during a time we hope sufficient to suppress experimental effects. Before the growth of the GaInP epilayer, the sample surface is checked by XPS revealing the absence of contamination especially in C or O. The growth is resumed by slowly heating the sample to the growth temperature (400 or 500 °C) without any element V beam. The RHEED shows a (2×4) reconstruction from the beginning to the end of the sample heating. The Ga and In shutter are opened and PH_3 switched to the cracker cell simultaneously.

For samples consisting of 10 ML of GaInP on GaAs grown with this modified procedure at 400 or 500 °C, the variations of As $3d$/P $2p$ intensity ratios with the polar angle are depicted in Fig. 5 together with simulations. The agreement between experimental data and a simulation assuming an abrupt GaInP on GaAs interface is quite good at 400 and 500 °C, demonstrating that the GaInP on GaAs interface is intrinsically quasi-abrupt. To improve the agreement between experiment and simulations, we assume the existence of an arsenic segregation. This effect is described using the kinetic model of segregation we have developed previously for group III elements.[15] In the case of anions, this model is modified to take into account the As desorption. In our case this effect is important especially at the highest temperature. For instance, in Fig. 5, the As $3d$/P $2p$ intensity ratios are always greater at 400 than at 500 °C, probably due to a partial desorption of As surface atoms at the higher growth temperature. The desorption has been included in the model by subtracting an amount of arsenic proportional to the As con-

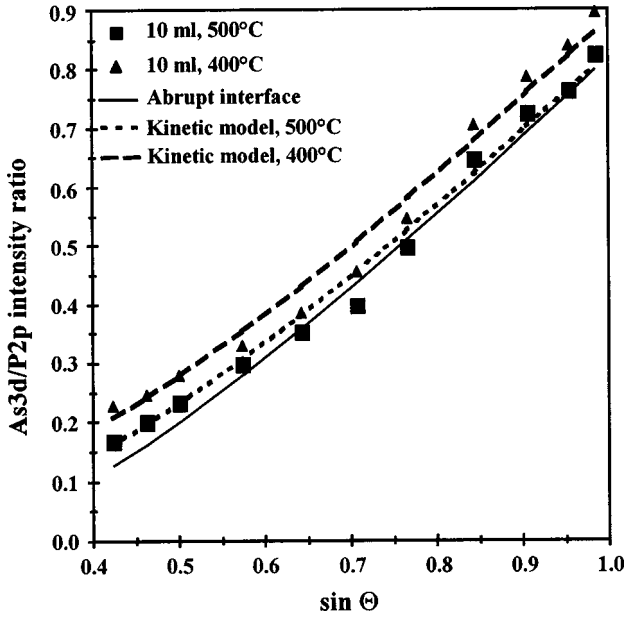

FIG. 5. Experimental and calculated polar angle dependence of the As $3d$/P $2p$ intensity ratio after azimutal average for a nominally 10 ML thick GaInP epilayer grown on GaAs at 400 and 500 °C with a one night growth interruption between the GaAs buffer and the GaInP epilayer.

centration of the surface monolayer after the exchange process. The proportion is kept constant along the growth. Hence the fit parameters for the modified kinetic model of segregation are the two energy barriers for exchange and the desorption coefficient.

The best agreement between experiments and simulations using the modified kinetic model of segregation is obtained with energy barriers of 1.68 and 1.8 eV both at 400 and 500 °C and reevaporation coefficients of 0 and 0.1 at 400 and 500 °C, respectively. Calculated As $3d$/P $2p$ intensity ratios derived using this segregation model are shown in Fig. 5. With this kinetic model, the As surface concentration is less than 5% both at 400 and 500 °C. For these samples, the weak As segregation causes a broadening of the GaInP on the GaAs interface over 3 ML. Hence this interface is quasi-abrupt and it is then meaningful to determine the valence band offset between GaInP and GaAs by XPS.

In the case of GaInP/GaAs the valence band offset can be measured using the As and P or As and In core levels. We present a determination using the narrowest and the most intense lines of these elements, i.e., As $3d_{5/2}$, P $2p_{3/2}$, In $3d_{5/2}$ and In $4d_{5/2}$. This choice allows a precise determination of the positions necessary to improve the accuracy of the measurement. The results of the determination are summarized in Table I for the two growth temperatures (500 and 400 °C). The mean value of the valence band offset is ≈0.30 eV with a dispersion of ±50 meV, in good agreement with a commonly accepted experimental value of 0.330 eV[31] measured using photoluminescence under pressure. Moreover, this value agrees quite well with theoretical predictions in the 0.32–0.39 eV range.[53] It is, to our knowledge, the first XPS determination of the valence band offset between GaInP and GaAs in agreement with a theoretical calculation. We think that this is probably due to the growth of a quasi-abrupt interface by the suppression of the experimental effects inducing the As/P interdiffusion.

TABLE I. Valence band offset values ΔE_v determined by XPS using various core level lines for the GaInP on GaAs interface at 400 and 500 °C with one night growth interruption.

ΔE_v	500 °C	400 °C
As $3d_{5/2}$–P $2p_{3/2}$	0.266 eV	0.285 eV
As $3d_{5/2}$–In $4d_{5/2}$	0.299 eV	0.291 eV
As $3d_{5/2}$–In $3d_{5/2}$	0.345 eV	0.335 eV

IV. CONCLUSION

In this work we present an XPS characterization of the GaInP on GaAs interface grown by GSMBE. This interface has often been described as diffuse, but we show that the interface broadening is due mainly to experimental effects. In our case, these effects could be a gas mixture in the vent line or in the cracker cell since they are common for arsine and phosphine. We show that, when they are suppressed, the GaInP on GaAs interface is quasi-abrupt. Surface segregation of indium and arsenic with respect to gallium and phosphorus limits the abruptness of the interface. However indium segregation in GaInP is reduced with respect to that in GaInAs at the same growth temperature. Furthermore, As segregation is weak and likely partially compensated by desorption at the surface for growth temperatures of 500 °C or higher. In summary the intrinsic interdiffusion at the GaInP on GaAs interface is weak. This allows us to measure the valence band offset between GaInP and GaAs, obtaining a value of ≈0.3±50 meV. This is the first XPS determination of the GaInP/GaAs valence band offset in agreement with theoretical predictions.

ACKNOWLEDGMENTS

The authors gratefully acknowledge C. Coinon for his technical assistance and J. Barrette for a critical reading of the manuscript.

[1] G. Margaritondo, J. Vac. Sci. Technol. B **11**, 1362 (1993).
[2] Y. Foulon, C. Priester, G. Allan, J. C. Garcia, and J. P. Landesman, J. Vac. Sci. Technol. B **10**, 1754 (1992).
[3] C. Priester, G. Allan, and M. Lannoo, J. Vac. Sci. Technol. B **11**, 1638 (1993).
[4] W. Seidel, O. Krebs, P. Voisin, J. C. Harmand, F. Aristone, and P. Voisin, Phys. Rev. B **55**, 56 (1997).
[5] J. M. Sallese, S. Taylor, H. J. Bühlmann, J. F. Carlin, A. Rudra, R. Houdré, and M. Ilegems, Appl. Phys. Lett. **65**, 341 (1994).
[6] S. S. Rao, W. P. Gillin, and K. P. Homewood, Phys. Rev. B **50**, 8071 (1994).
[7] J. M. Moison, C. Guille, F. Houzay, F. Barthe, and M. Van Rompay, Phys. Rev. B **40**, 6149 (1989).
[8] S. V. Ivanov, P. S. Kop'ev, and N. N. Ledentsov, J. Cryst. Growth **104**, 345 (1990).
[9] J. Massies, J. F. Rochette, and P. Delescluse, J. Vac. Sci. Technol. B **3**, 613 (1985).
[10] H. S. Hansen, A. Bensaoula, S. Tougaard, J. Zborowski, and A. Ignatiev, J. Cryst. Growth **116**, 271 (1992).
[11] J. M. Gérard, Appl. Phys. Lett. **61**, 2096 (1992).
[12] J. M. Gérard and J. Y. Marzin, Phys. Rev. B **45**, 6313 (1991).
[13] K. Muraki, K. Fukatsu, and Y. Shiraki, Appl. Phys. Lett. **61**, 557 (1992).

[14] J. F. Zheng, J. D. Walker, M. B. Salmeron, and E. R. Weber, Phys. Rev. Lett. **72**, 2414 (1994).
[15] O. Dehaese, X. Wallart, and F. Mollot, Appl. Phys. Lett. **66**, 52 (1995).
[16] N. Grandjean, J. Massies, and M. Leroux, Phys. Rev. B **53**, 998 (1996).
[17] J. F. Nützel and G. Abstreiter, Phys. Rev. B **53**, 13 551 (1996).
[18] M. Mesrine, J. Massies, C. Deparis, N. Grandjean, and E. Vanelle, Appl. Phys. Lett. **68**, 3579 (1996).
[19] T. Anan, S. Sugou, K. Nishi, and T. Ichihashi, Appl. Phys. Lett. **63**, 1047 (1993).
[20] W. Wu, S. L. Skala, J. R. Tucker, J. W. Lyding, A. Seabaugh, E. A. Beam III, and D. Jovanovic, J. Vac. Sci. Technol. A **13**, 602 (1995).
[21] R. Benzaquen, A. P. Roth, and R. Leonelli, J. Appl. Phys. **79**, 2640 (1996).
[22] H. Y. Lee, M. D. Crook, M. J. Hafich, J. H. Quigley, G. Y. Robinson, D. Li, and N. Otsuka, Appl. Phys. Lett. **55**, 2322 (1989).
[23] J. C. Garcia, P. Maurel, P. Bove, and J. P. Hirtz, Jpn. J. Appl. Phys., Part 1 **30**, 1186 (1991).
[24] A. Freundlich, A. Bensaoula, A. H. Bensaoula, and V. Rossignol, J. Vac. Sci. Technol. B **11**, 843 (1993).
[25] A. Y. Lew, C. H. Yan, C. W. Tu, and E. T. Yu, Appl. Phys. Lett. **67**, 932 (1995).
[26] T. Nittono, S. Sugitani, and F. Hyuga, J. Appl. Phys. **78**, 5387 (1995).
[27] T. Kobayashi, K. Taira, F. Nakamura, and H. Kawai, J. Appl. Phys. **65**, 4898 (1989).
[28] K. Kodama, M. Hoshino, K. Kitahara, M. Takikawa, and M. Ozeki, Jpn. J. Appl. Phys., Part 2 **25**, L127 (1986).
[29] M. A. Haase, M. J. Hafich, and G. Y. Robinson, Appl. Phys. Lett. **58**, 616 (1991).
[30] T. W. Lee, P. A. Houston, R. Kumar, X. F. Yang, G. Hill, M. Hopkinson, and P. A. Claxton, Appl. Phys. Lett. **60**, 474 (1992).
[31] M. Leroux, M. L. Fille, B. Gil, J. P. Landesman, and J. C. Garcia, Phys. Rev. B **47**, 6465 (1993).
[32] J. P. Landesman, J. C. Garcia, J. Massies, G. Jezequel, P. Maurel, J. P. Hirtz, and P. Alnot, J. Vac. Sci. Technol. B **10**, 1761 (1992).
[33] D. A. Shirley, Phys. Rev. B **5**, 4709 (1972).
[34] C. S. Fadley, Prog. Surf. Sci. **16**, 275 (1984).
[35] M. Seelmann-Eggebert and H. J. Richter, Phys. Rev. B **43**, 9578 (1991).
[36] G. Grenet, E. Bergignat, M. Gendry, M. Lapeyrade, and G. Hollinger, Surf. Sci. **352–354**, 734 (1996).
[37] J. J. Joyce, M. Del Guidice, and J. H. Weaver, J. Electron Spectrosc. Relat. Phenom. **49**, 31 (1989).
[38] G. Le Lay, D. Mao, A. Kahn, Y. Hwu, G. Margaritondo, Phys. Rev. B **43**, 14 301 (1991).
[39] R. W. Grant, E. A. Kraut, S. P. Kowalczyk, and J. R. Waldrop, J. Vac. Sci. Technol. B **1**, 320 (1983).
[40] J. R. Waldrop, S. P. Kowalczyk, R. W. Grant, E. A. Kraut, and D. L. Miller, J. Vac. Sci. Technol. **19**, 573 (1981).
[41] K. Hirakawa, Y. Hashimoto, and T. Ikoma, Appl. Phys. Lett. **57**, 2555 (1990).
[42] S. P. Kowalczyk, E. A. Kraut, J. R. Waldrop, and R. W. Grant, J. Vac. Sci. Technol. **21**, 482 (1982).
[43] J. R. Waldrop, R. W. Grant, and E. A. Kraut, J. Vac. Sci. Technol. B **7**, 815 (1989).
[44] J. R. Waldrop, R. W. Grant, and E. A. Kraut, J. Vac. Sci. Technol. B **11**, 1617 (1993).
[45] J. R. Waldrop, E. A. Kraut, C. W. Farley, and R. W. Grant, J. Appl. Phys. **69**, 372 (1991).
[46] G. Martin, S. Srite, A. Botchkarev, A. Agarwal, A. Rockett, H. Morkoç, W. R. L. Lambrecht, and B. Segall, Appl. Phys. Lett. **65**, 610 (1994).
[47] G. Biasiol, L. Sorba, G. Bratina, R. Nicolini, A. Franciosi, M. Peressi, S. Baroni, R. Resta, and A. Baldereschi, Phys. Rev. Lett. **69**, 1283 (1992).
[48] M. Cantile, L. Sorba, S. Yildirim, P. Faraci, G. Biasiol, A. Franciosi, T. J. Miller, and M. I. Nathan, Appl. Phys. Lett. **64**, 988 (1994).
[49] E. T. Yu, E. T. Croke, and T. C. Mc Gill, Appl. Phys. Lett. **56**, 569 (1990).
[50] W. X. Ni and G. V. Hansson, Phys. Rev. B **42**, 3030 (1990).
[51] *Handbook of Chemistry and Physics* edited by D. R. Lide. (CRC, Boca Raton, FL, 1994).
[52] O. Dehaese, X. Wallart, O. Schuler, and F. Mollot, Appl. Surf. Sci. **123/124**, 523 (1998).
[53] Y. Foulon, C. Priester, G. Allan, J. C. Garcia, J. P. Landesman, and M. Leroux, Phys. Rev. B **46**, 1886 (1992).

of wafer A, which can be recycled. Wafer B plays the role of stiffener, so the microsplitting develops differently to in the case of a free surface. Indeed, elastic deformation of the thin film is impossible and consequently, due to the local stress, splitting of the full wafer occurs. This stiffener effect is obtained by high quality bonding. The macroscopic view of the transferred wafer shows a good transfer on the full wafer (Fig. 3); note the existence of a few defects near the flat section. The cross-section of this structure exhibits a good quality bonding interface, a high microroughness surface due to the splitting (Fig. 4). The microroughness, determined with a Tencor profilometer, indicates an RMS roughness of ~15nm.

(iv) Step 4: A final polish has to be carried out after splitting to eliminate the disturbed region on the surface. This work is in progress.

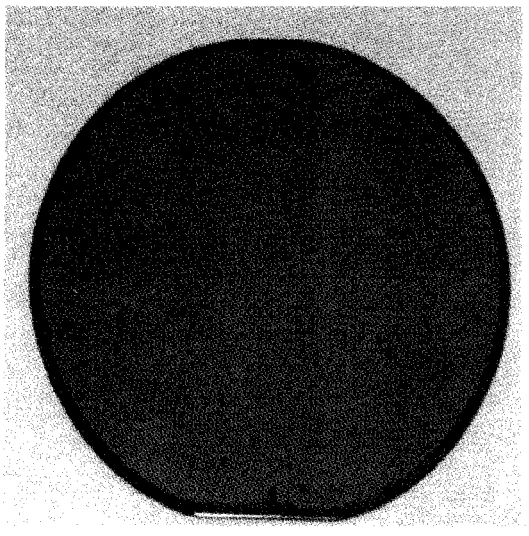

Fig. 3 *Photograph of GaAs film transferred onto 3in silicon wafer*

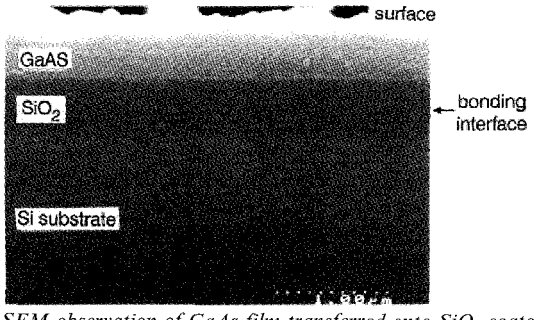

Fig. 4 *SEM observation of GaAs film transferred onto SiO_2 coated silicon substrate*

Conclusion: We have demonstrated, for the first time, the feasibility of transferring thin monocrystalline GaAs film onto an Si substrate using the 'IMPROVE' process. This prepares the way for achieving new architectures with III-V materials.

Acknowledgments: This work was funded by CEA and PICOGIGA.

17 December 1997
Electronics Letters Online no: 19980265

E. Jalaguier, B. Aspar, S. Pocas, J.F. Michaud, M. Zussy and M. Bruel (*LETI-CEA Grenoble, Département de Microtechnologies, 17 rue de Martyrs, 38054 Grenoble Cedex 9, France*)

A.M. Papon (*LETI-CEA Grenoble, Département Optronique, 17 rue des Martyrs, 38054 Grenoble Cedex 9, France*)

References

1 MORI, K., TOKUTOME, K., and SUGOU, S.: 'Low-threshold pulsed operation of long-wavelength lasers on Si fabricated by direct bonding', *Electron. Lett.*, 1995, **31**, (4), pp. 284–285
2 BRUEL, M.: 'Silicon on insulator material technology', *Electron. Lett.*, 1995, **31**, (14), pp. 1201–1202
3 Smart-Cut® is a trade mark of the SOITEC company
4 DI CIOCIO, L., LE TIEC, Y., LETERTRE, F., JAUSSAUD, C., and BRUEL, M.: 'Silicon carbide on insulator formation using the Smart Cut process', *Electron. Lett.*, 1996, **32**, (12), pp. 1144–1145
5 SNYMAN, H.C., and NEETHLING, J.H.: 'Transmission electron microscopy of extended crystal defects in proton bombarded and annealed GaAs', *Radiation Effects*, 1983, **69**, pp. 199–230
6 ASPAR, B., BRUEL, M., MORICEAU, H., MALEVILLE, C., POUMEYROL, T., PAPON, A.M., CLAVERIE, A., BENASSAYAG, G., AUBERTON-HERVÉ, A.J., and BARGE, T.: 'Basic mechanisms involved in the Smart-Cut® process', *Microelectron. Eng.*, 1997, **36**, pp. 233–240
7 TONG, Q.-Y., GUTJAHR, K., HOPFE, S., GÖSELE, U., and LEE, T.-H.: 'Layer splitting process in hydrogen-implanted Si, Ge, SiC, and diamond substrates', *Appl. Phys. Lett.*, 1997, **70**, (11), pp. 1390–1392
8 MASZARA, W.P., GOETZ, G., CAVIGLIA, A., and MCKITTERICK, J.B.: 'Bonding of silicon wafers for silicon-on-insulator', *J. Appl. Phys.*, 1988, **64**, (10), pp. 4943–4950

V-band high-power/low-voltage InGaAs/InP composite channel HEMTs

P. Chevalier, X. Wallart, B. Bonte and R. Fauquembergue

The authors have developed 0.15μm gate length InAlAs/InGaAs/InP composite channel HEMTs with state-of-the-art power performance at 60GHz. An output power of 355mW/mm was obtained with 6.2dB linear power gain and 12% power-added-efficiency at a drain voltage of 2.5V.

InGaAs/InAlAs HEMTs on InP substrates have demonstrated excellent performance for low-noise applications in the millimetre wave range. Nevertheless, power HEMTs based on InGaAs channels are limited by the strong impact ionisation in this material. Thus, they suffer from high output conductance, low breakdown voltage and non-zero gate current due to hole generation. By decreasing the indium content in the InGaAs channel, impact ionisation can be reduced, but frequency performance and drain current are affected.

Another method for reducing impact ionisation is to substitute the lower part of the InGaAs channel by an InP layer. The main advantages of this composite channel structure are the higher value of the ionisation threshold energy in InP compared with InGaAs (1.69eV compared with 0.92eV), the conduction band discontinuity between the two materials (ΔE_c ($In_{0.53}Ga_{0.47}As$-InP) = 0.2eV), and the high-field electron transport properties in InP which are not so different from those of InGaAs.

We have shown, using Monte-Carlo simulations, that this type of structure reduces impact ionisation effects [1] due to hot electron transfer from InGaAs to InP. These results, experimentally confirmed [2], outline the interest of the InGaAs/InP/n^+-InP composite doped channel HEMT as a power device. Relatively few composite channel HEMTs with a doped sub-channel have been realised [3, 4]. The obtained results have shown the ability of this device to deliver power in the K-band at a high drain voltage [5]. In this Letter, we present state-of-the-art power results at 60GHz, obtained at a low voltage with a 0.15μm gate length composite channel HEMT.

The composite channel structure was grown on a (100)-oriented InP substrate using a Riber-32P gas source molecular beam epitaxy (GS-MBE) system. The epitaxial layers, shown in Fig. 1, consist of a conventional InAlAs/InGaAs lattice-matched structure with a $5 \times 10^{12}cm^{-2}$ delta-doped layer and a composite doped channel with 12nm of undoped InGaAs, a 4nm undoped InP spacer and an 8nm InP sub-channel doped to $2 \times 10^{18}cm^{-3}$. The undoped InP spacer was inserted to avoid Si diffusion into the InGaAs channel. The sheet resistance of the epilayer was 180Ω/□.

$2 \times 50 \times 0.15\mu m^2$ HEMTs were fabricated using a trilayer resist gate technology. The fabrication began with the realisation of source and drain ohmic contacts. They were formed using Ni/Ge/Au/Ni/Au metallisation and rapid thermal annealing at 315°C for 10s in an N_2/H_2 atmosphere. A contact resistance of 0.13Ω/mm was obtained. Device isolation was performed by chemical mesa etching down to the InAlAs buffer layer with an H_3PO_4:H_2O_2:H_2O

etchant. HCl:H_2O was used to etch the sub-channel of InP. The T-gate was defined within a source-drain separation of 1.3μm, in one step, using electron-beam lithography on a trilayer resist system (PMMA/P(MMA-MAA)/PMMA). After the chemical recess using a selective etchant (succinic acid: H_2O_2), the gate was metallised with Ti/Pt/Au, followed by a 15min, 290°C anneal. As a final step, thick Ti/Au probing pads were deposited. The devices were non-passivated.

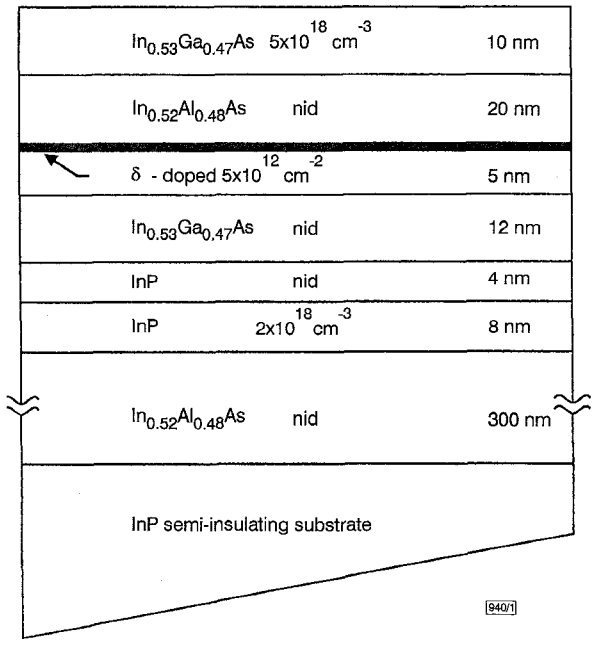

Fig. 1 *GaInAs/InP composite channel HEMT structure*

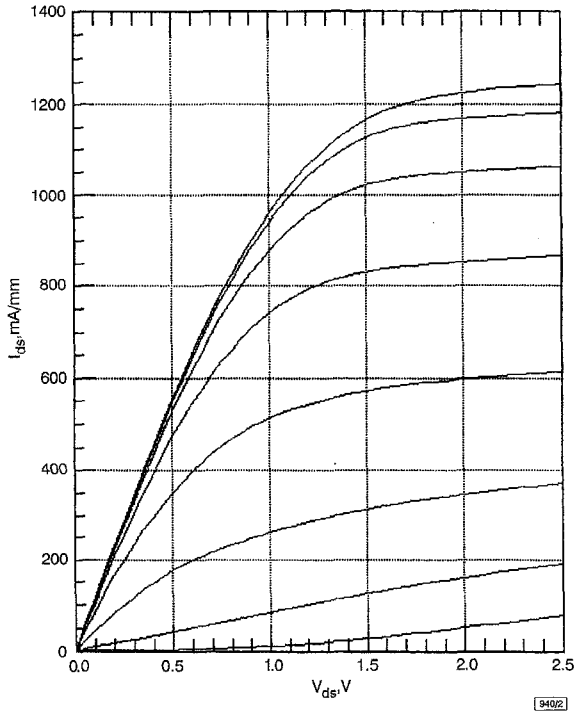

Fig. 2 *Current voltage characteristics of 0.15 × 2 × 50μm² composite channel HEMT*

Gate voltage ranges from 0.4 to –2.4V with 0.4V step

The typical current-voltage characteristics of the 2 × 50 × 0.15μm² device is shown in Fig. 2. The InGaAs/InP/n^+-InP composite channel device exhibits a current density of ~1100mA/mm at V_{ds} = 1.5V and V_{gs} = 0V and 1250mA/mm at V_{ds} = 2.5V and V_{gs} = +0.4V. A source to drain breakdown voltage > 3V was obtained. This value is very interesting if we consider the short source-to-drain spacing (1.3μm) and the width of the gate recess (300nm).

The microwave performance was measured using on-wafer probing techniques. S-parameters were extracted from 1 to 50GHz under an optimum DC bias. The extrinsic current gain cutoff frequency F_T and the maximum unilateral gain cutoff frequency F_{MAX} were determined from extrapolation with a –20dB/decade slope of the current gain H_{21}^2 and the unilateral gain U. RF characteristics were measured at drain voltages of +1.5 and +2V. The transconductance peak was ~950mS/mm at 1.5V and 860mS/mm at 2V. The associated output conductances were, respectively, 125and 85mS/mm. Values of F_T = 150GHz and F_{MAX} = 200GHz have been obtained at V_{ds} = 1.5V.

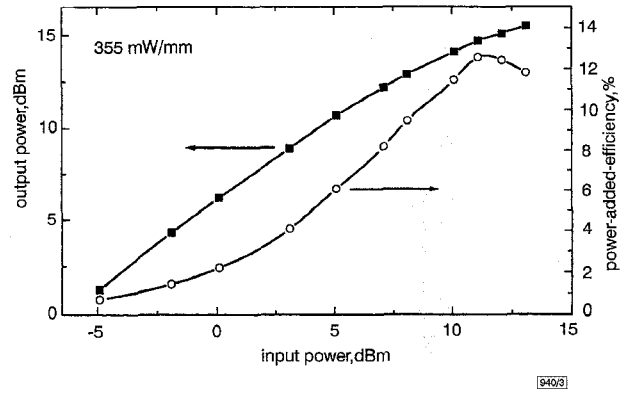

Fig. 3 *Output power and PAE at 60GHz of a 0.15 × 2 × 50μm² composite channel HEMT*

V_{ds} = 2.5V, V_{gs} = –1.2V

The power performance was measured in class A at 60GHz using an on-wafer probe system. The mechanical tuners were adjusted to obtain the maximum output power and minimum reflected input power. The measured input and output powers were corrected in order to take into account the losses of the RF probes and the waveguide. The evolution of output power and power-added-efficiency (PAE) against input power, measured at a drain bias of V_{ds} = 2.5V and a gate bias of V_{gs} = –1.2V, are plotted in Fig. 3. The device generates 355mW/mm output power with 6.2dB linear power gain, 28% drain efficiency and 12% PAE. The maximum power was achieved far above the 1dB gain compression, which explains the low PAE compared to the drain efficiency. This distinctive feature can be attributed to the small aspect ratio (gate length/gate-to-channel separation), unfavourable to low output conductance and high gate resistance.

In summary, composite channel power HEMTs have successfully been realised with a high power performance in the V-band at a low drain-to-source voltage of 2.5V, which is very interesting for low voltage applications. In addition, these results were obtained for a power non-optimised device: a gate centred in the 1.3μm source-drain spacing, with a narrow gate recess, and a lattice-matched Schottky barrier. Consequently, significant improvements in structure and device technology are being studied to develop MMIC circuits based on these InP composite channel HEMTs. Our aim is to introduce a hole barrier by using a strained Schottky layer and to determine the best compromise between gate length, MAG and frequency of operation.

Acknowledgments: The authors would like to thank D. Theron and F. Dessenne for their helpful discussions and E. Delos for RF measurements. This work has been financed by French MOD (DGA).

16 December 1997

Electronics Letters Online No: 19980254

P. Chevalier, X. Wallart, B. Bonte and R. Fauquembergue (*Institut d'Electronique et de Microélectronique du Nord, U.M.R.-C.N.R.S. 9929, Département Hyperfréquences et Semiconducteurs, Avenue Poincaré BP 69, 59652 Villeneuve d'Ascq, France*)

References

1 BOUREL, P., BADIROU, M., DESSENNE, F., THOBEL, J.L., and FAUQUEMBERGUE, R.: 'A Monte-Carlo study of impact ionisation in InP LM-HEMT'. 4th Int. Seminar on Simulation of Devices and Technologies, Berg-en-Dal, South Africa, 1995, pp. 50–53

2 CHEVALIER, P., DESSENNE, F., BADIROU, M., THOBEL, J.L., and FAUQUEMBERGUE, R.: 'Interest of 0.15μm gate length InGaAs/InP composite channel HEMTs for millimeter-wave MMIC amplifiers'. 5th IEEE Int. Workshop on High Performance Electron Devices for Microwave and Optoelectronic Applications, London, UK, 1997, pp. 193–198

3 ENOKI, T., ARAI, K., KOHZEN, A., and ISHII, Y.: 'Design and characteristics of InGaAs/InP composite-channel HFET's', *IEEE Trans. Electron Devices,* 1995, **42**, (8), pp. 1413–1418

4 MATLOUBIAN, M., JELLOIAN, L.M., LUI, M., LIU, T., LARSON, L.E., NGUYEN, L.D., and LE, M.V.: 'GaInAs/InP composite channel HEMT's', *IEEE Trans. Electron Devices,* 1993, **40**, (11), pp. 2112

5 SHEALY, J.B., MATLOUBIAN, M., LIU, T., VIRK, R., PUSL, J., and NGO, C.: 'K-band high-power/efficiency/breakdown GaInAs/InP composite channel HEMT's', *IEEE Microw. Guided Wave Lett.,* 1997, **7**, (9), pp. 261–263

Compensation for saturation effects in FIR-NLMS system identification

P. Händel

An adaptive scheme is derived to be used in combination with the normalised least mean squares algorithm for finite impulse response models (FIR-NLMS), to combat nonlinear imperfections of the plant to be identified. The scheme is shown to outperform FIR-NLMS when a test system that consists of a variable static nonlinearity in cascade with a linear filter is identified.

Introduction: One of the most widely used algorithms for on-line system identification is the normalised least mean squares for finite impulse response models (FIR-NLMS) [1]. A typical system identification setup is shown in Fig. 1, where x_k and y_k are the measured input and output signals from the plant to be identified. The success of a system identification experiment by FIR-NLMS depends on several issues related to the plant, such as complexity (model order selection), linearity, stationarity, and properties of external disturbances e_k, as well as on the properties of the stimulus x_k, that, in particular, has to be persistently exciting.

The objective of this Letter is to derive a low-complexity add-on algorithm in order to improve performance (in terms of residual error) of FIR-NLMSs when the plant includes a class of nonlinear imperfections. The proposed add-on scheme has only one parameter, b, that is adaptively adjusted to the data. A smooth static nonlinearity is utilised, that for small values of b is approximately linear, and for large b is an approximation of a scaled sign-function. For easy reference, the FIR-NLMS compensated for nonlinear imperfections is denoted C-FIR-NLMS. The performance of C-FIR-NLMS is investigated by identification of the test system in Fig. 1. The test system may, for example, be a rough description of an acoustic plant, where the gain control and the fixed limiter

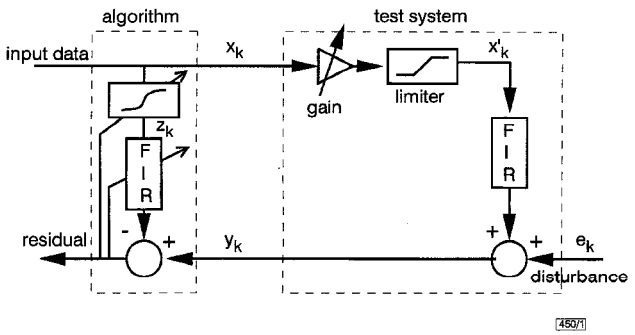

Fig. 1 *Test system containing a variable gain, a fixed limiter, and a 74-tap FIR filter with unity gain*

For identification purposes, an $(L+1)$-tap FIR-NLMS is combined with the proposed adaptive compensator for saturation effects describe an (analogue) amplifier and loudspeaker, and where the FIR model describes the impulse response of the acoustic cavity. At low volumes the loudspeaker output is a linear function of the input to the amplifier, but at high volumes the output is severely distorted due to saturation effects in the amplifier, or loudspeaker imperfections.

FIR-NLMS with compensation for saturations: For simplicity, let x_k be bounded by ±1. Consider the following static nonlinear transformation of x_k:

$$z_k = \frac{\arctan(e^b x_k)}{e^b} \qquad k = 0, 1, \ldots \tag{1}$$

where b is a free parameter. For $b \ll 0$, e^b is small and $\arctan(e^b x_k) \simeq e^b x_k$, and thus $z_k \simeq x_k$. On the other hand, for $b \gg 0$, e^b is large and $z_k \simeq c \cdot \text{sign}[x_k]$, where $c = \pi/2e^b$. For practical applications, b values in the range (–1, 3) seem to be sufficient, meaning that e^b spans the interval 0.37–20. Let z_k be the input data to an FIR-NLMS (see Fig. 1). Then, the residual error is given by (^{T} denotes transpose)

$$\varepsilon_k(b) = y_k - \mathbf{h}^T \mathbf{z}_k = y_k - \mathbf{h}^T \frac{\arctan(e^b \mathbf{x}_k)}{e^b} \tag{2}$$

where $\mathbf{x}_k = (x_k, \ldots, x_{k-L})^T$ and $\mathbf{z}_k = (z_k, \ldots, z_{k-L})^T$. The notation $\arctan(\mathbf{x})$, where $x = (x_0, \ldots, x_L)^T$, is a short notation for the vector with components $\arctan(x_\ell)$, $\ell = 0, \ldots, L$. The negative gradient of $\varepsilon_k(b)$ with respect to b is necessary, that is

$$-\frac{\partial \varepsilon_k(b)}{\partial b} = \sum_{\ell=0}^{L} h_\ell \left(\frac{x_{k-\ell}}{1 + e^{2b} x_{k-\ell}^2} - z_{k-\ell} \right) \tag{3}$$

Replacing $\varepsilon_k(b)$ and $\partial\varepsilon_k(b)/\partial b$ with running estimates, a recursive prediction error algorithm for the adaptive update of b is easily constructed [2]. Combining the resulting algorithm with the FIR-NLMS scheme results in the C-FIR-NLMS as summarised below.

$$\hat{a}_k = \exp(\hat{b}_{k-1}) \tag{4}$$

$$z_k = \frac{\arctan(\hat{a}_k x_k)}{\hat{a}_k} \tag{5}$$

$$\mathbf{z}_k = (z_k, z_{k-1}, \ldots, z_{k-L})^T \tag{6}$$

$$\varepsilon_k = y_k - \mathbf{h}_{k-1}^T \mathbf{z}_k \tag{7}$$

$$\mathbf{h}_k = \mathbf{h}_{k-1} + \frac{\mu \mathbf{z}_k}{\mathbf{z}_k^T \mathbf{z}_k} \varepsilon_k \tag{8}$$

$$\psi_k = \frac{x_k}{1 + \hat{a}_k^2 x_k^2} - z_k \tag{9}$$

$$\Psi_k = (\psi_k, \psi_{k-1}, \ldots, \psi_{k-L})^T \tag{10}$$

$$R_k = \lambda R_{k-1} + (\mathbf{h}_k^T \Psi_k)^2 \tag{11}$$

$$\hat{b}_k = \hat{b}_{k-1} + \frac{\mathbf{h}_k^T \Psi_k}{R_k} \varepsilon_k \tag{12}$$

where eqns. 4 and 5 form the nonlinear transformation of x_k; eqns. 6 – 8 define the FIR-NLMS algorithm [1], and eqns. 9 – 12 form the adaptive update of b.

The recursions (eqns. 4–12) in combination with the stability monitoring: $\hat{b}_k \in (b_{min}, b_{max})$, and gain control $R_k > R_{min}$ for some small R_{min} completes the C-FIR-NLMS. Typical values are $b_{min} = -1$, $b_{max} = 3$, and $R_{min} = 0.01$. In eqn. 11, λ is a design variable $\lambda < 1$ that controls the speed of the convergence of $\hat{b}_k$.

Performance evaluation: The test system used in the simulation study consists of a variable gain, a limiter, and a 74-tap FIR filter, see Fig. 1. The output from the limiter is $x_k^L = x_k$ for $|x_k| \leq 1$ and $x_k^L = \text{sign}[x_k]$ for $|x_k| > 1$, where sign[·] is the sign function. By assumption x_k is bounded by ±1, and thus the test system is linear for gains below 0dB. In the limit that the gain tends to $+\infty$, the output is $x_k^L = \text{sign}[x_k]$. The FIR filter has unity static gain, and its impulse response is shown in Fig. 2. In the experiment, x_k is a 7s sequence of male Finnish speech samples of absolute level –16.9dB. The speech signal is sampled at 8kHz. The external disturbance e_k is zero mean white Gaussian with absolute level –45dB.

The performance, measured in terms of residual error of the C-

Best Combination Between Power Density, Efficiency, and Gain at V-Band with an InP-Based PHEMT Structure

S. Piotrowicz, C. Gaquiere, *Member, IEEE*, B. Bonte, E. Bourcier, D. Theron, *Member, IEEE*, X. Wallart, and Y. Crosnier

***Abstract*— In this letter, we report on the state-of-the-art combination at V-band between simultaneously power density (370 mW/mm), power-added efficiency (28.3%), and power gain (5.2 dB) of InP pseudomorphic HEMT's biased at a low drain voltage of 2 V. The performance of these double delta-doped pseudomorphic AlInAs/GaInAs HEMT's on InP with an original strain compensated channel was measured at 60 GHz. This demonstrates a good potentiality for low-voltage applications in order to reduce the power supply of systems.**

I. Introduction

A LOT of work has been done on InP-based HEMT's for low-noise or low-power applications because they demonstrated higher microwave performance superior than those of any other transistor [1]. In the case of low noise, many devices have been realized with a lattice-matched channel, allowing a high conduction band discontinuity at the InGaAs/InAlAs heterostructure interface, an excellent electron mobility, and peak velocity in the InGaAs channel [2]. These advantages can be improved by increasing the indium mole fraction [3]. In the case of power amplifiers, high breakdown voltages are more crucial than for low-noise amplifiers. That is why many authors have reported structures where the channel is often lattice matched [4], [5] and the aluminum fraction in the $Al_xIn_{(1-x)}As(x > 0.48)$ barrier is increased. To our knowledge, the best result in term of output power with an InP-based HEMT at around 60 GHz has been obtained by Matloubian *et al.* [4] with an output power of 180 mW (400 mW/mm), a power-added efficiency (PAE) of 27%, and 3-dB gain at 3.5-V drain-to-source voltage.

However, in the case of low-supply applications, the dc bias is limited [6]. Hence, to obtain high power density, it is necessary to achieve high current density. For this reason, in this work we report the fabrication and measurements of an original InP power PHEMT with a strain-compensated channel and two delta-doped planes in order to reach a very high current density. A high aluminum fraction in the barrier has also been inserted to increase the conduction band discontinuity. Power measurements at 60 GHz represent to our knowledge the best combination between a power density of 370 mW/mm, a PAE of 28.3%, and power gain of 5.2 dB.

Manuscript received August 4, 1997. This work was supported by the French MOD (DGA).

The authors are with the Institiut d'Electronique et de Microelectronique du Nord, 59652 Villeneuve D'ASCQ, France.

Publisher Item Identifier S 1051-8207(98)00862-9.

II. Device Design

To achieve high current densities with power HEMT's, we have used, an original strain-compensated layer. A cross section of the power HEMT considered is shown in Fig. 1. The layers were grown by molecular beam epitaxy on a semi-insulated InP substrate. The buffer consists of a 100-nm AlInAs layer and a 300-nm-thick AlInAs layer grown at low temperature (400 °C). The active part of the structure is a 15-nm $Ga_{0.35}In_{0.65}As$ pseudomorphic channel with two 5-nm AlInAs spacer layers on both side of the channel. The bottom AlInAs layer is lattice matched with a δ-doped plane at 2×10^{12} cm^{-2}. To improve the Schottky-barrier height of the gate, a 15-nm undoped pseudomorphic $Al_{0.65}In_{0.35}As$ layer with a δ-doped plane of 4×10^{12} cm^{-2} was grown. Finally, a 7-nm doped (5×10^{18} cm^{-3}) GaInAs layer was grown to facilitate ohmic contact formation. The two-dimensional electron gas (2-DEG) was formed in the pseudomorphic GaInAs channel by electron transfer from silicon δ doping above and below the AlInAs layer. The dual δ-doped structure provides high carrier concentration in the channel and leads to a high current density which benefits the power device performance. Hall measurements indicate, at room temperature, an electron sheet charge density of 4.6×10^{12} cm^{-2} with an approximate mobility of 15 000 cm^2/V·s. The fabricated device has a total gate width of 2×50 μm with a 0.25-μm gate length.

III. Device Performance

These InP HEMT's have demonstrated a peak transconductance Gm of 800 mS/mm. They exhibit a full channel current $I_{\max}$ of 1480 mA/mm (defined as the drain saturation current density measured at a gate-to-source voltage of 0.6 V) measured at a drain to source voltage of 2 V. The gate-to-drain or gate-to-source diodes breakdown voltages measured at 1 mA/mm of gate current are 4.5 V. The turn-on voltage and the pinch-off voltage are, respectively, 0.9 and -2.5 V.

S-parameter measurements of the devices were performed from 0.5 to 75 GHz using automatic network analyzers. An intrinsic current gain cutoff frequency (F_T) of 105 GHz and a maximum available gain of 10 dB at 60 GHz have been obtained at a drain bias of 2 V. The power performance of the HEMT were measured at 60 GHz using an on wafer probe system. Mechanical tuners were adjusted to obtain maximum output power and minimum reflected input power.

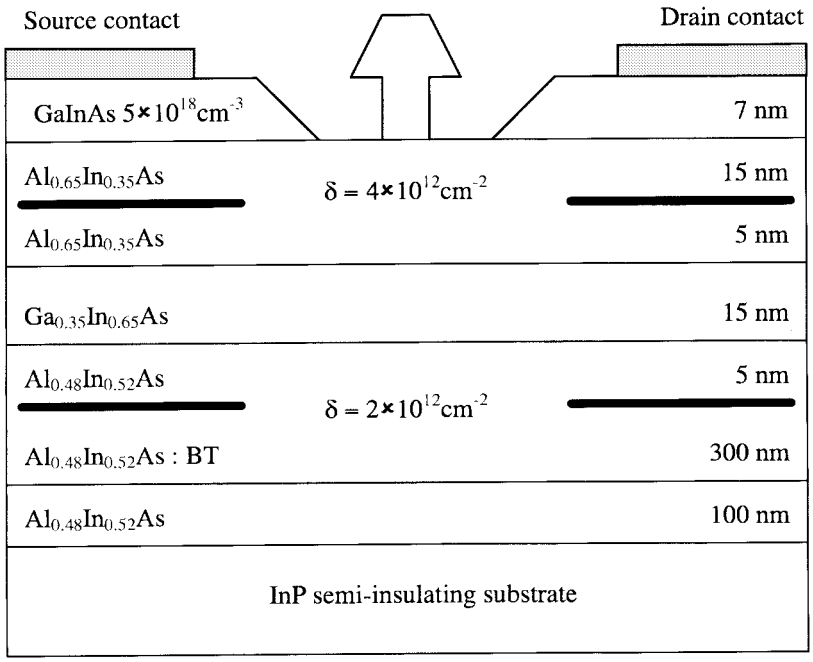

Fig. 1. Cross section of the double δ-doped pseudomorphic $Al_{0.65}In_{0.35}As$/ $Ga_{0.35}In_{0.65}As$/InP HEMT.

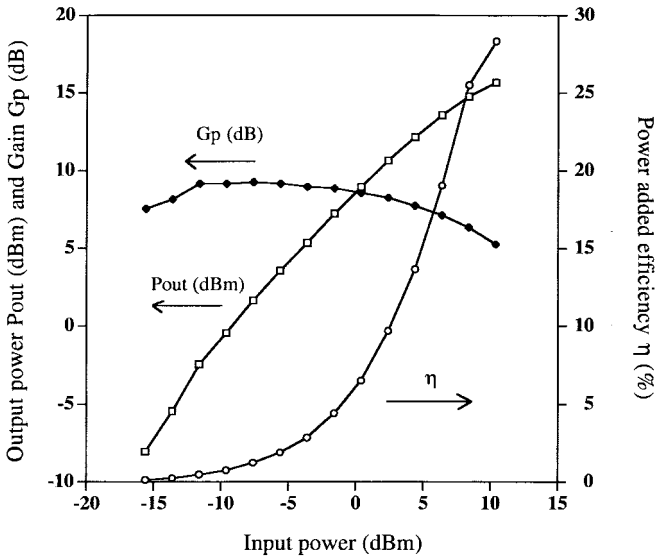

Fig. 2. Power characteristics at 60 GHz for the following bias conditions: $V_{ds} = 2$ V and $V_{gs} = -1.5$ V.

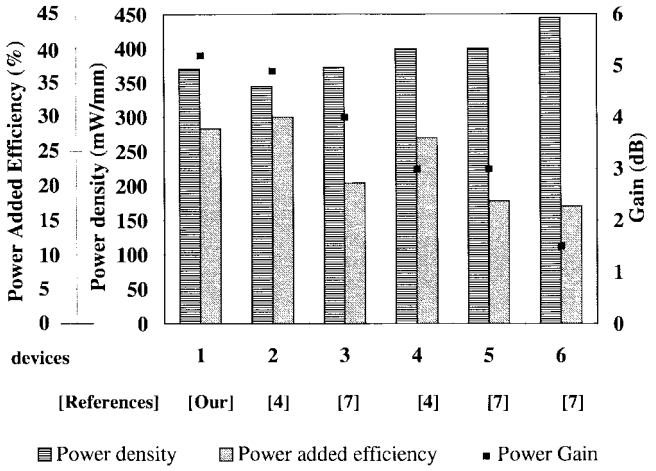

Fig. 3. Comparison of the state-of-the-art power density, PAE, and power gain on discrete devices at about 60 GHz on InP.

The measured input and output power were corrected in order to take into account the losses of the probes and the waveguide. The measured power performance of devices biased at a V_{ds} of 2 V and V_{gs} of -1.5 V to operate in class A are shown in Fig. 2. They have demonstrated a maximum output power of 15.7 dBm corresponding to a power density of 370 mW/mm with a PAE of 28.3% and 5.2-dB gain. In order to compare our results with other power devices at 60 GHz on InP HEMT, we report Fig. 3 a graph with the most significantly published results. Even if our devices exhibit a power density slightly inferior to the other, it seems to be the best compromise between the three items: power density, gain, and efficiency. We have obtained less power density but much more PAE and gain than devices numbered 3, 4, 5 and 6. The devices numbered 2 have a slightly better PAE (30%) than our devices but a gain and power density inferior. That is why we can consider that, to our best knowledge, we have achieved the state-of-the-art combination between simultaneously power density, PAE, and power gain.

The fabricated double δ-doped HEMT has demonstrated good potentiality for low-voltage operation in power conditions. The reduction of the power consumption of circuits allows to decrease the number of the battery cells and then to the reduction of the size and weight of systems.

IV. Conclusion

In this letter, we report on state-of-the-art combination between power density, PAE, and power gain on original InP PHEMT's with a strain compensated layer. Power measure-

ments at 60 GHz have given a power density of 370 mW/mm with a PAE of 28.3% and 5.2-dB gain at a low drain-to-source voltage of 2 V. These devices exhibit a current density as high as 1480 mA/mm. They have demonstrated a good potentiality for low-voltage operation in order to reduce the power consumption of systems. By further optimization of the gate recess dimensions and also incorporating a 0.15-μm gate length in our power PHEMT's, we expect some improvement of the power performance of these transistors in V-Band.

ACKNOWLEDGMENT

The authors would like to acknowledge M. Zaknoune for his helpful discussions and F. Diette for device processing.

REFERENCES

[1] P. M. Smith, S.-M. J. Liu, M.-Y. Kao, S. C. Wang, K. H. G. Duh, S. T. Fu, and P. C. Chao, "W band high efficiency InP based power HEMT with 600 GHz $f_{\max}$," *IEEE Microwave Guided Wave Lett.*, vol. 5, pp. 230–232, July 1995.

[2] L. Tran, R. Isobe, M. Delaney, R. Rhodes, D. Jang, J. Brown, L. Nguyen, M. Le, M. Thompson, and T. Liu, "High performance, high yield millimeter-wave MMIC LNA's using InP HEMT's," in *IEEE MTT-S Dig.*, 1996, pp. 9–12.

[3] H. Wang, R. Lai, D. C. W. Lo, D. C. Streit, P. H. Liu, R. M. Dia, M. W. Pospieszalski, and J. Berenz, "A 140 GHz monolithic low noise amplifier," *IEEE Microwave Guided Wave Lett.*, vol. 5, pp. 150–152, May 1995.

[4] M. Matloubian, L. M. Jelloian, A. S. Brown, L. D. Nguyen, L. E. Larson, M. J. Delaney, M. A. Thompson, R. A. Rhodes, and J. E. Pence, "V band high efficiency high power AlInAs/GaInAs/InP HEMT's," *IEEE Trans. Microwave Theory Tech.*, vol. 41, pp. 2206–2209, Dec. 1993.

[5] R. Lai, G. I. Ng, D. C. W. Lo, T. Block, H. Wang, M. Biedenbender, D. C. Streit, P. H. Liu, R. M. Dia, E. W. Lin, and H. C. Yen, "A high efficiency 94 GHz 0.15 μm InGaAs/InAlAs/InP monolithic power HEMT amplifier," *IEEE Microwave Guided Wave Lett.*, vol. 6, pp. 365–367, Oct. 1996.

[6] Y. L. Lai, E. Y. Chang, C. Y. Chang, T. K. Chen, T. H. Liu, S. P. Wang, T. H. Chen, and C. T. Lee, "5 nm high power density dual delta doped power HEMT's for 3 V L band applications," *IEEE Electron Device Lett.*, vol. 17, pp. 229–231, May 1996.

[7] M. Matloubian, A. S. Brown, L. D. Nguyen, M. A. Melendes, L. E. Larson, M. J. Delaney, J. E. Pence, R. A. Rhodes, M. A. Thompson, and J. A. Henige, "High power V-band AlInAs/GaInAs on InP HEMT's," *IEEE Electron Device Lett.*, vol. 4, Apr. 1993.

Composition effect on the growth mode, strain relaxation, and critical thickness of tensile $Ga_{1-x}In_xP$ layers

X. Wallart,[a] O. Schuler, D. Deresmes, and F. Mollot
Institut d'Electronique et de Microélectronique du Nord, UMR–CNRS 8520, B.P. 69, 59652 Villeneuve d'Ascq, France

(Received 21 September 1999; accepted for publication 15 February 2000)

In this work, we compare the growth and relaxation behavior of tensile $Ga_{0.7}In_{0.3}P$/GaAs and $Ga_{0.2}In_{0.8}P$/InP layers using reflection high-energy electron diffraction, double-crystal x-ray diffraction, and atomic-force microscopy. Although the lattice mismatch is similar in both cases, we show that the relaxation process and the related critical thickness are very different and, hence, drastically dependent on the alloy composition. We interpret this result considering the predicted composition range for which alloy decomposition should occur. © *2000 American Institute of Physics.* [S0003-6951(00)05215-3]

Up to now, the reported work on strained-layer growth and relaxation of III–V semiconductors has been mainly concerned with two material systems, i.e., GaInAs/GaAs (Refs. 1 and 2) and GaInAs/InP.[3,4] From the great amount of reported studies, a picture of the relaxation behavior of compressive strained layers has emerged with the main emphasis put on the elastic strain value. Briefly, for strain values above 2%, elastic relaxation occurs first via the formation of coherent islands on the surface, what is called the two-dimensional to three-dimensional (2D–3D) growth-mode transition. On the contrary, for strain values below 2%, plastic relaxation occurs first. The case of tensile layers is less straightforward since the two above-mentioned relaxation processes seem more or less driven by the development of the surface roughness during growth. Regarding the relaxation behavior of strained GaInP layers, Matragano *et al.*[5] have investigated the relaxation of slightly strained (±0.5%) GaInP layers grown on GaAs by metalorganic chemical-vapor deposition (MOCVD) using double-axis x-ray diffraction. They show that strain relaxes anisotropically and that the anisotropy is more pronounced for tensile samples than for compressive ones. This anisotropy is also discussed by Bensaada *et al.*[6] for slightly tensile $Ga_xIn_{1-x}P$ layers ($0.01<x<0.12$) on InP obtained by MOCVD and observed by Cohen and co-workers[7,8] who report a critical thickness of 500 Å for $Ga_{0.25}In_{0.75}P$ tensile layers grown on InP by metalorganic molecular-beam epitaxy (MOMBE). Gonzalez *et al.*[9] have studied the relaxation behavior of compressive $Ga_{1-x}In_xP$ layers ($0.53<x<0.70$) and show that neither doping nor growth conditions have a strong influence on relaxation.

However, in most of the reported work on the relaxation of GaInP alloys as well as on other alloys, strain and composition effects are always correlated since the strain variation is obtained via a composition modification and vice versa. In this work, using reflexion high-energy electron diffraction (RHEED), double-crystal x-ray diffraction (DCXRD), and atomic-force microscopy (AFM), we compare the relaxation of tensile strained $Ga_{0.7}In_{0.3}P$ layers on GaAs(001) and $Ga_{0.2}In_{0.8}P$ layers on InP(001) substrates. We show that although the lattice mismatch is similar in both cases (+1.4%), the relaxation process is drastically different for the two alloy compositions under consideration. We interpret this result in term of spinodal decomposition of the GaInP alloys.

The samples are grown by gas-source molecular-beam epitaxy (Riber 32P) using cracked phosphine and arsine as element-V sources and standard effusion cells for elements III, on semi-insulating (001) GaAs or InP substrates. On the GaAs substrates, strained layers were grown either directly on a GaAs buffer layer or on a lattice-matched (LM) GaInP buffer layer. In the former case, after the growth of a GaAs buffer layer at 580 °C, the substrate temperature is lowered down to 520 °C during a 3 min growth interruption. The arsine flux is vented when the substrate temperature reaches 550 °C in order to keep a (2×4) reconstruction. Then, special care is taken in the gas commutation procedure to minimize As/P intermixing, i.e., the GaAs surface is exposed for 10 s to phosphorus flux before Ga and In shutters are opened. On InP substrates, the strained layer growth is only preceded by the growth of a InP buffer layer at 490 °C. Gallium and indium fluxes, determining growth rates and alloy compositions are measured by RHEED intensity oscillations on GaAs and InP, before the growth. The growth parameters of the strained GaInP layers are kept identical on both substrates, i.e., a growth rate of 0.7 ML/s and a PH_3 flow rate of 3 sccm. 20 keV RHEED patterns are recorded along both the [110] and [1-10] directions. From the analysis of the RHEED patterns, we deduce the thickness H_{3D} for which the transition from a two-dimensional to a three-dimensional growth mode occurs from the intensity increase of a 3D Bragg diffraction spot. *Ex situ* AFM images are acquired with a Digital Nanoscope III system working in the tapping mode.

We first investigate the case of tensile $Ga_{0.7}In_{0.3}P$ alloys grown at 520 °C on a LM GaInP buffer on GaAs substrates for which, during growth, the RHEED pattern exhibits a diffuse (2×1) reconstruction. The 2D–3D transition observed on the evolution of the 3D Bragg spot intensity [Fig. 1(a)] occurs abruptly around 1 ML. The increase of the phosphorus flux by a factor of 2 has no effect. At the 2D–3D transition, the RHEED pattern along the [110] direction exhibits 3D Bragg spots, whereas it shows a very diffuse pattern along the [1–10] direction with ''chevrons.'' This indicates the formation of 3D islands, elongated along the

[a]Electronic mail: xavier.wallart@iemn.univ-lille1.fr

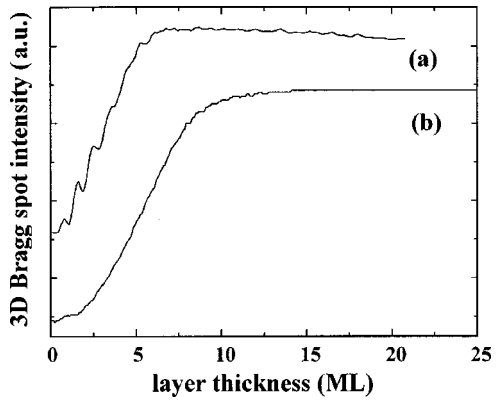

FIG. 1. Evolution of the 3D Bragg spot intensity vs thickness for $Ga_{0.7}In_{0.3}P$ layers grown at 520 °C either on a lattice-matched GaInP buffer layer (a) or on a GaAs buffer layer (b).

[1–10] direction. This value of H_{3D} is abnormally small since it is similar to that which we measure, in the same conditions, for the growth of GaP on GaAs for which the lattice mismatch is +3.6%.[10]

Since it has been reported that the buffer layer can greatly influence the 3D growth mode,[11] we then grow $Ga_{0.7}In_{0.3}P$ alloys directly on a GaAs buffer taking care of the gas commutation sequence as discussed above. As can be seen in Fig. 1(b), we note a similar rapid increase of the 3D Bragg spot intensity around 2 ML. This weak difference can be attributed to some residual As/P intermixing which lowers the strain of the growing layer. Nevertheless, the change of the buffer layer modifies only very slightly the relaxation, and the transition to a 3D growth mode occurs very rapidly. This 3D growth mode is further confirmed by the AFM images of Fig. 2. A 60-Å-thick $Ga_{0.7}In_{0.3}P$ film grown on a LM GaInP buffer layer [Fig. 2(a)] exhibits a peak-to-peak roughness of 50 Å and a random growth of 3D structures elongated along the [1–10] direction, as was deduced from the RHEED pattern. These structures are rather similar in Fig. 2(b) to a 120-Å-thick $Ga_{0.7}In_{0.3}P$ film grown directly on a GaAs buffer, the peak-to-peak roughness being slightly higher in this case and reaching 65 Å, due to the larger layer thickness.

We then study the growth of tensile strained $Ga_{0.2}In_{0.8}P$ alloys on InP at 520 °C. In this way, we can separate strain effects from compositional effects. Indeed, if the critical thickness is only determined by strain, the results should be the same for GaAs or InP substrates. During the growth of the strained layers on InP, the surface exhibits a (2×4) InP-like reconstruction, suggesting In segregation. The RHEED pattern does not exhibit a sharp 2D–3D transition but rather a growth roughening around 30 ML. This behavior is in agreement with the observations of Gendry and Hollinger[12] on the relaxation of tensile GaInAs layers on InP. Indeed, for a substrate temperature of 525 °C and for strains below 2%, they report a roughening of the surface rather than a 2D–3D transition. In order to get insight into the critical thickness in this case, we performed DCXRD experiments on $Ga_{0.2}In_{0.8}P$ layers of different thickness ranging from 110 to 700 Å. The spectra are displayed in Fig. 3 together with the simulations assuming a perfect pseudomorphic growth. Clearly, for the 110 Å layer, there is a good agreement between the experimental and simulated spectra. For the 280 Å layer, the experimental layer peak is slightly less intense and broader

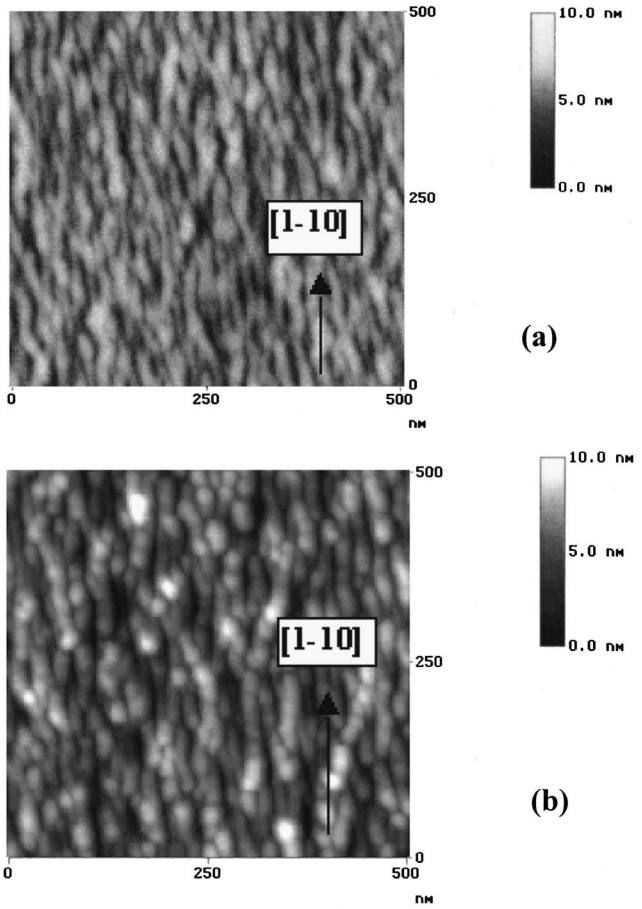

FIG. 2. AFM image of a 60-Å-thick $Ga_{0.7}In_{0.3}P$ layer grown at 520 °C on a lattice-matched GaInP buffer layer (a) and of a 120-Å-thick $Ga_{0.7}In_{0.3}P$ layer grown at 520 °C on a GaAs buffer layer (b).

than the simulated one and the Pendellösung oscillations are hardly distinguishable, indicating that plastic relaxation has started to occur. Finally, for the 700 Å case, the disagreement between experiment and simulation as regards the layer peak intensity, width, position, and the lack of Pendellösung oscillations evidences an advanced state of layer relaxation. We can then conclude that the 280 and 700 Å layers are

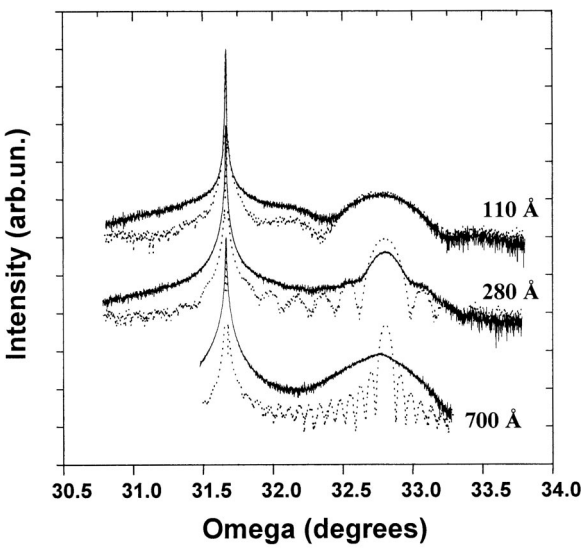

FIG. 3. DCXRD spectra and related simulations assuming pseudomorphic growth for 110-, 280-, and 700-Å-thick $Ga_{0.2}In_{0.8}P$ layers grown at 520 °C on InP.

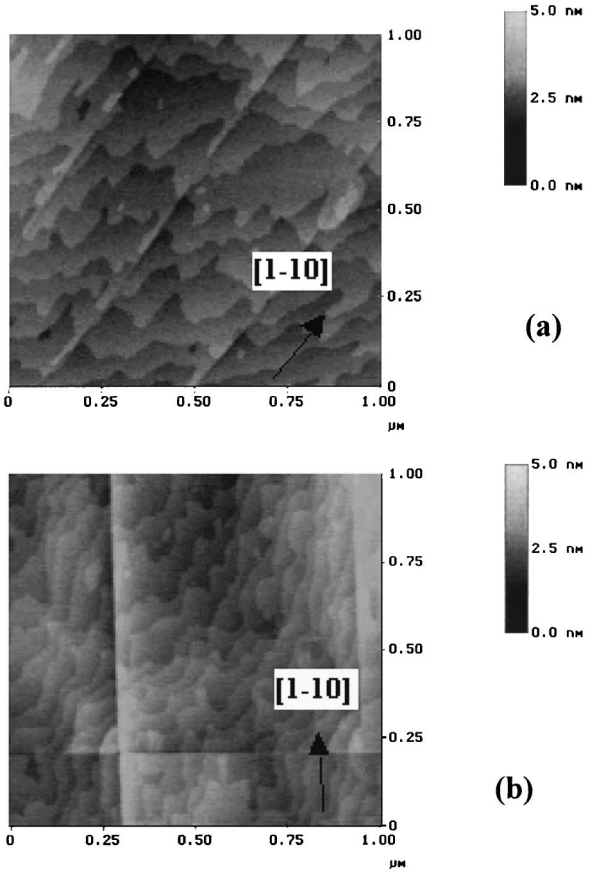

FIG. 4. AFM images of 110-Å-thick (a) and 700-Å-thick (b) $Ga_{0.2}In_{0.8}P$ layers grown at 520 °C on InP.

partially plastically relaxed, whereas the 110 Å one is still pseudomorphic or at the very early stages of relaxation.

Figure 4 displays the AFM images obtained on these samples. On the 110-Å-thick film [Fig. 4(a)] atomic steps are clearly resolved, evidencing a step-flow growth mode and the 2D character of the layer. Moreover, this image also reveals the presence of lines oriented along the [1–10] direction. The origin of these lines could be associated with the formation of misfit dislocations. We observe these lines only in the [1–10] direction, indicating that the film is at the very early stages of plastic relaxation. On the contrary, the 700-Å-thick layer [Fig. 4(b)], although still bi-dimensional, exhibits a cross-hatched surface characteristic of a more advanced state of relaxation. These observations are in good agreement with RHEED and DCXRD results. They confirm that the critical thickness for plastic relaxation of $Ga_{0.2}In_{0.8}P$ alloys on InP at 520 °C is 110 Å, rapidly following the growth roughening observed by RHEED after 90 Å. This value is significantly lower than that of 500 Å reported by Cohen and co-workers[7,8] for the growth of $Ga_{0.25}In_{0.75}P$ on InP by MOMBE. Since the growth temperature is rather similar in both cases, this difference may be ascribed to the investigation methods since Cohen and co-worker mainly use DCXRD. Indeed, we can note from the above results that AFM is more sensitive than DCXRD in detecting the onset of relaxation, suggesting that the value reported by Cohen and co-workers is probably overestimated.

The observed composition effect can hardly be ascribed to surface diffusion kinetics. Indeed, on InP substrates, the tensile layers are obtained for higher In contents than on the GaAs ones. Since, for a given substrate temperature, In atoms are more mobile than Ga ones, one would expect that higher In contents would promote a three-dimensional growth mode and, hence, then the critical thickness would be smaller on InP than on GaAs substrates, which is not the case.

In order to get insight into this behavior, we consider the data on the spinodal decomposition of alloys reported by Wei, Ferreira, and Zunger.[13] At 520 °C, for $Ga_{1-x}In_xP$, the indium composition range related to the spinodal domain roughly extents from 0.15 to 0.50 (whereas no decomposition occurs for GaInAs at this temperature). Considering now the case of $Ga_{0.7}In_{0.3}P$/GaAs, according to these data, alloy decomposition should occur, resulting in the formation of $Ga_{0.5}In_{0.5}P$ and $Ga_{0.85}In_{0.15}P$ alloys. Clearly, in this case, the Ga-rich alloy determines the critical thickness. This could explain the measured value of 1–2 ML. On the other hand, for $Ga_{0.2}In_{0.8}P$/InP, the alloy composition is far from the composition range of spinodal decomposition. This explains why, for a similar mismatch (+1.4%), the critical thickness is higher in this case. Of course, this explanation is only based on thermodynamic arguments neglecting strain and kinetics effects but seems to be a good starting point. More detailed models are then needed to take into account the interplay between alloy decomposition, strain, and kinetic effects, as well as the detailed structure of the growth front, the surface roughness, and the In segregation.

In this work, using RHEED, DCXRD, and AFM, we show that the relaxation of tensile $Ga_{0.7}In_{0.3}P$/GaAs layers and of $Ga_{0.2}In_{0.8}P$/InP layers is drastically different although the lattice mismatch is the same in both cases. The $Ga_{0.7}In_{0.3}P$/GaAs layers exhibit a 2D–3D transition for an abnormally small thickness of 1–2 ML. On the other hand, the critical thickness for $Ga_{0.2}In_{0.8}P$/InP layers lies around 100 Å and the films relax via the formation of misfit dislocations. This clearly evidences the effect of the alloy composition on the relaxation of tensile GaInP layers. Considering the composition range in which alloy decomposition can occur allows us to explain the observed results.

[1] B. Elman, E. S. Koteles, P. Melman, C. Jagannath, J. Lee, and D. Dugger, Appl. Phys. Lett. **55**, 1659 (1989).
[2] Y. Androussi, A. Lefebvre, C. Delamarre, L. P. Wang, A. Dubon, B. Courboulès, C. Deparis, and J. Massies, Appl. Phys. Lett. **66**, 3450 (1995).
[3] M. Gendry, V. Drouot, C. Santinelli, G. Hollinger, C. Miossi, and M. Pitaval, J. Vac. Sci. Technol. B **10**, 1829 (1992).
[4] Y. Robach, A. Solére, M. Gendry, and L. Porte, J. Vac. Sci. Technol. B **16**, 1786 (1998).
[5] M. J. Matragano, D. G. Ast, J. R. Shealy, and V. Kishnamoorthy, J. Appl. Phys. **79**, 8371 (1996).
[6] A. Bensaada, A. Chennouf, R. W. Cochrane, J. T. Graham, R. Leonelli, and R. A. Massut, J. Appl. Phys. **75**, 3024 (1994).
[7] G. M. Cohen, P. Zisman, G. Bahir, and D. Ritter, J. Vac. Sci. Technol. B **16**, 2639 (1998).
[8] G. M. Cohen, D. Ritter, V. Richter, and R. Kalisch, Appl. Phys. Lett. **74**, 43 (1999).
[9] L. Gonzalez, Y. Gonzalez, G. Aragon, M. J. de Castro, and T. Herrero, Proceedings of the VIII EuroMBE Workshop, Sierra Nevada (1995), p. 93.
[10] O. Schuler, X. Wallart, and F. Mollot, J. Comput. Phys. **201/202**, 280 (1999).
[11] J. Brault, M. Gendry, G. Grenet, G. Hollinger, Y. Desières, and T. Benyattou, Appl. Phys. Lett. **73**, 2932 (1998).
[12] M. Gendry and G. Hollinger, Proceedings of the International Conference on Semiconductor Heteroepitaxy, Montpellier (1995), p. 572.
[13] S. H. Wei, L. G. Ferreira, and A. Zunger, Phys. Rev. B **41**, 8240 (1990).

Interplay between segregation, roughness, and local strains in the growth of $Ga_{0.75}In_{0.25}P$ alloy

X. Wallart,[a] C. Priester, D. Deresmes, and F. Mollot
Institut d'Electronique et de Microélectronique du Nord, UMR-CNRS 8520, Avenue Poincaré, B.P. 69, 59652 Villeneuve d'Ascq Cédex, France

(Received 22 February 2000; accepted for publication 16 May 2000)

In this work, using reflexion high energy electron diffraction and atomic force microscopy, we compare the growth of strained $Ga_{0.75}In_{0.25}P$ alloys on GaAs(001) and GaP (001) substrates. We show that although the absolute strain value is similar in both cases, the transition from a bidimensional to a three-dimensional growth mode occurs much faster in the tensile case than in the compressive one. We interpret this result with a microscopic theoretical model which takes into account the interplay between a weak surface roughness, In vertical and lateral segregation, and strain effects. © *2000 American Institute of Physics.* [S0003-6951(00)00828-7]

The growth of strained epitaxial III–V semiconductor layers has attracted a lot of interest in the last decade due to improved electronic properties, as well as from a fundamental point of view of growth process studies. Up to now, reported work has been mainly devoted to the GaInAs alloy for which a combination of growth experiments on GaAs and InP substrates allows a rather complete study of the alloy growth for both compressive and tensile strains.

As an aluminum-free alloy with a rather large bandgap, GaInP is an interesting candidate for microwave and optoelectronics applications. However, growth of strained GaInP alloys[1–5] is much less documented than that of GaInAs ones. However, using both GaAs and GaP substrates, the cases of compressive and tensile strains can be investigated for various alloy compositions. In recent studies, we reported on the abnormal relaxation behavior observed for the growth of tensile GaInP layers on GaAs.[6] Briefly, during the growth of $Ga_{0.7}In_{0.3}P$ on GaAs ($\Delta a/a = +1.4\%$) at 520 °C, the two-dimensional to three-dimensional (2D–3D) transition is observed for a deposited thickness around 1–2 monolayers (MLs) which is much less than the critical thickness measured for the 2D–3D transition in the case of tensile $Ga_{0.75}In_{0.25}As$ layers on InP[7] ($\Delta a/a = +2\%$) at 525 °C, varying from 11 to 17 MLs according to the growth conditions. This difference could be attributed to spinodal decomposition which, for GaInP alloys near 500 °C, is predicted to occur for an indium content between 0.15 and 0.50 whereas, at the same growth temperature, no decomposition is expected for GaInAs alloys.[8] However, this explanation only relies on thermodynamic arguments for bulk materials and neglects the effect of strain and surface growth mechanisms. As regards the strain, the works of Cahn[9] and Glas[10] support the fact that only the absolute strain value affects the spinodal decomposition.

In order to test this hypothesis, using reflexion high energy diffraction (RHEED) and atomic force microscopy (AFM), we investigate the growth of the $Ga_{0.75}In_{0.25}P$ alloy both in compressive strain on GaP (001) substrates ($\Delta a/a = -1.9\%$) and in tensile strain on GaAs(001) substrates ($\Delta a/a = +1.8\%$). We show that although the alloy composition and the absolute strain value are the same in both cases, the relaxation behavior is very different and hence can hardly be accounted for in terms of spinodal decomposition of the alloy. We then tentatively explain our results within the frame of a model which takes into account the interplay between In segregation, surface roughness, and strain effects.

Samples are grown by gas source molecular beam epitaxy (Riber 32P) using cracked phosphine and arsine as element V sources and standard effusion cells for elements III, on semi-insulating (001) GaAs and undoped (001) GaP substrates. On GaAs substrates, strained layers are grown either directly on a GaAs buffer layer or on a lattice matched (LM) GaInP buffer layer. In the former case, after the growth of a GaAs buffer layer at 580 °C, the substrate temperature is lowered down to 520 °C during a 3 min growth interruption. The arsine flux is vented when the substrate temperature reaches 550 °C in order to keep a (2×4) reconstruction. Then special care is taken in the gas commutation procedure to minimize As/P intermixing, i.e., the GaAs surface is exposed to phosphorus flux for 10 s before Ga and In shutters are opened. On GaP substrates, the strained layer growth is preceded by the growth of a GaP buffer layer at 600 °C. The substrate temperature is then lowered down to 520 °C during a 3 min growth interruption and the phosphine flux is vented when the substrate temperature reaches 550 °C. Gallium and indium fluxes, determining growth rates and alloy compositions, are measured by RHEED intensity oscillations on GaAs and InP before the growth. The growth parameters of the strained GaInP layers are kept identical on both substrates, i.e., a growth rate of 0.7 ML/s and a PH_3 flow rate of 3 sccm. 20 keV RHEED patterns are recorded along either the [110] or the $[1\bar{1}0]$ directions. From the analysis of the RHEED patterns, we deduce the thickness H_{3D} for which the transition from a two-dimensional to a three-dimensional growth mode occurs from the intensity increase of a 3D Bragg diffraction spot. *Ex situ* AFM images are acquired with a Digital Nanoscope III system working in the tapping mode.

We first investigate the case of tensile $Ga_{0.75}In_{0.25}P$ alloys grown at 520 °C on a LM GaInP buffer on GaAs sub-

[a]Electronic mail: Xavier.Wallart@IEMN.Univ-Lille1.fr

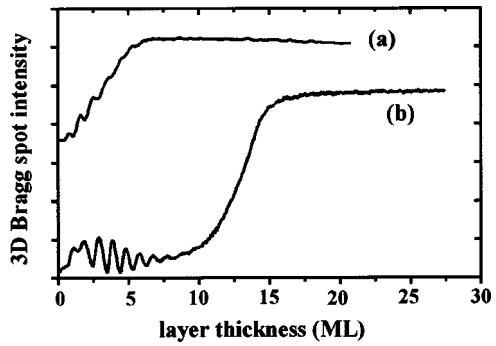

FIG. 1. 3D Bragg spot intensity evolution vs thickness for $Ga_{0.75}In_{0.25}P$ layers grown at 520 °C either on GaAs (a) or on GaP (b).

strates for which, during growth, the RHEED pattern exhibits a diffuse (2×1) reconstruction. The 2D–3D transition occurs abruptly for 1–2 MLs [Fig. 1(a)]. At the 2D–3D transition, the RHEED pattern along the [110] direction exhibits 3D Bragg spots whereas it is very diffuse along the [1–10] direction with ''arrow-head shapes.'' This indicates the formation of 3D islands, elongated along the [1–10] direction. This value of H_{3D} is abnormally small for a +1.8% lattice mismatch since it is similar to that we measure, in the same conditions, for the growth of GaP on GaAs for which the lattice mismatch is +3.6%.[6]

It has been reported that the buffer layer can greatly influence the 3D growth mode of InAs on InP.[11] However, in our case, when $Ga_{0.75}In_{0.25}P$ is grown directly on a GaAs buffer taking care of the gas commutation sequence as discussed above, the only observed difference with respect to the case of growth on a LM GaInP buffer layer is a slight increase of the H_{3D} thickness to 2–3 MLs. Figure 2(a) shows the AFM image of a 55 Å thick $Ga_{0.75}In_{0.25}P$ film grown on GaAs, which exhibits a peak-to-peak roughness of 40 Å and a random growth of 3D structures elongated along the [1–10] direction as was deduced from the RHEED pattern.

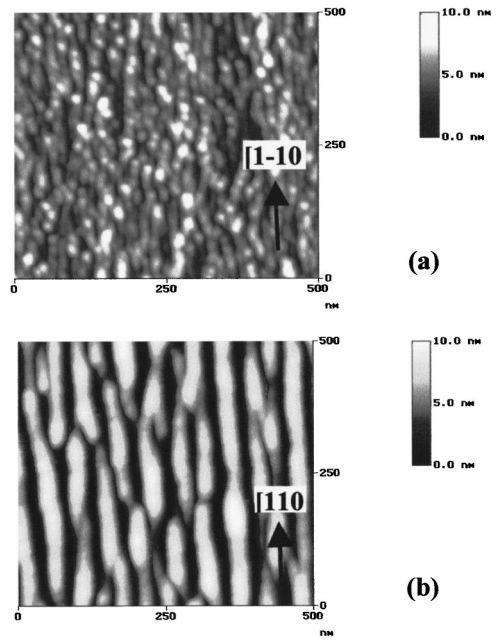

FIG. 2. AFM image of a 55 Å thick $Ga_{0.75}In_{0.25}P$ layer grown at 520 °C on a GaAs buffer layer (a) and of a 75 Å thick $Ga_{0.75}In_{0.25}P$ layer grown at 520 °C on a GaP buffer layer (b) (top views).

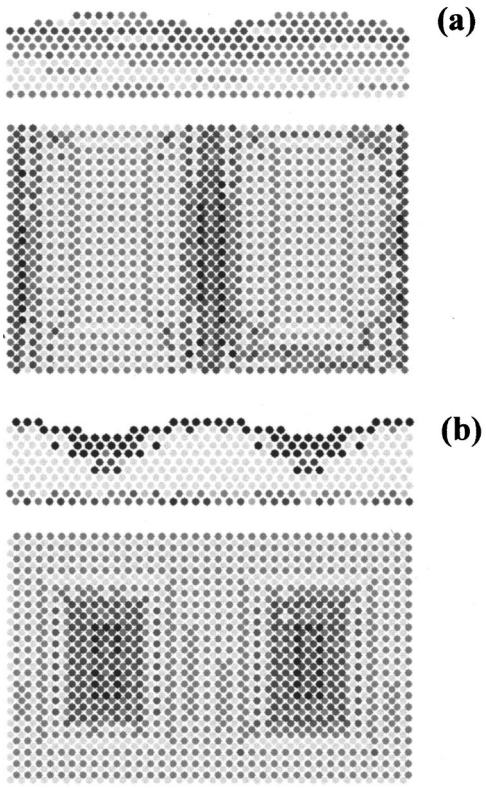

FIG. 3. Cross and top section views of the growth of $Ga_{0.75}In_{0.25}P$ on a rough surface with humps (a) and holes (b) after 5 MLs deposited thickness on GaAs (tensile case). Indium-rich atomic rows correspond to darker symbols and Ga-rich rows to brighter symbols.

We then consider the growth of compressively strained $Ga_{0.75}In_{0.25}P$ layers on GaP $(\Delta a/a=-1.9\%)$. During growth, starting with the (2×4) GaP reconstruction, the RHEED pattern turns first to a (2×2) one as long as 2D growth proceeds. When thickness increases, the (2×2) reconstruction progressively vanishes before the onset of 3D growth, occurring around 10 MLs, significantly larger than the H_{3D} measured in the previous case. More, at the 2D–3D transition, 3D Bragg spots are now observed along the [1–10] direction whereas arrow-head shapes appear along the [110] one. This indicates the formation of 3D islands, elongated along the [110] direction. The AFM image of a 75 Å thick $Ga_{0.75}In_{0.25}P$ [Fig. 2(b)] confirms the RHEED observations and evidences the formation of very well defined wire-like structures along the [110] direction with a peak-to-peak roughness around 70–80 Å.

As regards the above results, the measured critical thickness for the 2D–3D growth mode transition of $Ga_{0.75}In_{0.25}P$ compressive layers (10 MLs) lies in the same range as that reported for the growth of $Ga_{0.7}In_{0.3}As$ on GaAs[12] (9 MLs), so that we can infer that the involved relaxation processes are mainly similar in both cases. On the other hand, the relaxation process seems very different for the tensile layers although the composition and the absolute strain value are similar. This difference can hardly be explained by some spinodal decomposition of the alloy, since it is expected that this would affect tensile and compressive layers in the same way, which is obviously not the case.

In order to introduce surface and growth mechanisms and take advantage of previous work reported on AlInAs,[13,14]

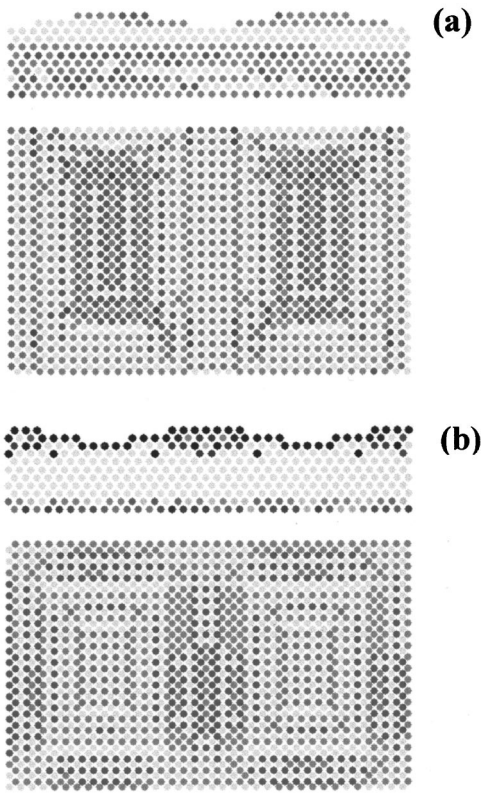

FIG. 4. Cross and top section views of the growth of $Ga_{0.75}In_{0.25}P$ on a rough surface with humps (a) and holes (b) after 5 MLs deposited thickness on GaP (compressive case). Indium-rich atomic rows correspond to darker symbols and Ga-rich rows to brighter symbols.

we develop a microscopic model combining the effect of In segregation, surface roughness, and strain effects. Details on the model are given elsewhere.[13] Briefly, for the sake of simplicity, we consider two types of surface roughness: either made of 2–3 MLs high platelets or made of 2–3 MLs deep holes. We consider periodic systems with two humps or two holes per period. This type of surface morphology is though to describe well a growth front morphology within a bidimensional growth mode. The used period size (which corresponds to a somewhat ''theoretical diffusion length'') is about 100–200 Å, which is smaller than typical diffusion lengths under usual growth conditions. This ensures the relevance of the description. As regards In segregation, as bulk diffusion is negligible at usual molecular beam epitaxy (MBE) growth temperature, the allowed exchange of cations belong either to the surface layer or to the underlying layer. Then, for modeling the growth process itself, one ML of random alloy is deposited on the surface and allowed to exchange all over the period. Figures 3 and 4 depict the variations of the alloy composition according to this model for the tensile and compressive $Ga_{0.75}In_{0.25}P$ alloys, respectively, after the deposition of 5 MLs for the two types of considered surface roughness (holes or platelets). Clearly, in the tensile case (Fig. 3), we note strong composition modulations associated with the formation of a locally Ga-rich alloy at the top of the humps and In-rich alloy in the holes. On the contrary, for the same deposited thickness in the compressive case (Fig. 4), composition modulations are much less pronounced and the alloy looks rather like a random one. We can separate the physics included in our model into two parts. First, the roughness combined with surface tension criterions leads to some vertical and lateral cation segregation (In accumulation at the surface, near the sloping areas in both systems). The second point differentiates between the two cases. In GaInP/GaAs, both binaries are mismatched to the substrate, the strain-induced decomposition is efficient all over the system and develops, inducing an early 2D–3D growth mode transition. This is not the case for GaInP/GaP where the Ga-rich areas spread all over the system with no adding driving force for segregation.

On InP substrates, surface roughening has already been reported to be important in the growth of tensile $Ga_{0.75}In_{0.25}As$ layers and responsible for a lower 2D–3D critical thickness than that measured for the growth of compressive $Ga_{0.18}In_{0.82}As$ layers.[15] However, in this study, the absolute strain value is similar in both cases (tension and compression), but the alloy compositions are largely different, making a detailed comparison difficult. Here, considering the growth of the same alloy on two different substrates, we show that the surface roughness promotes large composition modulations in the tensile case and hence strongly affects the 2D–3D critical thickness whereas its effect is much less important in the compressive case.

To summarize, using RHEED and AFM, we have investigated the growth of $Ga_{0.75}In_{0.25}P$ alloys on both GaAs(001) and GaP(001) substrates at 520 °C. We have observed that the critical thickness for the 2D–3D growth mode transition is largely smaller in the tensile case (on GaAs) than in the compressive case (on GaP) although the absolute strain value is the same in both cases. Then, we have shown that these results can be correctly explained by a microscopic model taking into account the interplay between In segregation, a weak surface roughness, and strain effects.

The authors are grateful to C. Coinon for his technical assistance in the MBE experiments.

[1] M. J. Matragano, D. G. Ast, J. R. Shealy, and V. Kishnamoorthy, J. Appl. Phys. **79**, 8371 (1996).
[2] A. Bensaada, A. Chennouf, R. W. Cochrane, J. T. Graham, R. Leonelli, and R. A. Massut, J. Appl. Phys. **75**, 3024 (1994).
[3] G. M. Cohen, P. Zisman, G. Bahir, and D. Ritter, J. Vac. Sci. Technol. B **16**, 2639 (1998).
[4] G. M. Cohen, D. Ritter, V. Richter, and R. Kalisch, Appl. Phys. Lett. **74**, 43 (1999).
[5] L. Gonzalez, Y. Gonzalez, G. Aragon, M. J. de Castro, and T. Herrero, Proceedings of the VIIth EuroMBE Workshop, Sierra Nevada, 93 (1995).
[6] O. Schuler, X. Wallart, and F. Mollot, J. Cryst. Growth **201/202**, 280 (1999).
[7] D. Jacob, Y. Androussi, T. Benabbas, P. François, D. Ferré, A. Lebebvre, M. Gendry, and Y. Robach, J. Cryst. Growth **179**, 331 (1997).
[8] S. H. Wei, L. G. Ferreira, and A. Zunger, Phys. Rev. B **41**, 8240 (1990).
[9] J. W. Cahn, Acta Metall. **9**, 795 (1961).
[10] F. Glas, Phys. Rev. B **55**, 11 277 (1997).
[11] J. Brault, M. Gendry, G. Grenet, G. Hollinger, Y. Desières, and T. Benyattou, Appl. Phys. Lett. **73**, 2932 (1998).
[12] Y. Androussi, A. Lefebvre, C. Delamarre, L. P. Wang, A. Dubon, B. Courboulès, C. Deparis, and J. Massies, Appl. Phys. Lett. **66**, 3450 (1995).
[13] C. Priester and G. Grenet, J. Vac. Sci. Technol. B **16**, 2421 (1998).
[14] C. Priester and G. Grenet, Phys. Rev. B **61**, 16029 (2000).
[15] M. Gendry and G. Hollinger, *Proceedings of the International Conference on Semiconductor Heteroepitaxy*, Montpellier (World Scientific, Singapore, 1995), p. 572.

Relationship between surface reconstruction and morphology of strained $Ga_{1-x}In_xP$ layers grown on GaP (001) by gas-source molecular-beam epitaxy

X. Wallart,[a] D. Deresmes, and F. Mollot
Institut d'Electronique et de Microélectronique du Nord, UMR-CNRS 8520, Avenue Poincaré, B.P. 69, 59652 Villeneuve d'Ascq Cedex, France

(Received 2 January 2001; accepted for publication 9 March 2001)

We study the growth of strained $Ga_{1-x}In_xP$ layers on GaP (001) by gas-source molecular-beam epitaxy for x varying from 0.25 to 1. At a growth temperature of 520 °C, we find two main differences with respect to the well known GaInAs/GaAs system. First, for $0.25 \leqslant x \leqslant 0.5$, we observe the development of wire-like structures oriented along the [110] direction and on the other hand, the growth of InP on GaP leads to the formation of huge dots in small density. The influence of the growth parameters such as the growth temperature or the phosphine flow rate is presented. The whole set of results is discussed in light of recent work on the phosphide surface reconstructions with a particular emphasis on the role of the cation-rich one. © *2001 American Institute of Physics.* [DOI: 10.1063/1.1371242]

The formation of three-dimensional (3D) structures during the growth of strained layers has become a subject of great interest in recent years. In the III–V semiconductor field, most of the studies have been concerned with the growth of the GaInAs alloy on GaAs or InP. In these systems, apart from the strain value, previous work has stressed the influence of the surface reconstructions[1] and the nature of the buffer layer[2] on the onset of 3D growth and on the 3D morphology. In comparison with the growth of strained arsenides, the growth of strained phosphides is much less documented, especially considering molecular-beam epitaxy growth. Previous work on the growth of strained GaInP alloys have mainly focused on the growth on GaAs[3] or InP[4,5] substrates whereas a few studies have explored the growth of InP on GaP either by organometallic vapor-phase epitaxy[6,7] or by chemical beam epitaxy.[8] However, no systematic study on GaP substrates has been undertaken.

In this work, using reflection high-energy electron diffraction (RHEED) and atomic force microscopy (AFM), we investigate the growth of strained GaInP layers on GaP (001) substrates by gas-source molecular-beam epitaxy. Significant differences exist with respect to the case of arsenides and we show that they can be accounted for considering recent results on phosphide surface reconstructions and we especially point out the role of the (2×4) cation-rich reconstruction.

Samples are grown by gas-source molecular-beam epitaxy (Riber 32P) using cracked phosphine and standard effusion cells for elements III, on undoped (001) GaP substrates. The strained layer is preceded by a 2000-Å-thick GaP buffer layer grown at 600 °C. The temperature is then lowered down to 520–400 °C during a 3 min growth interruption, then the strained layer is grown. Gallium and indium fluxes, determining growth rates and alloy compositions, are measured by RHEED intensity oscillations on GaAs and InP, respectively, before the growth. The growth rate of the strained GaInP layers lies in the 0.3–0.7 monolayer per second (ML/s) range except for the growth of InP for which it has been reduced to 0.1 ML/s. We have used $2PH_3$ flow rate values. The first one is a standard value (3 sccm in our system) we use to obtain good quality InP or lattice matched GaInP layers on GaAs and hereafter referred as the standard P_2 flux. The second one is three times higher (9 sccm) and is hereafter referred as the high P_2 flux. 20 keV RHEED patterns are recorded along both the [110] and the [1-10] directions on two different samples. *Ex situ* AFM images are acquired with a Digital Nanoscope III system working in the tapping mode.

We first examine the growth of strained $Ga_{1-x}In_xP$ alloys for $0.25 \leqslant x \leqslant 0.5$. During the growth at 520 °C with a standard P_2 flux, whatever the In content, starting with the (2×4)GaP reconstruction, the RHEED pattern immediately changes to a (2×2) one as long as 2D growth proceeds. When thickness increases, the (2×2) reconstruction progressively vanishes and the transition from a 2D to a 3D growth mode occurs. At the 2D–3D transition, RHEED 3D Bragg spots are observed along the [1-10] direction, whereas, along the [110] direction, the pattern is very diffuse with arrow-head shapes. This indicates the formation of elongated platelets along the [110] direction which is further confirmed by the AFM image [Fig. 1(a)] exhibiting wire-like structures along the [110] direction. This is markedly different from the $Ga_{1-x}In_xAs$//GaAs case for which circular dots are observed for $0.3 < x < 0.5$.[9] Wire-like structures have been reported for the growth of InAs on InGaAs[2] under As-rich conditions but these structures are elongated along the [1-10] direction. In this case, the orientation of the wire-like structures can be explained from a kinetic point of view by an enhanced surface diffusion of the impinging cations along the dimer rows, and from an energetic point of view by a preferential development of straight step edges along the [1-10] direction, both typical of the As-stabilized arsenide surfaces.[10,11]

This elongated morphology is strongly modified by an increase of the P_2 flux. Indeed, under the high P_2 flux, the

[a]Electron mail: xavier.wallart@iemn.univ-lille1.fr

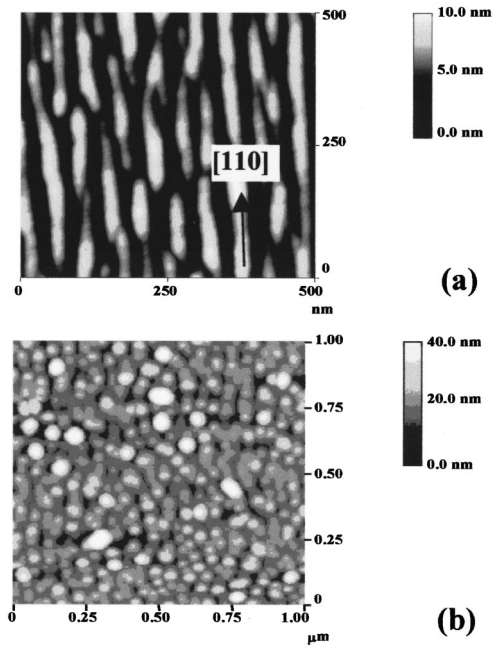

FIG. 1. AFM images of a 27-ML-thick $Ga_{0.75}In_{0.25}P$ layer grown on GaP at 520 °C under a standard P_2 flux (a) and of a 26-ML-thick $Ga_{0.7}In_{0.3}P$ layer grown on GaP at 520 °C with a high P_2 flux (b).

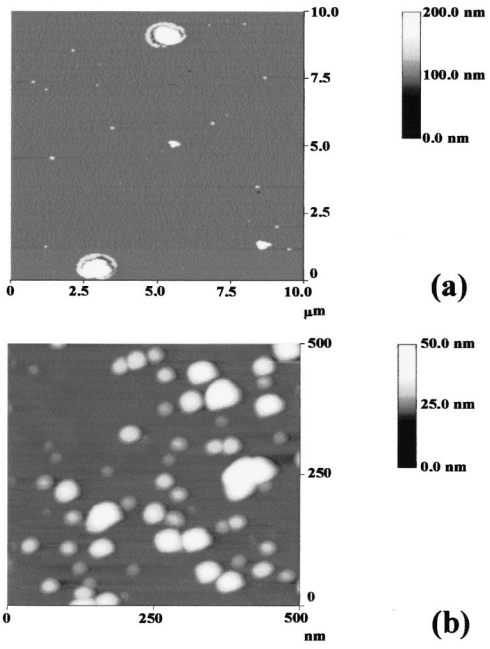

FIG. 3. AFM images after the growth of 3.3 MLs of InP on GaP at 520 °C (a) and 400 °C (b) under a standard P_2 flux.

RHEED pattern exhibits first a faint (3×2) reconstruction before turning to the (2×2) one and, at the onset of 3D growth, Bragg spots are observed in both azimuths. This is characteristic of the formation of dots as revealed by the AFM image of Fig. 1(b).

Turning now to the case of the growth of InP on GaP, at 520 °C with a standard P_2 flux, the RHEED pattern exhibits a (2×2) reconstruction before Bragg spots appear along both azimuths. The 2D–3D transition occurs abruptly at 2.1 MLs (Fig. 2). The film morphology after deposition of 3.3 MLs is characterized by two families of islands [Fig. 3(a)]. The first one corresponds to huge islands (~1 μm wide, ~2000 Å high) with a low density around $10^6/cm^2$. The second one is related to smaller dots (~1000 Å wide, ~400 Å high) with a higher density around $10^7/cm^2$. Using the high P_2 flux at the same growth temperature does not modify the RHEED pattern neither the critical thickness but leads to an increase of the dot density to $4\times10^8/cm^2$ with a more homogeneous dot size (~1000 Å wide, ~400 Å high). Then, at 520 °C, we get rather large dots with a small density which is very different from the InAs/GaAs system[12] where typical islands are 200–300 Å wide and a few tens of angstroms high with a much higher density above $10^{10}/cm^2$. On the contrary, when growth occurs at 400 °C with a standard P_2 flux, the RHEED pattern exhibits a (3×2) reconstruction before the 2D–3D transition which, in this case, is less abrupt than at 520 °C but occurs at 1.7 MLs (Fig. 2). The resulting island size is more homogeneous with a mean width of 500 Å, mean height of 150 Å and a density around $2.10^{10}/cm^2$ [Fig. 3(b)]. This dot size and density are closer to what is observed in the InAs/GaAs system. Nevertheless, we are left with an unusual behavior since the critical thickness decreases with decreasing growth temperature although kinetic factors usually lead to the increase of the critical thickness when the growth temperature decreases.[13] This implies that the onset of 3D growth is not kinetically controlled in this case.

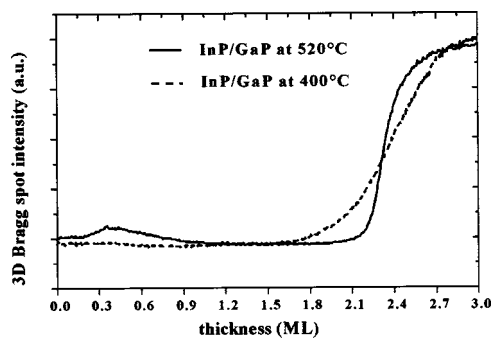

FIG. 2. RHEED Bragg spot intensity evolution during the growth of InP on GaP at 520 °C (full line) and 400 °C (dashed line) under a standard P_2 flux.

In order to get insight into these findings, we consider recent results reported on the phosphide surface reconstructions.[14–16] According to them, two different (2×4) reconstructions exist for GaP(001) heated under UHV conditions: a P-rich one, around 500 °C, which looks like the $\beta2$ (2×4) GaAs one and a Ga-rich one, around 600 °C, described by a mixed dimer model, characterized by the formation of Ga dimers along the [110] direction. For InP(001), at 370 °C, Esser *et al.*[14] observe a (2×4) reconstruction that they describe by a two-domain surface composed of P-rich $(2\times1)/(2\times2)$ and In-rich (2×4) domains whereas above 400 °C the observed (2×4) seems to be only an In-rich reconstruction with the mixed-dimer model. Under the same experimental conditions, i.e., heating of an InP(001) surface under UHV, Labella *et al.*[16] observe a (2×4) reconstruction above 310 °C and then a $c(2\times8)$ above 340 °C. They infer that the $c(2\times8)$ could be probably described by a slightly modify mixed-dimer model. More, these latter authors show that under a P_2 flux, the only observed reconstruction above 450 °C is the $c(2\times8)$.

Coming back to our results, under standard P_2 flux at 520 °C, we are in experimental conditions for which the (2

$\times 4$) GaP is P rich whereas the (2×4) InP is In rich. Then, during the growth of the GaInP alloy, the two reconstructions compete and only the main feature of each one will be preserved. For the P-rich GaP one, the main feature is the formation of P dimers along [1–10] whereas the In-rich InP one is mainly characterized by the formation of In dimers along [110]. The combination of both In and P dimers then lead to the observed (2×2) reconstruction. On the other hand, during the growth of strained $Ga_{1-x}In_xP$ layers on GaP, In segregation leads to an In enrichment of the surface. For the In content under investigation ($0.25 \leqslant x \leqslant 0.5$), typical segregation energies of 0.1–0.2 eV[17] lead to a surface In composition above 0.5 at the end of the 2D growth regime, i.e., just before the onset of 3D growth. This in turn implies that In dimers dominate over P dimers, i.e., that the surface is rather cation stabilized. In the case of cation-stabilized growth of $Ga_{0.18}In_{0.82}As$ on InP, Robach *et al.*[18] observe the preferential formation of straight step edges along the [110] direction parallel to the cation dimers which tends to show that on cation-stabilized surfaces, 3D structures will preferentially develop along this direction. This energetic argument of preferential formation of step edges parallel to the cation dimers together with the kinetic argument of an enhanced surface diffusion of the impinging species along the dimer direction (as in the arsenide surface case) are both in favor of the formation of elongated structures oriented along the In dimers direction at the onset of 3D growth. Then during the 3D growth, although the (2×2) reconstruction vanishes due to the surface roughness, we are still in experimental conditions which promote the formation of surface In dimers and, hence, of wire-like structures along the [110] direction [Fig. 1(a)]. The increase of the P_2 flux promotes the formation of P dimers, reducing the number of In surface dimers. Hence, the surface is no longer cation stabilized, but rather characterized by a balanced mixture of anion and cation dimers. In this case, no particular direction is favored as regards the step edges formation as well as the surface diffusion length: this results in the formation of dots instead of wires, in agreement with the observations of Fig. 1(b).

As regards the growth of InP on GaP at 520 °C, the (2×2) reconstruction is observed mainly during the growth of the first monolayer when the competition between the two (2×4) reconstructions once again occurs. After the 2D–3D transition, due to the large mismatch, dots are formed instead of wires. The large dimensions of these dots are clearly related to very large surface diffusion lengths associated with the In-rich InP surface. This behavior has been observed on GaAs surfaces too for which it has been shown that the cation diffusivity is higher on the cation-rich surface than on the anion-rich one.[19,20] The increase of the P_2 flux in this case reduces the surface diffusion length and hence the dot size but the general trend is similar. However, when decreasing the growth temperature to 400 °C, the P dimers formation is favored since this temperature becomes rather close to the transition temperature reported between the P-rich (2×1) and the In-rich (2×4) InP reconstructions. Then, at 400 °C, P dimers dominate and the surface is anion stabilized as in the arsenide case and that is why we observe the same critical thickness than in the InAs/GaAs system with rather similar dot size. Finally, as regards the increase of the critical thickness from 1.7 to 2.1 MLs when the growth temperature is raised, it cannot be explained by In desorption solely since it has been shown that the re-evaporated In fraction amounts to a few percents only during InP growth at 520 °C.[21] Hence, we relate it mainly to surface energetics and not to kinetic factors. The (2×2) cation-rich reconstruction observed at 520 °C is more energetic than the (3×2) one at 400 °C for which the formation of surface P dimers is favored. This surface tension then delays the 2D–3D transition as also reported in the arsenide case.[1]

In this work, we show that the growth of strained $Ga_{1-x}In_xP$ layers on GaP (001) presents marked differences with respect to that of GaInAs on GaAs, i.e., the formation of wire like structures oriented along the [110] direction for $0.25 \leqslant x \leqslant 0.5$ and the very large size and low density of the dots formed during the growth of InP on GaP at 520 °C. We interpret these results considering the competition between the P-rich GaP and In-rich InP surface reconstructions occurring under our experimental conditions and leading to cation-stabilized surfaces. Finally, we show that when these conditions are modified in order to promote a P-rich surface, then the growth tends to behave as in the GaInAs/GaAs case.

[1] M. Gendry, G. Grenet, Y. Robach, P. Krapf, L. Porte, and G. Hollinger, Phys. Rev. B **56**, 9271 (1997).
[2] J. Brault, M. Gendry, G. Grenet, G. Hollinger, Y. Desières, and T. Benyattou, Appl. Phys. Lett. **73**, 2932 (1998).
[3] M. J. Matragano, D. G. Ast, J. R. Shealy, and V. Kishnamoorthy, J. Appl. Phys. **79**, 8371 (1996).
[4] A. Bensaada, A. Chennouf, R. W. Cochrane, J. T. Graham, R. Leonelli, and R. A. Massut, J. Appl. Phys. **75**, 3024 (1994).
[5] G. M. Cohen, D. Ritter, V. Richter, and R. Kalisch, Appl. Phys. Lett. **74**, 43 (1999).
[6] K. Borgi, F. Hassen, H. Maaref, A. Daami, and G. Bremond, Microelectron. J. **30**, 637 (1999).
[7] Y. Nabetani, K. Sawada, Y. Furukawa, A. Wakahara, S. Noda, and A. Sasaki, J. Cryst. Growth **193**, 470 (1998).
[8] B. Junno, T. Junno, M. S. Miller, and L. Samuelson, Appl. Phys. Lett. **72**, 954 (1998).
[9] C. W. Snyder, B. G. Orr, D. Kessler, and L. M. Sander, Phys. Rev. Lett. **66**, 3032 (1991).
[10] J. Sudijimo, M. D. Johnson, C. W. Snyder, M. B. Elowitz, and B. G. Orr, Phys. Rev. Lett. **69**, 2811 (1992).
[11] J. E. Northrup and S. Froyen, Phys. Rev. B **50**, 2015 (1994).
[12] P. Chen, Q. Xie, A. Madhukar, L. Chen, and A. Konkar, J. Vac. Sci. Technol. B **12**, 2568 (1994).
[13] M. Gendry, V. Drouot, C. Santinelli, G. Hollinger, C. Miossi, and M. Pitaval, J. Vac. Sci. Technol. B **10**, 1829 (1992).
[14] N. Esser, W. G. Schmidt, J. Bernholc, A. M. Frisch, P. Vogt, M. Zorn, M. Pristovsek, W. Richter, F. Bechstedt, Th. Hannappel, and S. Visbeck, J. Vac. Sci. Technol. B **17**, 1691 (1999).
[15] A. M. Frisch, W. G. Schmidt, J. Bernholc, M. Pristovsek, N. Esser, and W. Richter, Phys. Rev. B **60**, 2488 (1999).
[16] V. P. LaBella, Z. Ding, D. W. Bullock, C. Emery, and P. M. Thibado, J. Vac. Sci. Technol. A **18**, 1492 (2000).
[17] O. Dehaese, X. Wallart, O. Schuler, and F. Mollot, J. Appl. Phys. **84**, 2127 (1998).
[18] Y. Robach, A. Solène, M. Gendry, and L. Porte, J. Vac. Sci. Technol. B **16**, 1786 (1998).
[19] J. H. Neave, P. J. Dobson, B. A. Joyce, and J. Zhang, Appl. Phys. Lett. **47**, 100 (1985).
[20] J. M. Van Hove and P. I. Cohen, J. Cryst. Growth **81**, 13 (1987).
[21] M. B. Panish and H. Temkin, *Gas Source Molecular Beam Epitaxy* (Springer, Berlin, 1993), p. 25.

ELSEVIER

Surface Science 506 (2002) 203–212

SURFACE SCIENCE

www.elsevier.com/locate/susc

A combined RHEED and photoemission comparison of the GaP and InP(0 0 1) (2 × 4) surface reconstructions

Xavier Wallart *

Institut d'Electronique et de Microélectronique du Nord, UMR-CNRS 8520, Avenue Poincaré, B.P. 69, F-59652 Villeneuve d'Ascq Cédex, France

Received 22 October 2001; accepted for publication 2 February 2002

Abstract

In this work, we compare the (2 × 4) reconstructions of GaP and InP(0 0 1) surfaces. Two different (2 × 4) reconstructions are detected by reflection high energy electron diffraction for both materials. Photoemission experiments reveal that the high temperature one is cation-rich whereas the low temperature one is anion-rich. High resolution spectra on the high temperature (2 × 4) reconstructions exhibit surface components which are in agreement with what is expected from the mixed-dimer model in both cases. As regards the low temperature (2 × 4) GaP, a second surface component on the P 2p core level line reveals that two different atomic sites exist for the P-atoms at the surface which is different from the $\beta 2$ (2 × 4) geometry. The low temperature (2 × 4) InP is more phosphorus-rich and turns to be a mixture between the (2 × 1) and the high temperature (2 × 4) reconstructions. © 2002 Published by Elsevier Science B.V.

Keywords: Reflection high-energy electron diffraction (RHEED); Molecular beam epitaxy; X-ray photoelectron spectroscopy; Surface relaxation and reconstruction; Gallium phosphide; Indium phosphide

1. Introduction

The reconstruction of arsenide surfaces has been a subject of interest for a long time and now, we have got a rather detailed picture of the atomic structure of the main reconstructions observed during epitaxial growth. Until recently, the situation was completely different as regards the phosphide surface reconstructions for which the knowledge was relatively poor. However, recent work has allowed a better insight in the GaP(0 0 1) and InP(0 0 1) surface reconstructions. Low energy electron diffraction or reflection high energy electron diffraction (RHEED) observations performed on surfaces prepared either by molecular beam epitaxy (MBE) [1,2] or metalorganic vapor-phase epitaxy [3,4] reveal three main reconstructions with decreasing phosphorus coverage: a (2 × 2) then a (2 × 1) and finally a (2 × 4) one. The (2 × 1) reconstruction has been studied by scanning tunneling microscopy (STM) [5], soft X-ray photoemission spectroscopy (SXPS) [6] and reflectance anisotropy spectroscopy (RAS) [7] and the results have been interpreted in terms of a surface terminated by buckled phosphorus dimers. Using SXPS

* Tel.: +33-320-19-78-57; fax: +33 -320-19-78-92.
E-mail address: xavier.wallart@iemn.univ-lille1.fr (X. Wallart).

0039-6028/02/$ - see front matter © 2002 Published by Elsevier Science B.V.
PII: S0039-6028(02)01428-0

and STM, Vogt et al. [8] have investigated a more P-rich $(2 \times 1)/(2 \times 2)$ surface for which they propose a model consisting of P-dimers oriented along [1 1 0] adsorbed on a complete P-layer. As regards the less P-rich (2×4) surfaces, the most striking feature is the existence of a cation-rich (2×4) reconstruction which has no counterpart in the arsenides for which cation-rich surfaces exhibit a (4×2) reconstruction. Indeed, Frisch et al. [9] suggest the existence of at least two different (2×4) surface phases for GaP, depending on the Ga content on the surface. Based on both RAS experiments and density-functional theory in local-density approximation (DFT-LDA) calculations, the authors describe the Ga-rich one by mixed Ga–P dimers on top of a Ga-terminated surface [10] (mixed dimer model) whereas for the less Ga-rich one, they suggest the formation of P–P dimers in a $\beta 2$ (2×4) geometry as observed on GaAs. As regards InP, it appears that the (2×4) is always associated with an In-rich surface [11–14] described by the mixed dimer model [15].

Most of the above results have been derived from RAS, STM experiments and from DFT-LDA calculations. Some XPS experiments have been reported but mainly on the P-rich (2×1) surface or on the cation-rich surfaces. That is why, in this work, we have undertaken a study of GaP and InP reconstructions by RHEED and XPS focusing on the anion- and cation-rich (2×4) reconstructions. Using angle-resolved XPS, (AR-XPS) we probe the surface composition whereas high resolution XPS spectra allows us to determine the surface components associated with the various reconstructions.

2. Experimental

Samples are grown by Gas Source Molecular Beam Epitaxy in a Riber 32P reactor, using standard effusion cells for the elements III and cracked phosphine on undoped GaP(0 0 1) substrates and Fe doped InP(0 0 1) ones. After the growth of a 2000 Å thick buffer layer, the samples are cooled down under phosphorus in order to prepare the richer P surface. They are then heated up either under UHV or under a phosphorus flux in order to examine the various surface reconstructions in both cases. For some of these, we perform XPS measurements. In this case, the desired reconstruction is prepared by a careful heating and cooling down to room temperature of a P-rich surface under UHV conditions (pressure in the low 10^{-10} Torr range) before transferring the sample to the XPS chamber connected under UHV to the growth chamber. During cooling down, the RHEED pattern is monitored to ensure it remains unchanged. The XPS system is a Physical Electronics model 5600, modified by SINVACO in order to analyze 3 in. MBE samples. We use a monochromatic AlKα X-ray source for which the ultimate overall resolution as measured from the FWHM of the Ag 3d5/2 line is 0.45 eV. The acceptance angle of the analyzer has been set to 14° and the angle between the incident X-rays and the analyzer is 90°. The direction of photoelectrons is given by the polar angle θ, as referenced to the sample surface. To obtain angle dependent XPS results, the polar angle is varied from 25° to 75°. The intensity of the various XPS core levels (CLs) are measured as the peak area after standard background subtraction according to the Shirley procedure [16]. Photodiffraction effects are often prominent on single crystals [17] and, as they superimpose to the XPS signal variations relative to the concentration gradient, they can make concentration profile determination rather difficult. To minimize these effects, we perform an average of the different XPS CL intensities with respect to the azimuth [18]. Then, we calculate intensity ratios between XPS lines either of P 2p and Ga 3d or of P 2p and In 4d with close binding energies [19]. For the high resolution XPS results, we apply the deconvolution procedure proposed by Joyce et al. [20]. In this procedure, the Ga 3d and In 4d CLs are synthesized using Voigt functions by a doublet for the 3/2 and 5/2 components whereas the P 2p CL is modeled by a doublet for the 1/2 and 3/2 components. The branching ratios are theoretical ones and the splitting energies are fixed at 0.45 eV between Ga 3d3/2 and Ga 3d5/2, 0.86 eV between In 4d3/2 and In 4d5/2 and 0.85 eV between P 2p1/2 and P 2p3/2, which are typical values for these CLs [21]. The best fit is obtained through a least-square minimization procedure. High res-

olution spectra have been recorded at a low (25°) and a high (75°) electron takeoff angles in order to evidence surface components. These latter are modeled with the same parameters than the bulk component, i.e. the Gaussian and Lorentzian broadening are kept fixed for each component of a given CL.

3. Results

We first discuss our RHEED observations upon annealing a phosphorus-rich sample under UHV. On both substrates, from lower to higher temperatures, we first observe a (2×2) diagram followed by a (2×1) one, then appears a low temperature (2×4) (LT(2×4)) pattern and finally a high temperature (2×4) (HT(2×4)) one. The main feature which allows us to distinguish the LT and HT (2×4) is the $\times 4$ RHEED pattern observed when the electron beam is along the $[1\,-1\,0]$ direction. Indeed, in this direction, the LT(2×4) exhibit intermediate streaks which are clearly weaker than the main spots whereas for the HT-(2×4), the intermediate streaks sharpen in bright spots. This is illustrated by the intensity profiles along the [1 1 0] direction for both reconstructions in Fig. 1. When performing the annealing under a phosphorus flux (3 sccm phosphine flow rate in Fig. 2), the prominent effect for both materials is to shift the transition temperatures between the various reconstructions to higher values. The main differences between GaP and InP are the transition temperatures between the various reconstructions (Fig. 2) and also the behavior of the LT(2×4). In the case of GaP, this reconstruction occurs within a rather wide temperature range (100 °C) whereas for InP, it only exists for a 40 °C temperature range and the associated pattern is weak. When performing the annealing under a phosphorus flux, the LT(2×4) GaP $\times 4$ RHEED pattern exhibits bright intermediate spots characteristic of a well-ordered surface reconstruction preceding the evolution towards the HT(2×4) for which the intermediate spots are even sharper and brighter. On the other hand, for InP, the LT(2×4) $\times 4$

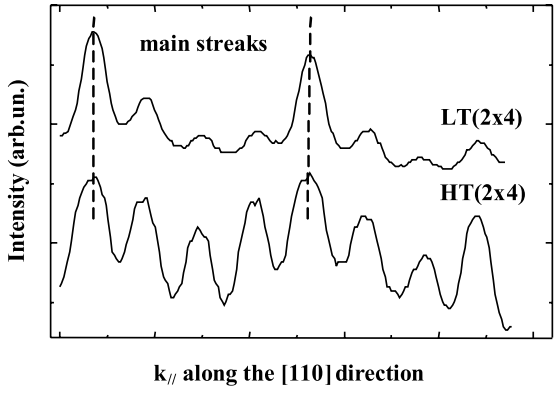

Fig. 1. RHEED intensity profiles along the [1 1 0] direction for the LT and HT (2×4) GaP reconstructions obtained by annealing under UHV conditions.

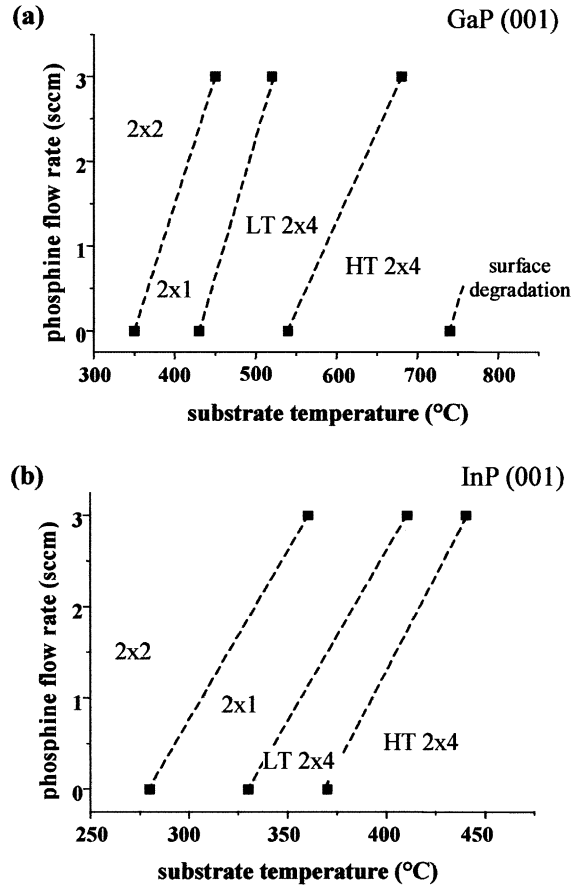

Fig. 2. Evolution of the surface reconstruction versus the annealing temperature for a GaP(0 0 1) (a) and InP(0 0 1) (b) sample with and without phosphorus flux.

RHEED pattern remains still characterized by weak intermediate streaks. Then, at this point, it is not so clear that the observed LT(2×4) is indeed a true reconstruction for InP or only a transition reconstruction between the (2×1) and the HT(2×4). These trends agree rather well with previously published results on InP and GaP [2,3]. On InP, we cannot resolve the c(4×4) observed by LaBella et al. [2] at low temperatures, neither the c(2×8) they detect at high temperatures. In the following, we now focus on the two different (2×4) reconstructions we get.

Turning first to the ARXPS measurements, Fig. 3 shows the evolution of the P 2p/Ga 3d (a) and P 2p/In 4d (b) intensity ratios versus the photoelectron takeoff angle for GaP and InP respectively. On this kind of plot, higher values at low takeoff angles than at high ones are related to a P-rich surface. This is obviously the case for the (2×2) reconstruction for both GaP and InP. The solid lines in Fig. 3 represent the simulated evolution in a layer-by-layer model for a P-rich surface assuming a phosphorus surface coverage of 2 monolayers (MLs) for GaP and 2.5 MLs for InP. These findings are in good agreement with those of Li et al. [4] and Vogt et al. [8] who observe a phosphorus surface coverage of 2 MLs for the (2×2) InP surface. The relative sensitivity factors between P 2p and Ga 3d or In 4d are needed for the simulations. We have used the values obtained for the LT(2×4) at a 75° takeoff angle in order to minimize surface effects, since, in both cases, the evolution is rather flat in this case. For the LT(2×4), the evolution of the intensity ratios is well described by a simulated one assuming a phosphorus surface coverage of 0.75 (dashed line) as in a $\beta 2$ (2×4) reconstruction. On the contrary, in the case of the HT(2×4), we observe a slight increase of the intensity ratios with increasing takeoff angles, characteristic of a cation-rich surface. This evolution is rather well depicted in both cases, assuming that the surface is terminated by a cation plane (short-dashed line). From these measurements, we conclude that the LT(2×4) is probably a P-rich surface whereas the HT(2×4) is a cation-rich surface.

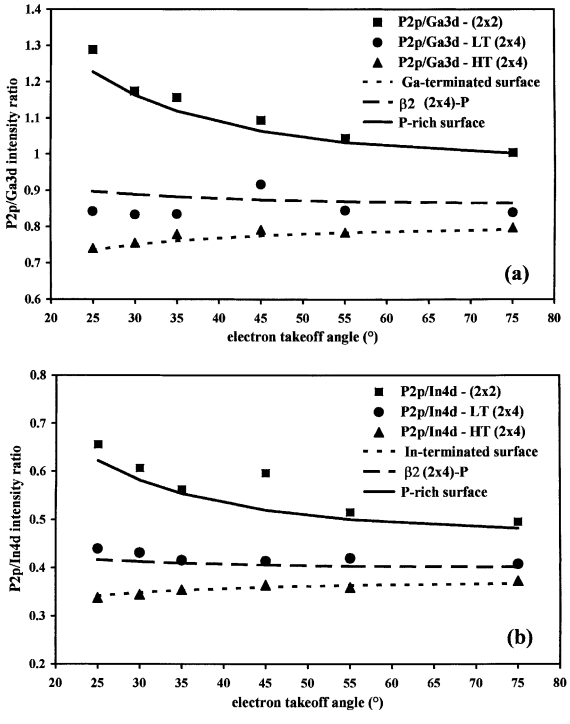

Fig. 3. Evolution of the P 2p/Ga 3d (a) and P 2p/In 4d (b) intensity ratios versus electron takeoff angle for various GaP and InP reconstructions. The solid lines are calculated ratios for a P-rich surface, assuming a phosphorus surface coverage of 2 MLs for GaP and 2.5 MLs for InP.

As regards the high resolution XPS results, we first discuss in details the results relative to GaP and then compare them to those recorded on InP. The results of the peak decomposition for the various surface reconstructions are summarized in Table 1. Fig. 4a shows the P 2p CLs for the (2×2), LT(2×4) and HT(2×4) reconstructions for a 25° electron takeoff angle, evidencing the differences according to the surface reconstruction. In order to get insight in the surface components, Fig. 4b and c compare the P 2p CL for the two different (2×4) reconstructions and for two takeoff angles: a grazing one (25°) which is more surface sensitive and a rather normal one (75°) which is more bulk sensitive. For the LT(2×4) surface (Fig. 4b), the comparison of the P 2p CLs at 25° and 75° evidences differences both on the high and low binding energy side whereas for the HT(2×4) (Fig. 4c), differences are mainly located on the high binding energy side of the CL. This indicates that

Table 1
Summary of the surface component binding energy shifts according to the surface reconstruction. All energies are in eV

Surface reconstruction	P 2p			Ga 3d		In 4d	
	S1	S2	S3	S1	S2	S1	S2
HT(2 × 4) GaP	−0.40/−0.45	–	–	−0.55/−0.60	+0.40/+0.45	–	–
LT(2 × 4) GaP	−0.40/−0.45	+0.35/+0.40	–	−0.55/−0.60	+0.40/+0.45	–	–
HT(2 × 4) InP	−0.25/−0.30	–	–	–	–	−0.50/−0.55	+0.40/+0.45
LT(2 × 4) InP	–	+0.35/+0.40	+1.05/+1.10	–	–	−0.50/−0.55	+0.40/+0.45

for the LT(2 × 4), one more surface component is needed than for the HT(2 × 4) (Fig. 4c). This is indeed confirmed by the peak decompositions presented in Fig. 5a and b for a 25° takeoff angle. In the HT(2 × 4) case (Fig. 5b), apart from the main bulk contribution, only one surface component S1 appears at ≈−0.40/−0.45 eV. For the LT(2 × 4) (Fig. 5a) a second surface component S2 appears at +0.35/+0.40 eV. This second surface component is the main difference between the P 2p CLs recorded on the two (2 × 4) surface reconstructions.

Fig. 6a and b compare the Ga 3d CLs for the two different (2 × 4) reconstructions, once again at two electron takeoff angles 25° and 75°. Differences between the two angles are observed on the high and low binding energy sides of the peak, suggesting the presence of two surface components. Fig. 7a and b show the result of the peak decompositions for a 25° takeoff angle. In both cases, two surface components appear at ≈−0.55/−0.60 eV (S1) and ≈+0.40/+0.45 eV (S2). The difference between the 2 reconstructions arises from the relative intensity of S1 and S2. In the LT(2 × 4) case (Fig. 7a), the S1 component is very weak compared to S2 whereas for the HT(2 × 4) (Fig. 7b), S2 decreases and S1 increases which leads to a rather similar intensity for these two components.

Turning now to the InP case, the results recorded on the HT(2 × 4) are similar to those presented above on the HT(2 × 4) GaP reconstruction. The P 2p CL (Fig. 8, dotted line) is very close to that recorded on the HT(2 × 4) GaP surface (Fig. 4a, dotted line). Indeed the peak decomposition (Fig. 9b) reveals only one surface component S1 at ≈−0.25/−0.30 eV from the bulk peak. The In 4d CL (Fig. 10b) is characterized by a low binding energy surface component S1 at ≈−0.50/−0.55 eV and a high binding energy surface component S2 at ≈+0.40/+0.45 eV from the bulk component.

On the contrary, for the LT(2 × 4) InP, the P 2p CL is very different from that recorded on the LT(2 × 4) GaP (Figs. 8 and 4a, dashed lines), especially on the high binding energy side of the peak. Clearly, a new high binding energy component is present on both LT(2 × 4) and (2 × 2) reconstructions as indicated by the dashed-dotted line in Fig. 8. This is confirmed in Fig. 9a where the peak decomposition shows the presence of a new component S3 at ≈+1.10 eV from the bulk one. For this component the total broadening has been increased to ensure a good fit. The broadening has been taken from the decomposition of the P 2p CL on the (2 × 2) InP surface. In this case, the S2 component is still present whereas the S1 is hardly detected (not shown on Fig. 9a). Finally, Fig. 10a presents the decomposition of the In 4d CL for the LT(2 × 4) reconstruction which exhibits two surface components similar to those observed on the HT(2 × 4) surface. As in the GaP case, we note that the main difference between the two reconstructions comes from the intensity ratio between S1 and S2 with an increase of the S1 intensity and a decrease of the S2 one going from the LT(2 × 4) to the HT(2 × 4).

4. Discussion

RHEED observations suggest the existence of a LT and a HT (2 × 4) reconstructions for both GaP and InP. ARXPS measurements show that the LT

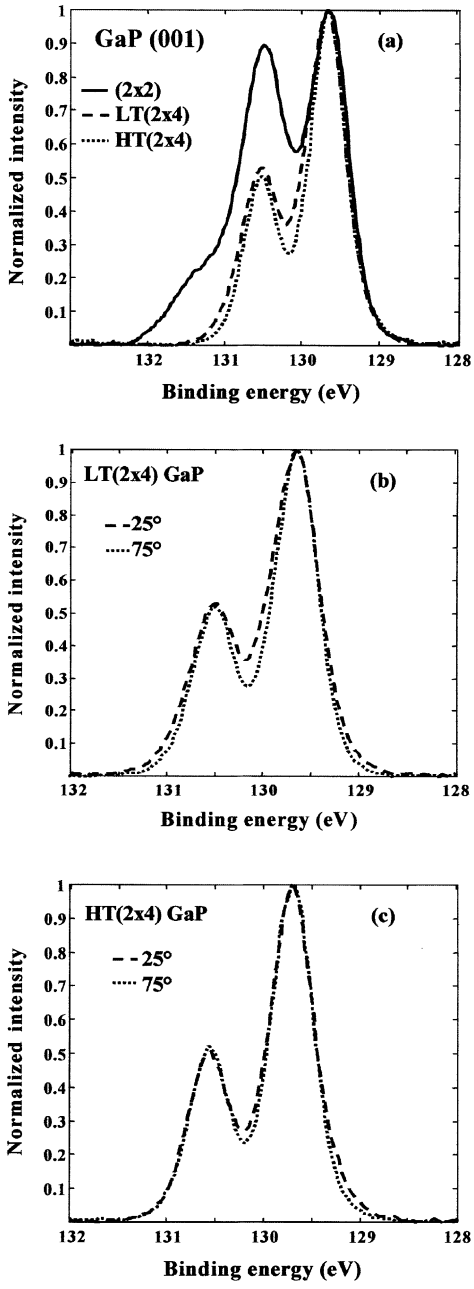

Fig. 4. P 2p XPS CL for the (2 × 2), LT(2 × 4) and HT(2 × 4) GaP reconstructions (a). P 2p CL at 25° and 75° electron takeoff angles for the LT(2 × 4) (b) and HT(2 × 4) (c).

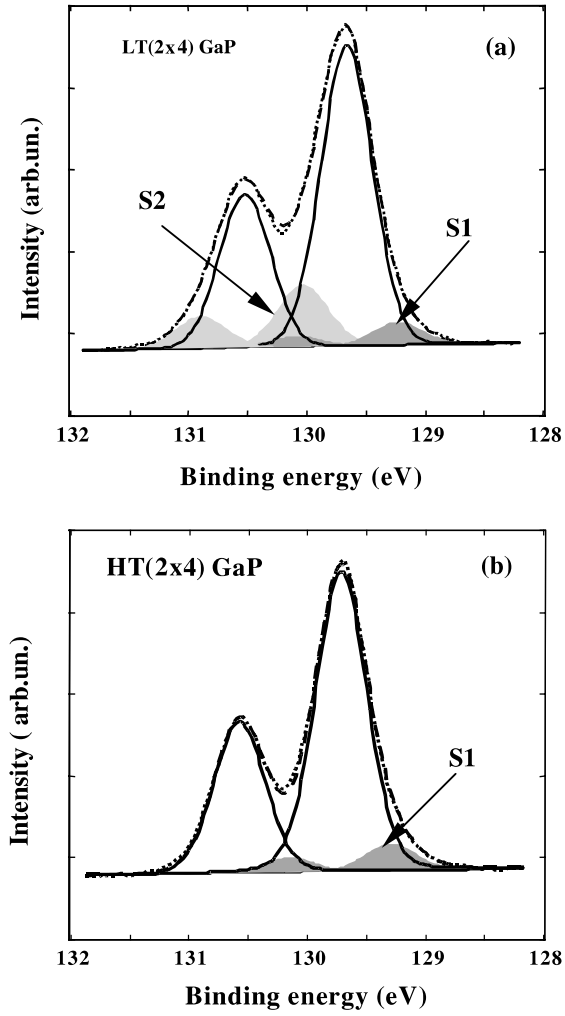

Fig. 5. P 2p CL decomposition for the LT(2 × 4) (a) and HT(2 × 4) (b) GaP surfaces at an electron takeoff angle of 25°. Shaded areas indicate surface components; the full lines are related to the bulk one; the dashed line is the resulting fit and the dotted line is the experimental data.

one is P-rich whereas the HT one is cation-rich. The high resolution XPS spectra on the HT(2 × 4) reveal one low binding energy surface component for the P 2p CL. For the Ga 3d and In 4d CLs, two surface components are detected. These findings are in good agreement with previous results [15,22–24]. The value of the various binding energy shifts are rather comparable, the differences coming mainly from a better experimental resolution in previous work, thanks to the use of synchrotron facilities. These results have been interpreted by Schmidt et al. [15] and Vogt et al. [25] in terms of charge transfer associated with the various surface

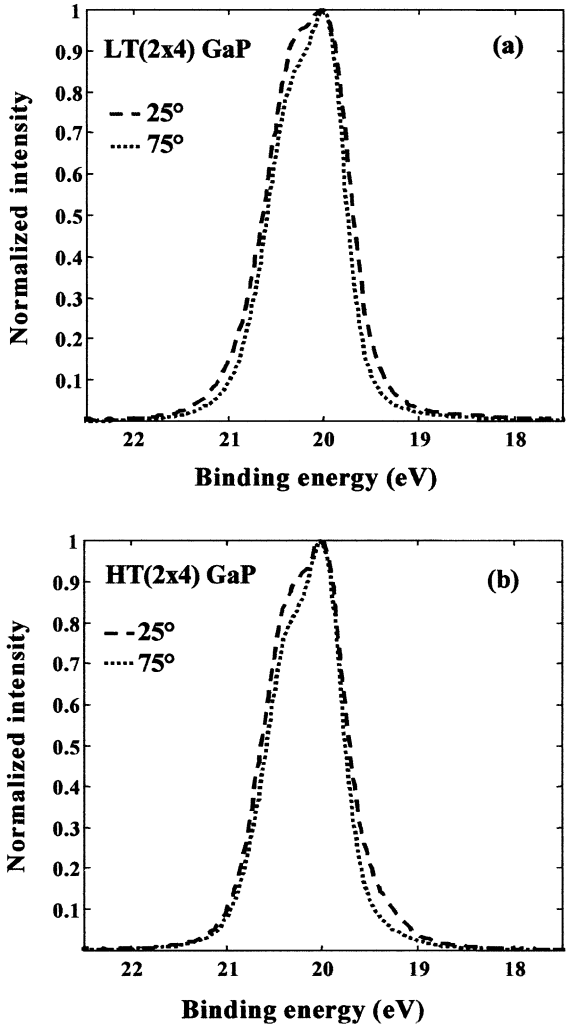

Fig. 6. Ga 3d CL at 25° and 75° electron takeoff angles for the LT(2 × 4) (a) and HT(2 × 4) (b).

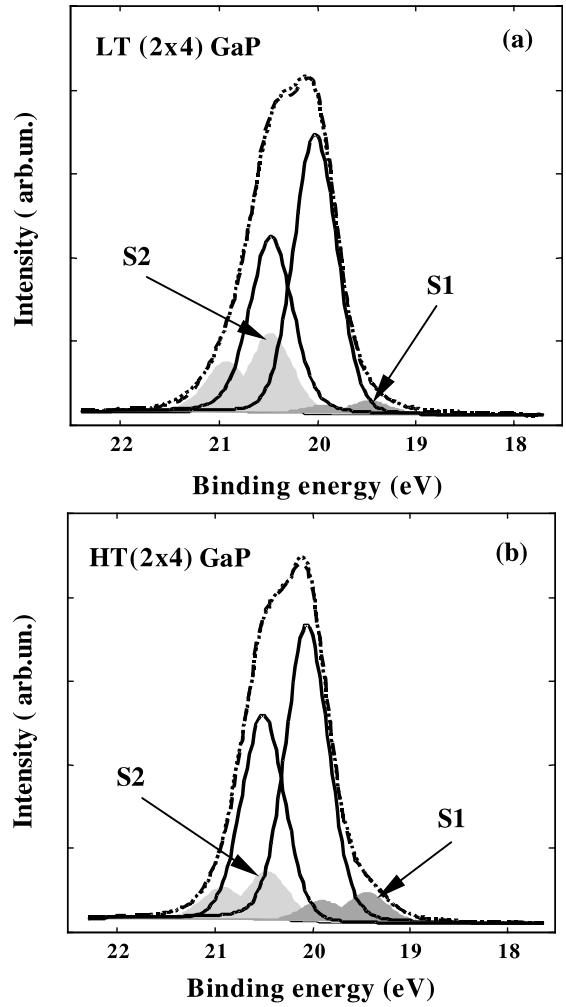

Fig. 7. Ga 3d CL decomposition for the LT(2 × 4) (a) and HT(2 × 4) (b) GaP surfaces at an electron takeoff angle of 25°. Shaded areas indicate surface components; the full lines are related to the bulk one; the dashed line is the resulting fit and the dotted line is the experimental data.

components. The S1 surface component of the P 2p CL would be associated with the P-atom in the mixed dimer whereas the S1 and S2 surface components in the Ga 3d or In 4d CLs would correspond to two different surface sites for the cation atom in the mixed-dimer model.

Going from the LT to the HT (2 × 4) reconstruction, the relative increase of the low binding energy surface component (S1) in the Ga 3d or In 4d CL is very similar to what is observed from the As-rich (2 × 4) to the Ga-rich (4 × 2) GaAs surfaces [26,27]. This trend agrees well with the above findings that the LT(2 × 4) is P-rich whereas the HT(2 × 4) is Ga- or In-rich. Nevertheless, for the LT(2 × 4) GaP reconstruction, a second surface component S2 at ≈+0.35–0.40 eV clearly appears in the P 2p CL. For the LT(2 × 4) GaP surface, Esser et al. [3] have proposed the formation of P–P dimers in a $\beta 2$ (2 × 4) geometry as in the GaAs case. For the $\beta 2$ (2 × 4) GaAs surface, the As3d CL exhibits one low binding energy

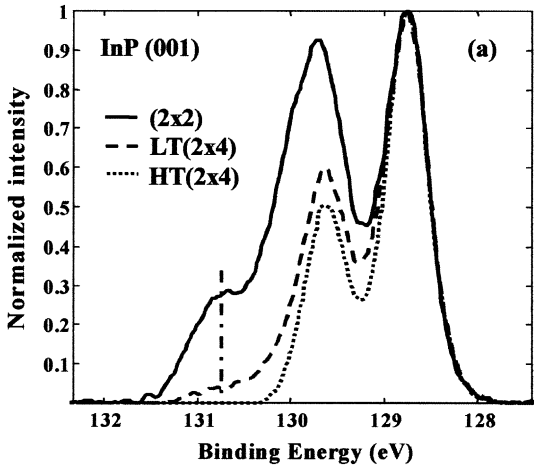

Fig. 8. P 2p XPS CL for the (2 × 2), LT(2 × 4)and HT(2 × 4) InP reconstructions.

surface component at ≈−0.40 eV and sometimes a high binding energy surface one at ≈+0.6 eV [26–29]. This latter one has been related to elemental arsenic on the surface. However, S2 cannot be related to elemental phosphorus on the surface since Yang et al. as well as Vogt et al. [1,6] have shown that elemental phosphorus produces a component shifted from ≈1 eV from the bulk one. This in turn implies that the structure of this LT(2 × 4) GaP should be different from the $\beta 2$ (2 × 4) GaAs. The two surface components S1 and S2 then suggest two different atomic sites for the P-atoms on the surface, S1 associated with a negative charge transfer and S2 with a positive one.

For the LT(2 × 4) InP, the high binding energy surface component at ≈1 eV in the P 2p CL (S3) is clearly related to elemental phosphorus present on the surface as in the case of the (2 × 2) or (2 × 1) reconstructions [1,6]. The presence of the S2 one still shows the existence of atomic sites for the P-atoms experiencing a positive charge transfer. Nevertheless, since the low binding energy surface component S1 is extremely weak, this indicates that this reconstruction is different from a $\beta 2$ (2 × 4) one. The presence of the S3 component shows that this surface is more P-rich than the LT(2 × 4) GaP one and this tends to confirm that this reconstruction is a mixture between the (2 × 1) and the HT(2 × 4) as suggested by Esser et al. [3].

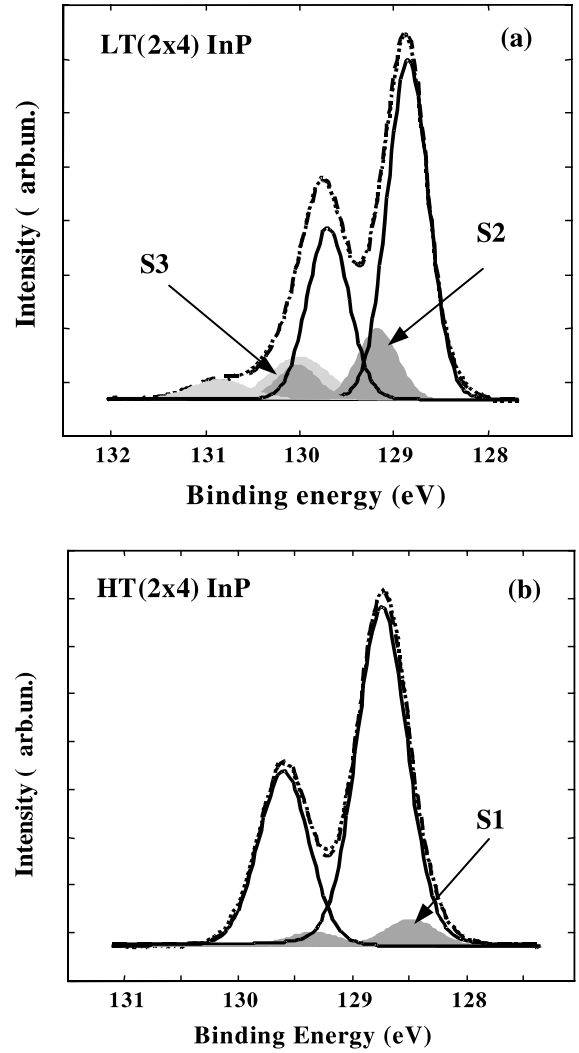

Fig. 9. P 2p CL decomposition for the LT(2 × 4) (a) and HT(2 × 4) (b) InP surfaces at an electron takeoff angle of 25°. Shaded areas indicate surface components; the full lines are related to the bulk one; the dashed line is the resulting fit and the dotted line is the experimental data.

5. Conclusion

From RHEED observations, we have shown that both InP and GaP exhibit two different (2 × 4) reconstructions. From ARXPS measurements, the LT one is slightly P-rich whereas the HT one is cation-rich. HRXPS spectra confirm these trends for the HT ones. For both InP and

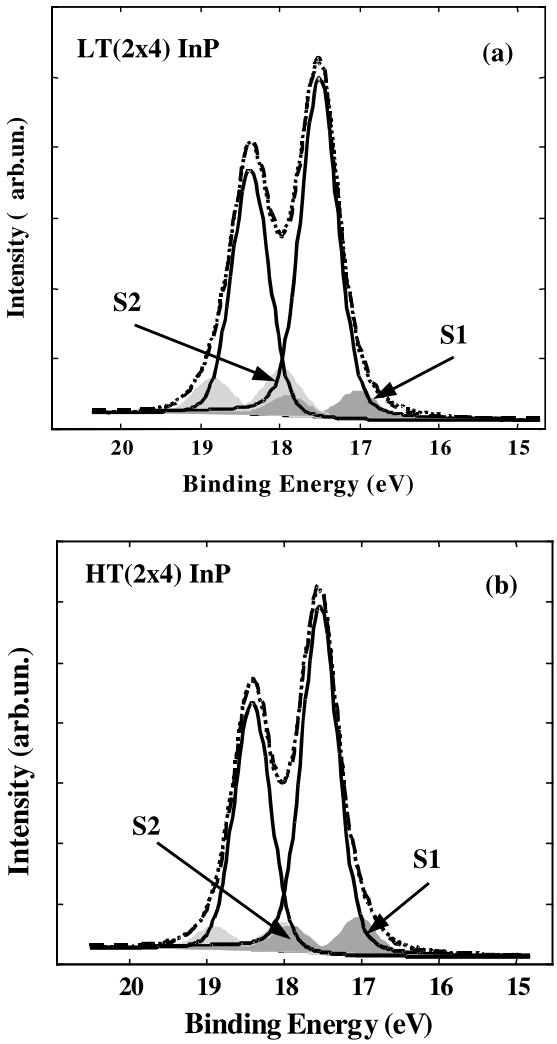

Fig. 10. In 4d CL decomposition for the LT(2 × 4) (a) and HT(2 × 4) (b) InP surfaces at an electron takeoff angle of 25°. Shaded areas indicate surface components; the full lines are related to the bulk one; the dashed line is the resulting fit and the dotted line is the experimental data.

GaP, only one surface component is detected in the P 2p CL and two surface components in the Ga 3d or In 4d CLs, in agreement with what is expected from the mixed-dimer model. For the LT one, a second surface component is detected in the P 2p CL for the GaP surface which cannot be attributed to elemental phosphorus on the surface. This kind of component has no counterpart in the (2 × 4)GaAs case and then the LT(2 × 4) GaP atomic structure is probably different from the $\beta 2$ (2 × 4) GaAs one. The evolution of the surface components S1 and S2 in the Ga 3d and In 4d CLs between the LT and HT (2 × 4) is in good agreement with that observed in the GaAs case when going from the As-rich (2 × 4) to the Ga-rich (4 × 2) surface. This confirms that the LT(2 × 4) is a P-rich surface whereas the HT one is a Ga- or In-rich one. Finally, in the InP case, the LT(2 × 4) exhibits a component associated with elemental phosphorus on the surface. This indicates that this surface is more P-rich than the LT(2 × 4) GaP one and is probably a mixture of (2 × 1) and HT(2 × 4) domains on the surface.

Acknowledgements

The author is grateful to Mr. F. Mollot for fruitful discussions and his critical reading of the manuscript as well as to Mr. C. Coinon for his technical assistance in the MBE experiments.

References

[1] B.X. Yang, Y. Ishikawa, T. Ozeki, H. Hasegawa, Jpn. J. Appl. Phys. 35 (1996) 1267.
[2] V.P. LaBella, Z. Ding, D.W. Bullock, C. Emery, P.M. Thibado, J. Vac. Sci. Technol. A 18 (2000) 1492.
[3] N. Esser, W.G. Schmidt, J. Bernholc, A.M. Frisch, P. Vogt, M. Zorn, M. Pritovsek, W. Richter, F. Bechstedt, Th. Hannapel, S. Visbeck, J. Vac. Sci. Technol. B 17 (1999) 1691.
[4] L. Li, Q. Fu, C.H. Li, B.K. Han, R.F. Hicks, Phys. Rev. B 61 (2000) 10223.
[5] L. Li, B.K. Han, Q. Fu, R.F. Hicks, Phys. Rev. Lett. 82 (1999) 1879.
[6] P. Vogt, A.M. Frisch, Th. Hannapel, S. Visbeck, F. Willig, Ch. Jung, R. Follath, W. Braun, W. Richter, N. Esser, Appl. Surf. Sci. 166 (2000) 190.
[7] M. Zorn, B. Junno, T. Trpk, S. Bose, L. Sammuelson, J.T. Zettler, W. Richter, Phys. Rev. B 60 (1999) 11557.
[8] P. Vogt, Th. Hannapel, S. Visbeck, K. Knorr, N. Esser, W. Richter, Phys. Rev. B 60 (1999) R5117.
[9] A.M. Frisch, W.G. Schmidt, J. Bernholc, M. Pritovsek, N. Esser, W. Richter, Phys. Rev. B 60 (1999) 2488.
[10] K. Lüdge, P. Vogt, O. Pulci, N. Esser, F. Bechstedt, W. Richter, Phys. Rev. B 62 (2000) 11046.
[11] C.D. MacPherson, R.A. Wolkow, C.E.J. Mitchell, A.B. McLean, Phys. Rev. Lett. 77 (1996) 691.

[12] D. Pahlke, J. Kinsky, Ch. Schulz, M. Pritovsek, M. Zorn, N. Esser, W. Richter, Phys. Rev. B 56 (1997) R1661.
[13] M. Shimomura, N. Sanada, G. Kaneda, T. Takeuchi, Y. Suzuki, Y. Fukuda, W.R.A. Huff, T. Abukawa, S. Kono, H.W. Yeom, A. Kakiraki, Surf. Sci. 412/413 (1998) 625.
[14] S. Mirbt, N. Moll, K. Cho, J.D. Joannopoulos, Phys. Rev. B 60 (1999) 13283.
[15] W.G. Schmidt, F. Bechstedt, N. Esser, M. Pritovsek, Ch. Schulz, W. Richter, Phys. Rev. B 57 (1998) 14596.
[16] D.A. Shirley, Phys. Rev. B 5 (1972) 4709.
[17] C.S. Fadley, Prog. Surf. Sci. 16 (1984) 275.
[18] M. Seelmann-Eggebert, H.J. Richter, Phys. Rev. B 43 (1991) 9578.
[19] G. Grenet, E. Bergignat, M. Gendry, M. Lapeyrade, G. Hollinger, Surf. Sci. 352–354 (1996) 734.
[20] J.J. Joyce, M. Del Guidice, J.H. Weaver, J. Electron Spectrosc. Relat. Phenom. 49 (1989) 31.
[21] G. Le Lay, D. Mao, A. Kahn, Y. Hwu, G. Margaritondo, Phys. Rev. B 43 (1991) 14301.
[22] M. Shimomura, N. Sanada, G. Kaneda, T. Takeuchi, Y. Suzuki, Y. Fukuda, W.R.A. Huff, T. Abukawa, S. Kono, H.W. Yeom, A. Kakizaki, Surf. Sci. 412/413 (1998) 625.
[23] N. Sanada, S. Mochizuki, S. Ichikawa, N. Utsumi, M. Shimomura, G. Kaneda, A. Takeuchi, Y. Suzuki, Y. Fukuda, S. Tanaka, M. Kamata, Surf. Sci. 419 (1999) 120.
[24] P. Vogt, K. Lüdge, M. Zorn, M. Pritovsek, W. Braun, W. Richter, N. Esser, J. Vac. Sci. Technol. B 18 (2000) 2210.
[25] P. Vogt, K. Lüdge, M. Zorn, M. Pritovsek, W. Braun, W. Richter, N. Esser, Phys. Rev. B 62 (2000) 12601.
[26] G. Le Lay, D. Mao, A. Kahn, Y. Hwu, G. Margaritondo, Phys. Rev. B 43 (1991) 14301.
[27] S. Heun, M. Sugiyama, S. Maeyama, Y. Watanabe, K. Wada, M. Oshima, Phys. Rev. B 53 (1996) 13534.
[28] I.M. Vitomirov, A.D. Raisanen, A.C. Finnefrock, R.E. Viturro, L.J. Brillson, P.D. Kirchner, G.D. Petit, J.M. Woodall, J. Vac. Sci. Technol. B 10 (1992) 1898.
[29] M. Larive, G. Jezequel, J.P. Landesman, F. Solal, J. Nagle, B. Lépine, A. Taleb-Ibrahimi, G. Indlekofer, X. Marcadet, Surf. Sci. 304 (1994) 298.

Why do (2×4) GaAs and InAs (001) surfaces exposed to phosphorus have so different behavior? Elastic strain arguments

X. Wallart,[a] C. Priester, D. Deresmes, T. Gehin, and F. Mollot
Institut d'Electronique et de Microélectronique du Nord, UMR CNRS 8520, Avenue Poincaré, B.P. 69, 59652 Villeneuve d'Ascq Cedex, France

(Received 9 April 2002; accepted for publication 14 June 2002)

When exposed to phosphorus, the (2×4) GaAs surface tends rapidly to roughen whereas it is not the case for the (2×4) InAs one, even after long exposure times. X-ray photoemission measurements show that the incorporated phosphorus amount is similar in both cases. The elastic energy difference between these two materials with incorporated phosphorus, calculated within the valence force field approximation, appears to be strong enough to explain this phenomenon. The role of surface reconstruction, mainly dimerization, on phosphorus incorporation is also emphasized. © *2002 American Institute of Physics.* [DOI: 10.1063/1.1499230]

The growth of epitaxial heterostructures involving both arsenic and phosphorus based *III–V* semiconductors remains a challenge due to the significant anion intermixing occurring at the interfaces.[1–5] Both interfaces do not behave symmetrically since As is more easily incorporated in a phosphide overlayer than P in an arsenide one.[6] The most common recipe used to reduce anion intermixing is to make a growth interruption at the interface during which the arsenide surface is exposed to a phosphorus flux or vice versa.[7–9] This kind of procedure then raises the question of the reactivity of an arsenide surface to a phosphorus flux and of a phosphide surface to an arsenic one. The most extensively studied case is that of InP with As since it occurs directly when the InP substrate oxide removal is performed under an As overpressure.[10] In this case, it has been shown that a thin InAs layer, around 2 monolayers (MLs) thick, is formed at the surface.[11] The As/P exchange reaction at the InP (001) surface has recently been investigated in light of the influence of the surface reconstruction on the formation of three-dimensional structures.[12,13] As regards GaAs surfaces, Jönsson *et al.*[14] have shown that a metalorganic vapor phase epitaxy grown As-rich $c(4\times4)$ GaAs surface reacts with PH_3 to form a single-layer P-terminated structure for temperatures below 600 °C. This structure is not stable at higher temperatures leading to a surface roughening at 650 °C. This trend has also been noted by Mahalingham *et al.*[15] from transmission electron microscopy observations on InGaP/GaAs supperlattices. From photoluminescence measurements, Aurand *et al.*[16] have shown that a GaP-rich layer up to 2 MLs thick is formed at the GaAs surface when exposed to cracked phosphine for a few tens of seconds. Nevertheless, very little has been reported on the reactivity on an InAs surface exposed to a phosphorus flux.

So, we have undertaken a comparison of the GaAs and InAs (001) surface behavior when exposed to a phosphorus flux. Although one could expect a rather similar behavior of these two binaries, we observed significant differences. Indeed, even after the incorporation of several phosphorus MLs, the InAs surface is still flat, whereas the GaAs one becomes rough after the incorporation of only 1–1.5 phosphorus MLs. Using valence force field calculations, we show that this difference is related to the elastic energy differences occurring upon phosphorus incorporation in both systems.

Samples are grown by gas-source molecular-beam epitaxy (MBE) in a Riber 32P reactor, using standard effusion cells for the elements III and cracked phosphine and arsine on undoped GaAs(001) and InAs(001) substrates. 4000 Å thick buffer layers are grown at 630 °C on GaAs and 500 °C on InAs, using a 1 ML/s growth rate. After growth, both samples exhibit a clear (2×4) reflection high-energy electron diffraction (RHEED) pattern, characteristic of As-rich surfaces. Then, the InAs samples are kept under an arsenic flux before the exposure to the phosphorus flux whereas GaAs samples are cooled down to 500 °C, the arsenic flux being vented below 550 °C to preserve the (2×4) reconstruction, before the phosphorus exposure (3 sccm phosphine flow rate) at 500 °C.[17] For both samples, during the cooling down to room temperature, the phosphorus flux is vented when the substrate temperature reaches 400 °C to avoid any phosphorus accumulation at the surface and the RHEED pattern is monitored to ensure it remains unchanged. We perform x-ray photoelectron spectroscopy (XPS) measurements with a monochromatic Al $K\alpha$ x-ray source on some of the samples by transferring them to the XPS chamber connected under an UHV to the growth chamber. Details of the data processing procedure are given elsewhere.[5] Finally, samples have been examined "*ex situ*" by atomic force microscopy (AFM), using a Digital Nanoscope III, working in the tapping mode.

Upon exposure to a 3 sccm phosphine flow rate at 500 °C, starting with the (2×4) reconstruction, the InAs surface first exhibits a change to a (2×2) pattern after 30 s exposure and then again a (2×4) pattern after 60 s. This pattern is characterized by intermediate streaks as bright as the main ones in the ×4 azimuth [inset in Fig. 1(a)] and is similar to that observed on the InP surface. In this case, we never detect any trend to a surface roughening until 30 min exposure time which is the longest we explored in this work. On the contrary, in the GaAs case, the starting (2×4) pattern is progressively lost with the appearance of arrow-headed shaped spots in the ×4 azimuth around 70 s exposure time, indicating the beginning of the surface roughening which

[a]Electronic mail: xavier.wallart@iemn.univ-lille1.fr

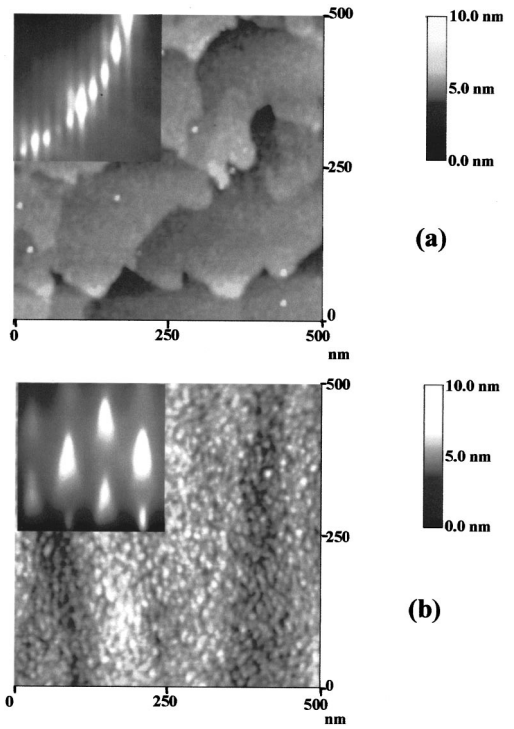

FIG. 1. AFM image of a (2×4) InAs surface exposed for 10 min. (a) and of a (2×4) GaAs one exposed for 5 min (b) to a cracked phosphine flux (3 sccm) at 500 °C. The insets show the corresponding RHEED patterns along the [110] azimut.

develops as exposure goes on, resulting in a spotty pattern after a few minutes [inset in Fig. 1(b)]. These findings are confirmed by the AFM observations which clearly indicate that the InAs surface is still smooth with clearly visible atomic steps [Fig. 1(a)], whereas the GaAs one becomes rough with small dots formation [Fig. 1(b)] after the phosphorus exposure.

In order to evaluate the phosphorus incorporated in the samples, we perform XPS measurements on both type of surfaces after 60 s exposure, i.e., just before the onset of roughening on GaAs, and after 10 and 30 min on InAs. Figure 2 shows the measured intensity ratios between the As $3d$ and P $2p$ core levels (CLs) versus the sine of the polar angle of detection with respect to the surface plane. The increase of these ratios with increasing angle clearly indicates that phosphorus is located at the sample surface. However, the P $2p$ CL does not exhibit the high binding energy component (≈1

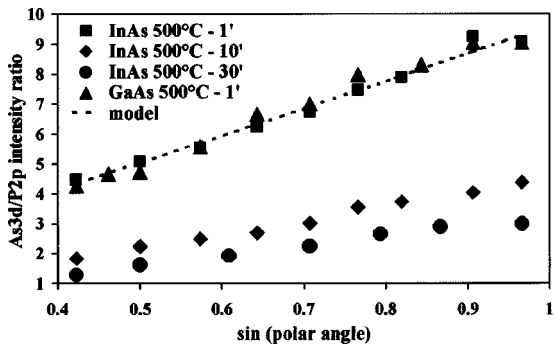

FIG. 2. As $3d$/P $2p$ XPS intensity ratios versus sine of polar angle after exposure of (2×4) GaAs and InAs surfaces to phosphorus. The dashed line represents the calculated ratios assuming the formation of a surface layer extending on 3 MLs with 50% P and 50% As.

eV shifted from the main one) characteristic of elemental phosphorus on the surface.[18] This indicates that there is no phosphorus accumulation at the surface during the cooling down of the sample. From Fig. 2, it is obvious that the amount of phosphorus in the GaAs and InAs samples after 60 s exposure is quite similar. From the experimental curves, it is possible to get an estimate of the amount of phosphorus in the sample although it is not possible to recover a unique concentration profile inside the sample, since different concentration profiles can lead to a rather similar agreement with the experiment. Then, it is necessary to assume the composition profile *a priori* and calculate the related intensity ratios. For the sake of simplicity, we use a square one with a constant phosphorus concentration on a given depth. This procedure requires a relative sensitivity factor between As $3d$ and P $2p$ CLs for which we use data recorded on MBE grown GaP and GaAs surfaces. For a 60 s exposure time, a good agreement between calculated and experimental intensity ratios is then found for a surface layer extending over 3 MLs with 50% phosphorus, i.e., a total amount of 1.5 MLs. A more interesting quantity is the incorporated phosphorus amount, i.e., the total amount minus the phosphorus amount lying in the outermost atomic plane, this latter being too sensitive to the cooling down procedure to be meaningful. The determination of the phosphorus amount in the outermost surface plane is not easy and that is why we consider two extreme cases. In the first one, we assume that the surface is terminated by a complete anion atomic plane whereas in the second one, we suppose a cation-rich surface terminated by a complete cation atomic plane. In the first case, the incorporated phosphorus is 1 ML whereas in the second, it increases to 1.5 MLs. The actual surface is in between these two extreme cases and we can safely conclude that after 60 s exposure time, the incorporated phosphorus amount lies between 1 and 1.5 MLs. More, the InAs surface exhibits still a clear reconstruction without any roughening for incorporated phosphorus quantities considerably larger than that detected at the onset of roughening on GaAs. Then, the difference observed in the behavior of the two surfaces around 60–70 s exposure can not be related to a significantly different incorporated amount of phosphorus.

Since growth roughening is often related to the elastic energy of the system, we have described the two systems we are interested in by means of a valence force field model. We have chosen, as in Ref. 19, a Keating's description[20] and the parameters for GaAs, GaP, InAs, and InP are those of Ref. 21. In our experiments, the increase in elastic energy is due to the replacement of As atoms by P ones. Thus, we have first calculated the substitutional energy of P atoms in GaAs or InAs assuming various surface reconstructions: (2×1) or $\beta 2$ (2×4) anion rich and (1×2) cation rich.[22] We note the peculiar importance of dimerization since for a (2×1) anion-rich surface, due to the presence of anion dimers, two different sites, α (below dimers) or β (between dimers), occur on the anion plane just below the surface with a large difference in substitutional energy, in agreement with previous work.[19] For a (1×2) cation-rich surface the inequivalent α and β sites are located in the second anion plane below the surface whereas for the $\beta 2$ (2×4) surface, one gets several different α-type and β-type sites located in the two upper planes be-

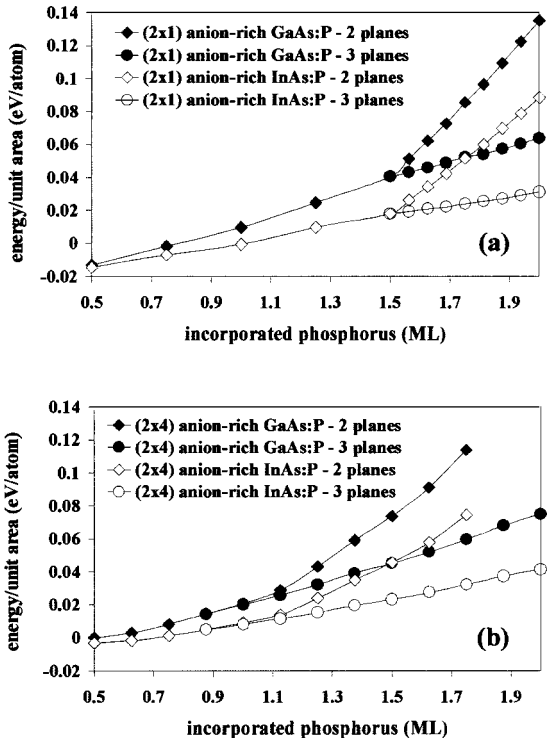

FIG. 3. Elastic energy differences between the systems with and without phosphorus for a (2×1) (a) and a $\beta 2$ (2×4) (b) surface reconstruction, considering phosphorus incorporation on two or three atomic planes below the surface.

low the surface. The calculated substitutional energy is roughly twice as large in GaAs (average value:45 meV/solute atom) than in InAs (25 meV/solute atom). This is mainly due to the bond strength difference between GaP and InP.

Nevertheless, the observed difference in substitutional energy is not sufficient to explain our experimental evidences since it considers only one single P atom in a GaAs or InAs matrix whereas, for a greater amount of incorporated phosphorus, elastic interaction between P atoms is efficient and needs to be taken into account. To go further, we perform the elastic energy calculation for a given amount of incorporated phosphorus on a definite depth. In Fig. 3, we plot the energy difference between the system with and without phosphorus incorporation. For these calculations, guided by the XPS results, we focus on an incorporated phosphorus amount ranging from 0.5 to 2 MLs and extending 2 or 3 MLs from the surface. The distribution of P atoms within the allowed two or three atomic planes is achieved by minimizing the elastic energy of the system. For any surface reconstruction, once again, energies are roughly twice as large in GaAs than in InAs. Moreover, one can note a rapid increase in the energy difference above 1.2 ML [for the $\beta 2$ (2×4) surface, 1.5 ML for the (2×1) one] incorporated phosphorus in the sample, if a two plane extension is considered. This increase corresponds to P atoms occupying less favorable (β-type) sites. From a kinetic point of view, since the GaAs bond is stronger than the InAs one, one can assume that the energetic barrier for phosphorus diffusion will be larger in GaAs than in InAs. This in turn tends to increase the elastic energy more rapidly in the GaAs (two plane extension) than in the InAs case (three plane extension) after 1.2 ML incorporated phosphorus. This 1.2 ML value is in good agreement with the above XPS determination of the phosphorus amount incorporated just before the onset of roughening on GaAs (between 1 and 1.5 MLs). This would explain why elastic energy relaxation occurs via surface roughening in the GaAs case.

We have compared the behavior of As-rich (2×4) GaAs and InAs surfaces exposed to a phosphorus flux at 500 °C. The InAs surface remains atomically flat with a clear (2×4) reconstruction after incorporation of several phosphorus MLs whereas the GaAs one becomes rough after incorporation of 1–1.5 MLs phosphorus. Using valence force field calculations, we show that this can be explained by the elastic energy differences occurring in these systems upon phosphorus incorporation and that the presence of surface dimers plays a key role in phosphorus incorporation.

The authors are grateful to G. Grenet for fruitful discussions and to C. Coinon for his technical assistance in the MBE experiments.

[1] M. Gerhardt, G. Kirpal, R. Schwabe, G. Benndorf, and V. Gottschalch, Thin Solid Films **392**, 85 (2001).
[2] R. Kudela, M. Kucera, B. Olejnikova, P. Elias, S. Hasenöhrl, and J. Novak, J. Cryst. Growth **212**, 21 (2000).
[3] Y. Moon, T.-W. Lee, S. Yoon, K. Yoo, and E. Yoon, J. Cryst. Growth **208**, 160 (2000).
[4] O. Schuler, O. Dehaese, X. Wallart, and F. Mollot, J. Appl. Phys. **84**, 765 (1998).
[5] O. Dehaese, X. Wallart, O. Schuler, and F. Mollot, J. Appl. Phys. **84**, 2127 (1998).
[6] M. B. Panish and H. Temkin, *Gas-Source Molecular Beam Epitaxy: Growth and Properties of Phosphorus Containing III–V Heterostructures* (Springer, Berlin, 1993).
[7] S. W. Chiou, C. P. Lee, J. M. Hong, C. W. Chen, and Y. Tsou, J. Cryst. Growth **206**, 166 (1999).
[8] Y. K. Fukai, F. Hyuga, T. Nittono, and K. Watanabe, J. Vac. Sci. Technol. B **17**, 2524 (1999).
[9] Y. Moon and E. Yoon, J. Cryst. Growth **212**, 61 (2000).
[10] J. M. Moison, M. Bensoussan, and F. Houzay, Phys. Rev. B **34**, 2018 (1986).
[11] G. Hollinger, D. Gallet, M. Gendry, C. Santinelli, and P. Viktorovitch, J. Vac. Sci. Technol. B **8**, 832 (1990).
[12] S. Yoon, Y. Moon, T. W. Lee, E. Yoon, and Y. D. Kim, Appl. Phys. Lett. **74**, 2029 (1999).
[13] H. Yang, P. Ballet, and G. Salamo, J. Appl. Phys. **89**, 7871 (2001).
[14] J. Jönsson, F. Reinhardt, M. Zorn, K. Ploska, W. Richter, and J. Rumberg, Appl. Phys. Lett. **64**, 1998 (1994).
[15] K. Mahalingham, Y. Nakamura, N. Otsuka, H. Y. Lee, M. J. Hafich, and G. Y. Robinson, J. Electron. Mater. **21**, 129 (1992).
[16] A. Aurand, J. Leymarie, A. Vasson, M. Mesrine, J. Massies, and M. Leroux, J. Appl. Phys. **89**, 3775 (2001).
[17] Following this procedure and according to the work of H. H. Farrell and C. J. Palmstrom [J. Vac. Sci. Technol. B **8**, 903 (1990)], for the (2×4) GaAs surface, we get is a $\beta 2$ one whereas for InAs, the (2×4) surface is probably a mixture of $\alpha 2$ and $\beta 2$ reconstructions according to the recent work of W. Barvosa-Carter, R. S. Ross, C. Ratsch, F. Grosse, J. H. G. Owen, and J. J. Zinck [Surf. Sci. **499**, L129 (2002)].
[18] P. Vogt, A. M. Frisch, Th. Hannapel, S. Visbeck, F. Willig, C. Jung, R. Follath, W. Braun, W. Richter, and N. Esser, Appl. Surf. Sci. **166**, 190 (2000).
[19] S. B. Zhang and A. Zunger, Appl. Phys. Lett. **71**, 677 (1997).
[20] P. N. Keating, Phys. Rev. **145**, 637 (1966).
[21] R. M. Martin, Phys. Rev. B **1**, 4005 (1970).
[22] For the (2×4) reconstruction, we have only considered the $\beta 2$ anion-rich one since the case of the $\alpha 2$ would be quite similar: Equivalent surface corrugation and a great amount of inequivalent α-type and β-type sites in the upper plane. As far as corrugation is concerned, our calculations clearly demonstrate that this short-range corrugation is completely inefficient: phosphorus incorporates below ridges as well as below trenches. The key parameter is definitely the presence of dimers.

Experimental and theoretical investigation of $Ga_{1-x}In_xAs$ surface reactivity to phosphorus

X. Wallart and C. Priester*
Institut d'Electronique de Microlectronique et de Nanotechnologie, UMR CNRS 8520, Boîte Postale 69, 59652 Villeneuve d'Ascq Cédex, France

(Received 6 March 2003; revised manuscript received 1 July 2003; published 11 December 2003)

$Ga_{1-x}In_xAs$ surfaces appear to show different behavior when exposed to phosphorus, depending on the In concentration. X-ray photoemission spectroscopy experiments provide information about phosphorus incorporation on several samples. Atomic-scale elastic energy calculations which include surface reconstructions emphasize the role or dimers for phosphorus incorporation and show a reasonable agreement for experiments that concern unstrained surfaces. Another roughening mechanism is proposed for strained surfaces.

DOI: 10.1103/PhysRevB.68.235314 PACS number(s): 82.45.Jn, 81.05.Ea, 81.65.−b, 82.80.Pv

I. INTRODUCTION

Heterostructures involving both arsenic and phosphorus based III-V semiconductors are of interest for optoelectronic as well as for microelectronic applications. However, the epitaxial growth of these structures with abrupt interfaces still remains a challenge whatever the growth technique used, i.e., metalorganic vapor phase epitaxy (MOVPE) or molecular-beam epitaxy (MBE).[1,2] Indeed, without any particular care, the resulting interfaces are diffuse with significant anion intermixing, due to various ''memory effects'' in the growth system, related to the anion overpressure during growth and to the high vapor pressure of arsenic and phosphorus.[3–8] Both interfaces do not behave symmetrically since As is more easily incorporated in a phosphide overlayer than P in an arsenide one.[9] The preferred recipe for reducing anion intermixing involves a growth interruption at the interface during which the arsenide surface is exposed for a given time to a phosphorus flux or vice versa.[10–13] A tradeoff has to be found for the best value of this exposure time which must be long enough to allow a good anion commutation but without degrading the interface quality.

This kind of procedure then raises the question of the reactivity of an arsenide surface to a phosphorus flux and of a phosphide surface to an arsenic flux. The most extensively studied case is that of InP under an As pressure since it occurs directly when people make the InP substrate oxide removal under an As overpressure.[14] In this case, it has been shown that a thin InAs layer around 2 ML (monolayers) thick is formed at the surface.[15] The As/P exchange reaction at the InP (001) surface versus substrate temperature has recently been investigated and the surface phase diagram has been determined, confirming that the substitution of As for P is limited to the two or three outermost monolayers.[16] On the same surface, Yoon *et al.*[17] and Yang *et al.*[18] have studied the influence of the V/III ratio or of the surface reconstruction on the formation of three-dimensional structures during As/P exchange reaction. As regards GaAs surfaces, Jönsson *et al.*[19] have shown that a MOVPE grown As-rich $c(4\times4)$ GaAs surface reacts with PH_3 to form a single-layer P-terminated structure for temperatures below 600 °C. They have observed that this structure is not stable at higher temperatures leading to surface roughening at 650 °C. This trend has been noted by Mahalingham *et al.*[20] from TEM observations on InGaP/GaAs superlattices. From photoluminescence measurements, Aurand *et al.*[21] have shown that a GaP-rich layer up to 2 ML thick is formed at the GaAs surface when exposed to cracked phosphine for a few tens of seconds. Nevertheless, very few is reported on the reactivity of an InAs surface exposed to a phosphorus flux.

In order to minimize the As incorporation in phosphides, the exposure of arsenides to phosphorus prior to the growth of a phosphide layer is required. That is why we have studied the surface reactivity of $Ga_{1-x}In_xAs$ alloys to a phosphorus flux. For a 500 °C substrate temperature, we find that, except for the InAs case ($x=1$), the surface roughens rather rapidly and that roughening occurs faster in the alloy case than in the GaAs one ($x=0$). We show that these observations cannot be attributed to different amounts of phosphorus incorporated in the layer, as determined by x-ray photoelectron spectroscopy (XPS). Using valence force field calculations and taking properly into account the surface reconstruction, we show that the difference between GaAs and InAs is related to the elastic energy differences occurring upon phosphorus incorporation in both systems. For the alloys, we show that, in the case of an average alloy matched to its substrate, the surface reconstruction, mainly dimers, induces some alloy ordering in the atomic layers very close to the surface, which renders less favorable phosphorus incorporation (above half a monolayer) as far as surface keeps flat.

II. EXPERIMENTAL

Samples are grown by gas source molecular-beam epitaxy in a Riber 32P reactor, using standard effusion cells for the elements III and cracked phosphine and arsine on undoped GaAs(001), InAs(001), and Fe-doped InP(001) substrates. We consider $Ga_{1-x}In_xAs$ alloys with four different In concentrations: $x=0$ (sample X0), 0.2 (sample X20), 0.53 (sample X53) and 1.0 (sample X100). The X0 sample is a 4000-Å-thick buffer layer grown at 630 °C on GaAs. For the X20 sample, we grow the same buffer layer followed by the growth of a 100 Å strained $Ga_{0.8}In_{0.2}As$ layer at 500 °C. The X53 sample is a 1000-Å-thick lattice-matched $Ga_{0.47}In_{0.53}As$ layer grown at 500 °C on a 2000-Å-thick InP buffer layer. Finally, the X100 sample is a 4000-Å-thick InAs buffer grown at 500 °C on InAs. The growth rate for all samples lies in the 0.7–1.0 ML/s. range. After growth, the samples

exhibit a clear (2×4) (samples X0, X53, and X100) or (2×3) (sample X20) reflection high-energy electron-diffraction (RHEED) pattern, characteristic of As-rich surfaces. Then the InAs and the alloy samples are kept under an arsenic flux for 2 min to allow surface smoothing before the exposure to the phosphorus flux. On the contrary, GaAs samples are cooled down to 500 °C, the arsenic flux being interrupted below 550 °C to preserve the (2x4) reconstruction, before the phosphorus exposure [3-SCCM phosphine flow rate) at 500 °C. Following this procedure, the (2×4) GaAs surface is $\beta2$ type[22] whereas the InAs one is probably a mixture between $\alpha2$ and $\beta2$ structures.[23] As regards the alloys, the (2×4) reconstruction occurring for sample X53 is probably closed to that of InAs due to In segregation, leading to an In-rich topmost layer. For the X20 sample, the observed (2×3) reconstruction has been described elsewhere.[24,25] For all samples, during the cooling down to room temperature, the phosphorus flux is interrupted when the substrate temperature reaches 400 °C to avoid any phosphorus accumulation at the surface and the RHEED pattern is monitored to ensure it remains unchanged. We perform XPS measurements on some of the samples by transferring them to the XPS chamber connected under UHV to the growth chamber. The XPS system is a Physical Electronics model 5600, modified by SINVACO in order to analyze 3-inch MBE samples. We use a monochromatic Al $K\alpha$ x-ray source and an analyzer pass energy of 12 eV. Under these conditions, the overall resolution as measured from the full width at half maximum of the Ag 3d5/2 line is 0.55 eV. The acceptance angle of the analyzer is set to 14° and the angle between the incident x rays and the analyzer is 90°. The direction of photoelectrons is given by the polar angle θ, as referenced to the sample surface. To obtain angle-dependent XPS results, the polar angle is varied from 25° to 75°. The intensity of the various XPS core levels (CL's) is measured as the peak area after standard background subtraction according to the Shirley procedure.[26] Photodiffraction effects are often prominent on single crystals[27] and, as they superimpose to the XPS signal variations relative to the concentration gradient, they can make concentration profile determination rather difficult. To minimize these effects, we perform an average of the different XPS core level intensities with respect to the azimuth.[28] Then, we calculate intensity ratios between the P $2p$ and As $3d$ CL's with close binding energies.[29] For the CL decomposition, we apply the deconvolution procedure proposed by Joyce *et al.*[30] In this procedure, the As $3d$ CL is synthesized using Voigt functions by a doublet for the 3/2 and 5/2 components whereas the P $2p$ CL is modeled by a doublet for the 1/2 and 3/2 components. The branching ratios are theoretical ones and the splitting energies are fixed at 0.69 eV between As $3d_{3/2}$ and As $3d_{5/2}$ and 0.85 eV between P $2p_{1/2}$ and P $2p_{3/2}$, which are typical values for these core levels.[31] The best fit is obtained through a least-square minimization procedure. The surface components are modeled with the same parameters than the bulk component, i.e., the Gaussian and Lorentzian broadening are kept fixed for each component of a given CL. This broadening is chosen as that obtained on (2×4) GaAs and InP surfaces analyzed in the same conditions. Finally, samples have been examined "*ex situ*" by atomic force microscopy (AFM), using a Digital Nanoscope III, working in the tapping mode.

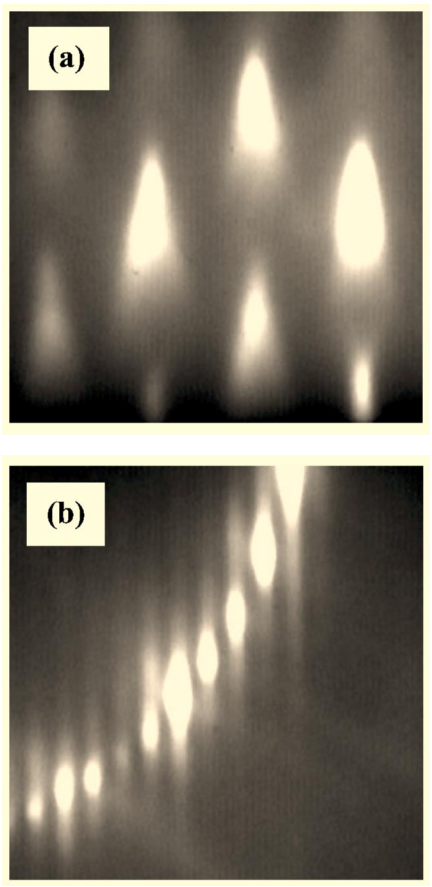

FIG. 1. RHEED patterns along the [110] azimuth of a (2×4) GaAs surface exposed for 5 min (a) and of a (2×4) InAs surface exposed for 10 min (b) to a cracked phosphine flux (3 SCCM) at 500 °C.

III. RESULTS

A. RHEED and AFM observations

Upon exposure to a 3-SCCM phosphine flow rate at 500 °C, for all samples except the InAs one, the starting RHEED pattern [(2×4) for samples X0 and X53, (2×3) for sample X20] is progressively lost with the appearance of arrow-headed shape spots in the [110] azimuth. This indicates that the surface roughens as exposure goes on, resulting in a spotty pattern after a few minutes [Fig. 1(a)]. As revealed by the evolution of the intensity of a three-dimensional (3D) Bragg spot (Fig. 2), roughening occurs more rapidly for the alloys (after roughly a 10-s exposure time) than for GaAs (after 70 s). In the same way, the transition from a 2D to 3D morphology is more abrupt for the X53 sample than for the X20 one. On the contrary, for the InAs sample, the RHEED pattern indicates that the reconstruction first starts as (2×4), then changes towards (2×2) after 30 s exposure and turns back towards a (2×4) pattern after 60 s. This pattern [Fig. 1(b)] is characterized by intermediate streaks as bright as the main ones in the [110]

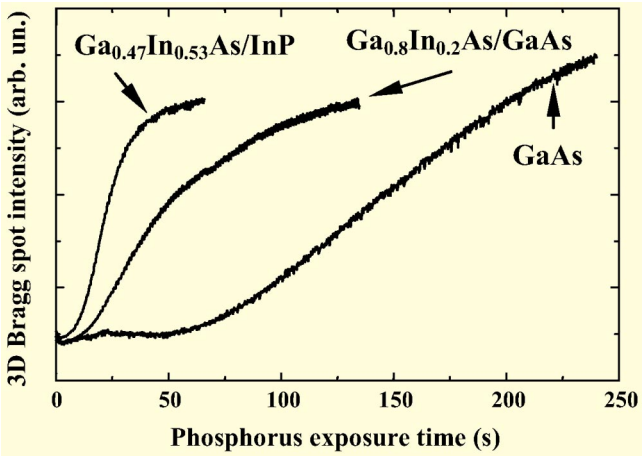

FIG. 2. 3D Bragg spot intensity evolution vs exposure time to a cracked phosphine flux (3 SCCM) at 500 °C for a (2×4) GaAs, a (2×3) $Ga_{0.8}In_{0.2}As$, and a (2×4) $Ga_{0.47}In_{0.53}As$ surfaces.

azimuth and is similar to that observed on a (2×4) InP surface. In this case, we never detect any trend to a surface roughening until 30 min exposure time which is the longest we explore in this work.

When increasing the substrate temperature to 600 °C or 650 °C for the X0 sample (GaAs), surface roughening tends to occur more rapidly than at 500 °C.

On the other hand, when decreasing the substrate temperature to 450 °C during the phosphorus exposure, samples X20 and X53 do not exhibit anymore a tendency to surface roughening. In this case, the starting reconstruction under As stabilization is a (1×3)–(4×3) one for both alloys. Upon P exposure, this reconstruction vanishes within 10 s and turns to a (3×4) for sample X53 and to a (3×2) for sample X20 after roughly 40 s. When P exposure goes on, the RHEED pattern keeps its 2D character for times as long as 10 min.

These findings are confirmed by the AFM observations. They clearly evidence that the InAs surface is still smooth with clearly visible atomic steps [Fig. 3(d)] after rather long exposure times (10 min). On the contrary, for the other samples, the surface becomes rough with small dots formation [Fig. 3(a–c)], even after short exposure times (a few tens of seconds). These observations indicate in which range kinetic limitations are ruling out surface roughening. In this paper we will mainly focus on experiments at 500 °C or more, for which the near equilibrium conditions are fulfilled.

B. XPS measurements

In light of the above observations, upon phosphorus exposure, the surface morphology evolution seems to depend on the sample composition. That is why we determine the incorporated phosphorus in different samples before the onset of roughening by XPS measurements. We perform them on X0 after 60-s exposure, on X20 and X53 after 10 s, and on X100 after 1-, 10-, and 30-min exposure at 500 °C. For X20, we also get XPS spectra after 5-min exposure at 450 °C. Figure 4 shows the measured intensity ratios be-

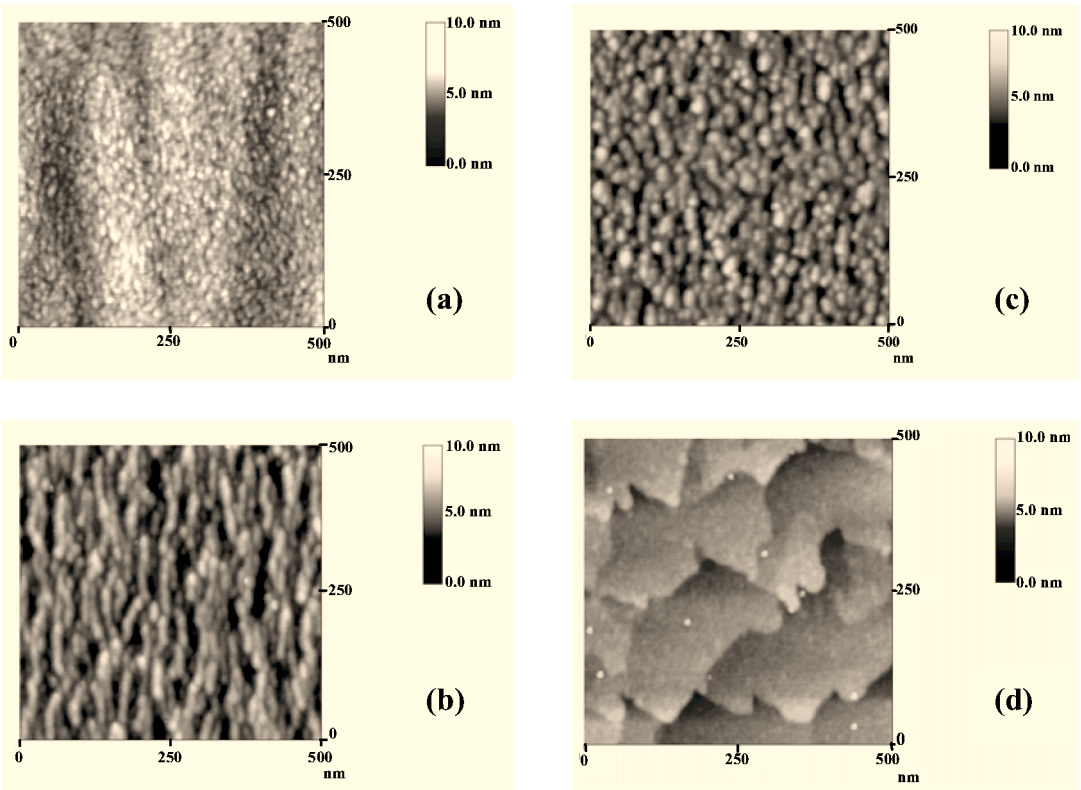

FIG. 3. AFM images of a (2×4) GaAs surface exposed for 5 min (a), of a (2×3) $In_{0.2}Ga_{0.8}As$ one exposed for 3 min (b) of a (2×4) $In_{0.53}Ga_{0.47}As$ one exposed for 3 min (c), and of a (2×4) InAs one exposed for 10 min (d) to a cracked phosphine flux (3 SCCM) at 500 °C.

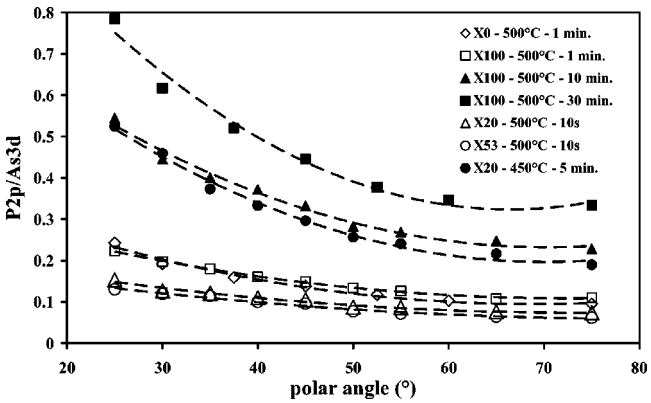

FIG. 4. P $2p$/As $3d$ XPS intensity ratios vs the detection polar angle with respect to the surface plane for samples X0 (GaAs), X20 ($In_{0.2}Ga_{0.8}As$), X53 ($Ga_{0.53}In_{0.47}As$), and X100 (InAs) exposed to a cracked phosphine flux (3 SCCM) at 450 °C or 500 °C.

tween the P $2p$ and As $3d$ CL's versus the detection polar angle with respect to the surface plane. The decrease of these ratios with increasing angle clearly indicates that phosphorus is mainly located near the sample surface and does not penetrate very deep in the sample. However, the P $2p$ CL does not exhibit the high binding-energy component (≈ 1 eV shifted from the main one) characteristic of elemental phosphorus on both InP and GaP surfaces.[32,33] This indicates that there is no phosphorus accumulation at the surface during the cooling down of the sample. From Fig. 4, at 500 °C, it is obvious that the amount of phosphorus in the X0 (GaAs) and X100 (InAs) samples after 60-s exposure is quite similar whereas it is smaller for the X20 and X53 samples after 10-s exposure.

From these experimental curves, it is possible to get an estimate of the amount of phosphorus in the sample although it is not possible to recover a unique concentration profile inside the sample, since different concentration profiles can lead to a rather similar agreement with the experiment. Then it is necessary to assume the composition profile *a priori* and to calculate the related intensity ratios. For sake of simplicity, we use a square profile with a constant phosphorus concentration on a given depth. For estimating the relative sensitivity factor between As $3d$ and P $2p$ CL's, we use MBE grown (2×4) GaAs and P-rich (2×4) GaP surfaces which present very close surface compositions although their atomic structures could differ.[33,34] Moreover, XPS data are recorded at normal emission from the surface in order to minimize surface effects. The most relevant quantity is the incorporated phosphorus amount, i.e., the total amount minus the phosphorus amount lying in the outermost atomic plane, this latter being too sensitive to the cooling down procedure to be meaningful. Since the determination of the incorporated P amount is not straightforward, we use the two different methods described below.

In the first method, we first try to get an estimate of the incorporated P amount by using the total As $3d$ and P $2p$ XPS intensities. We model the P $2p$/As $3d$ intensity ratios using a square concentration profile. The results of the fit are given in Table I, columns 3, c(P), and 4 d(P), first line for each sample. To interpret these results, we then consider two extreme cases. (i) in the first one, we assume that the surface is terminated by a complete anion atomic plane (which is then the outermost atomic plane); (ii) in the second one, we assume that the surface is terminated by a complete cation plane (the first anion plane is then the second atomic plane from the surface). For the anion-terminated surface, d(P) includes the phosphorus of the outermost anion plane which we do not consider as incorporated. The incorporated P amount is obtained by $c(\mathrm{P})*[d(P)-1]$ which gives the lower value of the range reported in column 5 in Table I. On the contrary, for the cation-terminated surface, the incorporated P amount is calculated via $d(\mathrm{P})*c(\mathrm{P})$, which gives the higher value of the range in column 5. Of course the actual surface is in between these two extreme cases and that is

TABLE I. Phosphorus concentration c(P) and in-depth penetration d(P) as deduced from XPS measurements according either to the total P $2p$ and As $3d$ intensities or to the bulk components extracted from the decomposition of the CL's.

Sample	Method	c(P)	d(P) : in-depth P penetration (ML)	Total amount of incorporated P (ML)
GaAs—500 °C	Total intensities	0.48	3	0.96–1.44
1 min	Bulk component intensities	0.55	2	1.10
InAs—500 °C	Total intensities	0.48	3	0.96–1.44
1 min	Bulk component intensities	0.58	2	1.16
InAs—500 °C	Total intensities	0.68	4	2.02–2.72
10 min	Bulk component intensities	0.77	3	2.31
InAs—500 °C	Total intensities	0.72	5	2.88–3.60
30 min	Bulk component intensities	0.84	4	3.36
$Ga_{0.8}In_{0.2}As$	total intensities	0.36	3	0.72–1.08
500 °C—10 s	Bulk component intensities	0.46	2	0.92
$Ga_{0.47}In_{0.53}As$	Total intensities	0.32	3	0.64–0.96
500 °C—10 s	Bulk component intensities	0.37	2	0.74
$Ga_{0.8}In_{0.2}As$	Total intensities	0.84	3	1.68–2.52
450 °C—10 s	Bulk component intensities	0.96	2	1.92

why this first method only provides a lower and a higher estimate of the incorporated P amount.

To get more precise results, we use a second method in which we decompose the P $2p$ and As $3d$ CL's in their bulk and surface components. We assume that the surface components are related to nonincorporated P and As, i.e., to P and As atoms which are located on the outermost atomic plane whereas the bulk components are related to As and P atoms located on the second anion atomic plane or deeper. In the CL's decomposition, we assume two surface components as previously done for GaAs surfaces[31] and for P-rich phosphide surfaces.[32,33] Figure 5 shows a typical decomposition of the P $2p$ and As $3d$ CLs. Doing so, for a 30 min exposure time of the X100 sample, we only need one surface component for the P $2p$ CL at lower binding energy as in the pure (2×4) InP surface case.[32,35] Then, after long P exposure times, the P $2p$ CL of the InAs surface becomes very close to that recorded on an InP (2×4) one, confirming the similarity observed in the RHEED patterns. Then we model the P $2p$ and As $3d$ bulk component intensity ratios by a square concentration profile. The results of the fit are given in Table I, columns 3, c(P), and 4, d(P), second line for each sample. This method allows us to get a more precise value of the incorporated P amount, reported in column 5

It is clear from Table I that the observed different behavior from the roughening point of view between X0 (GaAs) and X100 (InAs) at 500 °C cannot be accounted for by a significant difference in the amount of incorporated phosphorus. In the same way, the incorporated phosphorus amount before the onset of roughening is significantly lower in the X20 and X53 samples than in the X0 sample. On the contrary, for sample X100 after 30-min exposure for which the surface is still 2D, the incorporated phosphorus amount is considerably larger than that determined before the onset of roughening on sample X0 (GaAs). This implies that the tendency to surface roughening upon phosphorus exposure cannot be directly related to a more or less important amount of incorporated phosphorus. Finally, we can also note the effect of the growth temperature since for sample X20, at 450 °C, no surface roughening is observed after incorporation of 2-ML phosphorus whereas at 500 °C, surface roughening occurs for less than 1-ML incorporated phosphorus.

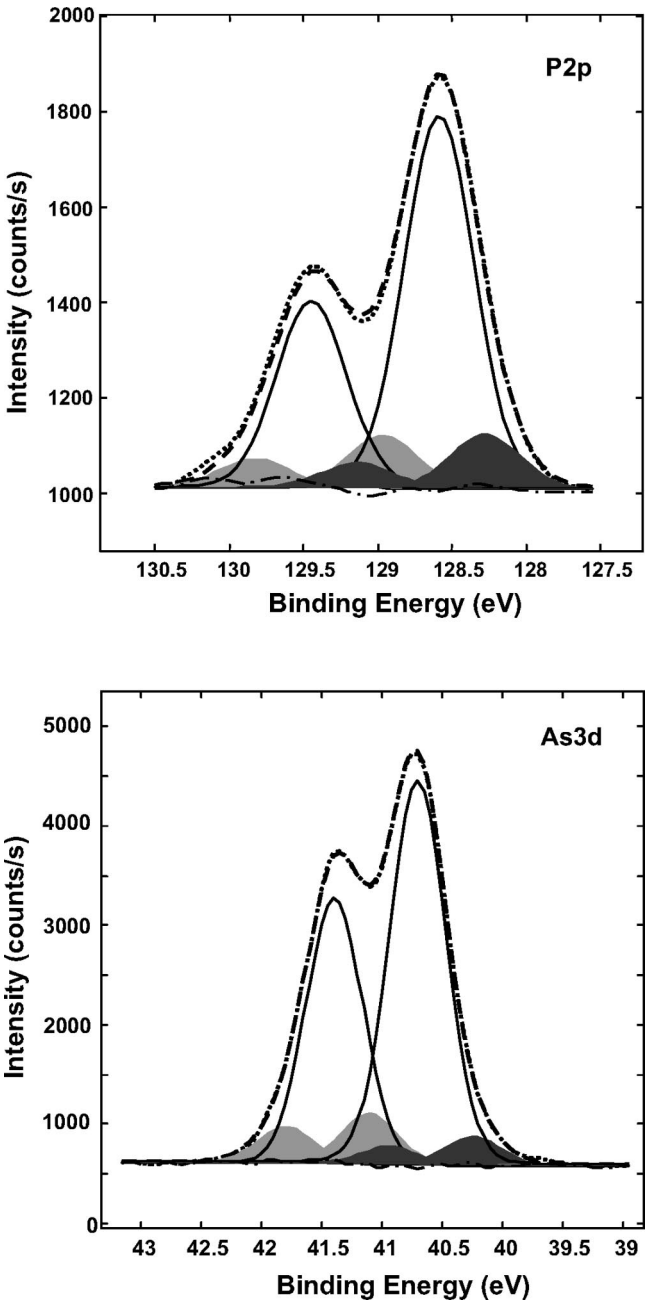

FIG. 5. Typical XPS core-level decomposition for P $2p$ and As $3d$ (sample InAs after 1-min exposure time at 500°C). The takeoff angle of the photoelectrons is 25° with respect to the surface plane. Shaded areas indicate surface components, the full lines are related to the bulk one, the dashed line is the resulting fit, the dotted line is the experimental data, and the dashed-dotted line is the residual of the fit.

IV. MODEL AND DISCUSSIONS

As the amount of incorporated phosphorus definitely cannot be the key parameter for the roughening onset, let us now consider the strain induced by phosphorus incorporation. For the samples under investigation here, the phosphorus incorporation tends either to induce a tensile strain in the surface layer (for samples X0, X53, and X100) or to reduce the initial compressive strain (for sample X20). For a given distribution of incorporated phosphorus, the mean induced tensile strain is similar for X0, X53, and X100 samples. Taking into account the amount of phosphorus incorporated in X0, X53, and X100 samples determined above, it is clear that the surface roughening of X0 and X53 samples cannot be explained by the mean induced tensile strain since X100 sample should exhibit surface roughening too, which is not the case. In the same way, this argument cannot account for earlier roughening on sample X53 than on X0 sample. Clearly, a more detailed picture is needed.

When looking at an atomistic picture of the surface layer, one important feature to consider is the tendency of the quaternary GaInAsP alloys to exhibit spinodal decomposition[36–38] to form GaP and InAs-rich regions. Considering thermodynamical calculations on spinodal decomposition

reported by LaPierre *et al.*[36,37] could be useful here for sample X53 for which the incorporation of phosphorus leads the resulting quaternary to fall inside the miscibility gap. However, the same calculations predict that the quaternary formed by P incorporation in the X20 sample falls mainly outside the miscibility gap and do not predict any miscibility gap for GaAsP. Then it is not possible to explain our results by a thermodynamic description of the spinodal decomposition even if this decomposition is indeed an important factor to be considered. Moreover, as outlined by LaPierre *et al.*,[36,37] the origin of the phase separation observed during the growth of the quaternary GaInAsP alloys is probably surface related and not a bulk effect. That is why we model the systems from a microscopic point of view, taking into account the surface reconstruction. Let us first present the results relative to the two binaries GaAs and InAs.

A. GaAs and InAs cases

Since growth roughening is often related to the elastic energy of the system, we describe the two systems we are interested in by means of a valence force field model. We choose, as in Ref. 39, a Keating's description,[40] and the parameters for GaAs, GaP, InAs, and InP are those of Ref. 41. In our experiments, the elastic energy increase is due to the replacement of As atoms by P ones. Thus we first calculate the substitutional energy of P atoms in GaAs or InAs assuming various surface reconstructions. First the simple and academic cases of (2×1) anion-rich and (1×2) cation rich are considered, as they are very helpful for enlightening the dimer role. For the anion-rich surfaces that present a (2×4) reconstruction, we only display results for the $\beta2(2\times4)$ as we have checked that an $\alpha2(2\times4)$ leads to similar results; this is due to equivalent surface corrugation and a great amount of inequivalent α- and β-type sites in the upper plane. As far as corrugation is concerned, our calculations clearly demonstrate that this short-range corrugation is less efficient than dimers: phosphorus incorporates below ridges as well as below trenches. The key parameter is definitely the presence of dimers: for a (2x1) anion-rich surface [Fig. 6(a)], due to the presence of anion dimers, two different sites, α (below dimers) or β (between dimers), occur on the anion plane just below the surface. As shown in Fig. 7, these two sites present a large difference in substitutional energy, in agreement with previous work.[39] For a (1×2) cation-rich surface [Fig. 6(b)], the inequivalent α and β sites are located in the second anion plane below the surface whereas for the $\beta2$ (2×4) surface (not represented in Fig. 6), one gets several different α-type and β-type sites located in the two upper planes below the surface.

The calculated substitutional energy is roughly twice as large in GaAs (average value—45 meV/solute atom) than in InAs (25 meV/solute atom). This is mainly due to the bond strength difference between GaP and InP which is also at the origin of the difference between the interaction parameter Ω involved in the calculation of the alloys mixing enthalpy (for GaAsP, the mean value of Ω is 35 meV (Ref. 42) whereas it is 15 meV for InAsP (Ref. 43).

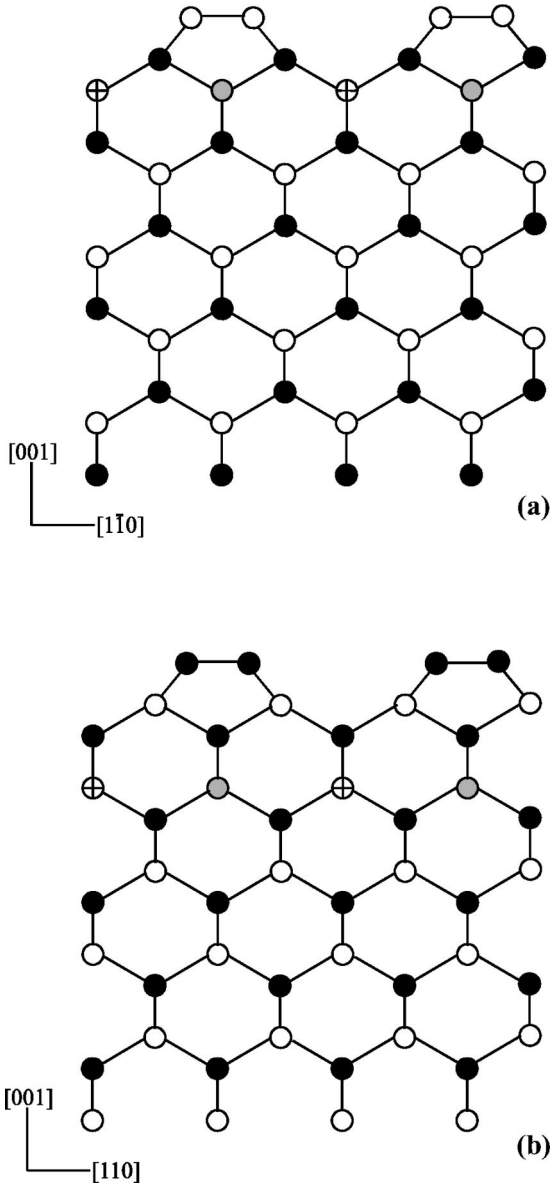

FIG. 6. Schematic drawing showing the existence of α and β sites for the incorporation of phosphorus in the second anion plane from the surface either for an anion-rich (2×1) reconstruction (a) or for a (1×2) cation-rich one (b). Filled circles are for cations, opened ones are for anions, gray ones are for the α sites, and the crossed ones for the β sites.

Nevertheless, the observed difference in substitutional energy is not sufficient to explain our experimental evidences since it considers only one single P atom in a GaAs or InAs matrix whereas, for a greater amount of incorporated phosphorus, elastic interaction between P atoms is efficient and needs to be taken into account. To go further, we perform the elastic energy calculation for a given amount of incorporated phosphorus on a definite depth. In Figs. 8 and 9, we plot the energy difference between the system with and without phosphorus incorporation for the (2×1) and (2×4) reconstructions, respectively. For these calculations, guided by the XPS results, we focus on an incorporated phosphorus amount ranging from 0.5 to 2 ML and extending 2 or 3 ML from the

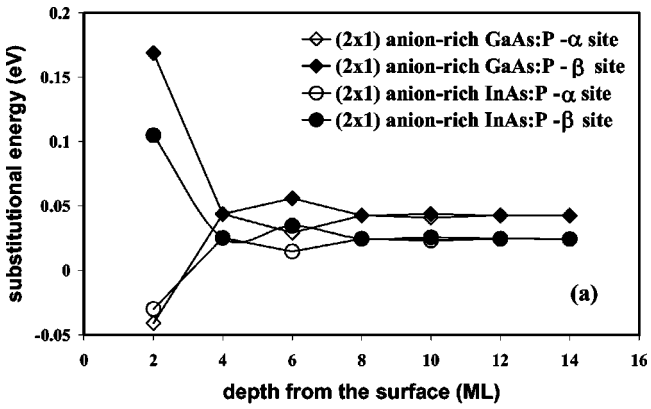

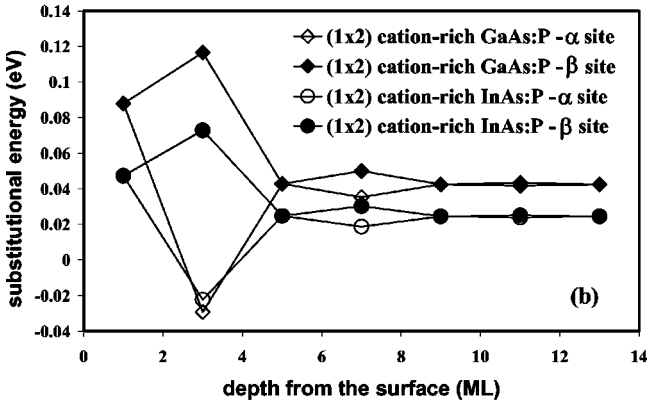

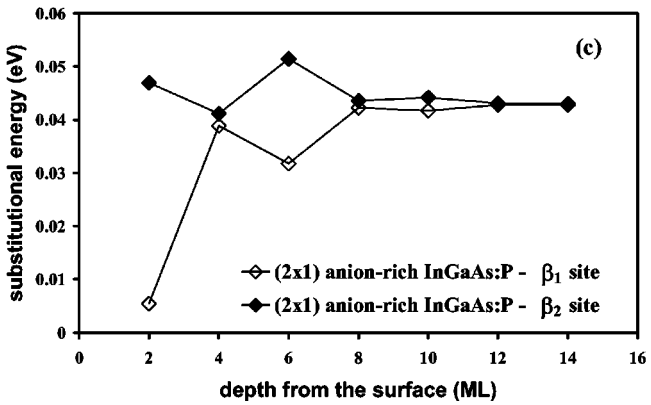

FIG. 7. Substitutional energy of P atoms in GaAs and InAs matrix, considering either an anion-rich (2×1) reconstruction (a) or a cation-rich (1×2) one (b), and in a $In_{0.5}Ga_{0.5}As$ one for a (2×1) anion-rich reconstruction (c).

surface. The distribution of P atoms within the allowed two or three atomic planes is got by minimizing the elastic energy of the system. Once again, energies are roughly twice as large in GaAs than in InAs. Moreover, in Fig. 9, one can note a rapid increase in the energy difference above 1.2 ML incorporated phosphorus in the sample, if a two plane extension is considered. This increase corresponds to P atoms starting to occupy less favorable (β-type) sites. This 1.2-ML value is in good agreement with the above XPS determination of the phosphorus amount incorporated just before the onset of roughening on GaAs (1.1 ML). Within this model,

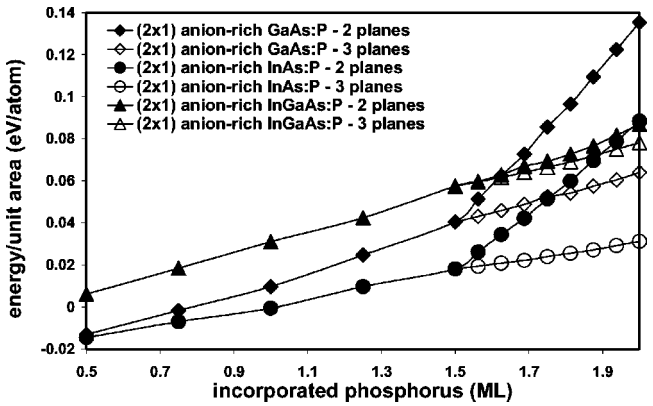

FIG. 8. Elastic energy differences between the systems with and without phosphorus for GaAs, InAs, and $Ga_{0.5}In_{0.5}As$ considering a (2×1) reconstruction and assuming phosphorus incorporation on two or three atomic planes below the surface.

we can infer that P incorporation occurs first on the most favorable sites (α type) of the first plane below the surface and on the equivalent sites of the second plane below the surface. Then, since diffusion is very weak in III-V semiconductors at 500 °C, the in-depth penetration of P is kinetically limited and P incorporation goes on with the occupation of the less favorable sites (β type) of the first plane under the surface. This leads to an important increase of the elastic energy, especially in the GaAs case, which in turn would explain the relaxation via surface roughening.

B. Alloy cases

In this case, we have first to examine the surface dimer effect on the cation distribution. Indeed, for the (1×2) cation-rich surface, we have shown above [Figs. 6(b) and 7(b)] that the presence of surface cation dimers leads to two inequivalent sites for P incorporation in the second anion plane from the surface (α site below the dimers, β site between the dimers). In the same way, for an anion-rich alloy surface, the presence of the anion dimers will lead to two inequivalent sites for the Ga atoms in the second cation plane

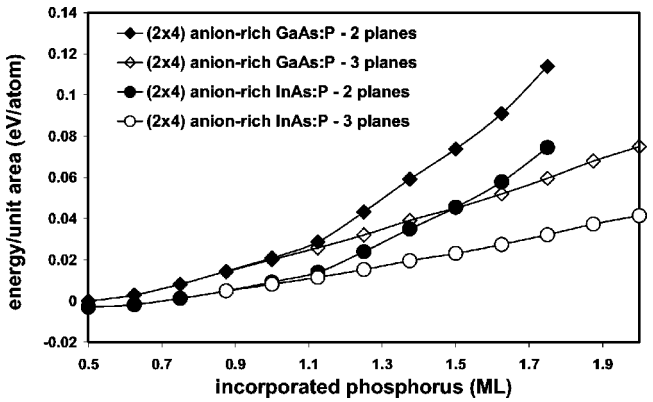

FIG. 9. Elastic energy differences between the systems with and without phosphorus for GaAs and InAs considering a (2×4) reconstruction and assuming phosphorus incorporation on two or three atomic planes below the surface.

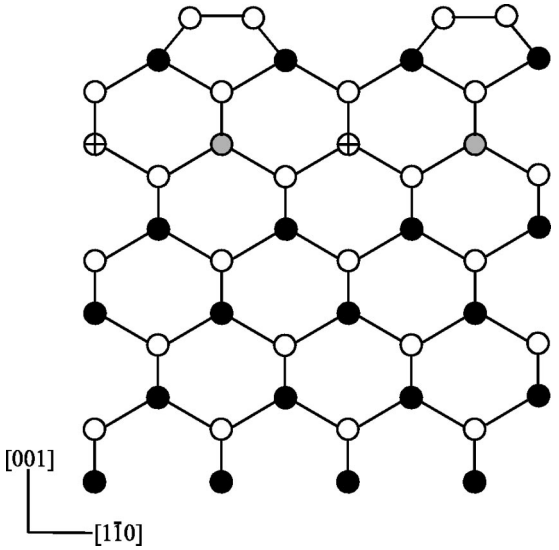

FIG. 10. Schematic drawing showing the existence of α and β sites for the Ga atoms in the second cation layer from the surface of $In_{0.5}Ga_{0.5}As$ due to the presence of As dimers. Filled circles are for cations, opened ones are for anions, gray ones are for the α sites, and the crossed ones for the β sites.

from the surface: a favorable one (α site) below the dimers and a more energetic one (β site) between the dimers (Fig. 10). This implies that the second cation plane will present a kind of ordering due to the anion dimers with Ga atoms preferentially below the dimers and In atoms preferentially between the dimers.[44] XPS Ga 3*d*-In 4*d* spectra recorded at 25° and 75° polar angles reveal a significant In 4*d* surface component associated with In segregation as observed in a previous work.[29] Then, in our model, in order to take into account In segregation towards the surface, the upper cation plane (where all sites are equivalent) is supposed to be purely In. For simplicity, as far as X53 sample is concerned, we assume that all other cation planes contain half In and half Ga atoms. In such a dimer induced surface ordered alloy, how altered are α and β sites for phosphorus incorporation? β sites keep repulsive, but a bit less repulsive than in binaries, as phosphorus incorporation will induce InP areas, obviously lattice matched to the InP substrate. This can be viewed in Fig. 7(c): β site substitution energy in the first layer is significantly lower in the alloy than in the binaries [Fig. 7(a)]. On the other hand, the sites located below the dimer rows are no longer attractive from phosphorus incorporation point of view, but become slightly repulsive, as incorporating P atoms in these sites creates lines of GaP bonds (Fig. 10), which are 7% mismatched to the substrate. Subsurface anion sites are thus never α type, but slightly (β_1) or strongly (β_2) β type: that's why the phosphorus incorporation curves for a 2×1 anion-rich surface displayed in Fig. 8 show InGaAs curves (triangles) lying significantly upper than both InAs (circles) and GaAs (diamonds) curves. This is the basic mechanism which explains why X53 roughens earlier than X0. If one turns to a more realistic 2×4 surface, surface cation ordering is a bit more complicated and InGaAs phosphorus incorporation curves lie clearly upper than GaAs curves only if one takes into account some In

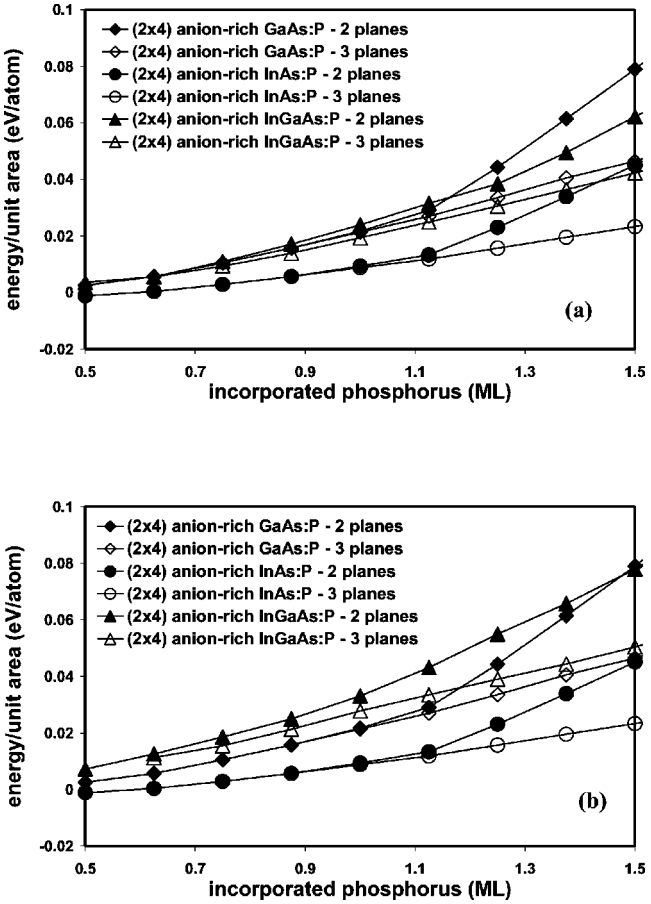

FIG. 11. Elastic energy differences between the systems with and without phosphorus for GaAs, InAs, and $In_{0.5}Ga_{0.5}As$ considering (2×4) reconstruction and the nominal In concentration in the second cation plane (a) and a slightly In depleted second cation plane (b).

depletion just below the In surface plane: Fig. 11(a) corresponds to the nominal In concentration in the second cation plane and Fig. 11(b) to an In depleted second cation plane (three In atoms and five Ga atoms in the surface unit cell). Under this assumption, the calculated phosphorus incorporation curves are in reasonable agreement with the experimental observation of the roughening of unstrained GaAs, InAs, and $Ga_{0.47}In_{0.53}As$ surface under phosphorus exposition.

These three systems are lattice matched to their substrate before incorporating phosphorus. This is not the case for $Ga_{0.8}In_{0.2}As$ on GaAs substrate. In this latter system indeed, phosphorus incorporation first tends to lower the mean strain in the alloy. This explains why, at low phosphorus exposure temperatures (450 °C), a rather great amount of phosphorus is incorporated very fast near the surface, as reported in Table I. For this reason, one would expect that, at usual phosphorus exposure temperatures, $Ga_{0.80}In_{0.20}As$ would roughen later than GaAs. That is what the model shows if one calculates the equivalent of Fig. 11 for this strained alloy: either one considers a $\beta2$ 2×4 reconstruction or the more realistic (2×3) (which also exhibits surface anion dimers, as shown in Ref. 25), the $Ga_{0.8}In_{0.2}As$ curves lie lower than GaAs ones. However, this comparison assumes

equivalent initial surface roughnesses in strained and unstrained samples before phosphorus exposure. This is probably not the case: the strained sample would probably present long-range and smooth surface undulations, which cannot be detected by RHEED observations, in order to slightly relax the stored elastic energy. These undulations will favor the wirelike roughening which is observed on AFM views (Fig. 3). Let us note that for the unstrained samples X0 and X53 the roughening morphology is dotlike. On the other hand, AFM view of a $Ga_{0.3}In_{0.7}As$ film grown on an InP substrate and exposed to phosphorus also displays a wire-like morphology after roughening. Last, let us note that if the phosphorus incorporation was enhancing the average strain instead of reducing it (e.g., $Ga_{0.7}In_{0.3}As$ on InP), both roughening mechanisms would compete.

V. CONCLUSIONS

In this work we have studied the surface reactivity of $Ga_{1-x}In_xAs$ alloys to a phosphorus flux, and we have shown that for a 500 °C substrate temperature, except for the InAs case, the surface roughens rather rapidly and that roughening occurs more rapidly in the alloy case than in the GaAs one. These observations could not be attributed to different amounts of phosphorus incorporated in the layer, as determined by x-ray photoelectron spectroscopy (XPS). We have proposed a model which emphasizes the role of surface reconstruction, and more precisely of dimers: they tend to order the surface ternary (GaAsP, InAsP) or quaternary (GaInAsP) alloys, and thus govern the calculated phosphorus incorporation curves, which are in reasonable agreement with surface roughening observations. Valence force field calculations, taking properly into account the surface reconstruction, show that the difference between GaAs and InAs is related to the elastic energy differences occurring upon phosphorus incorporation in both systems. For the alloy matched to its substrate, the surface reconstruction, mainly dimers, induces some alloy ordering in the atomic layers very closed to the surface, which renders less favorable phosphorus incorporation (above half a monolayer) as far as surface keeps flat. In the case of strained alloys the roughening mechanism is completely different (large wires are used instead of initially small dots which ripen), and is related to initial smooth undulations of the strained alloy film. In this paper we have chosen to focus on roughening mechanisms, but we have also shown that this roughening can be experimentally avoided by making use of the kinetic limitations associated with lower substrate temperature.

ACKNOWLEDGMENTS

We wish to acknowledge Dominique Deresmes for AFM measurements, C. Coinon for his technical assistance in the MBE experiments, and D. Vignaud for a critical reading of this manuscript.

*Electronic address: catherine.priester@isen.fr

[1] M. Gerhardt, G. Kirpal, R. Schwabe, G. Benndorf, and V. Gottschalch, Thin Solid Films **392**, 85 (2001).
[2] R. Kudela, M. Kucera, B. Olejnikova, P. Elias, S. Hasenhrl, and J. Novak, J. Cryst. Growth **212**, 21 (2000).
[3] J.C. Garcia, P. Maurel, P. Bove, and J.P. Hirtz, J. Appl. Phys. **30**, 1186 (1991).
[4] W. Wu, S.L. Skala, J.R. Tucker, J.W. Lyding, A. Seabaugh, E.A. Beam III, and D. Jovanovic, J. Vac. Sci. Technol. A **13**, 602 (1995).
[5] O. Schuler, O. Dehaese, X. Wallart, and F. Mollot, J. Appl. Phys. **84**, 766 (1998).
[6] O. Dehaese, X. Wallart, O. Schuler, and F. Mollot, J. Appl. Phys. **84**, 2127 (1998).
[7] Y. Moon, T-W. Lee, S. Yoon, K. Yoo, and E. Yoon, J. Cryst. Growth **208**, 160 (2000).
[8] R. André, S. Wey, and C.W. Tu, J. Cryst. Growth **235**, 65 (2002).
[9] M. B. Panish and H. Temkin, *Gas Source Molecular Beamp Epitaxy: Growth and Properties of Phosphorus Containing III-V Heterostructures* (Springer, Berlin, 1993).
[10] M.J. Hafich, J.H. Quigley, R.E. Owens, G.Y. Robinson, D. Li, and N. Otsuka, Appl. Phys. Lett. **54**, 2686 (1989).
[11] S.W. Chiou, C.P. Lee, J.M. Hong, C.W. Chen, and Y. Tsou, J. Cryst. Growth **206**, 166 (1999).
[12] Y.K. Fukai, F. Hyuga, T. Nittono, K. Watanabe, and H. Sugahara, J. Vac. Sci. Technol. B **17**, 2524 (1999).
[13] Y. Moon and E. Yoon, J. Cryst. Growth **212**, 61 (2000).
[14] J.M. Moison, M. Bensoussan, and F. Houzay, Phys. Rev. B **34**, 2018 (1986).
[15] G. Hollinger, D. Gallet, M. Gendry, C. Santinelli, and P. Viktorovitch, J. Vac. Sci. Technol. B **8**, 832 (1990).
[16] C.H. Li, L. Li, D.C. Law, S.B. Visbeck, and R.F. Hicks, Phys. Rev. B **65**, 205322 (2002)
[17] S. Yoon, Y. Moon, T.W. Lee, E. Yoon, and Y.D. Kim, Appl. Phys. Lett. **74**, 2029 (1999).
[18] H. Yang, P. Ballet, and G. Salamo, J. Appl. Phys. **89**, R7871 (2001).
[19] J. Jönsson, F. Reinhardt, M. Zorn, K. Ploska, W. Richter, and J. Rumberg, Appl. Phys. Lett. **64**, 1998 (1994).
[20] K. Mahalingham, Y. Nakamura, N. Otsuka, H.Y. Lee, M.J. Hafich, and G.Y. Robinson, J. Electron. Mater. **21**, 129 (1992).
[21] A. Aurand, J. Leymarie, A. Vasson, M. Mesrine, J. Massies, and M. Leroux, J. Appl. Phys. **89**, 3775 (2001).
[22] H.H. Farrell and C.J. Palmstrom, J. Vac. Sci. Technol. B **8**, 903 (1990).
[23] W. Barvosa-Carter, R.S. Ross, C. Ratsch, F. Grosse, J.H.G. Owen, and J.J. Zinck, Surf. Sci. **499**, L129 (2002).
[24] M. Sauvage-Simkin, Y. Garreau, R. Pinchaux, M.B. Véron, J.P. Landesman, and J. Nagle, Phys. Rev. Lett. **75**, 3485 (1995).
[25] L. Bellaiche, K. Kunc, M. Sauvage-Simkin, Y. Garreau, and R. Pinchaux, Phys. Rev. B **53**, 7417 (1996).
[26] D.A. Shirley, Phys. Rev. B **5**, 4709 (1972).
[27] C.S. Fadley, Prog. Surf. Sci. **16**, 275 (1984).
[28] M. Seelmann-Eggebert and H.J. Richter, Phys. Rev. B **43**, 9578 (1991)
[29] G. Grenet, E. Bergignat, M. Gendry, M. Lapeyrade, and G. Hollinger, Surf. Sci. **352-354**, 734 (1996).
[30] J.J. Joyce, M. Del Guidice, and J.H. Weaver, J. Elec. Spectrosc. Relat. Phenom. **49**, 31 (1989).

[31] G. Le Lay, D. Mao, A. Kahn, Y. Hwu, and G. Margaritondo, Phys. Rev. B **43**, 14 301 (1991).
[32] P. Vogt, A.M. Frisch, Th. Hannapel, S. Visbeck, F. Willig, Ch. Jung, R. Follath, W. Braun, W. Richter, and N. Esser, Appl. Surf. Sci. **166**, 190 (2000).
[33] X. Wallart, Surf. Sci. **506**, 203 (2002).
[34] N. Esser, W.G. Schmidt, J. Bernholc, A.M. Frisch, P. Vogt, M. Zorn, M. Pristovsek, W. Richter, F. Bechstedt, Th. Hannapel, and S. Visbeck, J. Vac. Sci. Technol. B **17**, 1691 (1999).
[35] W.G. Schmidt, F. Bechstedt, N. Esser, M. Pristovsek, Ch. Schultz, and W. Richter, Phys. Rev. B **57**, 14 596 (1998).
[36] R.R. Lapierre, T. Okada, B.J. Robinson, D.A. Thompson, and G.C. Weatherly, J. Cryst. Growth **155**, 1 (1995).
[37] R.R. Lapierre, T. Okada, B.J. Robinson, D.A. Thompson, and G.C. Weatherly, J. Cryst. Growth **158**, 6 (1996).
[38] X. Wu and G.C. Weatherly, J. Cryst. Growth **233**, 88 (2001).
[39] S.B. Zhang and A. Zunger, Appl. Phys. Lett. **71**, 677 (1997).
[40] P.N. Keating, Phys. Rev. **145**, 637 (1966).
[41] R.M. Martin, Phys. Rev. B **1**, 4005 (1970).
[42] S.H. Wei, L.G. Ferreira, and A. Zunger, Phys. Rev. B **41**, 8240 (1990).
[43] *Numerical Data and Functional Relationships in Science and Technology*, edited by O. Madelung, M. Schultz, and H. Weiss, Landolt-Börnstein, New Series, Group III, Vol. 17 (Springer-Verlag, Berlin, 1982).
[44] Similar dimers effect on ordering has been previously described for bulk InGaP(100) alloys, see M. Zorn *et al.*, Phys. Rev. B **60**, 8185 (1999), and references therein.

Résumé

La fabrication d'hétérostructures de semi-conducteurs III-V de qualité repose sur la connaissance des surfaces, l'optimisation de la formation des interfaces et la maîtrise de la relaxation des couches contraintes. Nous montrons d'abord par une étude en diffraction et spectroscopie d'électrons que la reconstruction de surface des semi-conducteurs III-V phosphorés est différente des reconstructions couramment observées sur les arséniés. Nous abordons ensuite le problème des interfaces à anion commun pour lequel nous proposons un modèle cinétique prenant en compte l'effet de la température de croissance sur les mécanismes d'échange et de ségrégation en surface. Pour les interfaces différant par leurs anions, la corrélation des résultats de diverses techniques nous conduit à une description précise de la composition chimique de ces interfaces en fonction des conditions de croissance et de son influence sur les propriétés électroniques de l'hétérostructure. L'obtention d'interfaces les plus abruptes possible nous amène à étudier la réactivité de surface des arséniures sous flux de phosphore pour laquelle nous déterminons les facteurs essentiels : dimères d'anions en surface et énergie de liaison des binaires impliqués. L'effet de la contrainte sur la morphologie des couches de semi-conducteurs phosphorés présente des similitudes et des différences avec le cas des arséniés. Nous proposons une interprétation de ces différences soulignant le rôle des reconstructions de surface spécifiques aux phosphorés.

Nous envisageons ensuite l'utilisation de ces hétérostructures dans des transistors à effet de champ à modulation de dopage. Nous optimisons la croissance de structures à double plan de dopage, à canaux composites et étudions les limites des approches pseudomorphique et métamorphique pour les canaux en InGaAs à fort taux d'indium. Nous discutons enfin de l'intérêt des semi-conducteurs antimoniés pour améliorer les résultats obtenus avec les arséniés et phosphorés.